Aus der Klinik für Neurologie

der Heinrich-Heine-Universität Düsseldorf

Klinikdirektor: Univ.- Prof. Dr. Dr. Sven Meuth

The impact of complement on neuromuscular health

Habilitationsschrift

zur Erlangung der Venia Legendi für das Fach Experimentelle Neurologie

Fachbereich Humanmedizin

der Heinrich-Heine-Universität Düsseldorf

vorgelegt von

Dr. med. Christopher Nelke

2024

Inhaltsverzeichnis

Erklärung

Hiermit versichere ich an Eides statt, dass ich die vorgelegte Habilitationsschrift eigenständig und ohne unerlaubte Hilfsmittel angefertigt habe.

Ich versichere, dass bei den wissenschaftlichen Untersuchungen, die Gegenstand dieser Habilitationsschrift sind, ethische Grundsätze sowie die Grundsätze und Empfehlungen zur Sicherung guter wissenschaftlicher Praxis beachtet wurden. Weiterhin versichere ich, dass es für meine Person weder laufende noch abgeschlossene, erfolglose Habilitationsverfahren gibt.

Düsseldorf, April 2024

Dr. Christopher Nelke

List of publications/Publikationsliste

Diese kumulative Habilitationsschrift beruht auf den nachfolgend aufgelisteten Publikationen. Die mit einem * gekennzeichneten Arbeiten wurden in gleichberechtigter Erstautorenschaft der ersten Autoren und Autorinnen publiziert. In Klammern ist der Science Citation Index („Impact-Faktor“, IF) für die entsprechende Publikation angegeben.

1. **Nelke C***, Müntefering T*, Cengiz D, Theissen L, Dobelmann V, Schroeter CB, Block H, Preuße C, Michels APE, Lichtenberg S, Pawlitzki M, Pfeuffer S, Huntemann N, Zarbock A, Briese T, Kittl C, Dittmayer C, Budde T, Lundberg IE, Stenzel W, Meuth SG, Ruck T. K2P2.1 is a regulator of inflammatory cell responses in idiopathic inflammatory myopathies. J Autoimmun. 2023 Nov 5;142:103136. doi: 10.1016/j.jaut.2023.103136. PMID: 37935063. **[IF: 14.5]**
2. **Nelke, C.,** Schroeter, C.B., Theissen, L. et al. Senescent fibro-adipogenic progenitors are potential drivers of pathology in inclusion body myositis. Acta Neuropathol (2023). https://doi.org/10.1007/s00401-023-02637-2. **[IF: 12.7]**
3. **Nelke C***, Schroeter CB*, Stascheit F, Huntemann N, Pawlitzki M, Willison A, Räuber S, Melzer N, Distler U, Tenzer S, Stühler K, Roos A, Meisel A, Meuth SG, Ruck T. Eculizumab treatment alters the proteometabolome beyond the inhibition of complement. JCI Insight. 2023 Jul 10;8(13):e169135. doi: 10.1172/jci.insight.169135. PMID: 37227781; PMCID: PMC10371336. **[IF: 8.0]**
4. **Nelke C***, Stascheit F*, Eckert C, Pawlitzki M, Schroeter CB, Huntemann N, Mergenthaler P, Arat E, Öztürk M, Foell D, Schreiber S, Vielhaber S, Gassa A, Stetefeld H, Schroeter M, Berger B, Totzeck A, Hagenacker T, Meuth SG, Meisel A, Wiendl H, Ruck T. Independent risk factors for myasthenic crisis and disease exacerbation in a retrospective cohort of myasthenia gravis patients. J Neuroinflammation. 2022 Apr 12;19(1):89. doi: 10.1186/s12974-022-02448-4. PMID: 35413850; PMCID: PMC9005160. **[IF: 9.5]**
5. **Nelke C***, Schroeter CB*, Stascheit F, Pawlitzki M, Regner-Nelke L, Huntemann N, Arat E, Öztürk M, Melzer N, Mergenthaler P, Gassa A, Stetefeld H, Schroeter M, Berger B, Totzeck A, Hagenacker T, Schreiber S, Vielhaber S, Hartung HP, Meisel A, Wiendl H, Meuth SG, Ruck T. Eculizumab versus rituximab in generalised myasthenia gravis. J Neurol Neurosurg Psychiatry. 2022 May;93(5):548-554. doi: 10.1136/jnnp-2021-328665. Epub 2022 Mar 4. PMID: 35246490; PMCID: PMC9016243. **[IF: 11.2]**
6. **Nelke C***, Schroeter CB*, Pawlitzki M, Meuth SG, Ruck T. Cellular senescence in neuroinflammatory disease: new therapies for old cells? Trends Mol Med. 2022 Oct;28(10):850-863. doi: 10.1016/j.molmed.2022.07.003. Epub 2022 Aug 12. PMID: 35965205. **[IF 13.6]**

Abbreviations/Abkürzungsverzeichnis

3-hydroxy-3-methylglutaryl-CoA reductase	HMGCR
Acetylcholine receptor	AChR
Arachidonic acid	AA
B cell receptor	BCR
C3a receptor	C3aR
C5a receptor	C5aR
Complement factor 3	C3aR
Complement factor D	CFD
Complement factor H	CFH
Dermatomyositis	DM
Differentially expressed genes	DEGs
Early-onset MG	EOMG
Experimental autoimmune myasthenia gravis	EAMG
Fibrillin	FBN1
Fibro-adipogenic progenitor	FAP
Food and Drug Administration	FDA
Gene Set Enrichment Analysis	GSEA
iC3b/C3dg/C3d-binding complement receptor 2	CR2
Immune-mediated necrotizing myopathy	IMNM
Immunofluorescence staining	IF
Immunosuppressive treatments	IST
Impact factor	IF
Inclusion body myositis	IBM
Inflammatory myopathies	IIM
Intravenous immunoglobulins	IVIG
Late-onset MG	LOMG
Leukotrien A4	LTA4
Leukotrien B4	LTB4
Low-density lipoprotein receptor–related protein 4	LRP4
Lumican	LUM
Mammalian target of rapamycin	mTOR
Membrane attack complex	MAC
Minimal manifestation status	MMS
Muscle-specific kinase	MuSK
Myasthenia gravis	MG
Myasthenia Gravis Foundation of America	MGFA
Myasthenic crisis	MC
Neuromuscular junction	NMJ
Non-diseased controls	NDC
Odds ratio	OR
Plasma exchange	PLEX
polymorphonuclear leukocytes	PMN
Quantitative myasthenia gravis	QMG
Senescence-associated secretory phenotype	SASP
Signal recognition particle	SRP
Single nuclei RNA-seq	snRNA

Sodium	Na
Sparse partial least squares discriminant analysis	sPLS-DA
Standard deviation	SD
T cell receptor	TCR
T cells re-expressing CD45RA	TEMRA
T helper 1	TH1
Uniform manifold approximation and projection	UMAP

Figures/Abbildungen

1. Zusammenfassung

Das Komplementsystem ist ein integraler Teil des Immunsystems und hilft bei der Erkennung und Beseitigung von Krankheitserregern. Neben seiner Rolle als Protein-Netzwerk im Blut ist das Komplementsystem auch an der Regulation der adaptiven Immunität beteiligt. Zusätzlich zu diesen Funktionen im extrazellulären Raum hat das Komplementsystem ebenfalls eine neue Rolle in der intrazellulären Umgebung. Aktuelle Forschungsarbeiten haben gezeigt, dass das Komplementsystem ebenfalls intrazelluläre Prozesse wie Metabolismus, Autophagie oder Genexpression reguliert. Die Gesamtheit dieser extra- und intrazellulären Komplement-Aktivität wird als „Complosom“ bezeichnet, und seine Störung ist mit einer Vielzahl von Erkrankungen verbunden.

Diese Arbeit untersucht die Rolle des Komplementsystems bei neuromuskulären Erkrankungen, wobei sowohl die traditionellen extrazellulären Funktionen als auch die neueren intrazellulären Rollen im Fokus stehen. Im Kontext neuromuskulärer Erkrankungen wird die extrazelluläre Komplementaktivierung durch Myasthenia gravis veranschaulicht. Bei dieser antikörpervermittelten Autoimmunerkrankung trägt die Komplementaktivierung zur Zerstörung der postsynaptischen Membran bei, was die Anzahl der Rezeptoren und Natriumkanäle reduziert. Ein besseres Verständnis dieses Signalweges konnte die therapeutische Landschaft der MG erweitern und neue Signaturen bei Patienten und Patientinnen mit Myasthenia gravis aufzeigen.

Auf der anderen Seite beleuchtet diese Arbeit die Bedeutung des intrazellulären Komplementsystems am Beispiel der idiopathischen entzündlichen Myopathien. Bei diesen Erkrankungen ist die Hemmung des extrazellulären Komplements weniger wirksam. Gleichzeitig deuten aktuelle Daten darauf hin, dass intrazelluläre Komplementkomponenten in bei der Einschlusskörper Myositis, einer Unterform dieser Erkrankungen, beteiligt sind. Die Dysregulation von intrazellulären Komplementproteinen, insbesondere C3, könnte die Immunantwort und das Verhalten von Fibroblasten regulieren. Dies weist auf die Notwendigkeit weiterer Forschung hin, um die Rolle des intrazellulären Komplements bei neuromuskulären Erkrankungen besser zu verstehen.

In Summe diskutiert diese Arbeit die Bedeutung des extra- und intrazellulären

Komplementsystems bei neuromuskulären Erkrankungen und zeigt auf wie Diagnostik und Therapie durch ein besseres Verständnis dieses Systems verbessert werden können.

2. Introduction

Discovered over a century ago by Jules Bordet [1], the complement system has been viewed as a serum-effective arm of innate immunity that 'complemented' the action of antibodies during the detection and elimination of bloodborne pathogens.

As our understanding of the individual components within the complement system deepened, it became evident that this system plays a crucial role as a mediator in acute inflammatory reactions guiding migration and activation of innate immune cells [2]. Surprisingly, ongoing research initiated in the 1980s demonstrated that complement receptor signalling on B and T cells also constitutes an integral component of both the humoral and adaptive immune responses [3,4].

The serum-effective activity of extracellular complement has been in the scientific spotlight for decades. Here, complement is required for the bodies defence machinery against invading pathogens. Indeed, from an evolutionary viewpoint, the complement system has been conserved for more than 500 million years, as evidenced from genetic studies of common ancestors of Eumetazoa [5]. The initial activation mechanism of the ancient complement system is thought to closely resemble the mammalian lectin and alternative activation pathways, primarily focused on opsonization and induction of inflammatory pathways. This ancient complement system remained largely unchanged across most deuterostomes until the emergence of jawed vertebrates. During this evolutionary stage, the genetic landscape underlying the complement system shifted introducing the classical and lytic pathways to the pre-existing complement system [5]. This transformation marked the evolution from the primitive complement system to the complement system that is at the centre of our current understanding [5].

Still, our understanding of the complement system and its subsequent functions continues to expand, revealing a more intricate compartmentalization than previously assumed [3,4]. The activation of complement is not confined to extracellular spaces but also extends intracellularly, spanning diverse cell populations and various tissues. These pathways of intracellular complement have been termed as the „complosome" and are subject of ongoing research, uncovering compelling evidence of their involvement in novel and non-canonical functions. Remarkably, the complosome

actively engages in fundamental cellular processes like metabolism, autophagy, and gene expression [3,4,6]. This newly appreciated role in cell biology underscores the impact of disruptions in complosome activities on prevalent human diseases. Conditions ranging from recurrent infections to arthritic diseases, atherosclerosis, and cancer are increasingly linked to perturbations in the complosome.

This work explores the evolving role of the complement system in neuromuscular diseases. First, we will explore the „canonical“ activation of complement in the extracellular environment and its influence on neuromuscular disorders. A special emphasis will be placed on the development of therapies targeting the complement system. Second, we will highlight the „non-canonical“ intracellular role of complement in neuromuscular diseases and discuss its potential implications in understanding pathophysiological mechanisms. Finally, this work aims to amalgamate contemporary perspectives on both extracellular and intracellular complement activities, thereby offering a comprehensive synthesis of our present comprehension in this field.

3. Extracellular complement and its impact on neuromuscular diseases

The human complement system is a complex network involving over 50 proteins [7]. These proteins can be found circulating in the blood or residing as cell membrane-bound proteins. Among these proteins, C3 and C5 stand out as major effector molecules, primarily produced by the liver in a pro-enzymatic form. Activation of complement C3 and C5 occurs when various activation pathways are triggered in response to pathogen- or damage-associated molecular patterns [7]. This initial recognition leads to the creation of C3 and C5 convertases, subsequently resulting in the cleavage and activation of C3 into C3a and C3b, and C5 into C5a and C5b, respectively. The assembled C5b unit combines with serum proteins C6 through C9 to generate the membrane attack complex (MAC). The MAC, in turn, directly lyses pathogens or harmful target cells. Additionally, C3b opsonizes microbes and deleterious host cells, marking them for destruction by scavenger cells [7].

The receptors responsible for binding the anaphylatoxins C3a and C5a – the C3a receptor (C3aR) and C5a receptors 1 and 2 (C5aR1 and C5aR2), respectively – are expressed by a wide array of host immune and non-immune cells [8]. Stimulation of these receptors triggers diverse responses, including endothelial activation to facilitate adhesion and the influx of immune cells into tissues, contraction of smooth muscle cells, and the recruitment and activation of innate immune cells [7]. All these processes

are fundamental to the classic inflammatory reaction and are widely acknowledged as canonical complement functions.

While historically recognized as a key player of innate immunity, the complement system also plays a pivotal role in orchestrating adaptive immunity. One such example is the significance of the iC3b/C3dg/C3d-binding complement receptor 2 (CR2) acting as a co-stimulatory molecule for B cells [9–11]. Its function significantly reduces the threshold of B cell receptor (BCR) signaling, amplifying it by up to 10,000-fold. Similarly, CD46, a complement regulator and receptor capable of binding and deactivating C3b and C4b, offers co-stimulatory signals to human CD4+ T cells [11]. These signals are essential for the induction of T helper 1 (TH1) cell responses. The viewpoint that complement constitutes an integral part of adaptive immunity clarifies the extensive influence of complement dysregulation across various human disease states mediated by both innate and adaptive immunopathology.

3.1. Myasthenia gravis as prototypical complement-mediated autoimmune disease

A primary example of complement in autoimmunity is myasthenia gravis (MG). A rare and heterogenous condition, MG is characterized by the disruption of signal transmission across the neuromuscular junction (NMJ) [6,12]. The diverse manifestations of MG lead to its classification into distinct subtypes based on variations in autoantibodies and the clinical presentation of symptoms. The most frequent antibody detected in MG (80 to 85% of patients) is directed against the acetylcholine receptor (AChR), densely distributed on the postsynpatic membrane of the NMJ [6,12]. The mechanisms through which these AChR autoantibodies operate to disrupt synaptic transmission at the NMJ encompass the following mechanisms [13]:

Inhibition of acetylcholine binding: By obstructing the binding sites for acetylcholine on AChRs.

Accelerated degradation of AChRs: Prompting the internalization and breakdown of AChRs cross-linked by these autoantibodies.

Complement activation: This process triggers damage to the postsynaptic membrane at the NMJ, resulting in a decrease in membrane surface area, along with a reduction in both the number of AChRs and voltage-gated sodium ion (Na+) channels.

MG patients without AChR antibodies may, instead, demonstrate antibodies

recognizing the muscle-specific kinase (MuSK) or low-density lipoprotein receptor–related protein 4 (LRP4). These antibodies are rare and only detected in approximately 5% or less than 1% of patients, respectively [13]. Intriguingly, the anti-MuSK-antibody is mostly composed by IgG4 and, therefore, unlikely to induce complement activation as effector mechanism. Instead, these anti-MuSK-antibodies disrupt the signalling pathway of MuSK by obstructing the interaction between agrin, LRP4, and MuSK, resulting in reduced AChR density [13].

In the following sections, we will focus on the activation of complement by AChR-antibodies and its implications within the context of MG.

3.2. Evidence for complement activation as pathophysiological driver of MG

Multiple lines of evidence suggest complement in the pathogenesis of MG including human and animal studies [13]. First, immunization against the AChR was employed to generate models of experimental autoimmune myasthenia gravis (EAMG) [14]. Here, active or passive EAMG models showcased the deposition of complement revealing the co-localization of IgG, C3, and MAC deposits specifically at the NMJ. These deposits correlate with the deterioration of the postsynaptic membrane, debris accumulation within the synaptic space, AChR loss from the endplate region, and a noticeable decrease in miniature endplate potential amplitude [14]. Studies using knockout mice lacking either C3 or C4 have a notably decreased occurrence of active EAMG compared to their wild-type counterparts. Despite observing IgG deposits at the NMJ in both C3- and C4-deficient animals, MAC formation is largely absent in these knockout mice. Similar outcomes are observed in animals lacking C5 or C6. In C5-deficient mice, immunofluorescence detects IgG and C3 at the NMJ, but not the MAC [14,15].

In humans, alterations in the concentrations of different complement proteins within the serum of MG patients indicated the active involvement of complement components in the disease's pathogenesis. Further studies employing electron microscopy and immunohistochemistry to study the NMJ in MG patients, as pioneered by the late Andrew Engels, demonstrated the localization of IgG antibodies alongside complement components C3 and C9 specifically on the postsynaptic membrane [16,17]. Furthermore, these elements were identified on fragments of deteriorating junctional folds found within the synaptic space. This localization underlines the role of complement activation

in the structural and functional alterations observed at the NMJ in individuals with MG.

3.3. The need for novel therapeutics in MG

Owing to advancements in treatment strategies and diagnostic tools, the therapeutic outcomes for the majority of MG patients have improved [12,18]. However, there exists a distinct subgroup within the population of MG patients, often labeled as refractory, who continue to experience symptoms despite therapy. These patients commonly face disease exacerbations and myasthenic crisis (MC), which substantially contribute to the overall disease burden. Despite progress in diagnosing and treating MG, individuals experiencing MC still confront a considerable mortality rate, estimated at around 5–12%. The necessity for hospitalization, coupled with the burden of managing the disease and the expenses associated with available rescue therapies, underscores the critical importance of both preventing and effectively managing MC.

Indeed, we observed that in a retrospective, observational cohort study of MG patients between 2000 and 2021 from eight tertiary hospitals in Germany the risk for MC remained high with 26.3% of patients experiencing MC during their individual course of disease [12]. This study underscores the high disease burden in the time before the advent of targeted complement therapies. In this cohort, mean age at disease onset was 52.7 years (standard deviation (20) 20.0) and at diagnosis 53.5 years (SD 19.8). Early disease onset before the age of 50 years occurred in 300 patients (36.8%), while 510 patients (62.6%) were late-onset MG (LOMG) [12]. The follow-up time was 62.6 months (SD 73.3) after diagnosis. Out of 815 patients, 217 patients (26.3%) experienced a MC during their disease course while 225 patients (27.6%) experienced a disease exacerbation. Potential risk factors for the occurrence of a MC or disease exacerbation were interrogating using a model of multivariate Cox regression. In this cohort, the Myasthenia Gravis Foundation of America (MGFA) class, as surrogate marker for clinical severity, correlates inversely with the risk for MC (**Figure 1A, B**). Further, patients with anti-MuSK-antibodies have a higher risk for experiencing MC or disease exacerbation (**Figure 1C, D**) [12].

Intriguingly, the efficacy of therapeutic management of MG is associated with the occurrence of MC and disease exacerbations [12]. Minimal manifestation status (MMS) is defined in accordance with the MGFA as no symptoms of functional limitation from MG but weakness on examination only detectable by examination. To exclude bias due to patients presenting with MC or exacerbation as first manifestation, patients with a

clinical event up to 6 months after diagnosis were excluded from the analysis of treatment response. The risk was reduced for achieving MMS for MC (OR 0.32 95% CI 0.17–0.61, $p = 0.002$) and for exacerbation (OR 0.50 95% CI 0.34–0.70, $p < 0.001$) [12]. In line, patients without MMS are at an increased for MC and disease exacerbations as compared to patients achieving MMS (**Figure 1E, F**). The analysis of cortisone, as binary variable, and dosage, as continuous variable, as predictors for MC or exacerbation did not influence the risk for MC (OR 1.12 95% CI 1.05–1.33, $p = 0.16$) and exacerbation (OR 1.09 95% CI 1.01–1.45, $p = 0.42$) when compared with patients who did not receive cortisone. In the group of cortisone-treated patients, assessment of cortisone dose did not reveal an association with the risk for MC (OR 1.27 95% CI 1.16–1.65, $p = 0.23$) or exacerbation (OR 1.52 95% CI 1.34–1.72, $p = 0.18$) [12].

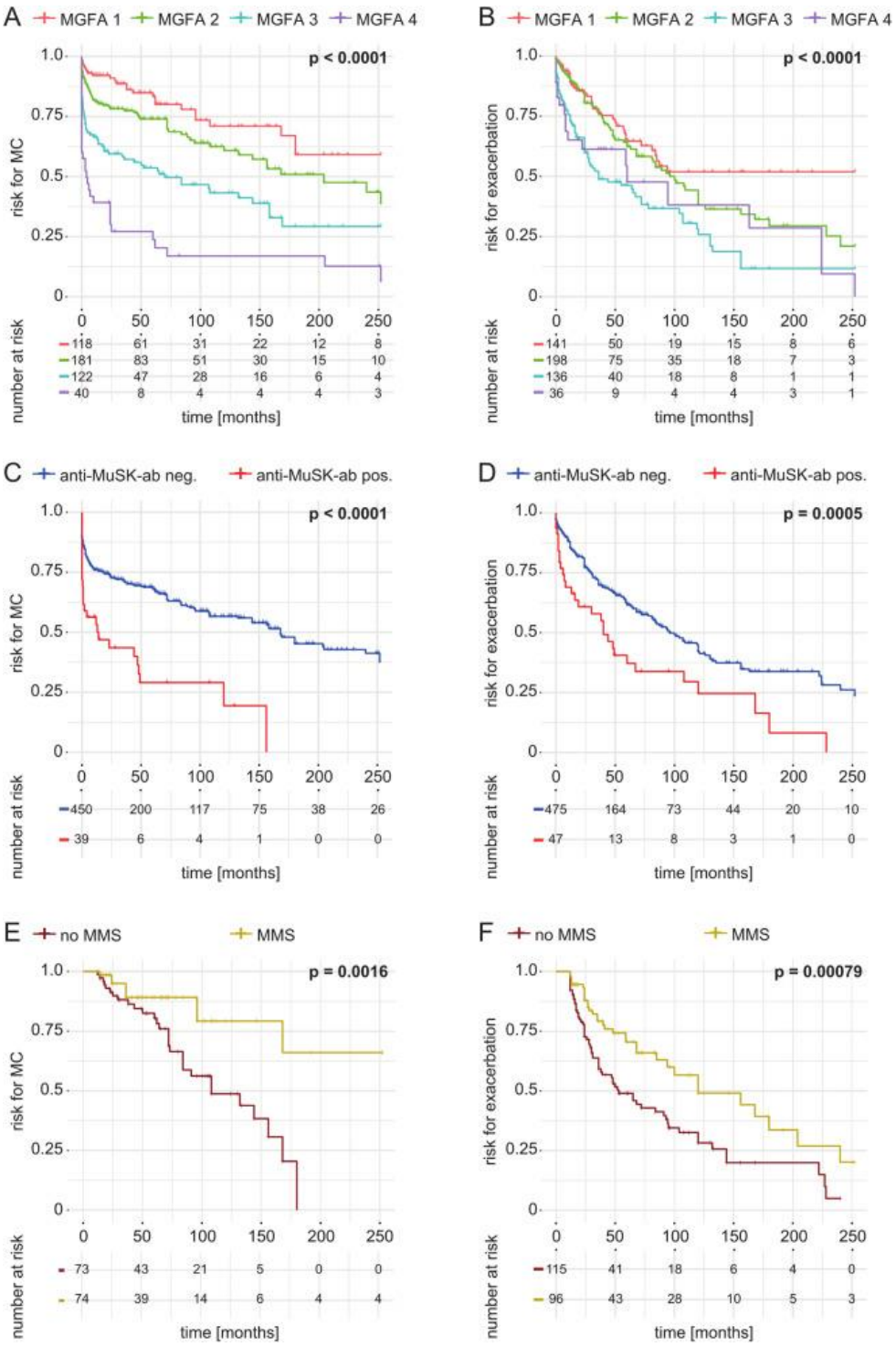

Figure 1: Survival analysis of MC and disease exacerbation. Survival curves displaying the time (in months) between diagnosis and the first MC (myasthenic crisis) or exacerbation. (**A**) Survival graph displaying the time to MC according to MGFA class. (**B**) Survival graph displaying the time to exacerbation according to MGFA class. (**C**) Survival graph displaying the time to MC according to anti-Musk-ab status. (**D**) Survival graph displaying the time to exacerbation according to anti-Musk-ab status. (**E**) Survival graph displaying the time to MC according to minimal manifestation status (MMS) at 12 months after diagnosis. (**F**) Survival graph displaying the time to exacerbation according to MMS at 12 months after diagnosis. Significance between survival curves was assessed by logrank testing. ****$p < 0.0001$ ***$p < 0.001$, **$p < 0.01$, *$p < 0.05$. Mit freundlicher Genehmigung des Verlags aus Nelke

et al. 2022.

This data suggests that a subgroup of patients continue to experience severe disease despite treatment and that patients are at an increased risk for life-threatening MC if symptoms are left unchecked.

3.4. Novel therapeutics in the management of MG

The existing standard of treatment for MG includes broad immunosuppressive treatments (IST) such as corticosteroids, azathioprine, methotrexate or mycophenolate mofetil as well as immunomodulatory treatments such as plasma exchange (PLEX) and intravenous immunoglobulins (IVIG) [13].

This spectrum was expanded in 2017 with the admission of eculizumab. This recombinant humanized monoclonal antibody binds to C5 inhibiting its breakdown into C5a and C5b, thereby preventing the formation of the MAC [19]. Eculizumab pioneered targeted complement therapies and was initially recognized by the Food and Drug Administration (FDA) in 2007 for treating paroxysmal nocturnal hemoglobinuria. In the phase 3 trial REGAIN, eculizumab demonstrated a convincing benefit in patients with refractory generalized MG, despite not achieving a 100% response rate. The majority of patients still required continuous, long-term therapy with other ISTs. Based on these findings, eculizumab became the first complement-targeted therapy for MG [19].

However, there remains a lack of evidence comparing different treatment approaches in MG [20]. In a retrospective, observational study, we assessed rituximab and eculizumab as treatments for generalized, therapy-resistant anti-AChR-antibody positive MG. The primary outcome parameter utilized was the change from the baseline quantitative myasthenia gravis (QMG) score, assessed over a 24-month follow-up period. Specific study outcomes were predetermined before data analysis commenced [20]. A total of 77 patients were included and matched by propensity score matching using an optimal full matching approach as to avoid a selection of patients to remain unmatched. The balance between the two groups was assessed by comparing the standardised mean differences of the covariates before and after propensity score adjustment. Using a model of optimal full matching, we achieved standardised mean differences for the selected covariates below 0.1 indicating adequate balancing of the two groups [20].

Table 1: Baseline characteristics of patients

	Rituximab-treated patients	Eculizumab-treated patients	P value
Patients, n	57	20	
Age at baseline, years, mean (SD)	46.5 (17.1)	45.4 (15.2)	0.791
Age at diagnosis, years, mean (SD)	40.8 (18.2)	36.5 (12.2)	0.351
Early onset MG, n (%)	36 (63.1)	16 (80.0)	0.266
Late onset MG, n (%)	21 (36.9)	4 (20.0)	0.266
Female patients, n (%)	35 (62.5)	12 (54.6)	0.610
Disease duration, years, mean (SD)	6.3 (4.5)	8.8 (6.3)	0.068
QMG score at baseline, mean (SD)	10.7 (5.1)	13.2 (5.2)	0.056
MGFA status at maximum severity, n (%)			
I	0 (0.0)	0 (0.0)	0.335
II	16 (28.1)	10 (50.0)	
III	20 (35.1)	5 (25.0)	
IV	16 (28.1)	3 (15.0)	
V	7 (12.2)	2 (10.0)	
History of thymectomy, n (%)	29 (50.8)	13 (65)	0.308
Confirmed thymoma, n (%)	8 (14.0)	4 (20.0)	0.487
Total number of previous ISTs, median (minimum–maximum)	2 (2–3)	2 (2–3)	0.285
Previous disease modifying therapy, n (%)			
Azathioprine	49 (85.9)	18 (90.0)	0.729
Mycophenolate	26 (45.6)	14 (70.0)	0.072
Methotrexate	24 (42.1)	7 (35.0)	0.608
Cyclosporine	7 (12.2)	5 (25.0)	0.279
Cortisone at baseline, mg, mean (SD)	6.0 (10.3)	10.4 (12.6)	0.121
Number of previous MC, median (minimum–maximum)	1 (0–3)	1 (0–3)	0.971

Table 1: Baseline refers to the first infusion of rituximab or eculizumab. Disease duration was defined as the time between symptom onset and baseline. Patients with rituximab were compared with patients receiving eculizumab by two-sided Student's t-test (*) or Fisher's exact test (#). P values are given; significance cut-off was $p<0.05$. Abbreviations: IST, immunosuppressive therapy; MC, myasthenic crisis; MG, myasthenia gravis; MGFA, Myasthenia Gravis Foundation of America; QMG, quantitative myasthenia gravis. Mit freundlicher Genehmigung des Verlafs aus Nelke, Schroeter et al. 2022.

Patients treated with eculizumab experienced a stronger benefit from the treatment compared to those on rituximab (QMG at 12 months: rituximab 11.2 (SD 7.3) vs. eculizumab 8.4 (SD 6.1); p=0.021, **Figure 2**) [20]. Furthermore, we assessed the change

to the QMG score from baseline and at 24 months between the rituximab (n=54) and eculizumab (n=19) cohorts. Eculizumab-treated patients displayed a stronger reduction in the QMG score compared to rituximab-treated patients at 24 months (QMG at 24 months: rituximab 11.2 (SD 6.4) vs. eculizumab 9.6 (SD 8.5); p<0.001). Notably, the presence of a thymoma did not affect the QMG score changes at 12 or 24 months (p=0.123 and p=0.848, respectively).

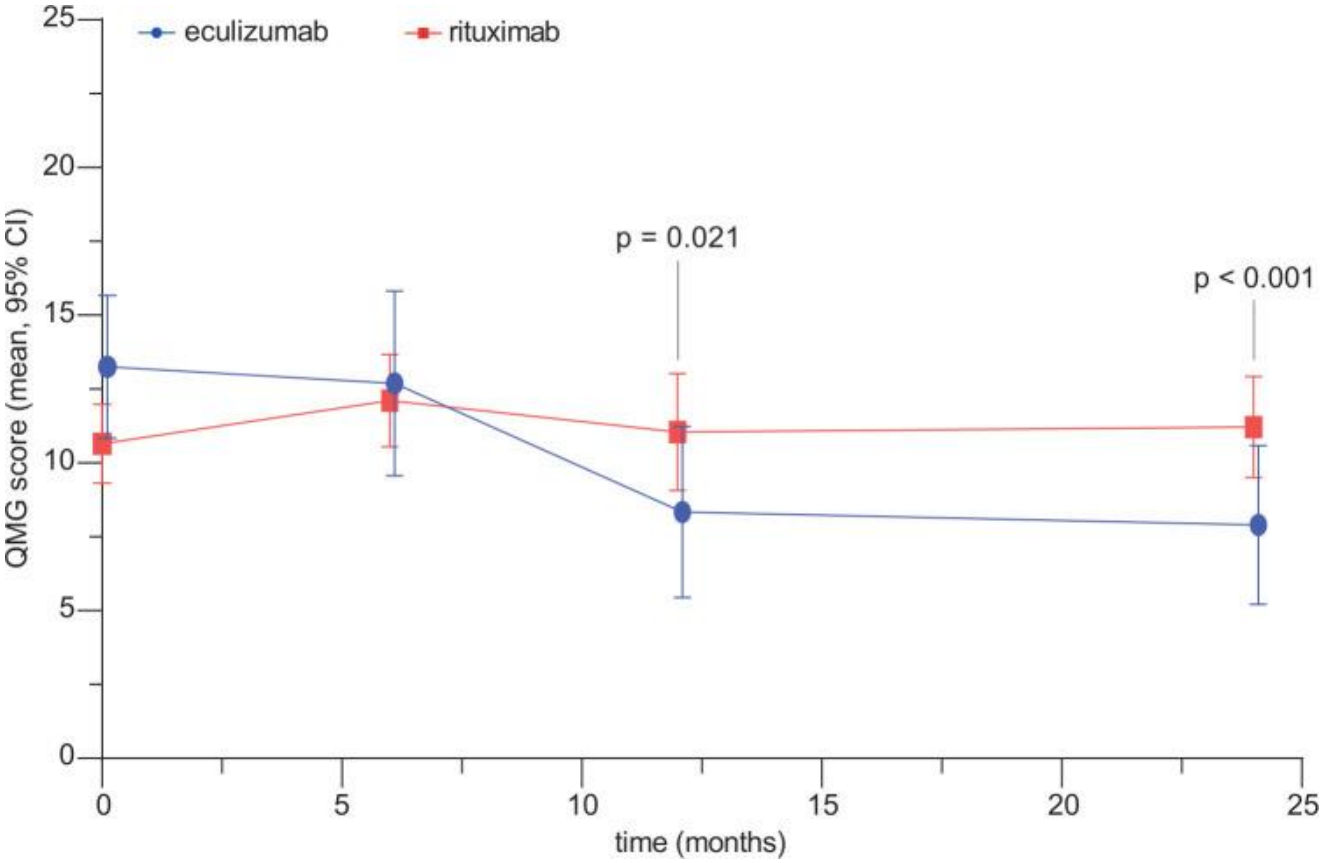

Figure 2: Changes to baseline QMG score. QMG scores were assessed at 6, 12 and 24 months. Baseline is defined as start of rituximab or eculizumab therapy. Differences between groups were assessed in a model of optimal full propensity score matching. Patients were matched for QMG score at baseline, sex, age at diagnosis, age at baseline and thymoma. Error bars display mean (95% CI). ***p<0.001, **p<0.01, *p<0.05, p≥0.05, not significant. Mit freundlicher Genehmigung des Verlags aus Nelke, Schroeter et al. 2022.

In respect to the occurrence of MC during the 24 month observation period, there were nine patients in the rituximab group who experienced a MC, whereas two patients showed deterioration in the eculizumab group. However, this discrepancy did not achieve statistical significance (MC, n (%), rituximab 15 (15.8%) vs. eculizumab 2 (10.0%), p=0.510). Interestingly, the time to MC did not display variance between rituximab- and eculizumab-treated patients (**Figure 3A**). At 12 month follow-up, there was a difference in the rate of patients achieving MMS between the two groups. Six

patients achieved MMS in the rituximab group (n=56, 10.7%), while seven patients achieved MMS in the eculizumab treatment group (n=19, 36.8%; p=0.031, **Figure 3B**). This effect persisted at the 24 month assessment, with seven patients reaching MMS after rituximab (n=54, 12.9%) and seven patients after eculizumab treatment (n=19, 36.8%; p=0.015). However, one eculizumab patient and three rituximab patients were excluded from the analysis due to insufficient information regarding their rescue therapies [20].

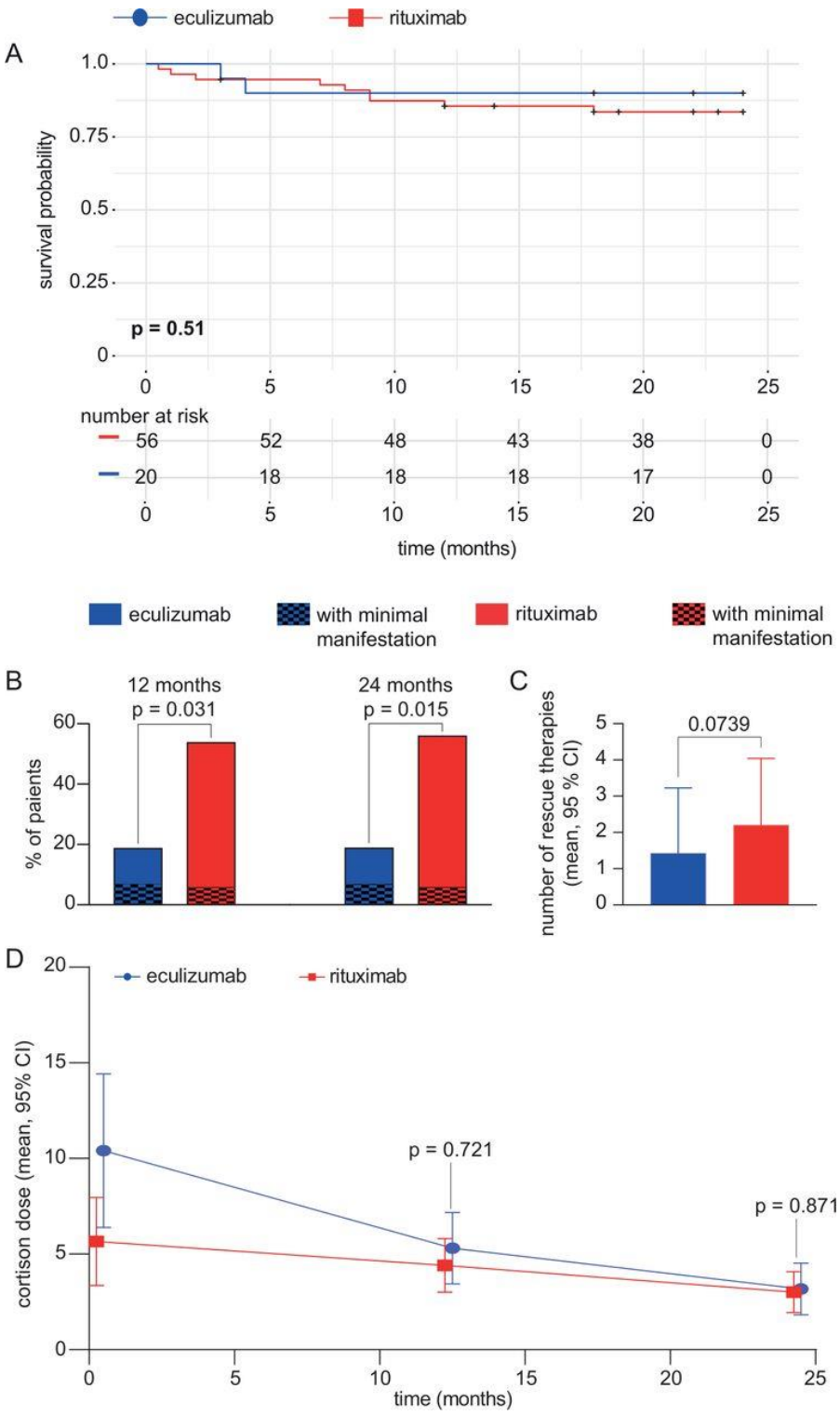

Figure 3: Time to myasthenic crisis after baseline. (A) Kaplan-Meier curve displaying time to myasthenic crisis after baseline. Baseline is defined as start of rituximab or eculizumab therapy. Differences between groups were assessed by logrank test. (B) Number of patients achieving minimal manifestation after 12 and 24 months of treatment according to treatment. (C) Number of rescue therapies per patient in the 24 months observation period. Differences between groups were assessed by two-sided Student's t-test. (D) Change to cortisone dose at baseline at 12 and 24 months of treatment. Error bars display mean (95% CI). **p<0.01, *p<0.05, p≥0.05, not significant. Mit freundlicher Genehmigung des Verlags aus Nelke et al. 2023.

The utilization of rescue therapies did not significantly differ between the rituximab and eculizumab groups, as indicated by the number of rescue therapies required per patient during the 24-month observation period (number of rescue therapies per patient (SD): rituximab 2.20 (1.83), eculizumab 1.42 (1.81); p=0.073) (**Figure 3C**). Additionally, both

groups were able to reduce their prednisolone dose after initiating treatment (**Figure 3D**). Notably, no significant difference was detected between the groups concerning the change in baseline prednisone dose at 12 months (prednisone dose at 12 months, mg (SD): rituximab 4.01 (4.90), eculizumab 5.30 (5.63); p=0.721) or at 24 months of treatment (prednisone dose at 24 months, mg (SD): rituximab 2.75 (3.67), eculizumab 3.17 (2.88); p=0.871).

Taken together, these data underline the value of targeted complement therapies for the management of MG. Still, there remains a substantial risk for MC independent of treatment strategies underscoring the need for intensified monitoring for patients at risk.

3.5. „Off-target“ effects of complement-inhibition with eculizumab

While eculizumab has exhibited remarkable effectiveness, even in instances of autoimmune diseases resistant to treatment, further studies into the long-term safety implications and treatment outcomes are needed. This need is underscored by a recent surge of novel complement inhibitors approved for the treatment of MG, such as ravulizumab[18] (monoclonal antibody targeting C5 with longer efficacy than eculizumab) or zilucoplan[21] (small molecule targeting C5 with subcutaneous application). As introduced above, complement is likely to impact not only aspects of innate and adaptive immunity, but also to regulate metabolic functions [4]. Consequently, the therapeutic suppression of the terminal complement cascade is likely to exert broader influences on human biology beyond solely inhibiting the formation of the MAC.

To address this viewpoint, we employed a combined proteomic and metabolomic approach to study the serological profile of anti-AChR-antibody MG patients treated with eculizumab [6]. Investigating the impact of eculizumab on both the serum proteome and metabolome, we enrolled three cohorts of patients with MG, each matched in terms of age and sex. These cohorts comprised individuals treated with either eculizumab or azathioprine (the most common first-line therapy), as well as treatment-naive patients serving as the control group. At the time of sampling, patients across all groups were around 55 years old, with an equal distribution of 2 women and 8 men in each cohort. Among the eculizumab-treated patients, there was an average of 2.8 (with a standard deviation of 1.6) prior ISTs, while those receiving azathioprine had an average of 1.5 (with a standard deviation of 2.5) previous ISTs [6]. Notably, thymectomy had been performed in three individuals from the eculizumab-treated group, one from the

treatment-naive group, and 5 from the azathioprine-treated group. All thymectomies took place at least 6 months prior to the patients' inclusion in the study. Importantly, there were no discernible differences in steroid dosage between patients treated with eculizumab and those treated with azathioprine (p = 0.68) [6].

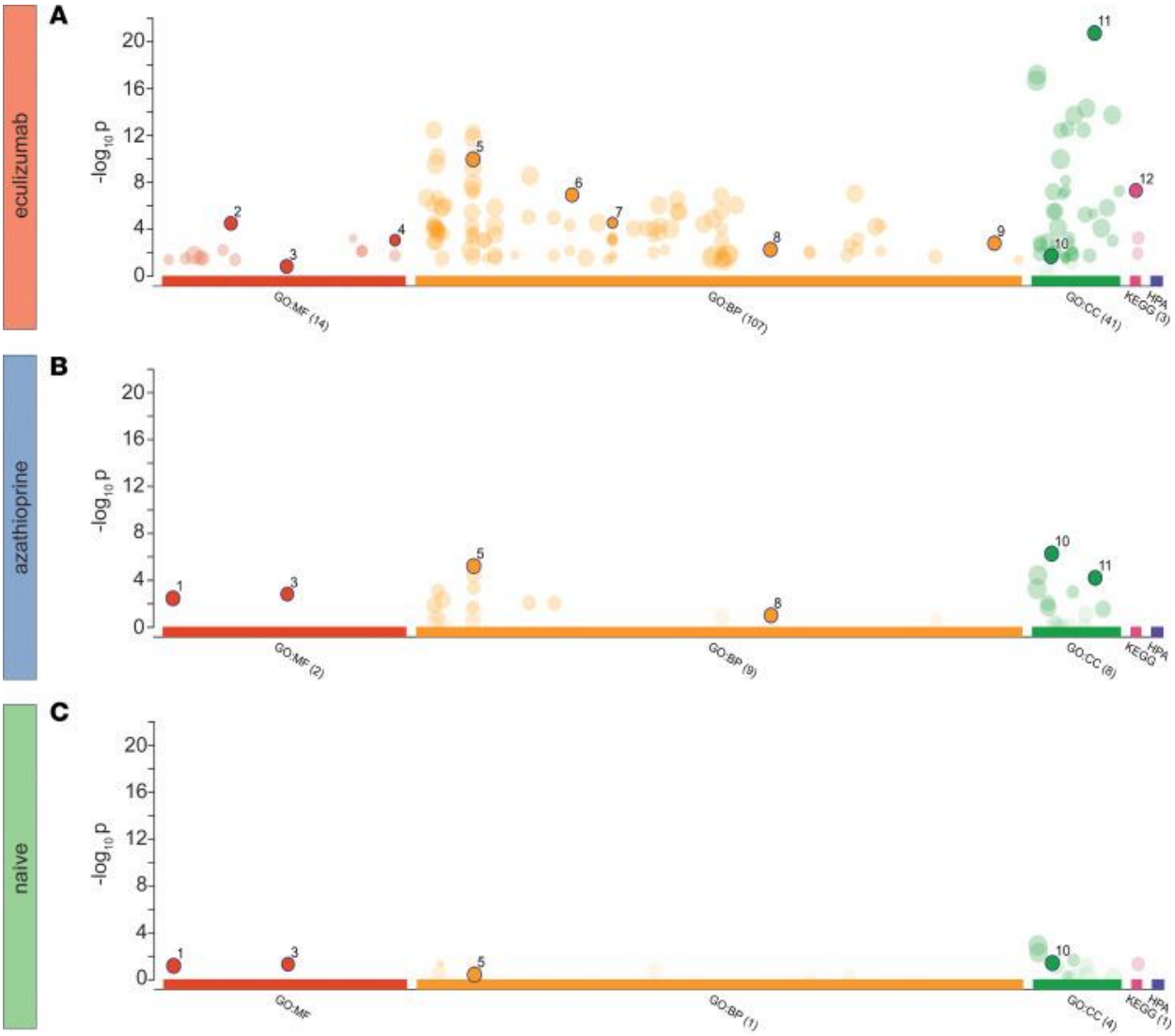

D

ID	Source	Term name	p (eculizumab)	p (azathioprine)	p (naïve)
1	GO-MF	antigen binding	1.000	3.795×10^{-3}	7.216×10^{-2}
2	GO-MF	antioxidant activity	3.405×10^{-5}	1.000	1.000
3	GO-MF	immunoglobulin receptor binding	1.572×10^{-1}	1.651×10^{-3}	5.236×10^{-2}
4	GO-MF	cholesterol transfer activity	9.141×10^{-4}	1.000	1.000
5	GO-BP	complement activation	1.168×10^{-10}	6.749×10^{-6}	4.002×10^{-1}
6	GO-BP	regulation of complement activation	1.296×10^{-7}	1.000	1.000
7	GO-BP	high-density lipoprotein particle remodeling	3.029×10^{-5}	1.000	1.000
8	GO-BP	regulation of wound healing	5.789×10^{-3}	1.072×10^{-1}	1.000
9	GO-BP	cellular detoxification	1.661×10^{-3}	1.000	1.000
10	GO-CC	immunoglobulin complex	2.138×10^{-2}	5.858×10^{-7}	4.086×10^{-2}
11	GO-CC	blood microparticle	2.016×10^{-21}	6.743×10^{-5}	1.000
12	KEGG	complement and coagulation cascades	5.420×10^{-8}	1.000	1.000

Figure 4: Gene set enrichment. (A–C) Manhattan plot illustrating functional enrichment of differentially regulated proteins (fold-change > 1.5) from the MF (molecular function), BP (biological process), CC

(cellular component), KEGG (Kyoto Encyclopedia of Genes and Genomes), and HPA (Human Protein Atlas) databases, respectively. The analysis was performed using the R package gprofiler2 with g:SCS multiple-testing correction method applying significance threshold of 0.05. The –log10 P value is indicated on the y axis. IDs next to circles are annotated in D. Related GO terms and functional pathways were clustered together. **(D)** Table displaying GO terms and functional pathways of interest shown in A–C. N = 10 per group. GO, gene ontology. Mit freundlicher Genehmigung des Verlags aus aus Nelke, Schroeter et al. 2022.

We performed Gene Set Enrichment Analysis (GSEA) to study the serum proteome of each cohort. Here, biological processes (BPs) displayed distinct alterations in the eculizumab cohort, particularly in respect to complement activation and the regulation of complement activation, likely attributed to the accumulation of terminal complement factors. Intriguingly, serum samples from patients treated with eculizumab also displayed significant alterations in high-density lipoprotein particle remodelling, regulation of wound healing, and cellular detoxification processes when compared to both azathioprine-treated and treatment-naive patients (**Figure 4A**). Concerning cellular components (CCs), the eculizumab group exhibited enrichments in GO terms associated with immunoglobulin complexes and blood microparticles, among others (**Figure 4B, C, D**). Analysis of the KEGG pathway highlighted an upregulation in complement and coagulation cascades within the eculizumab-treated cohort. However, analysis of the HPA database did not reveal any significant functional enrichments [6].

Next, we integrated the metaobolimc data. Here, we observed an alteration in the arachidonic acid metabolism due to eculizumab treatment. After data pre-processing and metabolite identification, we selected 289 unique metabolites for downstream analysis. Leveraging sparse partial least squares discriminant analysis (sPLS-DA), known for handling noisy data with high collinearity, we tailored a model to suit our metabolomics data and reduced the dataset dimensionality (**Figure 5A**). Each of the three groups exhibited distinct metabolome signatures. In order to identify altered pathways, we conducted functional enrichment analysis specific to the eculizumab-treated cohort using the KEGG database (**Figure 5B**). Notably, the linoleic acid metabolism pathway emerged as the most enriched functional pathway within the eculizumab-treated cohort. Building upon our earlier observation of reduced ALOX5 levels in the proteomic data, we hypothesized that the blockade of complement by eculizumab in patients leads to an alteration in arachidonic acid (AA) metabolism [6]. This might be relevant as linoleic acid serves as a precursor lipid metabolized to AA.

We observed a positive correlation between 5-HPETE and ALOX5. Hence, we suspected that the decreased ALOX5 levels result in a disruption of AA metabolism and inhibition of downstream production of leukotrienes given that ALOX5 metabolizes AA to leukotrienes. Specifically, ALOX5 metabolizes AA to generate 5-HPETE, which undergoes further processing to leukotriene A4 (LTA4). Our comparison between groups revealed a reduction in 5-HPETE levels in the serum of eculizumab-treated patients (**Figure 5C).** Importantly, 5-HPETE is a precursor metabolite to LTA4, an initiator of downstream leukotriene synthesis. However, our metabolomics approach could not definitively detect LTA4. Apart from its involvement in the leukotriene pathway, AA also serves as a precursor in prostaglandin metabolism. To investigate potential disturbances in prostaglandin metabolism, we assessed levels of PGH2 resulting from PGH2 synthase enzymatic activity (**Figure 5D**). Surprisingly, PGH2 levels remained unchanged across all groups. To validate our earlier findings using a different methodological approach, we conducted a targeted analysis of PGH2 and LTA4 via ELISA. These metabolites are pivotal precursors in both prostaglandin and leukotriene metabolism. LTA4 levels were diminished in eculizumab-treated patients, while PGH2 levels remained consistent across groups (**5E and F**). To confirm these observations, we obtained longitudinal samples from patients undergoing eculizumab treatment. Specifically, we collected serum samples from 5 patients who had transitioned from azathioprine to eculizumab (**Figure 5G**). These patients, with an average age of 52.5 years (ranging from 31 to 73), comprised 3 men and 2 women. Following the switch, azathioprine was discontinued, and patients received eculizumab treatment for 3 months before serum sample collection. Throughout this period, glucocorticoid dosages remained stable across all patients, averaging 5 mg (with a standard deviation of 2.5). We assessed LTA4 and PGH2 levels via ELISA, comparing their statuses during eculizumab treatment and prior. Consistently, LTA4 exhibited decreased levels in eculizumab-treated patients, while PGH2 levels remained unchanged (**Figure 5H and I**) [6].

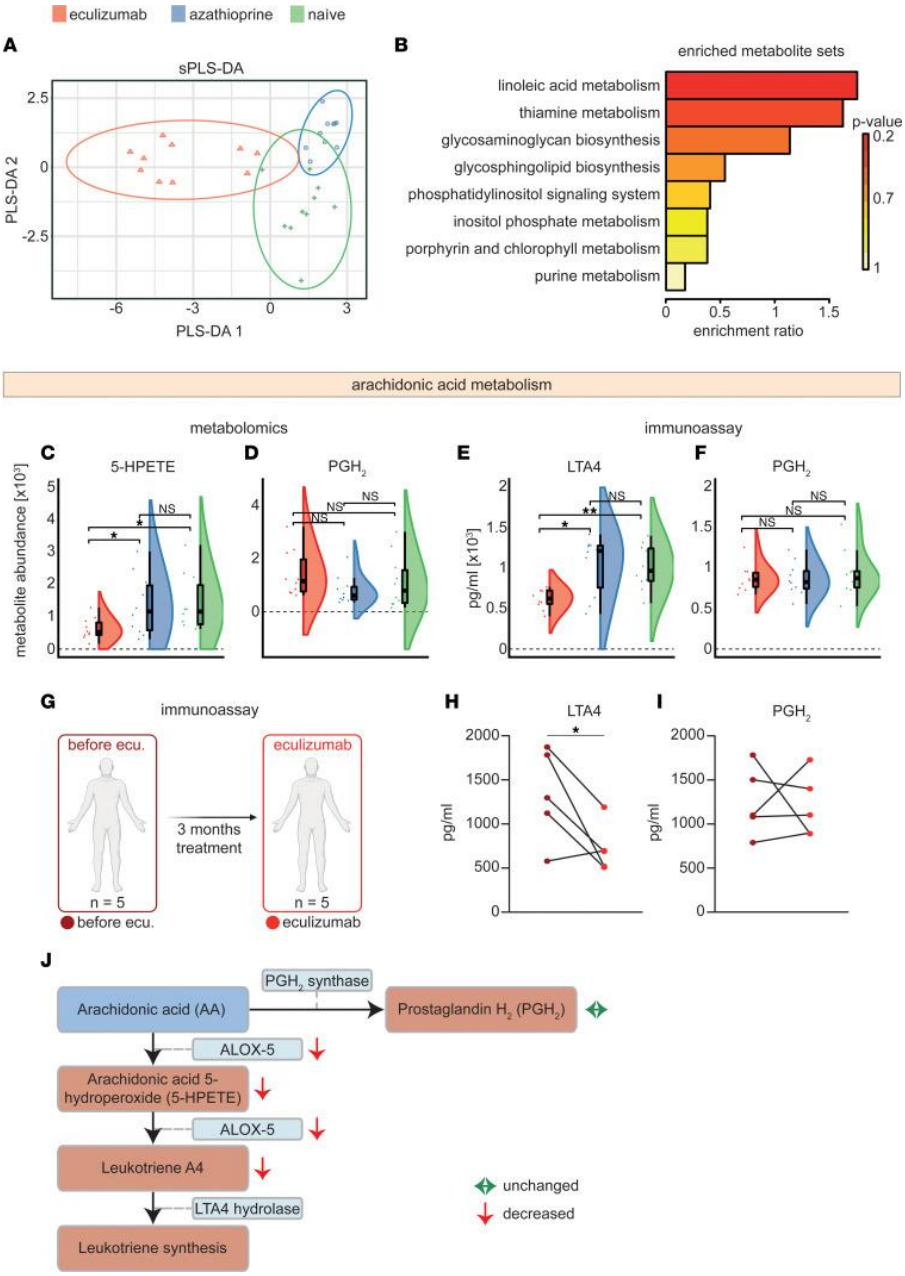

Figure 5: (A) sPLS-DA score plot showing the metabolite data set for different groups. Prediction ellipses are 95% CI. **(B)** Functional enrichment analysis of the eculizumab cohort compared with other groups. Enrichment was performed by MetaboAnalystR package version 3.0 set to GSEA using the KEGG database. **(C and D)** Metabolite abundance of 5-HPETE and PGH2 displayed as raincloud plots. Metabolite levels were determined by metabolomic analysis. **(E and F)** Metabolite abundance of LTA4 and PGH2 displayed as raincloud plots. Metabolite levels were determined by immunoassay. Whiskers are 1.5 IQR. **(G)** For longitudinal analysis, samples were acquired from 5 patients before and under eculizumab treatment. **(H)** Longitudinal analysis shows reduction of LTA4 level in eculizumab-treated patients. **(I)** PGH2 levels remained unchanged after switching to eculizumab. "Before eculizumab" and "eculizumab" are represented in dark red and red, respectively. **(J)** Schematic overview of AA metabolism. Changes observed in this study are indicated by arrows. N = 10 per group. 5-HPETE, arachidonic acid 5-hydroperoxide; GSEA, gene set enrichment analysis; LTA4, leukotriene A4; PGH2, prostaglandin H2; sPLS-DA, sparse partial least squares discriminant analysis. Mit freundlicher Genehmigung des Verlags aus Nelke, Schroeter et al. 2022.

Finally, we aimed to understand the mechanistic connection between inhibiting the terminal complement pathway and the resultant alterations in the ALOX5 metabolism. Previous studies have highlighted that the binding of the C5aR instigates the synthesis and discharge of leukotrien B4 (LTB4). LTB4, a downstream product of AA and LTA4, demonstrates pro-inflammatory properties. Consequently, the activity of ALOX5 is

crucial for the generation of LTB4. We hypothesized that reduced engagement of the C5aR leads to the downregulation of ALOX5 activity in response to C5 inhibition, subsequently reducing both LTA4 and LTB4 levels. To validate this hypothesis, we employed an in vitro model utilizing polymorphonuclear leukocytes (PMNs), the immune cells primarily involved in ALOX5 metabolism. To confirm ALOX5's ability to produce LTB4 in PMNs, we exposed these cells to escalating concentrations of recombinant C5a (**Figure 6A**) and quantified LTB4 using an ELISA. Consistent with earlier findings, C5a prompted the release of LTB4 in a dose-dependent manner. Based on these findings, we opted to proceed with 500 ng/mL of C5a for subsequent experiments. Subsequently, our aim was to establish the necessity of C5aR for LTB4 release in PMNs. For this purpose, PMNs were incubated with both C5a and PBS as a control (**Figure 6B**). We utilized the C5aR inhibitor PMX53 to investigate whether the interaction between C5a and C5aR is required for LTB4 generation. Notably, co-incubation with PMX53 (10 nM) resulted in diminished LTB4 release. Additionally, when PMNs were incubated with C5a and the ALOX5 inhibitor zileuton (100 µM), it similarly led to reduced LTB4 levels. These collective findings imply that the interaction between C5a and C5aR triggers the synthesis of leukotrienes by ALOX5.

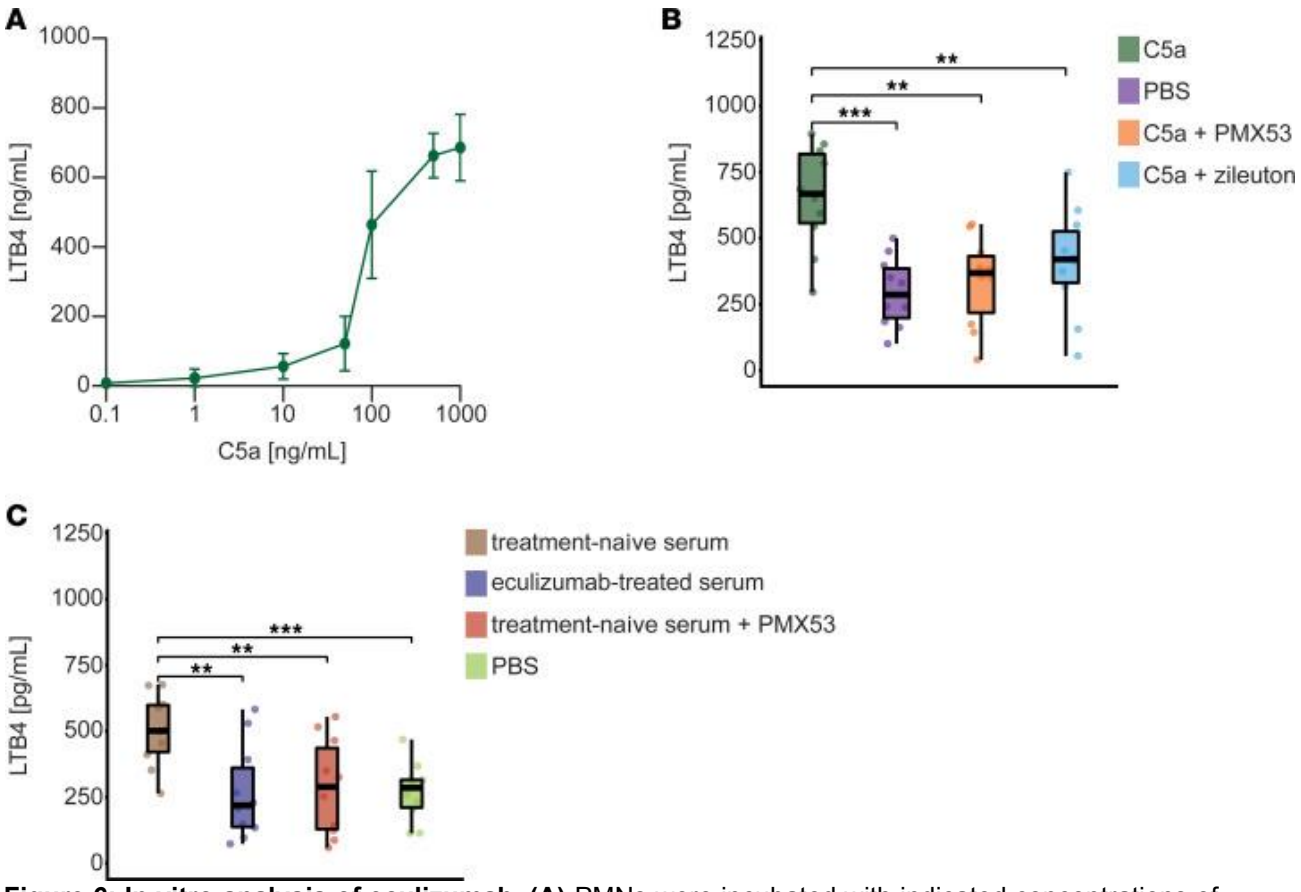

Figure 6: In vitro analysis of eculizumab. (A) PMNs were incubated with indicated concentrations of

recombinant C5a for 6 hours. **(B)** PMNs were incubated with indicated substances (C5a 500 ng/mL, C5a + PMX53 10 nM, C5a + zileuton 100 µM, or PBS) for 6 hours (n = 10 per group). **(C)** PMNs were incubated with indicated serum from treatment-naive patients with MG or eculizumab-treated patients with MG for 6 hours. PMNs were also incubated with treatment-naive serum and a final concentration of PMX53 of 10 nM or PBS for 6 hours (n = 10 per group). Groups were compared by 2-sided Student's t test. ***P < 0.001, **P < 0.01. ALOX5, arachidonate 5-lipoxygenase; LTB4, leukotriene B4; PMNs, polymorphonuclear leukocytes. Mit freundlicher Genehmigung des Verlags aus Nelke, Schroeter et al. 2022.

Subsequently, considering that the C5 inhibitor eculizumab obstructs the cleavage of C5 and the release of C5a, we hypothesize that this mechanism was accountable for the observed effects. To investigate this hypothesis, we exposed PMNs to the serum obtained from the 10 treatment-naive patients involved in this study, alongside serum from patients treated with eculizumab (**Figure 6C**). Upon exposure to the serum from treatment-naive patients, we observed higher levels of LTB4 compared to incubation with eculizumab-treated serum or PBS. Additionally, we treated PMNs with the serum from treatment-naive patients in combination with the C5aR inhibitor PMX53. Interestingly, this combination led to reduced LTB4 levels, indicating that the interaction between C5a and C5aR is pivotal for the impact of eculizumab on downstream products resulting from ALOX5 metabolism.

In summary, it appears that eculizumab prevents the engagement of C5aR on PMNs by impeding the generation of C5a. Activation of C5aR is crucial for initiating ALOX5 processing AA; hence, eculizumab might attenuate the production of subsequent leukotrienes resulting from this pathway.

3.6. Outlook on complement-targeting therapies for MG

The advent of complement-targeting therapies has introduced a groundbreaking shift to the landscape of MG treatments. These therapies constitute a new class of drugs that offer high efficacy while circumventing the drawbacks associated with broad immunosuppression. However, it's crucial to acknowledge specific adverse effects, such as increased susceptibility to encapsulated bacteria, and also to investigate potential "off-target" effects like modulation of AA metabolism that require further exploration.

Going forward, the development of additional options for complement inhibition is likely. These upcoming agents will vary in their administration methods (oral, intravenous, or subcutaneous) and treatment duration [13]. Such advancements are expected to provide

clear advantages for both physicians and patients, facilitating tailored treatment options that align with individual patient needs. Yet, several lingering questions within the field require answers: Are the efficacy profiles of different treatment agents comparable? How do co-existing health conditions impact treatment outcomes? What are the potential long-term consequences of prolonged complement inhibition? Furthermore, understanding the factors and mechanisms contributing to treatment non-responsiveness remains an important area of inquiry. Addressing these unresolved aspects will be crucial in advancing the field and refining the management of MG through complement-targeting therapies.

Finally, we discuss MG and its therapeutic landscape as example of extracellular complement activity as we assume that the prevention of MAC formation is the primary driver of treatment efficacy. However, the extent to which inhibiting the formation of C5a contributes to the effect of complement inhibition remains unclear. C5a, known for its interaction with a myriad of receptors, undergoes rapid degradation by carboxypeptidases, transforming into C5aDesArg, which exhibits a half-life of less than 5 minutes *in vivo* [22]. As a result, studying C5a is notoriously challenging, and its implications for intracellular signalling are likely underestimated, despite its significance.

4. Intracellular complement and its impact on neuromuscular diseases

In the previous section, we discussed extracellular complement activation in the context of MG as prototypical disease mediated by pathogenic antibodies. While inhibition of extracellular complement provided a substantial treatment benefit in MG, this efficacy is not readily replicated across complement-related conditions. Here, we will explore how intracellular complement might impact neuromuscular diseases, such as idiopathic inflammatory myopathies (IIM), and how its compartmentalization might hinder contemporary treatment approaches.

Over the last decade, numerous studies have provided evidence for a novel aspect of complement function: intracellular complement activation. Coined as the „complosome“ [3,4], this intricate protein complex operates intracellularly, distinct from the extracellular complement system. Notably, complosome constituents not only interact internally but also engage with other intracellular defence mechanisms like the inflammasome, autophagosomes, and the ribosomal machinery [3,4]. The proteins constituting the complosome are encoded by the same genes responsible for the circulating

complement system, such as C3 or C5. Placed in an intracellular context, specific proteases and convertases cleave internal C3 and C5 beneath the cell membrane or within subcellular compartments. While most complosome components originate from within cells, intracellular C3 can also originate externally or from the cell surface, integrating into the functionally active intracellular complosome [3,4,23].

The essential components of the complosome - C3, C5, their activation products, receptors, and some regulators - have been identified within various intracellular compartments, including the mitochondria, cytoplasm, or endoplasmic reticulum, and even the nucleus [3,4,23]. These diverse intracellular locations allow for distinct functional roles, diverging from those attributed to classical complement pathways. Specifically, the complosome contributes to fundamental cellular processes such as cell metabolism, gene expression regulation1, and autophagy. Intracellular receptors like mitochondrial, lysosomal, and/or endosomal C3aR and C5aR1 mediate their functions by initiating signalling cascades akin to those triggered by their „classical complement" counterparts present on the cell surface. This interaction occurs in spatial separation from extracellular complement components. Moreover, comeplement components also contribute to immune cell signalling, secreted either in an autocrine or paracrine fashion or expressed on the cell surface, challenging the separation between extra- and intracellular complement.

While the prospect of intracellular complement activity is novel, its implications for neuromuscular health and disease is intriguing. To exemplify this new prospect, we will examine inclusion body myositis (IBM) as unique neuromuscular entity that presents an ongoing therapeutic challenge [24].

4.1. On the pathophysiology of inclusion body myositis

IBM falls within the spectrum of IIMs, a category encompassing dermatomyositis (DM), immune-mediated necrotizing myopathy (IMNM), myositis in antisynthetase syndrome, and a group of non-specific IIM [24]. However, these classifications likely do not encompass the full range of IIM types. Among IIM, IBM is unique as it does not occur in children, has a relatively 'pure' muscle phenotype, and shows only subtle therapeutic response to contemporary treatments, if at all, making IBM difficult to contextualize immunologically [25].

Initial observations by the late Kichii Arahata regarding cytotoxic CD8+ T cell infiltration in the endomysium were later reinforced by studies indicating the clonal expansion of CD8+ T cells and their T cell receptor (TCR) repertoire in IBM. Recent advancements

in this line of argument have emerged through the discovery of effector memory T cells re-expressing CD45RA (TEMRA) and CD8+ T cells exhibiting an exhausted phenotype, characterized by the presence of CD57 and KLRG1 expressions, among other markers. The existence of degenerative aspects like rimmed vacuoles and protein accumulations has sparked an ongoing debate about IBM's underlying pathophysiology (**Figure 7A - F**). Taken together, the pathophysiology remains enigmatic: Convincing arguments for an autoimmune origin of the disease are contrasted by a resistance to immunosuppresive or immunoregulatory therapies [24].

4.2. A case study of cell-autonomous mechanisms in IBM

One potential explanation for IBM's resistance to treatment could lie in the initiation of cell-autonomous mechanisms that drive disease progression independent of ongoing inflammatory activity [24]. Skeletal muscle comprises both myogenic and non-myogenic cells whose intricate interplay is crucial for maintaining muscle health and resolving inflammation. However, IBM introduces a persistent state of inflammation within this compartment, potentially disrupting the balance of these cells and leading to a harmful muscle state. In response to chronic stress or damage, cells can enter a state of stable cell cycle arrest known as cellular senescence. These senescent cells maintain their influence on the surrounding environment by adopting a specific senescence-associated secretory phenotype (SASP), characterized by the release of immunomodulatory cytokines, growth factors, and proteases. Building upon this perspective, the accumulation of senescent cells in skeletal muscle might represent a cell-autonomous mechanism through which resident cells in the muscle perpetuate localized inflammation and foster fibrotic remodelling in IBM [24].

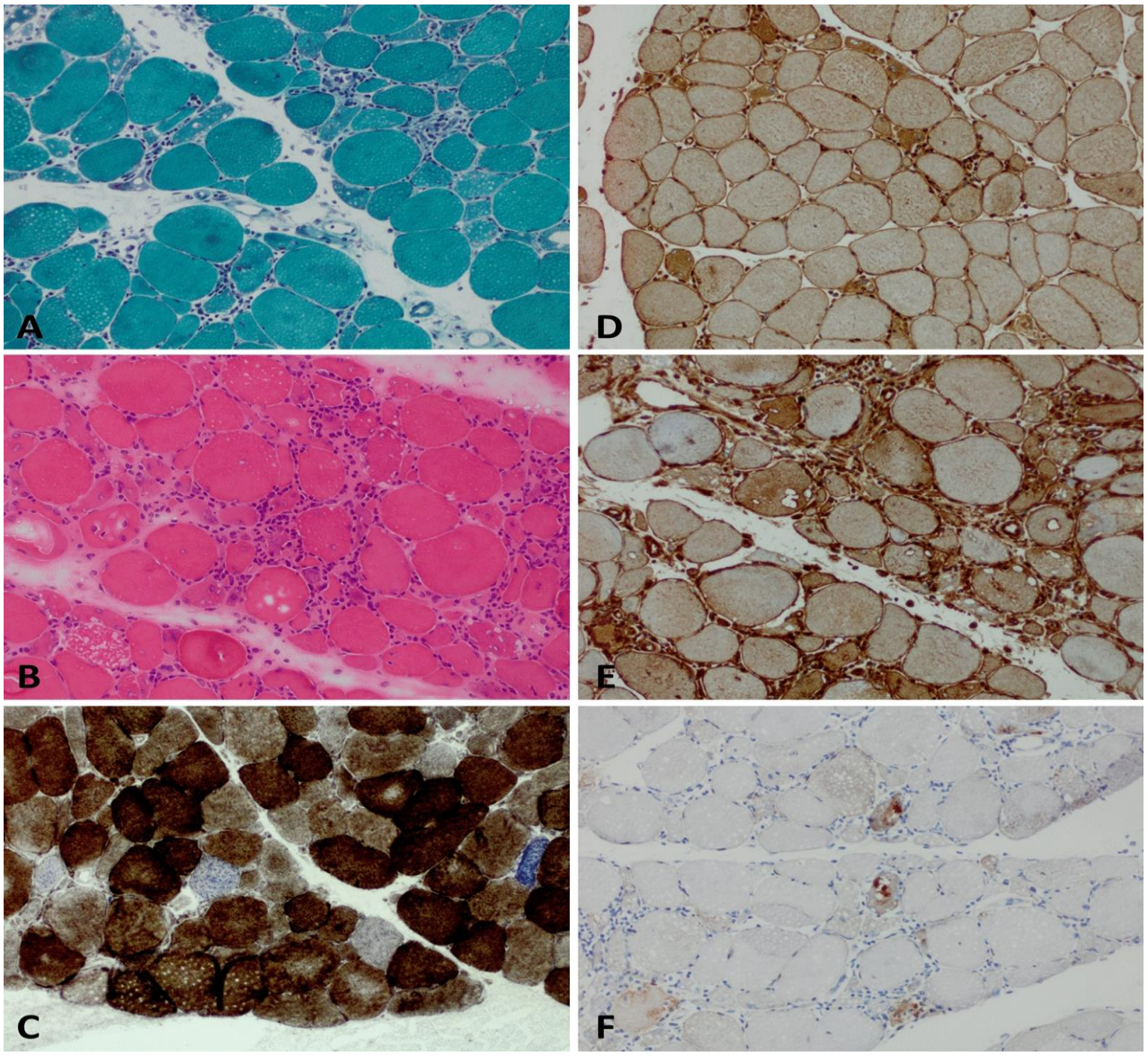

Figure 7: Characteristic pathomorphology of IBM. Pathomorphological characteristics of IBM patients as seen on muscle biopsy. **(a)** Pronounced fiber size variation with hypotrophic and hypertrophic fibers as well as internalized nuclei, myofiber necrosis and endomysial lymphocytic infiltrates and rimmed vacuoles. Gömöri trichrome staining (× 200). **(b)** Pronounced fiber size variation with hypotrophic and hypertrophic fibers as well as internalized nuclei, myofiber necrosis, endomysial lymphocytic infiltrates and rimmed vacuoles. H&E staining (× 200). **(c)** Presence of COX-negative, SDH-positive myofibers. COX-SDH staining (× 200). **(d)** Myofibers display sarcolemmal (and sarcoplasmic) positivity for MCH class I. MHC class I staining (× 100). **(e)** Myofibers display sarcolemmal (and sarcoplasmic) positivity for MHC class II. MHC class II staining (× 100). **(f)** Coarse p62+ autophagic material mostly localized in vacuoles. p62 staining (× 200). From Nelke et al. 2022. COX cytochrome oxidase immunohistochemistry; H&E hematoxylin and eosin; IBM inclusion body myositis; MHC major histocompatibility complex; SDH succinate dehydrogenase. Mit freundlicher Genehmigung aus Nelke et al. 2023.

To understand whether IBM instigates cell-autonomous mechanisms, we studied

cellular senescence in the skeletal muscles of IBM patients and compared them with those of non-diseased controls (NDC) and IMNM as diseased control. First, we sought to determine whether the number of senescent cells is altered in IBM compared to NDC and IMNM patients. For this purpose, we recruited a multicentric cohort of 48 patients (16 per group). Given that age is likely to have a major impact on the development of cellular senescence, NDC and IMNM patients were matched to IBM by age to account for this confounder. Our initial focus was on examining p21, a well-established marker indicative of cellular senescence. We evaluated the presence of p21+ cells using immunofluorescence (IF), requiring clear co-localization of p21 and DAPI within the cell nuclei to classify cells as p21+ (**Figure 8A**). The quantity of p21+ cells was higher in IBM patients compared to both NDC and IMNM patients (**Figure 8B**). To further substantiate these findings, we conducted gene-level analysis via PCR, observing a higher expression of CDKN1A (which codes for p21) in IBM patients compared to NDC or IMNM (**Figure 8C**). Intriguingly, a significant proportion of p21+ cells were located in the perimysial area in IBM. To discern the source of these cells, we also tallied the number of p21+ myonuclei (**Figure 8D**), defined as nuclei situated within the boundaries of the respective myofiber (**Figure 8E**) [26]. Interestingly, both IBM and IMNM patients exhibited similar quantities of p21+ myonuclei, suggesting that non-myogenic cells within the skeletal muscle might predominantly adopt a senescent phenotype in IBM. Building on this observation, our goal was to investigate senescence at the individual cell (or nucleus) level within the landscape of both myogenic and non-myogenic cells present in IBM-afflicted muscles.

To this purpose, we conducted single nuclei RNA-seq (snRNA) on samples from three IBM patients and three NDCs [26]. Post quality control, approximately 30,000 nuclei were processed, with around 13,000 from IBM muscle samples and about 17,000 from NDC samples, integrated into a batch-corrected expression matrix for subsequent analysis. Using graph-based clustering via uniform manifold approximation and projection (UMAP), we identified nine primary cell types or subtypes based on distinct marker gene expressions (**Figure 9A, B**). These cell types were classified based on the expression of recognized markers, drawing from earlier transcriptomic investigations of skeletal muscle [27,28].

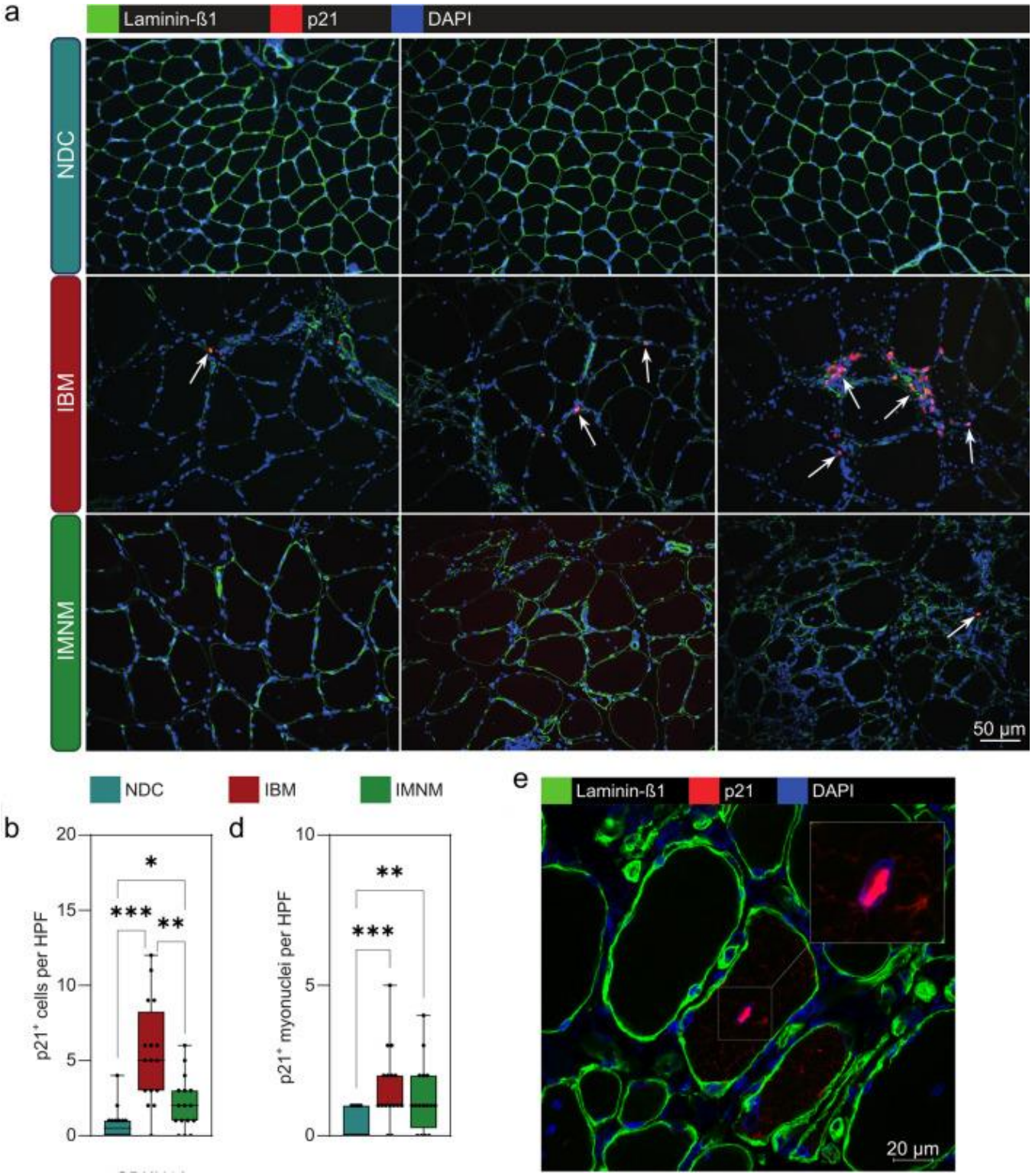

Figure 8: p21+ senescent cells are abundant in muscle of IBM. (a) Immunofluorescence staining of p21 (red), laminin-β1 (green), and DAPI (blue) in muscle specimens of NDCs (n = 16), IBM (n = 16), and IMNM (n = 16) patients. Arrows indicate single p21+ cells or clusters of p21+ cells. **(b)** p21 + cells were counted in randomly distributed 10 HPF (≙ 0.16 mm2). **(c)** RT-qPCR analysis of CDKN1A coding for p21 in muscle specimen (n = 16 per group). **(d)** Quantification of p21+ myonuclei in muscle in muscle specimen (n = 16 per group). **(e)** Exemplary image of a p21+ nucleus located inside a myofiber. Differences between groups were analysed by Kruskal–Wallis test followed by post hoc testing. *p < 0.05, **p < 0.01, ***p < 0.001. NDC non-diseased control; HPF high-power field; IBM inclusion body

myositis; IMNM immune-mediated necrotizing myopathy; r2 coefficient of determination; RT-qPCR real-time quantitative polymerase chain reaction. Mit freundlicher Genehmigung aus Nelke et al. 2023.

To understand the distribution of senescence in myogenic and non-myogenic cells, we determined the expression of CDKN1A across the dataset (**Figure 9C**). To compare the cluster-specific frequencies, we calculated the number of CDKN1A expressing cells as percentage of all cells in a cluster for IBM and NDC (**Figure 9D**). As described in the previous section, the relative frequencies of CDKN1A+ nuclei were comparable between IBM and NDC for myonuclei. Intriguingly, the frequencies of CDKN1A expressing fibro-adipogenic progenitors (FAPs) were strongly increased in IBM compared to NDC. However, it should be noted that the expression of a single gene is unlikely to capture the heterogeneity of cellular senescence across tissues. To address this caveat and to further corroborate the engagement of senescence pathways, we determined the differentially expressed genes (DEGs) between IBM and NDC for all cell clusters. Next, we employed the SenMayo gene set for enrichment analysis. Briefly, the SenMayo gene set is a panel composed of 125 key genes associated with senescence signalling pathways. We chose SenMayo as this gene set has been benchmarked against existing senescence or SASP gene sets and outperformed the latter in the detection of senescent cells. DEG lists of all clusters were entered into GSEA for the SenMayo gene set (**Figure 9E**) [29]. Only the FAPs cell cluster was enriched for SenMayo in IBM compared to NDC. Taken together, snRNA-seq demonstrates the capability of discerning distinct cellular subtypes and suggests that non-myogenic cells assume a senescent phenotype in IBM [26].

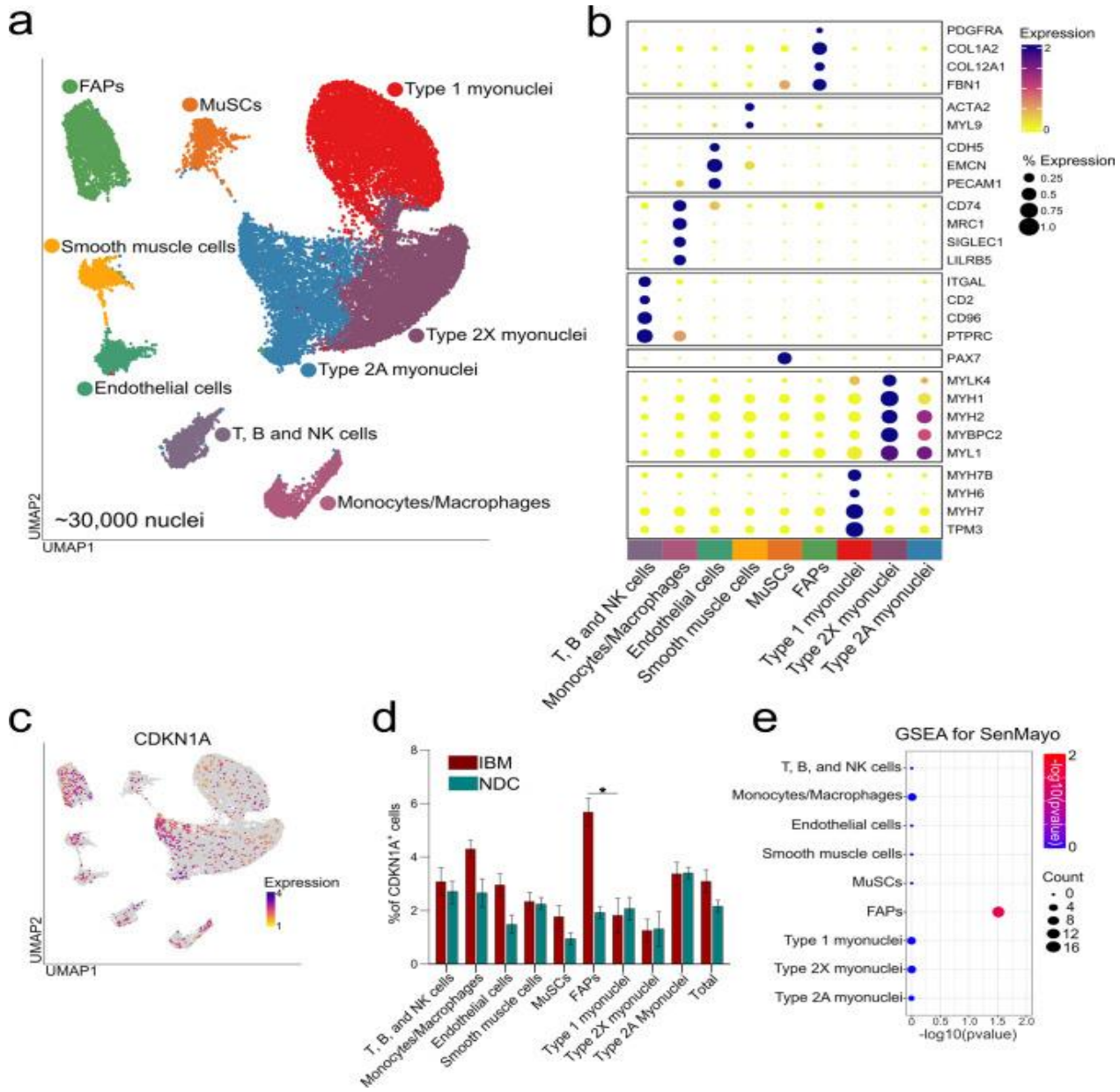

Figure 9: Single-nuclei RNA sequencing of IBM and NDC muscle. (a) UMAP embedding demonstrating distinct clusters of cell types and subtypes. **(b)** Clustered dot plot visualization of top-regulated marker genes. The mean expression for each cluster is indicated by colour code. **(c)** Expression of CKDN1A (coding for p21) across the UMAP embedding. **(d)** Frequency of CDKN1A+ cells for each cell cluster as indicated for IBM patients and NDC. **(e)** Gene set enrichment analysis (GSEA) for the SenMayo dataset. **p < 0.01. ACTA2 actin alpha 2; CDKN1A cyclin dependent kinase inhibitor 1A; CDH5 cadherin 5; COL collagen; EMCN endomucin; FBN1 fibrillin-1; ITGAL integrin subunit alpha L; LILRB5 leukocyte immunoglobulin like receptor B5; MRC1 mannose receptor C-type 1; MYBPC2 myosin binding protein C2; MYL9 myosin light chain 9; NDC non-diseased control; IBM inclusion body myositis; SIGLEC1 sialic acid binding Ig like lectin 1; TPM3 tropomyosin 3; PECAM1 platelet and endothelial cell adhesion molecule 1; PAX7 paired box 7; PTPRC protein tyrosine phosphatase type C (CD45); UMAP uniform manifold approximation and projection. Mit freundlicher Genehmigung aus Nelke et al. 2023.

Subsequently, our focus shifted towards the FAP population, and we isolated this particular cell cluster for in-depth examination (**Figure 10A**). FAPs represent lineage precursors of specialized non-myogenic cells, including activated fibroblasts, adipocytes, and osteogenic cells. We performed subclustering on these cells, identifying four distinct subpopulations of FAPs (**Figure 10B, C**). We identified marker genes for each FAP subtype, cross-referencing these findings with prior studies, including two FAP clusters unique to IBM patients. The first cluster was distinguished by the expression of lumican (LUM) and fibrillin-1 (FBN1). LUM+/FBN1+ FAPs were previously reported, resembling neprilysin (MME) expressing FAPs associated with fatty infiltration in skeletal muscle. Notably, we investigated the expression of CDKN1A across FAP subtypes and found it predominantly in the LUM+/FBN1+ FAP population. Consequently, we labelled these FAPs as CDKN1A+ to emphasize their senescent phenotype and connection to the p21 pathway. This specific FAP phenotype was exclusive to IBM patients and absent in NDCs (**Figure 10D, E**).

Given the scope of our study, we focused on the CDKN1A+ FAP population. Our goal was to ascertain if these FAPs displayed senescent characteristics. We identified marker genes for this cell cluster and conducted GSEA utilizing the Biological Processes (BP) database (**Figure 10F**). Notably, the most enriched term for the CDKN1A+ FAP population was the humoral immune response. This finding aligns with existing knowledge of the senescent phenotype, wherein these cells typically activate a pro-inflammatory secretome, such as SASP. To further substantiate the senescent profile of these FAPs, we performed GSEA for the SenMayo gene set. This analysis indicated that marker genes of CDKN1A+ FAPs were enriched for SenMayo, reinforcing the engagement of senescence pathways in these cells (**Figure 10G**). Moreover, CDKN1A+ FAPs appeared to activate the Jun/JunB signalling pathway, known to regulate fibroblast senescence by inhibiting insulin growth factor-1 (IGF-1) [29]. Surprisingly, these FAPs also exhibited upregulation of complement factors like complement factor 3 (C3), complement factor H (CFH), and complement factor D (CFD). In summary, CDKN1A + FAPs exhibit distinct hallmarks of cellular senescence, showcasing senescence markers, pro-inflammatory secretory features, pro-fibrotic surface molecules, a transcriptomic signature associated with senescence and expression of complement-related factors [26].

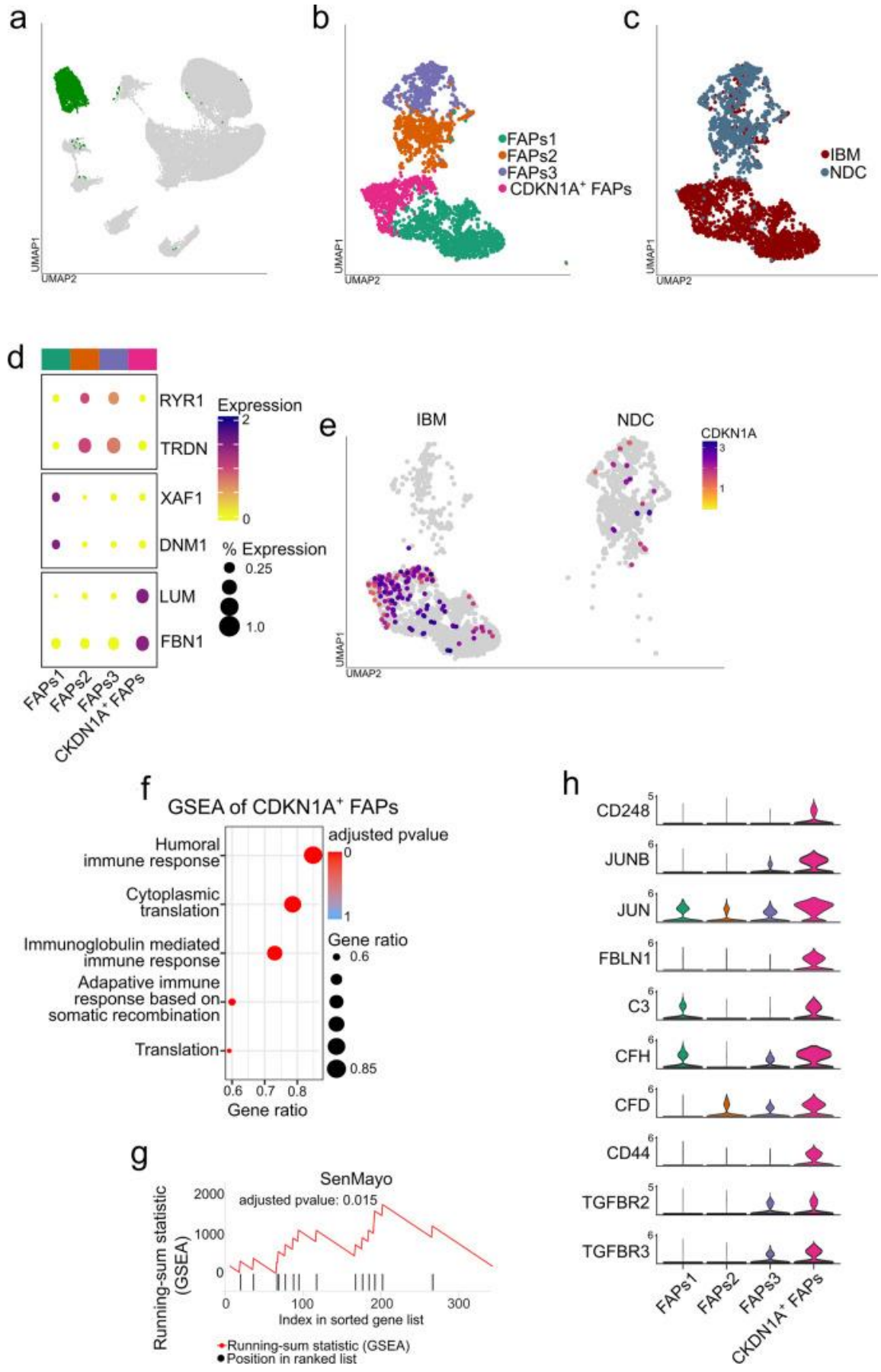

Figure 10: A novel population of senescent FAPs resides in IBM muscle. (a) UMAP embedding of the full dataset. FAPs are highlighted in green. **(b)** Subcluster analysis of the FAP population. **(c)** UMAP

embedding displaying the origin for each nucleus. **(d)** Clustered dot plot visualization of top-regulated marker genes. **(e)** Expression of CKDN1A (coding for p21) across the UMAP embedding split into the IBM (left) and NDC (right) datasets. **(f)** Gene set enrichment analysis (GSEA) for the GO-BP dataset for the CDKN1A+ FAP cluster. **(g)** GSEA analysis for the SenMayo dataset for the DEGs obtained from the CDKN1A+ FAP cluster. The running-sum statistic is in red, with the position in the ranked DEG list in black. Genes were sorted by fold change. **(h)** Violin plots displaying the normalized gene expression of the indicated genes for each FAP cluster. CDKN1A cyclin dependent kinase inhibitor 1A; DNM1 dynamin-1; FBN1 fibrillin-1; GO-BP gene ontology biological processes; LUM lumican; NDC non-diseased control; IBM inclusion body myositis; RYR1 ryanodine receptor 1; TRDN triadin; UMAP uniform manifold approximation and projection; XAF1 XIAP-associated factor 1. Mit freundlicher Genehmigung aus Nelke et al. 2023.

4.3. Inflammatory reprogramming linked to intracellular complement in IBM

Next, we focused on subpopulations of myonulcei with an inflammatory phenotype [26]. These myonuclei displayed distinct phenotypes based on their origin (**Figure 11A**). In IBM, these myonuclei exhibited elevated expression of marker genes such as C3 or HLA-A, distinguishing them from their counterparts in NDC. Moreover, these inflammatory myonuclei notably served as the primary source of transforming growth factor beta (TGFB1). To validate the presence of these myonuclei in muscle tissue, we conducted intracellular C3 IF staining. Remarkably, expression of C3 was solely detected in inflammatory myonuclei from IBM patients, not in other myonuclei subtypes in either NDC or IBM. This specificity suggests its potential as a distinctive marker (**Figure 11B**). Furthermore, myofibers exhibiting intracellular C3 staining were notably more abundant in IBM muscle compared to both NDC and IMNM muscle (**Figure 11C, D**). To further characterize these myofibers, we performed differential gene expression analysis comparing inflammatory myonuclei between IBM and NDC. GSEA focusing on these DEGs using the GO-BP database revealed the activation of various pro-inflammatory pathways. These included pathways related to the immunoglobulin-mediated immune response, adaptive immune response, innate immune response, and notably, the B cell-mediated immune response (**Figure 11E**). Collectively, these findings demonstrate the presence of an altered myofiber phenotype characterized by intracellular complement [26].

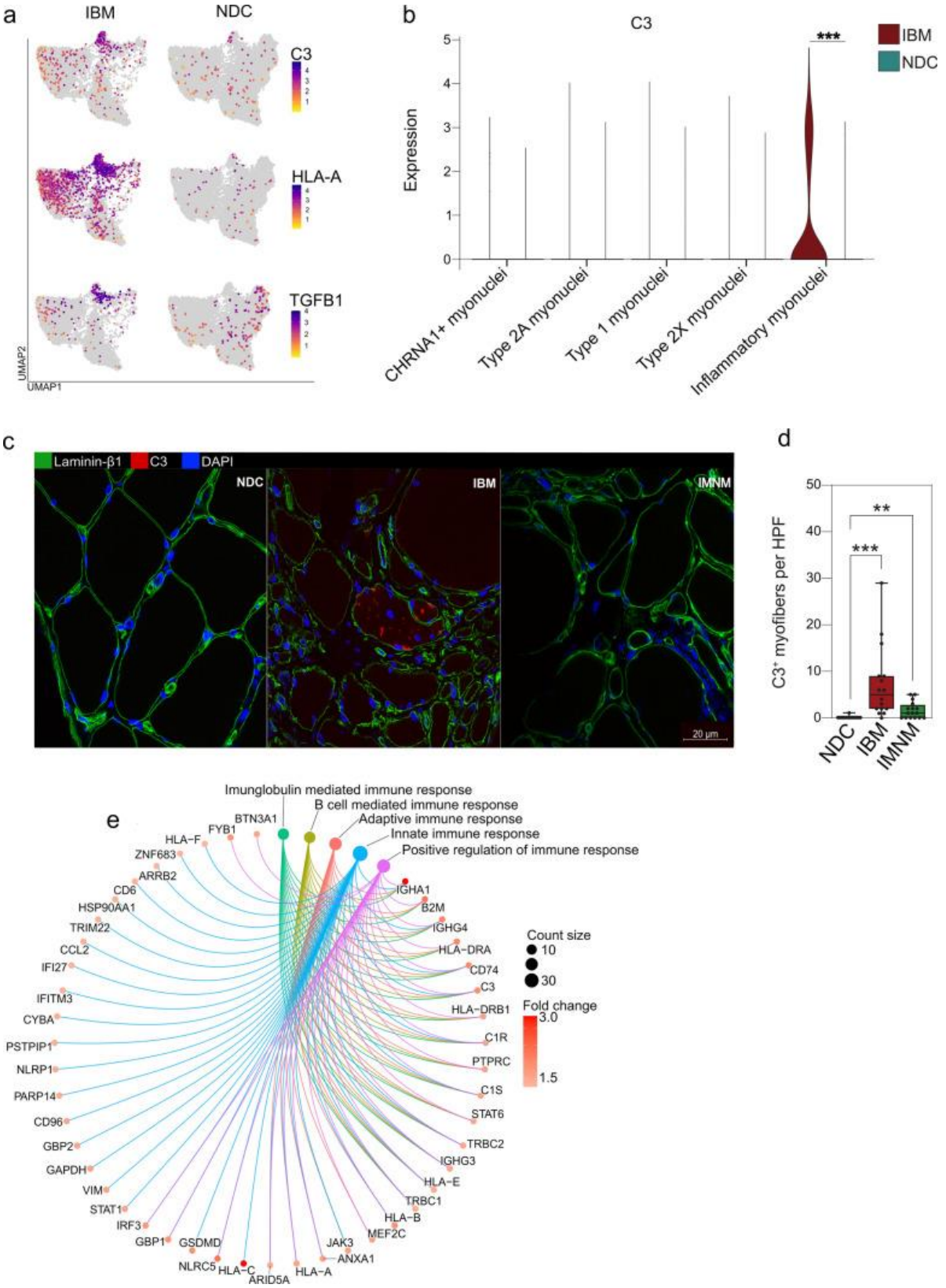

Figure 11: Skeletal muscle cells assume an inflammatory reprogramming in IBM. (a) UMAP embedding of the myonuclei split into IBM (left) and NDC (right). **(b)** Violin plot displaying the expression of complement factor 3 (C3) for each myonuclei subset for IBM and NDC. **(c)** Exemplary staining for C3 (red) laminin-β1 (green) and DAPI (blue) for NDC, IBM, and IMNM patients. **(d)** C3+ myofibers were counted in randomly distributed 10 HPF (≙ 0.16 mm2). **(e)**

Visualization of the gene set enrichment analysis (GSEA) for the GO-BP dataset as a gene concept network. CHRNA1 cholinergic receptor nicotinic alpha 1 subunit; HLA human leukocyte antigen; HPF high-power field; MYH myosin heavy chain; NDC non-diseased control; IBM inclusion body myositis; TGFB1 transforming growth factor beta 1; UMAP uniform manifold approximation and projection. Mit freundlicher Genehmigung aus Nelke et al. 2023.

4.4. Outlook on intracellular complement in neuromuscular diseases

The dysregulation of intracellular complement components was a consistent finding throughout our analysis of IBM. In our investigation, we observed a concurrent elevation of complement proteins, particularly C3, indicative of inflammatory states in both myogenic and non-myogenic cells. Intriguingly, the same set of genes responsible for generating the circulating complement system also encodes intracellular complement proteins. This observation emphasizes the crucial role of intracellular complement in governing tissue inflammation and influencing the transcriptomic programming of fibroblasts. A previous study highlighted that upon encountering recurring inflammatory stimuli, fibroblasts undergo a 'primed' state in both human and murine systems, rendering the tissue vulnerable to persistent inflammation [30]. Importantly, this transcriptomic shift is under the control of C3, its associated receptor C3a, and the mammalian target of rapamycin (mTOR) [30].

Building on this premise, our observations hint at the involvement of altered intracellular complement signalling, potentially contributing to the pathophysiology of IBM. This finding strongly suggests the need for further in-depth research to better comprehend the role and impact of intracellular complement factors in the context of inflammatory muscle diseases.

This need is further underpinned by a recent trial of zilucoplan in IMNM [31]. In contrast to IBM, IMNM is considered to harbour pathogenic autoantibodies targeting either the 3-hydroxy-3-methylglutaryl-CoA reductase (HMGCR) or the signal recognition particle (SRP) [31]. Despite attempts with off-label treatments such as intravenous immunoglobulin, glucocorticoids, and immunosuppressants, there are no approved therapies for IMNM, leaving many patients with sustained disease activity. Recent observations of complement-activating anti-HMGCR and anti-SRP autoantibodies, along with the identification of complement deposition on non-necrotic myofibers' sarcolemma, have given rise to the theory that complement activation might contribute to the pathology of IMNM. As a result, zilucoplan, an inhibitor of complement component 5 (C5), has been discussed as a potential therapeutic option.

Consequently, in a recent phase 2 multicenter, randomised, double-blind, placebo-controlled study of IMNM, zilucoplan was tested for efficacy. The primary efficacy endpoint was the percent change from baseline in serum CK levels [31]. Surprisingly, there was no statistically meaningful difference between zilucoplan and placebo in the percent change of CK levels. There also was no clinically relevant improvement over time within the treatment arm. The authors conclude: „C5 inhibition does not appear to be an effective treatment modality for IMNM. Rather than driving myofiber necrosis, complement activation may be secondary to muscle injury.“ [31]. This study outcome is surprising as it contrasts current viewpoints on complement. Despite the presence of pathogenic autoantibodies and the clear engagement of MAC on target structures, complement inhibition appeared to not be effective for controlling IMNM.

Collectively, these, and the findings presented before, question our current view on complement as pathogenic driver in inflammatory diseases affecting the neuromuscular system. Further research is required to understand the compartmentalized and context-specific role of complement. This effort could provide the groundwork for treatment approaches that are tailored to the specific profile of molecular patterns of complement signalling underlying neuromuscular diseases.

5. Bibliography

1. Schmalstieg, F. C. & Goldman, A. S. Jules Bordet (1870-1961): a bridge between early and modern immunology. *J Med Biogr* **17**, 217–224 (2009).
2. Mastellos, D. C., Hajishengallis, G. & Lambris, J. D. A guide to complement biology, pathology and therapeutic opportunity. *Nat Rev Immunol* (2023) doi:10.1038/s41577-023-00926-1.
3. Arbore, G., Kemper, C. & Kolev, M. Intracellular complement - the complosome - in immune cell regulation. *Mol Immunol* **89**, 2–9 (2017).
4. West, E. E. & Kemper, C. Complosome — the intracellular complement system. *Nat Rev Nephrol* 1–14 (2023) doi:10.1038/s41581-023-00704-1.
5. Elvington, M., Liszewski, M. K. & Atkinson, J. P. Evolution of the complement system: from defense of the single cell to guardian of the intravascular space. *Immunol Rev* **274**, 9–15 (2016).
6. Nelke, C. *et al.* Eculizumab treatment alters the proteometabolome beyond the inhibition of complement. *JCI Insight* **8**, e169135 (2023).
7. Reis, E. S., Mastellos, D. C., Hajishengallis, G. & Lambris, J. D. New insights into the immune functions of complement. *Nat Rev Immunol* **19**, 503–516 (2019).
8. van der Touw, W. *et al.* Receptors for C3a and C5a modulate stability of alloantigen-reactive induced regulatory T cells. *J Immunol* **190**, 5921–5925 (2013).
9. Kovács, K. G., Mácsik-Valent, B., Matkó, J., Bajtay, Z. & Erdei, A. Revisiting the Coreceptor Function of Complement Receptor Type 2 (CR2, CD21); Coengagement With the B-Cell Receptor Inhibits the Activation, Proliferation, and Antibody Production of Human B Cells. *Frontiers in Immunology* **12**, (2021).
10. Brown, S. L., Barrault, D. V., Phythian-Adams, A. & Knight, A. M. Lack of induced co-stimulation as a result of complement receptor 2 (CR2) ligation on mouse splenic B cells. *Int Immunol* **18**, 69–78 (2006).
11. Chen, L. & Flies, D. B. Molecular mechanisms of T cell co-stimulation and co-inhibition. *Nat Rev Immunol* **13**, 227–242 (2013).
12. Nelke, C. *et al.* Independent risk factors for myasthenic crisis and disease exacerbation in a retrospective cohort of myasthenia gravis patients. *J Neuroinflammation* **19**, 89 (2022).
13. Gilhus, N. E. *et al.* Myasthenia gravis. *Nat Rev Dis Primers* **5**, 30 (2019).
14. Fuchs, S., Aricha, R., Reuveni, D. & Souroujon, M. C. Experimental Autoimmune Myasthenia Gravis (EAMG): from immunochemical characterization to therapeutic approaches. *J Autoimmun* **54**, 51–59 (2014).
15. Tüzün, E. & Christadoss, P. Complement associated pathogenic mechanisms in myasthenia gravis. *Autoimmun Rev* **12**, 904–911 (2013).
16. Cenacchi, G., Papa, V., Fanin, M., Pegoraro, E. & Angelini, C. Comparison of muscle ultrastructure in myasthenia gravis with anti-MuSK and anti-AChR antibodies. *J Neurol* **258**, 746–752 (2011).
17. Kirby, T. Andrew Engel: 50 years of neuromuscular disorder research. *Lancet Neurol* **14**, 356 (2015).
18. Meisel, A. *et al.* Long-term efficacy and safety of ravulizumab in adults with anti-acetylcholine receptor antibody-positive generalized myasthenia gravis: results from the phase 3 CHAMPION MG open-label extension. *J Neurol* **270**, 3862–3875 (2023).
19. Howard, J. F. *et al.* Safety and efficacy of eculizumab in anti-acetylcholine receptor antibody-positive refractory generalised myasthenia gravis (REGAIN): a phase 3, randomised, double-blind, placebo-controlled, multicentre study. *Lancet Neurol* **16**, 976–986 (2017).
20. Nelke, C. *et al.* Eculizumab versus rituximab in generalised myasthenia gravis. *J Neurol Neurosurg Psychiatry* **93**, 548–554 (2022).
21. Howard, J. F. *et al.* Safety and efficacy of zilucoplan in patients with generalised myasthenia gravis (RAISE): a randomised, double-blind, placebo-controlled, phase 3 study. *Lancet Neurol* **22**, 395–406 (2023).
22. Bürgi, B., Brunner, T. & Dahinden, C. A. The degradation product of the C5a anaphylatoxin C5adesarg retains basophil-activating properties. *Eur J Immunol* **24**, 1583–1589 (1994).
23. Singh, P. & Kemper, C. Complement, complosome, and complotype: A perspective. *Eur J Immunol* **53**, e2250042 (2023).
24. Nelke, C., Kleefeld, F., Preusse, C., Ruck, T. & Stenzel, W. Inclusion body myositis and associated diseases: an argument for shared immune pathologies. *Acta Neuropathol Commun* **10**, 84 (2022).
25. Lundberg, I. E., de Visser, M. & Werth, V. P. Classification of myositis. *Nat Rev Rheumatol* **14**, 269–278 (2018).
26. Nelke, C. *et al.* Senescent fibro-adipogenic progenitors are potential drivers of pathology in inclusion body myositis. *Acta Neuropathol* (2023) doi:10.1007/s00401-023-02637-2.
27. Kim, M. *et al.* Single-nucleus transcriptomics reveals functional compartmentalization in syncytial skeletal muscle cells. *Nat Commun* **11**, 6375 (2020).
28. Soule, T. G. *et al.* A protocol for single nucleus RNA-seq from frozen skeletal muscle. *Life Sci Alliance* **6**, e202201806 (2023).
29. Saul, D. *et al.* A new gene set identifies senescent cells and predicts senescence-associated pathways across tissues. *Nat Commun* **13**, 4827 (2022).
30. Friščić, J. *et al.* The complement system drives local inflammatory tissue priming by metabolic reprogramming of synovial fibroblasts. *Immunity* **54**, 1002-1021.e10 (2021).

31. Mammen, A. L. *et al.* Zilucoplan in immune-mediated necrotising myopathy: a phase 2, randomised, double-blind, placebo-controlled, multicentre trial. *Lancet Rheumatol* **5**, e67–e76 (2023).

6. **Appendix**

Der Anhang der Publikationen erfolgt mit der freundlichen Genehmigung der Verlage.

Journal of Autoimmunity 142 (2024) 103136

Contents lists available at ScienceDirect

Journal of Autoimmunity

journal homepage: www.elsevier.com/locate/jautimm

$K_{2P}2.1$ is a regulator of inflammatory cell responses in idiopathic inflammatory myopathies

Christopher Nelke [a,1], Thomas Müntefering [a,1], Derya Cengiz [a,e], Lukas Theissen [a], Vera Dobelmann [a], Christina B. Schroeter [a], Helena Block [c], Corinna Preuße [c], Alexander P.E. Michels [a], Stefanie Lichtenberg [a], Marc Pawlitzki [a], Steffen Pfeuffer [b], Niklas Huntemann [a], Alexander Zarbock [c], Thorben Briese [d], Christoph Kittl [d], Carsten Dittmayer [e], Thomas Budde [f], Ingrid E. Lundberg [g], Werner Stenzel [e], Sven G. Meuth [a], Tobias Ruck [a,*]

[a] Department of Neurology, Medical Faculty, Heinrich-Heine-University, Duesseldorf, Germany
[b] Department of Neurology, University Hospital Gießen, Germany
[c] Department of Anesthesiology, Intensive Care and Pain Medicine, University of Muenster, Muenster, Germany
[d] Department of Trauma, Hand and Reconstructive Surgery, Westphalian Wilhelms University Muenster, Muenster, Germany
[e] Charité - Universitätsmedizin Berlin, Corporate Member of Freie Universität Berlin and Humboldt-Universität zu Berlin, Department of Neuropathology, Berlin, Germany
[f] Institute of Physiology I, University of Muenster, Germany
[g] Division of Rheumatology, Department of Medicine, Solna (MedS), K2, Karolinska Institutet, Stockholm, Sweden

ARTICLE INFO

Handling editor: M.E. Gershwin

Keywords:
$K_{2P}2.1$
KCNK2
TREK1
Myovascular unit
Idiopathic inflammatory myopathies
Barrier

ABSTRACT

$K_{2P}2.1$ (TREK1), a two-pore domain potassium channel, has emerged as regulator of leukocyte transmigration into the central nervous system. In the context of skeletal muscle, immune cell infiltration constitutes the pathogenic hallmark of idiopathic inflammatory myopathies (IIMs). However, the underlying mechanisms remain to be elucidated. In this study, we investigated the role of $K_{2P}2.1$ in the autoimmune response of IIMs. We detected $K_{2P}2.1$ expression in primary skeletal muscle and endothelial cells of murine and human origin. We observed an increased pro-inflammatory cell response, adhesion and transmigration by pharmacological blockade or genetic deletion of $K_{2P}2.1$ *in vitro* and in *in vivo* myositis mouse models. Of note, our findings were not restricted to endothelial cells as skeletal muscle cells with impaired $K_{2P}2.1$ function also demonstrated a strong pro-inflammatory response. Conversely, these features were abrogated by activation of $K_{2P}2.1$ and improved the disease course of a myositis mouse model. In humans, $K_{2P}2.1$ expression was diminished in IIM patients compared to non-diseased controls arguing for the translatability of our findings. In summary, $K_{2P}2.1$ may regulate the inflammatory response of skeletal muscle. Further research is required to understand whether $K_{2P}2.1$ could serve as novel therapeutic target.

1. Introduction

Idiopathic inflammatory myopathies (IIMs) are a spectrum of immune-mediated muscle diseases with heterogeneous clinical phenotypes. IIMs encompass different subtypes including dermatomyositis (DM), immune-mediated necrotizing myopathy (IMNM), anti-synthetase syndrome (ASyS), polymyositis and inclusion body myositis (IBM) [1,2]. These entities share common clinical symptoms of progressive muscle weakness, muscle pain and muscle fatigue but the molecular mechanisms leading to muscle weakness are unknown and likely to be diverse in different subsets of IIM. Some patients have infiltrates of immune cells in the muscle tissue whereas other have signs of fiber necrosis and yet a third group have minor detectable pathological features in the muscle biopsies. Although disease outcomes have substantially improved, current treatment options consist mainly of non-specific immunosuppression associated with limited efficacy [3,4].

* Corresponding author. Department of Neurology, University of Duesseldorf, Moorenstr. 5, D-40225 Duesseldorf, Germany.
E-mail address: tobias.ruck@med.uni-duesseldorf.de (T. Ruck).
[1] Contributed equally.

https://doi.org/10.1016/j.jaut.2023.103136
Received 3 May 2023; Received in revised form 12 October 2023; Accepted 18 October 2023
Available online 5 November 2023
0896-8411/

Hence, new therapeutic targets and strategies constitute an unmet need [5]. A hallmark of IIM pathology are immune cell infiltrates surrounding and sometimes invading muscle fibers or surrounding blood vessels. As such, autoreactive T cells and effector T cells are likely to contribute to the pathogenesis of IIMs and can be found in affected tissue of many patients [6–8]. Still, our knowledge on the role of other tissue-resident cells in IIMs, like fibroblasts, pericytes or endothelial cells remains incomplete.

Analogous to the concept of the neurovascular unit emphasizing the close structural and functional association of brain cells and microvasculature [9], muscle cells presumably form an interface with their surrounding vessels and constitute a functional unit regulating immune cell trafficking [10,11]. The endothelial cell barrier influences immune cell extravasation. Upregulation of adhesion molecules (ICAM-1 and VCAM-1) and pro-inflammatory cytokine secretion (IL-1α, IL-1β) accompanied by increased permeability (reduced VE-cadherin) are associated with immune cell infiltration and muscle damage in IIMs [12–17]. Treatment with glucocorticoid reduced expression of pro-inflammatory molecules (IL-1α, ICAM-1 and VCAM-1) on endothelial cells potentially correlated with muscle function [18]. Intriguingly, adhesion molecule and barrier function regulation are influenced by $K_{2P}2.1$ (TREK1), a mechano-gated potassium channel. In previous studies, we demonstrated that $K_{2P}2.1$ acts as a regulator of leukocyte transmigration through the blood-brain-barrier (BBB) into the central nervous system (CNS) [19]. Furthermore, inhibition of $K_{2P}2.1$ on primary mouse muscle cells resulted in impaired myoblast function and disruption of K^+/Ca^{2+} currents across the cell membrane [20]. Genetic depletion or inhibition induced secretion of pro-inflammatory cytokines and disturbed epithelial/endothelial barrier integrity in the lung, intestine or CNS [21–23]. Given the functional expression of $K_{2P}2.1$ in skeletal muscle and its critical role as regulator of barrier functions in endothelial cells, $K_{2P}2.1$ might be involved in the mechanisms underlying immune cell infiltration in IIMs. Consequently, we aimed to understand the role of $K_{2P}2.1$ in the pathophysiology of IIM.

2. Material and methods

2.1. Mice

All animal experiments of this study were approved by local authorities and the institutional Animal Care Committee (AZ: 84-02.04.2013.A264, 81-02.04.2021.A246). All animal procedures were performed in accordance with the European Union normative for care and use of experimental animals and the German Animal Protection Law. Mice were raised in an in-house animal facility or purchased from Charles River laboratories and kept in individually ventilated cages under Specific-Pathogen-Free conditions and fed ad libitum. All mice were on a C57BL/6J background. For experimental autoimmune myositis EAM induction or isolation of muscle and endothelial cells we used *Kcnk2*$^{-/-}$ [24] or C57BL/6J wildtype mice.

2.2. Human specimens

Muscle specimen were collected in the Clinic for Neurology, University Hospital Münster, and the Clinic for Neuropathology, Charité – University Medicine Berlin. Both ethical boards approved the study (Münster: 2017-671-f-S, 2017-023-f-S, Berlin: EA2/163/17). Informed oral and written consent was acquired from all patients prior study inclusion. Patients received muscle biopsies for routine diagnostic workup. Muscle biopsies were taken from the quadriceps vastus medialis muscle or the gastrocnemicus muscle. For IIM patients, a definitive histopathological diagnosis was required according to the current European League Against Rheumatism/American College of Rheumatology (EULAR/ACR) classification criteria [4]. We included 31 IIM patients in this study, including ASyS (n = 9), DM (n = 6), IMNM (n = 8) and IBM (n = 8). Clinical and epidemiological data, including antibody status, was recorded (Table 1). For comparison, we also recruited a cohort of non-diseased controls (n = 6, NDC). These were patients that underwent muscle biopsy for diagnostic purposes, but without any indication of inflammatory muscle disease. As such, they had suffered from myalgia, but objective muscle weakness and morphological abnormalities on skeletal muscle biopsy were absent. CK levels were normal and no signs of systemic inflammation and no myositis-specific antibodies (MSA) or myositis-associated antibodies (MAA) were detectable. Musle specimens had been cryopreserved at −80 °C prior to analysis. Besides, we collected primary human muscle cells (PHMC) from patients with an anterior cruciate ligament (ACL) reconstruction after obtaining written consent at the University Hospital Münster. After harvesting the semitendinosus tendon, the ACL graft was prepared on a graft preparation table. The remaining muscle on the proximal part of the tendon was removed and taken as sample and processed as described below. We included 10 samples of PHMC from ACL donors. These patients were on average 37 years old (standard deviation (SD) 15). 7 patients were male, 3 were female. Non of these patients had systemic diseases or known muscle disorders.

2.3. Isolation, purification and cultivation of primary murine cells

For primary murine muscle cell (PMMC) isolation, 1–7 days old mice pups and for primary murine muscle microvascular endothelial cell (PMMEC), 8–12 weeks old mice were sacrificed and muscle tissue from fore- and hindlimbs were separated from bones. Muscle tissue was dissociated as described before [11]. In brief, 2 mm^3 muscle cubes were dissociated homogenized by an insulin syringe and enzymatically digested with Collagenase/Dispase and DNase for 1.5 h at 37 °C.

For PMMC purification, we used the satellite cell isolation kit, mouse from Miltenyi Biotec (Germany). PMMC were cultured on laminin-coated 6-well plates in growth medium (40 % Ham's F10 nutrient, 9 % FCS, 1 % penicillin and streptomycin, 0.0025 % bFGF in DMEM). Differentiation of PMMC was initiated when cells reached over 90 % confluence by changing growth medium with a differentiation medium (2 % horse serum (PAA), 1 % penicillin and streptomycin in DMEM) and cultivation for 8 days.

For PMMEC purification, we depleted CD45$^+$ and accumulated CD31$^+$ cells by using magnetic Microbeads as described in Ref. [11]. For cultivation, we used a microvascular endothelial cell growth medium (PELO Biotech) on collagen-based coated 6-well plates until cells reached a confluent monolayer.

Murine T cells were isolated from spleens. After homogenization through a cell strainer (40 μm pore size) by an insulin syringe, Pan T cell isolation kit and a CD8a$^+$ T cell isolation kit from Miltenyi Biotech (Germany) were used to isolate T cells or CD8a$^+$ T cells of T cell receptor (TCR) transgenic mice (OT-1), respectively. Isolated T cells were stimulated by 2 μg/ml platebound purified anti-mouse CD3 antibody (clone 145-2C11, Biolegend) and 1 μg/ml soluble purified anti-mouse CD28 antibody (clone 37.51, Biolegend) in splenocyte complete medium (5 % FCS, 0.1 % 2-mercaptoethanol, 25 μg/ml gentamicin, 1 % NEAA, 10 mM HEPES in DMEM) for 48 h in a humidified incubator with 5 % CO_2 at 37 °C.

2.4. Isolation, purification and cultivation of primary human cells

Muscle tissue was dissociated by using a muscle dissociation kit from Miltenyi Biotech (Germany) and the program SMDK2 by a gentleMACS Dissociator with heaters.

For primary human skeletal muscle cell (PHMC) purification, we used a CD56 PE (clone N901, Beckman Coulter) antibody combined with PE Microbead magnetic separation. For cultivation, we used Biolaminin 521 LN coated 6-well plates and skeletal muscle cell growth medium from PELO Biotech. For all experiments, we used differentiated PHMCs by growing cells over 90 % confluence and changing growth to differentiation medium (basal media with 2 % horse serum and antibiotic, without growth factors, FCS or cortisol).

For primary human skeletal microvascular endothelial cell (PHMEC) purification, we depleted CD45$^+$ and enriched CD31$^+$ cells by using magnetic Microbeads from Miltenyi Biotech (Germany). For cultivation, we used a microvascular endothelial cell growth medium (PELO Biotech) with supplements (except hyrdrocortison) on collagen-based coated 6-well plates until cells reached a confluent monolayer.

Peripheral blood mononuclear cells (PBMC) were isolated via a density gradient and afterwards stimulated with 4 μg/ml platebound purified anti-human CD3 antibody (clone OKT3, Biolegend) and 2 μg/ml soluble purified anti-human CD28 antibody (clone CD38.2, Biolegend) in X-Vivo15 medium (Lonza) for 24 h in a humidified incubator with 5 % CO_2 at 37 °C.

2.5. Gene expression analysis

Mouse and human primary cells were stimulated for 24 h with 500 U/ml TNFα or left untreated and afterwards RNA was isolated by a RNA isolation Miniprep kit (Direct-Zol RNA Kit, Zymo Research). For cDNA synthesis, we used a standard protocol with random hexamer primers (Applied Biosystems). Quantitative real-time PCR (qRT-PCR) was performed using FAM-labelled *Kcnk2* Taqman primer (Applied Biosystems) for mouse (Mm01323942_m1) and human (Hs01005159_m1). VIC-labelled 18S rRNA Taqman primer was used for internal control. We performed a qRT-PCR and measured samples as duplicates. We calculated cycle threshold differences per sample (ΔCT), per group ΔΔCT and relative quantification ($2-\Delta\Delta CT$).

Table 1
Clinical characteristics of the cohort.

		ASyS (n = 9)	DM (n = 6)	IMNM (n = 8)	IBM (n = 8)	NDC (n = 6)
mean age at biopsy	years ± SD	55 ± 14	46 ± 12	50 ± 2	65 ± 20	45 ± 10
biological gender	♀/♂	55 %/56 %	50 %/50 %	50 %/50 %	75 %/25 %	50 %/50 %
antibody status*		Jo-1 33 % (n = 3) PL-7 33 % (n = 3) PL-12 33 % (n = 3)	TIF1-γ 33 % (n = 2) NXP2 16 % (n = 1) SAE 16 % (n = 1) MDA5 33 % (n = 2)	HMGCR 38 % (n = 3) SRP 38 % (n = 3) seronegative 25 % (n = 2)	cN-1A 50 % (n = 4) seronegative 50 % (n = 4)	100 % seronegative
creatine kinase	normal	11 %	16 %	0 %	50 %	100 %
	<10-fold	22 %	33 %	25 %	50 %	–
	>10-fold	22 %	33 %	25 %	–	–
	>30-fold unknown	44 %	16 %	25 %	–	–
		0 %	0 %	25 %	–	–
onset of symptoms	<1 year	11 %	33 %	50 %	25 %	50 %
	>1 year	33 %	33 %	25 %	25 %	50 %
	>5 years unknown	44 %	–	25 %	50 %	–
		11 %	33 %	–	–	–
symptoms	muscle symptoms	55 %	88 %	25 %	0 %	33 %
	pain (% of patients)	77 %	88 %	88 %	75 %	0 %
	weakness (% of patients)					
therapy	Corticosteroids	22 % (n = 2)	33 % (n = 2)	50 % (n = 4)	13 % (n = 1)	0 % (n = 0)
	% of patients with corticosteroids (n)	25 (25.5)	11.5 (10)	42 (35.7)	5 (0)	0
	Mean dose, mg (SD)					
	% of patients with DMDs	-33 %	-0 %	-25 %	-88 %	-0 %
	- naïve	-9 %	-0 %	-25 %	-0 %	-0 %
	- azathioprine	-18 %	-33 %	-0 %	-0 %	-0 %
	- MMF	-18 %	-33 %	-0 %	-0 %	-0 %
	- MTX	-18 %	-16 %	-25 %	-0 %	-0 %
	- cyclophosphamide	-0 %	-16 %	-25 %	-12 %	-0 %
	- unknown					

Abbreviations: ASyS, anti-synthetase syndrome; DM, dermatomyositis; DMD, disease-modifying drugs; IBM, inclusion body myositis; IMNM, immune mediated necrotizing myositis; NDC, non-diseased control; SD, standard deviation.
**Symptoms were subjective, in muscle biopsies no irregularities were found, no immune reactions and no signs of inflammation. CK levels were normal and no MSA or MAA were detected.
* Antibody status were determined by radio-immunoassay (RIA).

2.6. Histological staining

Immunofluorescence staining was performed with adherent cells (PMMC; PMMEC; PHMC; PHMEC) on coverslips or 10 μm tissue cryosections (lung, mouse muscle tissue EAM). Samples were fixed with 4 % paraformaldehyde at room temperature (RT) for 10 min. Then incubated with blocking solution (PBS with 1 % goat serum, 1 % donkey serum, 5 % BSA and 0.2 % Triton-X) at RT for 1 h. Samples were stained with primary antibodies ((rabbit anti TREK1 (Sigma-Aldrich #T6448), rat anti MHC-1 (abcam ab15681), rat anti CD4 (Biolegend 100506), rat anti CD8 (Serotec MCA1768T), rat anti CD11b (Serotec MCA711), Phalloidin CruzFluor™ 594 conjugate (Santa Cruz sc-363795), rat anti Pecam-1 (Santa Cruz Sc-52713)) in PBS, 5 % BSA, 1 % goat serum and 1 % donkey serum overnight at 4 °C. After three times of washing with PBS we performed a secondary antibody staining (Cy2 goat anti-rabbit (Dianova #111-225-144), Cy3 donkey anti-rat (Dianova #712-166-153)) in PBS, 5 % BSA at RT for 1 h. Samples were mounted with a mountant containing DAPI. Images were acquired with a fluorescence microscope (Keyence BZ-X). NDC, as described above, were employed as control for histological staining.

Histological staining of IIM patients was performed on 8 μm cryomicrotome sections as previously described [25]. The following antibodies were used for staining procedures: $K_{2P}2.1$ (Sigma, T6448), CD31 (DAKO, M0823), MHCn (Novocastra, NCL-MHCn), CD68 (DAKO, M0718), CD20 (DAKO, M0755), CD3 (Novacastra, NCL-CD3-PS1), CD4 (Zytomed, 503–3351), CD8 (DAKO, M7103), CD138 (DAKO, M7228), with secondary antibodies: Goat anti-rabbit horseradish peroxidase or

Goat anti-mouse Cy3 (Dianova, 115-165-062), Goat anti-rabbit Cy3 (Dianova, 111-166-003), Goat anti-rabbit AF488 (Invitrogen, A11008). Images were acquired with a fluorescence microscope (Olympus Bx53). The biopsies were blinded for quantification with the diagnosis not possible to identify from the label. The scoring was performed in randomly distributed 10 high power fields (HPF, based on the microscope used and the respective oculars ≙ 0.16 mm^2) as previously described [26].

We used irrelevant antibody stains (either mouse/rabbit monoclonal/polyclonal isotype controls) as negative controls, as well as omission of the primary antibody.

2.7. Western blot

Primary cells were sonicated in lysis buffer (50 mM TRIS pH7.5, 165 mM NaCl, 1 % SDS, 1x Protease Inhibitor cocktail tablets in ddH_2O) and incubated on ice for 30 min. After centrifugation, the supernatant was mixed in 5x reducing sample buffer (0.1 M Tris, 50 % glycerol, 5 % sodium dodecyl sulfate, 0.25 % bromophenolblue and 10 % β-mercaptoethanol) and heated for 5 min at 99 °C. Using a denaturating and reducing 10 % polyacrylamide gel we separated the proteinlysat. Afterwards, we transferred the proteins to a nitrocellulose membrane. For $K_{2P}2.1$ detection we blocked the membrane with 5 % milk/TBS and used afterwards a rabbit anti $K_{2P}2.1$ antibody (polyclonal, T6448, Sigma-Aldrich, 45 kDa). Peroxidase-conjugated secondary antibody to rabbit was added and was visualized by a chemiluminescence reaction (ECL, Amersham Bioscience). Hereafter, the membrane was cleared with 2 % sodium azide and beta-actin as loading control was detected.

2.8. Flow cytometry analysis

Muscle, endothelial cells as well as immune cells were identified and characterized by flow cytometry. Cultured primary muscle and endothelial cells were resuspended in phosphate buffered saline (PBS, Sigma-Aldrich) supplemented with 2 % heat-inactivated foetal bovine serum (FBS, GE Healthcare, Chicago, IL, USA) and 2 mM ethylenediaminetetraacetic acid (EDTA, Sigma-Aldrich). Approximately 1×10^6 cells were counted and used per sample and staining for all experiments. Cells were washed and additionally stained with the Aqua Fixable Viability Kit (Biolegend, San Diego, CA, USA) according to the manufacturer's manual to distinguish between dead and live cells. Cells were washed and resuspended in PBS/FBS/EDTA and analyzed by flow cytometry using a CytoFlex Flow Cytometer (Beckman Coulter, Brea, CA, USA). This flow cytometer is a 12-channel flow cytometer. Downstream analysis was performed using Kaluza (Beckman Coulter, Brea, CA, USA) v2.2. The gating strategy is demonstrated in Suppl. Fig. 1. An isotype control was included for each flow cytometric analysis and measured parallel to the experiment. Additionally, primary muscle and endothelial cells were treated with TNFα (500 U/ml) for 24 h. To mimic a decline of stimulation, medium of stimulated cells was refreshed every 24 h after stimulation (72–96 h). Additionally, muscle cells or endothelial cells were treated with or without $K_{2P}2.1$ modulators (BL-1249 10 μM, Spadin 1 μM, A2 6 μM, B3 4 μM, E1 7 μM). Corresponding isotypes were used as controls. For antibody staining, cells were incubated with fluorochrome-conjugated antibodies at 4 °C for 30 min in the dark. The following antibodies were used: PMMC/PMMEC: H-2kb (FITC, AF6-88.5), CD54 (APC, YN1/1.7.4), I-A/I-E (APC Cy7, M5/114.15.2); CD31 (PerCP-Cy5.5., MEC 13.3), CD106 (E460, 429). Immune cells: CD11c (FITC, N418), CD45R/B220 (PE, RA3-6B2), CD11b (PerCP/Cy5.5, M1/70), NK 1.1 (APC, PK136), CD8a (AF700, 53-6.7), CD45 (APC/Cy7, 30-F11), CD4 (PB, RM4-5), CD3 (BV 510, 17A2), CD49d (FITC, R1-2), CD11a (PE, 121/7), CD3 (PerCP/Cy5.5, 145-2C11), CD62L (PE Cy7, MEL-14), CD69 (APC, H1.2F3), CD8a (AF700, 53-6.7), CD25 (APC Cy7, 3C7), CD44 (BV510, IM7). PHMC and PHMEC: HLA A,B,C (FITC, W6/32), HLA-DR (APC, L243), CD54 (PB, HA58), CD31 (AF700, WM59), CD106 (APC, STA). PBMC: CD11b (FITC, ICRF44), CD56 (PerCP/Cy5.5, B159), CD3 (PE Cy7, SP34-2), CD11c (APC, SHCL3), CD20 (AF700, 2HF), CD4 (APC/Cy7, SK3), CD8a (PB, HIT8a).

2.9. Adhesion assay

PMMEC (4×10^4 cells) or PHMEC (6×10^4 cells per chamber) were seeded in ibidi® μ-slides IV 0.4. which were previously coated with speed coating solution (PELO Biotech). Cells were cultivated for at least 48 h in microvascular endothelial cell growth media (PELO Biotech) until the cells reached confluence. Different time points of inflammation were mimicked on EC. Cells were left untreated for 24 h (untreated). Then, cells were treated with TNFα 500U/ml for another 24 h (inflammation). After wash out, cells were left untreated for additional 24 h (post inflammation). In a set of experiments, cells were treated with $K_{2P}2.1$ modulators as described in flow cytometry analysis. Stimulated murine T cells or PBMC were added to PMMEC or PHMEC, respectively. Adhesion of immune cells was imaged with a Zeiss Axiovert A.1 microscope detecting bright-field images in a time series (1 image per 10 s for 30 min) under flow conditions (a flow rate of 0.25 dyn/cm^2). Immune cells were perfused by using a pump system. After 30 min the amount of adhered immune cells were analyzed by cell counting plugin from ImageJ.

2.10. Transmigration assay

To test the transmigratory capacity of immune cells, we performed a transmigration assay with minor modifications as described in Ref. [19]. PMMEC (4×10^4 cells) or PHMEC (6×10^4 cells) were seeded in a coated (Speed coating solution, PELO Biotech) insert of a transwell and cultivated for 48 h with microvascular endothelial cell growth medium (PELO Biotech). Under inflammatory conditions (as described in adhesion assay) or treatment with or without $K_{2P}2.1$ modulators (as described in flow cytometry analysis) we changed media and transferred 5×10^5 stimulated murine T cells or PBMC to PMMEC or PHMEC, respectively. After 8 h, we added Flow-Count Fluorosphere Beads (Beckman Coulter) to the migrated cells from the lower compartment. Cells were labelled with antibodies (see flow cytometry analysis) and absolute cell numbers were determined by flow cytometry.

2.11. Intravital microscopy of the cremaster muscle microcirculation

Intravital microscopy was performed in anesthetized mice as described before with modifications [27]. The cremaster muscle was inflamed by intrascrotal injection of 500 ng TNFα in 0.3 ml saline 2 h before cremaster muscle exteriorization. During intravital microscopy the exposed cremaster muscle was superfused with 1,25 mg/ml recombinant murine Exodus 2 (CCL21, Peprotech). CCL21 interacts with the CCR7 receptor to enable T cell migration and adhesion, but is not known to be chemotactic for monocytes [28]. As such, we chose CCL21 to enable T cell adhesion. T cells were stimulated as described above. Hereafter, viable T cells were collected by using a dead cell removal kit (Miltenyi Biotech) and labelled with a CellTracker™ Green CMFDA dye (Thermo Fisher). These cells were injected as short bolus via an artery femoralis catheter (2.5×10^7 cells/bolus). Intravital microscopy was conducted using fluorescence microscopy to determine leukocyte adhesion in the postcapillary venules of the inflamed cremaster muscle with a 40 × 0.75 NA water immersion objective (Axio Scope upright; Zeiss, Goettingen, Germany). In some experiments, Spadin (1 mM in 100 μl) or a monoclonal blocking VCAM antibody (200 μg in 100 μl; M/K-2.7, BioXCell) was injected 10 min prior the T-cell bolus. Recorded images were analyzed by ImageJ and AxioVision (Carl Zeiss) software. In postcapillary venules with a diameter of 20–40 μm numbers of adherent T cells were determined and calculated per mm^2. The microcirculation was recorded using digital cameras (Sensicam QE, Cooke, Romulus, MI or Axiocam, Zeiss, Oberkochen, Germany).

2.12. Cytotoxicity assay

To test the influence of skeletal muscle cells on the cytotoxicity of $CD8^+$ T cells we performed a flow-cytometry based co-culture cytotoxic assay. PMMC were stimulated and treated with $K_{2P}2.1$ modulators as described before. Afterwards, muscle cells were loaded with or without an ovalbumin peptide ($OVA_{257-264}$; SIINFEKL, EMC microcollections) for 1 h. Hereafter, medium was refreshed and stimulated $CD8a^+$ T cells (anti-CD3 coated 2 μg/ml, anti-CD28 soluble 1 μg/ml) were co-cultured with these PMMC for 24 h. Via flow cytometry $CD8a^+$ T cells were characterized (CD45 (APC/Cy7, 30-F11), CD3 (PerCP/Cy5.5, 145-2C11), CD8a (AF700, 53-6.7)) and the viability of PMMC was measured by Annexin V (FITC) and Fixable Viability Dye (FVD) eFlour™ 780 staining.

3. Experimental autoimmune myositis (EAM) experiments

We induced an experimental autoimmune myositis (EAM) in 8–12 week old female WT or *KCNK2*$^{-/-}$ mice with C-peptide fragment P13 in complete Freund's adjuvant (CFA) as described before [29]. Here, 200 μg/mouse of P13 peptide was subcutaneously injected in each flank (100 μl) of deeply anesthetized mice. On the day of immunization and two days later, a dose of 400 ng pertussis toxin (Alexis) was injected intraperitoneally (i.p.). In a subset of experiments, the $K_{2P}2.1$ activator BL-1249 was injected daily i.p. (1 mg/kg bodyweight). To evaluate the clinical disease course we performed Rotarod (RR) analysis over 2 min with an acceleration of 4–40 rounds per minute and five independent rounds. Two weeks before immunization, we started with a training phase and determined a median time on the Rotarod of each individual mouse. After immunization, we evaluated the mean time of five Rotarod rounds of each mouse daily. To calculate a Rotarod quotient, we divided the determined mean time per day after immunization by the individual median time of the training phase. For statistical analysis, we also calculated the mean Rotarod quotient for each animal from day 15 after immunization until day 30. For histological evaluation of EAM mice, we removed the quadriceps femoris and cryoconserved the tissue. Muscle tissues were sectioned (10 μm) and stained with hematoxylin and eosin (H&E) or with immunofluorescence antibodies (MHC-1, CD4, CD8, CD11b, as mentioned above). Muscle inflammation score (MIS) was determined as described before [29] of randomly chosen 8 areas. The evaluation was blinded and done by one person. Immune cells from spleen and inguinal lymph nodes were counted by a Casy Model TT cell counter (Innovatis AG). Immune cell characterization was performed by flow cytometry, and specific antibodies were used as mentioned above.

3.1. Electron microscopy

For ultrastructural analysis of skeletal muscle, we performed electron microscopy of a healthy human control and also two mice (C57BL/6). The healthy human control sample of a *M. biceps brachii* was part of an ongoing diagnostic analysis to exclude a myositis or myopathy, and routine light and electron microscopical analysis did not reveal ultrastructural abnormalities, beside a slightly thickened capillary basement membrane. All native samples were directly fixed in 2.5 % glutaraldehyde in 0.1 M sodium cacodylate buffer and further processed and embedded in resin according to a routine protocol as previously described for diagnostic samples (34266508). Semithin sections (500 nm) were prepared with an ultramicrotome (Ultracut E, Reichert-Jung) to select blocks for ultrastructural analysis. Ultrathin sections (60 nm) with virtual absence of limiting artifacts were prepared using pioloformcoated slot grids as described (large-scale digitization samples; LDS (34266508)), analyzed with a transmission electron microscope (Zeiss 902) and photographed using a 2 k side-mounted CCD camera (TRS). In sum, approximately 100 capillary profiles were recorded at 3000x, 7000x, 12,000x and 20,000x magnification to visualize capillary endothelial cells, pericytes, and also fibroblasts in their relation to surrounding skeletal muscle fibers.

3.2. Cytokine detection

We collected the supernatant of PMMC and PMMEC before (24 h), during (48 h) and after stimulation (72 h) with TNFα (500 U/ml). We quantified the secretion of IL-6, IL-1β, IL-10 and GM-CSF by ELISA according to the manufacturer's protocol (ebioscience). All experiments were performed in duplicates and luminescence was measured on a BetaPlate Reader (Tecan).

3.3. Statistical analysis

All results are presented as the mean ± SEM. D'Agostino-Pearson or Shapiro-Wilk test was used to evaluate a normal distribution. For analysis of two groups, we used a two-tailed *t*-test (unpaired/paired) or the Mann-Whitney *U* test or Wilcoxon rank sum test where as appropriate. Analysis of more than two groups were performed by using one-way ANOVA including post-test. For EAM Rotarod analysis, we used a two-way ANOVA. A p value ≥ 0.05 was classified as not significant, $p < 0.05$ (*) as significant, $p < 0.01$ (**) and $p < 0.001$ (***) as highly significant.

4. Results

4.1. $K_{2P}2.1$ expression is diminished in different IIM entities

The function and expression of $K_{2P}2.1$ channels in IIMs are currently unknown. To better understand the distribution of $K_{2P}2.1$ in muscle, we analyzed muscle specimen from IIM patients and NDCs using immunofluorescence (Fig. 1a). The clinical characteristics of this cohort, including the therapeutic agents administered at the time of biopsy, are given in Table 1. In line with previous reports [20,21,30], we focused our analysis of skeletal muscle fibers detecting $K_{2P}2.1$ on the cell membrane throughout the specimen (Fig. 1a). Although we detected $K_{2P}2.1$ across experimental groups, we observed differences in respect to the distribution of this ion channel. To interrogate this observation, we quantified the number of $K_{2P}2.1^+$ myofibers (Fig. 1b). Comparing NDCs (n = 6) and IIM patients (n = 31), we observed that the number of $K_{2P}2.1^+$ myofibers was reduced under inflammatory conditions. Of note, we also stratified IIM patients by steroid treatment as 9 out of 31 patients (29 %) received steroids at the time of biopsy with 9.8 mg (standard deviation (SD) 12 mg) per day. Comparing these treatment groups, patients treated with steroid as anti-inflammatory agent had higher numbers of $K_{2P}2.1^+$ myofibers as those patients without steroid treatment (Fig. 1c). Taken together, these observations indicate that muscle inflammation affects the distribution of $K_{2P}2.1$.

$K_{2P}2.1$ is downregulated in primary cells of murine muscle under inflammatory conditions.

To clarify the functional relevance of the diminished $K_{2P}2.1$ expression in human IIMs, we investigated the role of $K_{2P}2.1$ for the function of muscle resident cells. Electron microscopy identified close spatial relations between EC, scattered pericytes (not shown here),fibroblasts (FB), and myofibers (MF) (Fig. 2a). The close interaction of EC and skeletal muscle cells might therefore be particularly relevant for the immune cell infiltration and for $K_{2P}2.1$-related regulatory processes in IIMs. We found *Kcnk2* (gene for $K_{2P}2.1$) expression in differentiated primary murine muscle cells (PMMC) as well as primary murine muscle microvascular endothelial cells (PMMEC) both on gene (Fig. 2b) and protein level (Fig. 2c), whereas expression was higher in PMMC compared to PMMEC. Lung tissue was chosen as positive control given the strong expression of $K_{2P}2.1$ in this tissue as previously described [31]. To reciptulate inflammatory conditions, we employed TNFα as this cytokine is implicated in IIM pathophysiology in humans [26,32]. Here, both PMMC and PMMEC demonstrated downregulation of *Kcnk2* (Fig. 2d) and correspondingly on protein level (Fig. 2e). Of note, gene

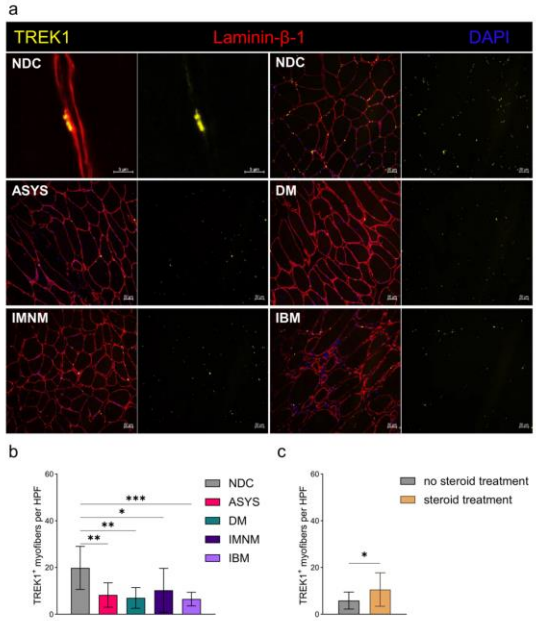

Fig. 1. $K_{2P}2.1$ expression in idiopathic inflammatory myopathy entities. (a) Immunofluorescence images of $K_{2P}2.1$ (yellow) in muscle specimen from non-disease control (NDC, n = 6) and idiopathic inflammatory myopathies (IIM). $K_{2P}2.1$ was detected directly adjacent to the muscle fiber membrane (stained with laminin-β-1 in red; top left image). Representative images of myofibers demonstrating different quantities of $K_{2P}2.1$ across IIM entities anti-synthetase syndrome (ASYS, n = 9), dermatomyositis (DM, n = 6), immune-mediated necrotizing myopathy (IMNM, n = 8) and inclusion body myositis (IBM, n = 8). (b) $K_{2P}2.1^+$ myofibers were counted in randomly distributed 10 high-power fields (HPF, ≙ 0.16 mm2). The biopsies were blinded for quantification, with the diagnosis impossible to identify from the label. $K_{2P}2.1^+$ cells were defined as cells with a clear expression of $K_{2P}2.1$ at the cell membrane. (c) Number of $K_{2P}2.1^+$ myofibers compared between IIM patients treated with steroids (n = 9) and without steroids (n = 22). Groups were compared by one-way ANOVA testing followed by post-hoc analysis. *p < 0.05, **p < 0.01, ***p < 0.001.

and protein expression showed fast dynamics in presence or absence of inflammatory stimuli. Downregulation of *Kcnk2* under inflammation was restored to baseline after wash out (Fig. 2f and g). Thus, muscle and endothelial cells respond to inflammatory conditions with downregulation of $K_{2P}2.1$.

4.2. Modulation of $K_{2P}2.1$ function alters inflammatory response of endothelial and muscle cells

Next, we investigated the consequences of $K_{2P}2.1$ function on immune properties of PMMC and PMMEC. Therefore, we used different $K_{2P}2.1$ modulators including spadin ($K_{2P}2.1$ inhibition) and BL-1249 ($K_{2P}2.1$ activation) in wildtype (WT) as well as genetic knockout

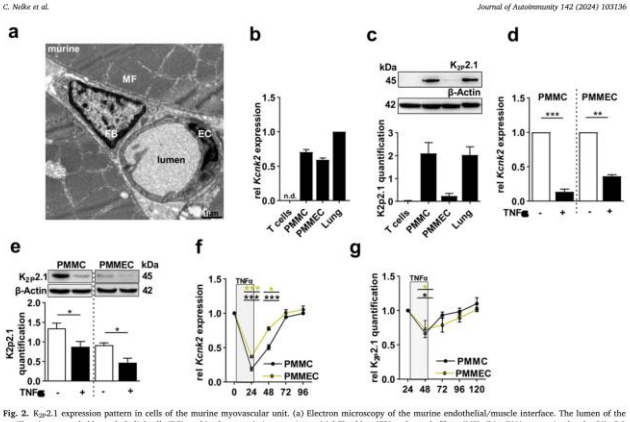

Fig. 2. $K_{2P}2.1$ expression pattern in cells of the murine myovascular unit. (a) Electron microscopy of the murine endothelial/muscle interface. The lumen of the capillary is surrounded by endothelial cells (EC), and in close proximity to an interstitial fibroblast (FB) and muscle fibers (MF). (b) mRNA expression levels of $K_{2P}2.1$ (gene: *Kcnk2*) in T cells, differentiated primary murine skeletal muscle cells (PMMC), primary murine skeletal microvascular endothelial cells (PMMEC) and lung tissue (n = 5). (c) Protein expression of $K_{2P}2.1$ and β-Actin as loading control measured by Western blot. Analyzed cell types: T cells, PMMC, PMMEC and lung tissue (n = 4). (d) mRNA expression levels of *Kcnk2* with or without TNFα inflammation of PMMC or PMMEC. The expression values were normalized to unstimulated cells (n = 5). (e) $K_{2P}2.1$ protein expression and β-Actin as loading control of unstimulated and TNFα-stimulated PMMC or PMMEC analyzed by Western blot (n = 4). $K_{2P}2.1$ (f) mRNA and (g) protein expression of PMMC (black) and PMMEC (corn yellow). Expressions were measured every 24 h without (0) or with TNFα stimulation (grey bar, 24) and every 24 h (48, 72) after washout of the stimulation. The expression levels were normalized to untreated cells (0) (n = 5). Statistics of mRNA expression levels were calculated with ΔC_t values. Statistics of Western blot analysis were calculated with ROI measurements analyzed by Image J. Groups were compared by two-sided Student's *T* test. All data are shown as mean±SEM. *p < 0.05, **p < 0.01, ***p < 0.001.

(*Kcnk2*$^{-/-}$) cells. On PMMC, higher levels of MHC-1, MHC-2 and ICAM-1 were observed in response to inflammatory conditions (Fig. 3a, b, c). Pharmacological $K_{2P}2.1$ blockade or genetic $K_{2P}2.1$ deficiency induced increased MHC-1 levels during and after inflammation with TNFα, while MHC-2 and ICAM-1 levels were unchanged in response to $K_{2P}2.1$ modulation on PMMC. Treatment with BL-1249 blunted the inflammatory response in respect to MHC-1 expression on PMMC. Conversely, on PMMEC, $K_{2P}2.1$ deficiency or treatment with spadin amplified the expression of MHC-1 as well as of the adhesion molecules ICAM-1 and VCAM-1 (Fig. 3d, e, f). The $K_{2P}2.1$ agonist BL-1249 had no statistically significant effect. Additionally, we investigated soluble pro-inflammatory cytokines secreted by muscle and endothelial cells under inflammatory conditions. IL-6 and the granulocyte-macrophage colony-stimulating factor (GM-CSF) were measured in supernatants of these cells. Interestingly, *Kcnk2*$^{-/-}$ and spadin-treated PMMC (Fig. 3g) and PMMEC (Fig. 3h) secreted significantly higher levels of IL-6 and GM-CSF before, during and after inflammation compared to WT control PMMC and PMMEC. BL-1249 reduced secretion of IL-6 and GM-CSF by PMMC at all time points. For PMMEC, we detected reduced IL-6 levels only after washout of inflammation. We found no significant changes in IL-1α and IL-10 production under modulation of $K_{2P}2.1$ function (Suppl. Fig. 2a). Taken together, $K_{2P}2.1$ blockade or deficiency leads to increased levels of pro-inflammatory cytokines and surface molecules *in vitro*.

4.3. $K_{2P}2.1$ is a regulator of immune cell migration and cytotoxicity in the context of muscle inflammation

Given the influence of $K_{2P}2.1$ modulation on expression of adhesion molecules and pro-inflammatory responses of PMMC and PMMEC, we next investigated the functional consequences for immune cell migration and cytotoxicity in the context of muscle inflammation. First, we performed a functional low physiological flow (0.25 dyn/cm^2) assay to characterize adhesion (Fig. 4a) and a boyden chamber assay to assess transmigration of T cells on/through a confluent PMMEC monolayer (Fig. 4c). For *Kcnk2*$^{-/-}$ PMMEC, we detected enhanced numbers of adherent (Fig. 4b) and transmigrated T cells (Fig. 4d) before, during and after inflammation compared to WT controls. Treatment of WT PMMEC with spadin led to an increase, whereas $K_{2P}2.1$ activation with BL-1249 induced a decrease of T cell adhesion and transmigration. To transfer these findings to an *in vivo* situation, we investigated the capability of T cell adhesion in the context of $K_{2P}2.1$ modulation using intravital microscopy of the cremaster muscle microcirculation (Fig. 4e). We detected increased numbers of T cell adhesion in *Kcnk2*$^{-/-}$ compared to WT mice already under basal conditions (Fig. 4f). Inflammation of the cremaster muscle further increased the adhesion of T cells both in *Kcnk2*$^{-/-}$ and WT animals. Spadin treatment enhanced T cell adhesion in WT, but not in *Kcnk2*$^{-/-}$ mice indicating a $K_{2P}2.1$ specific effect on immune cell adhesion. VCAM-1 blockade by a monoclonal antibody significantly diminished the number of adherent T cells, both in WT and *Kcnk2*$^{-/-}$

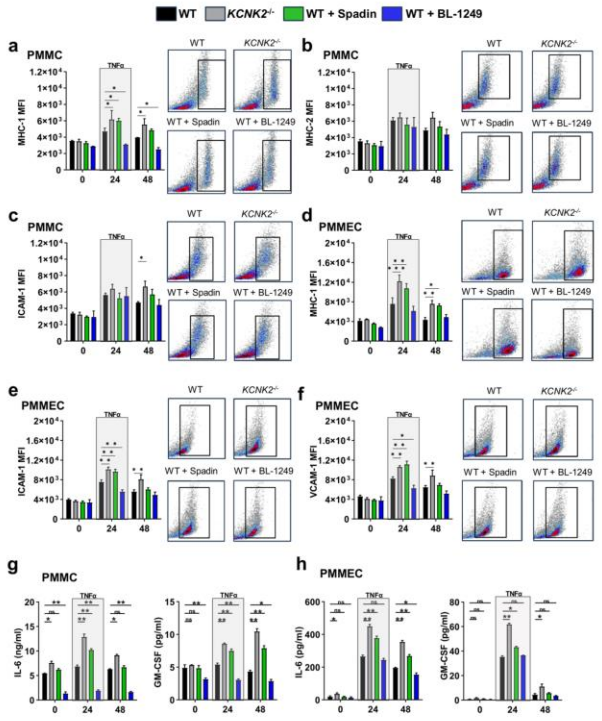

Fig. 3. Regulatory effect of $K_{2P}2.1$ on the inflammatory response of skeletal muscle and endothelial cells.
Untreated wildtype (WT), *Kcnk2*$^{-/-}$ cells or WT cells treated with Spadin ($K_{2P}2.1$ blocker) or BL-1249 ($K_{2P}2.1$ activator) were analyzed every 24 h without (0) or with stimulation of TNFα (24; grey bar) and each 24 h after washout (48, 72, 96) of the stimulation. Mean fluorescence intensities (MFI) of (a) MHC-1, (b) MHC-2, and (c) ICAM-1 on PMMC were measured by flow cytometry. MFI of (d) MHC-1, (e) ICAM-1 and (f) VCAM-1 are shown below. MFI levels were normalized to untreated and unstimulated WT cells, respectively. Representative scatter plots are shown for each experiment besides the corresponding bar plot for the 72 h time point. n = 10 for each experiment. (g) PMMC and (h) PMMEC cytokine secretion of IL-6 and GM-CSF at different time points of inflammation measured by ELISA (n = 5). Groups were compared by one-way ANOVA testing followed by post-hoc analysis. $^{*}p < 0.05$, $^{**}p < 0.01$, $^{***}p < 0.001$.

mice. Thus, $K_{2P}2.1$ regulates adhesion molecule level on PMMEC *in vitro* and *in vivo*.

In IIMs, infiltrating immune cells may exert cytotoxic effects towards skeletal muscle cells leading to their progressive destruction [1]. To understand the interaction between muscle fibers and cytotoxic T cells. We performed a flow cytometry-based cytotoxicity co-culture assay (Fig. 4g and h). Hence, we inflamed muscle cells in a time-dependent manner as described before and loaded these cells with or without an ovalbumin peptide ($OVA_{257\text{-}264}$). $CD8^+$ T cells isolated from OVA-specific TCR transgenic mice (OT-1) recognize $OVA_{257\text{-}264}$ in the context of MHC-1. These OT-1 $CD8^+$ T cells were stimulated and co-cultured with or without OVA-loaded muscle cells. We determined the number of live cells after incubation with $CD8^+$ T cells. Interestingly, $CD8^+$ T cell-mediated cytotoxicity was amplified in *Kcnk2*$^{-/-}$ muscle cells and in muscle cells treated with spadin with and without OVA loading (Fig. 4g and h). In contrast, BL-1249 blunted the cytotoxic effect of $CD8^+$ T cells on OVA loaded muscle cells. Taken together, these data suggest that $K_{2P}2.1$ may affect both immune cell migration and T cell-mediated cytotoxicity in skeletal muscle.

4.4. $K_{2P}2.1$ influences disease progression and inflammatory response in a small-peptide antigen-induced IIM animal model

Following our previous results, we next raised the question whether $K_{2P}2.1$ modulation can influence IIM disease progression *in vivo* and therefore we used the established C-peptide (P13) induced experimental

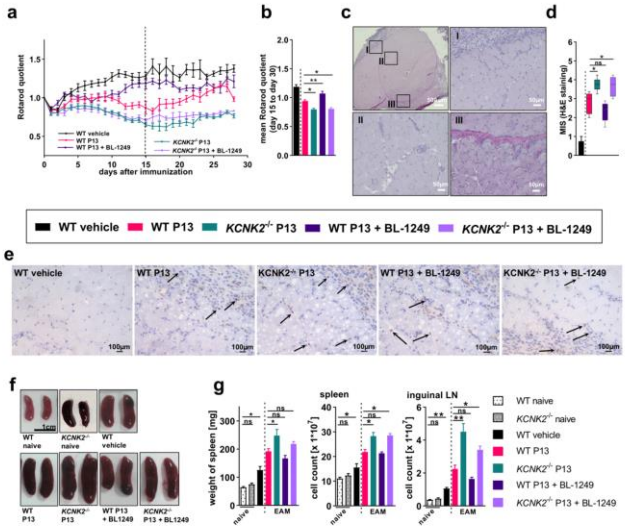

Fig. 5. Regulatory effect of $K_{2P}2.1$ in a small-peptide antigen-induced IIM animal model. The idiopathic inflammatory myopathy model or experimental autoimmune myositis (EAM) was induced by a small-peptide (P13) and vehicle as control, respectively. (a) The muscle strength of each individual animal was evaluated by a Rotarod quotient (mean Rotarod time of the respective day/median Rotarod time of previous 2 week training phase). Dashed line (day 15) indicates the day of analysis (n = 10 animals per group from 1 to 3 independent experiments). (b) The cumulative score from the Rotarod quotient as measured in (a) is shown for each experimental group. (c) H&E staining of a representative muscle section as overview and higher magnifications (fascicular (I), epimysial (II) and perimysial (III)). (d) Histological grading on numbers of necrotic fibers displayed as muscle inflammation score (MIS) in different experimental EAM groups. (e) Representative immunohistochemistry staining of muscle tissue from each experimental group. Sections were stained for MHC-1 (n = 5). Arrows indicate MHC-1 positive cells. (f) Exemplary images of spleens from naïve and EAM-induced WT and *Kcnk2*$^{-/-}$. (g) Spleen weights and count of cells isolated from spleen and inguinal lymph nodes (LN) of naïve and EAM animals. All data are shown as the mean ± SEM. A two-way ANOVA test was used to compare groups. $^{*}p < 0.05$, $^{**}p < 0.01$, $^{***}p < 0.001$.

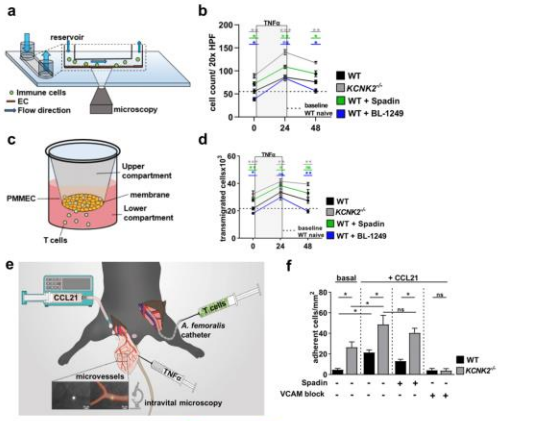

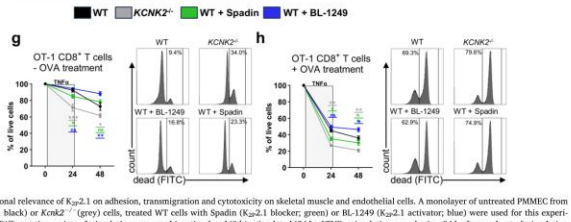

Fig. 4. Functional relevance of $K_{2P}2.1$ on adhesion, transmigration and cytotoxicity on skeletal muscle and endothelial cells. A monolayer of untreated PMMEC from wildtype (WT; black) or *Kcnk2*$^{-/-}$ (grey) cells, treated WT cells with Spadin ($K_{2P}2.1$ blocker; green) or BL-1249 ($K_{2P}2.1$ activator; blue) were used for this experimental setup. Different time points of stimulation were used (unstimulated (0 h), stimulated (24 h of TNFα stimulation, grey bar) or 24 h after washout of stimulation (48). (a) Illustration of the experimental setup for the low physiological flow (0.25 dyn/cm^2) adhesion assay. (b) Analysis of absolut immune cells counts adhered on a confluent endothelial cell (EC) monolayer within 30 min microscoped in by 20x High-power field (HFP) using Image J software. Statistical comparisons were made between WT and experimental groups. (c) Illustration of the experimental setup for a functional transmigration assay using Boyden chamber. (d) Absolut numbers of transmigrated stimulated immune cells after 6 h through an endothelial cell layer with predefined stimulatory and modulatory conditions. (e) Experimental setup for the intravital microscopy of the cremaster muscle microcirculation. TNFα was injected intrascrotally and the exposed cremaster muscle was superfused with CCL21. Fluorescence labelled T cells were injected intraarterially (i.a.) by a femoral catheter. Adherent T cells were observed via intravital microscopy using a Zeiss Axio Scope upright microscope, equipped with a 40x NA 0.75 water immersion objective. Scale bar represents 10 µm. (f) Intravital microscopy analysis of adherent T cells per mm^2 in cremaster muscle microvessels. Scrotum was stimulated with TNFα or without (basal), superfused with CCL21 and treated by i.a. injection with or without Spadin or a VCAM blocking antibody in wildtype (WT; black) or *Kcnk2*$^{-/-}$ (grey) animals (n = 12, n = 16). Treatment was done in parallel. PMMC were (g) untreated or (h) treated with $Ova_{257\text{-}264}$. Stimulated OT-1 $CD8^+$ T cells were co-cultured with PMMC and the viability was analyzed by flow cytometry (n = 5). Live cells were identified by Annexin-V/FVD staining. The percentage of live cells of the total PMMC is reported. 50,000 cells were analyzed per sample. Representative histograms are displayed beside each experiment. Data is shown as mean ± SEM. For (a,b) $^{*}p < 0.05$, $^{**}p < 0.01$, $^{***}p < 0.001$, determined by two-way ANOVA test and for (f) $^{*}p < 0.05$, determined by Student's t-test.

autoimmune myositis (EAM) mouse model [29]. We induced the disease in WT and $K_{2P}2.1$ deficient animals with or without BL-1249 treatment. Disease severity was measured by muscle strength, which we longitudinally detected by rotarod performance test. We defined a muscle strength basal level of each animal as median time on the Rotarod within a two weeks training period. P13 immunized WT mice (WT P13) demonstrated a substantially worsened motor performance compared to WT controls (WT vehicle) (Fig. 5a and b). Of note, the disease course in *Kcnk2*$^{-/-}$ P13 mice was significantly worse than in WT P13 mice. BL-1249 treatment ameliorated EAM disease course in WT P13 mice almost reaching motor performance of WT vehicle controls. As we did not observe any differences in motor performance in *Kcnk2*$^{-/-}$ P13 mice with or without BL-1249 treatment, this effect seems to be specific to $K_{2P}2.1$ modulation. Day 15 (dashed line) was defined as day of maximal muscle inflammation. H&E staining demonstrated immune cell infiltration in all EAM mice but not in WT vehicle animals, which were mainly observed in fascicular (I), epimysial (II) and perimysial (III, Fig. 5c) regions. To further assess whether $K_{2P}2.1$ affects muscle inflammation in EAM, we calculated the muscle inflammation score (MIS) as previously described [33,34]. Briefly, the MIS quantifies histomorphological abnormalities including immune cell infiltration, muscle atrophy and the number of necrotic fibers. Eight randomly chosen areas were quantified for each specimen by a blinded examiner. Here, *Kcnk2*$^{-/-}$ P13 mice demonstrated an enhanced MIS compared to WT P13.

In *Kcnk2*$^{-/-}$ P13 mice treated with or without BL-129t, we observed significant less necrosis compared to WT P13 animals, whereas we did not detect any relevant effects in BL-1249 P13 WT mice (Fig. 5d). We did not detect MHC-1$^+$ cells in WT vehicle treated animals, while we observed a higher number of MHC-1$^+$ cells in WT P13 animals, in *Kcnk2*$^{-/-}$ P13 animals and in BL-1249 treated *Kcnk2*$^{-/-}$ P13 animals (Fig. 5e). In comparison, the number of MHC-1$^+$ cells was diminished in BL-1249 treated WT P13 animals. Infiltrating immune cells comprised $CD4^+$, $CD8^+$ and $CD11b^+$ cells in all EAM (WT P13 and *Kcnk2*$^{-/-}$ P13) animals (Suppl. Fig. 3a). Investigating the peripheral immune response, we observed enlarged spleens in *Kcnk2*$^{-/-}$ P13 mice (Fig. 5f) accompanied by increased cell numbers in spleen and lymph nodes (LN) compared to WT P13 animals (Fig. 5g). BL-1249 did not induce a significant change to cell numbers of inguinal LN and spleen as compared to WT P13. Naïve *Kcnk2*$^{-/-}$ and WT animals did not show any significant differences.

In depth analysis of immune cells of the spleen and inguinal LN showed a slight shift to reduced T cell numbers ($CD4^+$ and $CD8^+$) and expanded B cells in *Kcnk2*$^{-/-}$ naïve compared to naïve WT animals (Suppl. Fig. 3b). In all spleens of EAM P13 and vehicle animals, we detected a shift towards monocytes and macrophages (MM), dendritic cell (DC) populations and B cells. Further, in EAM *Kcnk2*$^{-/-}$ mice demonstrated the strongest shift towards B cells accompanied by a T cell reduction in inguinal LN compared to all other groups. In addition, we observed a pronounced shift from naïve to T central (TCM) and T effector memory (TEM) cells of *Kcnk2*$^{-/-}$ P13 mice (Suppl. Fig. 3c) as well as enhanced T cell ($CD4^+$ and $CD8^+$) activation status in spleen and inguinal LN (Suppl. Figs. 3d and e) of *Kcnk2*$^{-/-}$ P13 mice. BL-1249 treatment significantly reduced those peripheral immune responses only in WT P13 mice. In summary, $K_{2P}2.1$ deficiency leads to a worsened EAM disease course associated with enhanced peripheral immune response and muscular immune cell infiltration, whereas $K_{2P}2.1$ activation specifically reverses those effects.

4.5. $K_{2P}2.1$ modulation influences the immune response of human muscle-derived cells

To translate our results from mouse *in vitro* and *in vivo* experiments to human tissue, we next investigated cells of the human myovascular unit. Similar to the murine ultrastrucutre, electron microscopy demonstrated an EC layer connected by tight junctions (TJ) surrounding capillaries as well as scattered pericytes and fibroblasts in close contact to the EC and myofibers (Fig. 6a). $K_{2P}2.1$ was expressed in PHMC and PHMEC on mRNA (Fig. 6b and c) and protein level (Fig. d). Similar to our findings in mice, we observed a significant and reversible downregulation of $K_{2P}2.1$ expression by TNFα treatment in differentiated PHMC and PHMEC (Fig. 6c, d, e). Next, we investigated whether pharmacological $K_{2P}2.1$ modulation has comparable functional consequences as observed in mice. For this purpose, we used the same experimental setups for human primary cells employing a time-dependent inflammation with TNFα. $K_{2P}2.1$ blockade by spadin led to an enhanced immune response with increased MHC-1, -2 and ICAM-1 expression on PHMC (mainly during and after inflammation) (Fig. 6f) and MHC-1, ICAM-1 and VCAM-1 expression on PHMEC (before, during and after inflammation) (Fig. 6g). In contrast, $K_{2P}2.1$ activation by BL-1249 treatment induced opposite effects. Activation of $K_{2P}2.1$ by BL-1249 led to an overall reduction of MHC-1 and both adhesion molecules (ICAM-1 and VCAM-1) before, during and after inflammation of PHMEC (Fig. 6f and g). Next, we investigated whether $K_{2P}2.1$ modulation also influences immune cell migration on/through PHMEC. Inflammation of PHMEC led to increased numbers of adherent and transmigrated PBMC. Those effects were further enhanced by spadin treatment, whereas BL-1249 treatment demonstrated opposite outcomes before, during and after inflammation (Fig. 6h and i). Thus, $K_{2P}2.1$ is functionally expressed in human skeletal muscle and muscle endothelial cells. Its pharmacological modulation can be used to modulate immune responses and immune cell migration in the context of muscle inflammation.

5. Discussion

The mechanosensitive outward rectifying potassium channel $K_{2P}2.1$ is expressed in several organs and tissues including brain, lung, kidney, heart and, notably, in the vascular system as well as smooth and skeletal muscle [35]. $K_{2P}2.1$ is one of the most studied channels of the K_{2P} family and involved in physiological and pathophysiological mechanisms [35]. Nevertheless, the role of $K_{2P}2.1$ in skeletal muscle and endothelial cells in the context of IIM remains poorly understood. Therefore, the present study aimed at understanding the mechanistic consequences of $K_{2P}2.1$ for immune function at the interface of skeletal muscle and vasculature. Here, we report a novel function for $K_{2P}2.1$ signaling as regulator of immune cell trafficking in skeletal muscle. $K_{2P}2.1$ modulation influenced disease severity in EAM and argues for $K_{2P}2.1$ as potential new therapeutic target for IIMs.

As previously reported for the central nervous system and the neurovascular unit [21], endothelial cells, but also pericytes and fibroblasts, presumably interact and regulate immune cell migration. In line, previous studies reported a comparable ultrastructure of murine and human muscle tissue characterized by the proximity of capillaries, satellite cells and other perivascular cells [36–38]. This observation might be of value to translate mechanisms of $K_{2P}2.1$ function from mice to human.

$K_{2P}2.1$ is expressed in muscle and muscle endothelial cells, but only infrequently in immune cells both of human and mouse origin. Inflammatory stimulation with TNFα leads to $K_{2P}2.1$ downregulation in typical $K_{2P}2.1$-expressing cell types with fast recovery after the inflammatory conditions have resolved. Similar effects have been reported for brain endothelial cells *in vitro* and *in vivo* [39], and in epithelial as well as endothelial cells in the intestine or nasal mucosa [22,23] during inflammation. Those observations indicate that $K_{2P}2.1$ is a regulator of cellular immune responses in different tissues of ectodermal and mesodermal origin. Consistent with this, increasing numbers of studies addressed $K_{2P}2.1$ modulation as potential therapeutic approach in the context of autoimmunity [21–23]. For this study, we employed *Kcnk2*$^{-/-}$ mice as well as established pharmacological modulators (spadin as inhibitor and BL-1249 as activator of $K_{2P}2.1$) [40]. Genetic deletion or treatment with spadin has been previously shown to induce secretion of pro-inflammatory cytokines and inflammation in the context of spinal cord or lung injury, intracerebral hemorrhage or

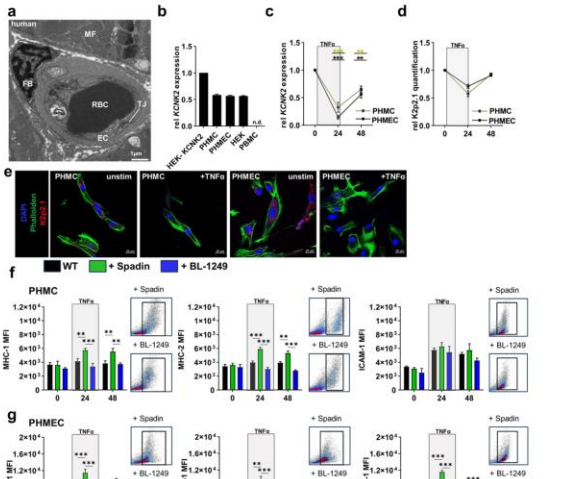

(caption on next page)

Fig. 6. $K_{2P}2.1$ expression pattern in cells of the human myovascular unit and its functional effect on the inflammatory response, adhesion and transmigration (a) Representative electron microscopy image of the human myovascular unit. A red blood cell (RBC) inside the capillary, surrounded by endothelial cells connected to each other by tight junctions (TJ). Fibroblasts (FB) are localized between EC and myofibers (MF) of the human muscle and can be differentiated from pericytes (not shown here) by absence of a basement membrane. (b) mRNA expression levels of *KCNK2* in peripheral blood mononuclear cells (PBMC), human embryonic kidney cells (HEK) as negative and HEK-*KCNK2* which constitutively expresses $K_{2P}2.1$ as positive control, respectively, as well as differentiated primary human kidney muscle cells (PHMC), primary human skeletal microvascular endothelial cells (PHMEC; n = 5). (c) Relative (rel) mRNA *KCNK2* or (d) $K_{2P}2.1$ protein expression determined of PHMC (black) or PHMEC (corn yellow) at different time points of stimulation by qPCR and flow cytometry, respectively. Cells were measured unstimulated (24), TNFα stimulated (48) or 24 h after (72) washout of the stimulation. The expression levels were normalized to unstimulated cells (24) (n = 6). (e) Representative immunofluorescence staining of unstimulated and TNFα stimulated PHMC or PHMEC for $K_{2P}2.1$ (red). DAPI (blue) and phalloidin (green). Cells were not permeabilized for this experiment. (f + g) Mean fluorescence intensities (MFI) of immune regulatory molecules (MHC-1, -2) adhesion (ICAM-1 and VCAM-1) expressed by PHMC and PHMEC were measured by flow cytometry and normalized to not stimulated, untreated cells (n = 6). Representative scatter plots are shown beside each experiment. (h) Stimulated PBMC were applied within 30 min under low flow ($0.25\ dyn/cm^2$) to unstimulated (24), stimulated (48, TNFα for 24 h, grey bar) or 24 h after washout (72) of PHMEC under untreated, Spadin or BL-1249 treatment conditions and counted per 20x High-power field (HPF). (i) Analysis of transmigrated PBMC towards a PHMEC monolayer treated with or without $K_{2P}2.1$ modulators during a stimulation interval. Dashed line displays the baseline of untreated and unstimulated PHMEC (n = 10). Statistics of mRNA expression levels were calculated with ΔC_T values. Data is shown as mean±SEM. Groups were compared by two-way ANOVA test. $^*p < 0.05$, $^{**}p < 0.01$, $^{***}p < 0.001$.

allergic reactions [22,23,41]. In line with these observations, we report that $K_{2P}2.1$ modulation promotes a pro-inflammatory cellular response of muscle and endothelial cells as evidenced by $K_{2P}2.1$ inhibition or deletion under basal and inflammatory conditions in both mouse and human tissue, respectively.

Here, we extend the knowledge of $K_{2P}2.1$ signaling to skeletal muscle and corroborate $K_{2P}2.1$ as driver of inflammation at the endothelial interface. Moreover, we demonstrate that $K_{2P}2.1$ is a central regulator of inflammatory cell responses not only for endothelial and epithelial barriers, but also for skeletal muscle cells and therefore the target cells in IIMs. Indeed, $K_{2P}2.1$ exerts a functional role in the context of IIM as disease severity of EAM is amplified in $K_{2P}2.1$ knockout mice. Functional deletion of *Kcnk2* enhances immune cell infiltration resulting in a worsended disease course. Following this line of argumentation, we hypothesized that $K_{2P}2.1$ activation might be of interest to dampen autoimmunity in the context of IIMs. Indeed, a recent study reported that $K_{2P}2.1$ activation results in reduced pro-inflammatory cytokine secretion of epithelial and alveolar cells following lung injury [31]. However, functional readouts of $K_{2P}2.1$ modulation are currently lacking *in vivo*. Thus, it is interesting to note that expression of pro-inflammatory molecules are diminished in response to BL-1249 in muscle and muscle endothelial cells. On a functional level, BL-1249 treatment improved muscle function in a model of EAM providing first *in vivo* evidence for a therapeutic effect of $K_{2P}2.1$ stimulation. On a cellular level, this effect was corroborated by reduced expression of costimulatory and adhesion molecules as well as cytokine production in response to $K_{2P}2.1$ activation.

$K_{2P}2.1$ likely exerts its immune regulatory effects via a number of mechanisms. Among these, restriction of immune cell trafficking across barriers is of particular importance. Indeed, we were able to demonstrate that $K_{2P}2.1$ modulates immune cell extravasation both *in vitro* and *in vivo*. Genetic depletion or pharmacological blockade promoted immune cell trafficking. Conversely, activation of $K_{2P}2.1$ had an opposite effect before and after inflammation in mouse and human cells, respectively. These findings can be attributed to adhesion molecule alterations on EC caused by $K_{2P}2.1$ modulation. Former studies are consistent with these findings, demonstrating that $K_{2P}2.1$ inhibition is associated with upregulation of adhesion molecules combined with downregulation of tight junction molecules in endothelial and epithelial cells in context of inflammatory processes [19,39]. These findings indicate $K_{2P}2.1$ as regulator of barrier function and integrity across tissues. Previously, we discussed potential mechanisms by which $K_{2P}2.1$ might influence barrier permeability in the context of the neurovascular unit [19]. Broadly, ion flux-dependent (e.g. alterations of Ca^{2+} homeostasis) or ion-flux independent mechanisms (e.g. interaction with the actin cytoskeleton [42]) are potentially implicated. Further investigations are needed to dissect the underlying pathways both in the context of the neurovascular unit and skeletal muscle.

A potential limitation of this study is introduced by the *Kcnk2*$^{-/-}$ model as this global knockout does not allow for discrimination between different cell types contributing to immune cell migration into skeletal muscle. Further studies might benefit from employing cell-specific knockouts to further dissect potential mechanisms. The absence of an effect for BL-1249 in *Kcnk2*$^{-/-}$ EAM argues for a specific $K_{2P}2.1$ mechanism in mice, an influence of BL-1249 on other potassium channels such as $K_{2P}10.1$ (TREK-2) cannot be excluded in human cell lines [43]. Specific $K_{2P}2.1$ modulators are needed to overcome this potential caveat. A further limitation to this work is potentially introduced by clinical and therapeutic heterogeneity among patients and subgroups. As such, immunomodulatory treatments might introduce a potential confounder in our analysis. To address this bias, we compared patients treated with glucocorticoids to those without. Here, we observed no meaningful differences between the two groups.

Succinctly, the present study provides evidence for $K_{2P}2.1$ as regulator of immune function in skeletal muscle exceeding an exclusive regulation of the endothelial barrier. $K_{2P}2.1$ inhibition or depletion leads to an increased pro-inflammatory response of muscle- and muscle endothelial cells, facilitates adhesion and transmigration of immune cells and aggravated EAM severity. Concurrently, $K_{2P}2.1$ activation ameliorates autoimmunity and results in a more beneficial course of EAM. Therefore, pharmacological modulation of $K_{2P}2.1$ might be of interest as a novel therapeutic strategy for IIM.

Funding

Study funding from the Deutsche Forschungsgemeinschaft (DFG) to CP (PR 1725/2-1) and TR (RU 2169/2-1). Additionally, TR was supported by the Else Kröner-Fresenius-Stiftung (2018_A03), the Federeal Ministry of Education and Research (BMBF, 01EC1901A) and the Deutsche Gesellschaft für Muskelerkrankte e.V. (DGM, Ru2/1 and Sc22/4). CN was supported by the Deutsche Gesellschaft für Muskelkranke e.V (DGM, Ne4/1). and the Interne Forschungsförderung of the Medical Faculty of the Heinrich-Heine University Duesseldorf.

Ethical approval

All procedures performed in studies involving human participants were in accordance with the ethical standards of the institutional and national research committee and with the 1964 Helsinki Declaration and its later amendments or comparable ethical standards. Informed consent was obtained from all patients and ethical approval was granted by the local ethical committee in Münster(2017-671-f-S, 2017-023-f-S).

Consent to publish

Informed consent was obtained from all individual participants included in the study.

Declaration of competing interest

The authors report no competing interests.

Appendix A. Supplementary data

Supplementary data to this article can be found online at https://doi.org/10.1016/j.jaut.2023.103136.

References

[1] S. Barsotti, I.E. Lundberg, Myositis an evolving spectrum of disease, Immunol. Med. 41 (2018) 46–54, https://doi.org/10.1080/13497413.2018.1481571.
[2] I.E. Lundberg, M. de Visser, V.P. Werth, Classification of myositis, Nat. Rev. Rheumatol. 14 (2018) 269–278, https://doi.org/10.1038/nrrheum.2018.41.
[3] K. Albrecht, D. Huscher, J. Callhoff, J.G. Richter, T. Alexander, J. Henes, A. Zink, Trends in idiopathic inflammatory myopathies: cross-sectional data from the German National Database, Rheumatol. Int. 40 (2020) 1639–1647, https://doi.org/10.1007/s00296-020-04634-0.
[4] I.E. Lundberg, A. Tjärnlund, M. Bottai, V.P. Werth, C. Pilkington, M. de Visser, L. Alfredsson, A.A. Amato, R.J. Barohn, M.H. Liang, J.A. Singh, R. Aggarwal, S. Arnardottir, H. Chinoy, R.G. Cooper, K. Dankó, M.M. Dimachkie, B.M. Feldman, I.G.-D. La Torre, P. Gordon, T. Hayashi, J.D. Katz, H. Kobayka, P.A. Lachenbruch, B. A. Lang, Y. Li, C.V. Oddis, M. Olesinska, A.M. Reed, L. Rutkowska-Sak, H. Sanner, A. Selva-O'Callaghan, Y.W. Song, J. Vencovsky, S.R. Ytterberg, F.W. Miller, L. G. Rider, EULAR/ACR classification criteria for adult and juvenile idiopathic inflammatory myopathies and their major subgroups, Ann. Rheum. Dis. 76 (2017) 1955–1964, https://doi.org/10.1136/annrheumdis-2017-211468.
[5] S. Baig, J.J. Paik, Inflammatory muscle disease - an update, Best Pract. Res. Clin. Rheumatol. 34 (2020), 101484, https://doi.org/10.1016/j.berh.2019.101484.
[6] A.E.R. Fasth, M. Dastmalchi, A. Rahbar, S. Salomonsson, J.M. Pandya, E. Lindroos, I. Nennesmo, K.-J. Malmberg, C. Söderberg-Naucler, C. Trollmo, I.E. Lundberg, V. Malmström, T cell infiltrates in the muscles of patients with dermatomyositis and polymyositis are dominated by CD28null T cells, J. Immunol. Baltim. Md 1950 183 (2009) 4792–4799, https://doi.org/10.4049/jimmunol.0903688.
[7] S.A. Greenberg, J.L. Pinkus, A.A. Amato, T. Kristensen, D.M. Dorfman, Association of inclusion body myositis with T cell large granular lymphocytic leukaemia, Brain J. Neurol. 139 (2016) 1348–1360, https://doi.org/10.1093/brain/aww024.
[8] S.A. Greenberg, J.L. Pinkus, S.W. Kong, C. Baecher-Allan, A.A. Amato, D. M. Dorfman, Highly differentiated cytotoxic T cells in inclusion body myositis, Brain 142 (2019) 2590–2604, https://doi.org/10.1093/brain/awz207.
[9] C. Iadecola, The neurovascular unit coming of age: a journey through neurovascular coupling in health and disease, Neuron 96 (2017) 17–42, https://doi.org/10.1016/j.neuron.2017.07.030.
[10] M. Kamiya, F. Mizoguchi, A. Takamura, N. Kimura, K. Kawahata, H. Kobsaka, A new in vitro model of polymyositis reveals CD8+ T cell invasion into muscle cells and its cytotoxic role, Rheumatol. Oxf. Engl. Sep (2020) 224–232, https://doi.org/10.1093/rheumatology/kez248.
[11] T. Müntefering, A.P.E. Michels, S. Pfeuffer, S.G. Meuth, T. Ruck, Isolation of primary murine skeletal muscle microvascular endothelial cells, J. Vis. Exp. JoVE. (2019), https://doi.org/10.3791/58901.
[12] I.M. Bronner, J.E. Hoogendijk, H. Veldman, M. Ramkema, M.A. van den Bergh Weerman, A.J.M. Rozemuller, M. de Visser, Tubuloreticular structures in different types of myositis: implications for pathogenesis, Ultrastruct. Pathol. 32 (2008) 123–126, https://doi.org/10.1080/01913120802209379.
[13] P. Englund, I. Nennesmo, L. Klareskog, I.E. Lundberg, Interleukin-1alpha expression in capillaries and major histocompatibility complex class I expression in type II muscle fibers from polymyositis and dermatomyositis patients: important pathogenic features independent of inflammatory cell clusters in muscle tissue, Arthritis Rheum. 46 (2002) 1044–1055, https://doi.org/10.1002/art.10140.
[14] S. Gao, X. Zuo, D. Liu, Y. Xiao, H. Zhu, H. Zhang, H. Luo, The roles of neutrophil serine proteinases in idiopathic inflammatory myopathies, Arthritis Res. Ther. 20 (2018) 134, https://doi.org/10.1186/s13075-018-1632-x.
[15] K. Nagaraju, L.G. Rider, C. Fan, Y.-W. Chen, M. Mitsak, R. Rawat, K. Patterson, C. Grundtman, F.W. Miller, P.H. Plotz, E. Hoffman, I.E. Lundberg, Endothelial cell activation and neovascularization are prominent in dermatomyositis, J. Autoimmune Dis. 3 (2006) 2, https://doi.org/10.1186/1740-2557-3-2.
[16] S. Sabbagh, I. Pinal-Fernandez, T. Kishi, I.N. Targoff, F.W. Miller, L.G. Rider, A. L. Mammen, Childhood Myositis Heterogeneity Collaborative Study Group, Anti-Ro52 autoantibodies are associated with interstitial lung disease and more severe disease in patients with juvenile myositis, Ann. Rheum. Dis. 78 (2019) 988–995, https://doi.org/10.1136/annrheumdis-2016-215004.
[17] M.A.A.G. Vianna, C.T.L. Borges, E.F. Borba, M.T.C. Caleiro, E. Bonfá, S.K.N. Marie, Myositis in mixed connective tissue disease: a unique syndrome characterized by immunohistopathologic elements of both polymyositis and dermatomyositis, Arq. Neuropsiquiatr. 62 (2004) 923–934, https://doi.org/10.1590/s0004-282x2004000600001.
[18] I.E. Lundberg, The role of cytokines, chemokines, and adhesion molecules in the pathogenesis of idiopathic inflammatory myopathies, Curr. Rheumatol. Rep. 2 (2000) 216–224, https://doi.org/10.1007/s11926-000-0082-y.
[19] S. Bittner, T. Ruck, M.K. Schuhmann, A.M. Herrmann, H.M. ou Maati, N. Bobak, K. Göbel, F. Langhauser, D. Stegner, P. Ehling, M. Borsotto, H.-C. Pape, B. Nieswandt, C. Kleinschnitz, C. Heurteaux, H.-J. Galla, T. Budde, H. Wiendl, S. G. Meuth, Endothelial TWIK-related potassium channel-1 (TREK1) regulates immune-cell trafficking into the CNS, Nat. Med. 19 (2013) 1161–1165, https://doi.org/10.1038/nm.3303.
[20] A.M. Afzali, T. Ruck, A.M. Herrmann, J. Iking, C. Sommer, C. Kleinschnitz, C. Preu, e, W. Stenzel, T. Budde, H. Wiendl, S. Bittner, S.G. Meuth, The potassium channels TASK2 and TREK1 regulate functional differentiation of murine skeletal muscle cells, Am. J. Physiol. Cell Physiol. 311 (2016) C583, https://doi.org/10.1152/ajpcell.00363.2015. C595p.
[21] S. Bittner, T. Ruck, J. Fernández-Orth, S.G. Meuth, TREK-king the blood-brain-barrier, J. Neuroimmune Pharmacol. Off. J. Soc. Neuroimmune Pharmacol. 9 (2014) 293–301, https://doi.org/10.1007/s11481-014-9530-9.
[22] Y. Fang, X. Huang, Y. Wan, H. Tian, Y. Tian, W. Wang, S. Zhu, M. Xie, Deficiency of TREK-1 potassium channel exacerbates secondary injury following spinal cord injury in mice, J. Neurochem. 141 (2017) 236–246, https://doi.org/10.1111/jnc.13980.
[23] Y. Fang, Y. Tian, Q. Huang, Y. Wan, L. Xu, W. Wang, D. Pan, S. Zhu, M. Xie, Deficiency of TREK-1 potassium channel exacerbates blood-brain barrier damage and neuroinflammation after intracerebral hemorrhage in mice, J. Neuroinflammation 16 (2019) 96, https://doi.org/10.1186/s12974-019-1485-5.
[24] C. Heurteaux, N. Guy, C. Laigle, N. Blondeau, F. Duprat, M. Mazzuca, L. Lang-Lazdunski, C. Widmann, M. Zanzouri, G. Romey, M. Lazdunski, TREK-1, a K+ channel involved in neuroprotection and general anesthesia, EMBO J. 23 (2004) 2684–2695, https://doi.org/10.1038/sj.emboj.7600234.
[25] C. Preuße, Y. Allenbach, O. Hoffmann, H.-H. Goebel, D. Pehl, J. Radke, A. Doeser, U. Schneider, R.H.E. Aiten, T. Kallinich, O. Benveniste, A. von Moers, B. Schoser, U. Schara, W. Stenzel, Differential roles of hypoxia and innate immunity in juvenile and adult dermatomyositis, Acta Neuropathol. Commun. 4 (2016) 45, https://doi.org/10.1186/s40478-016-0308-5.
[26] C. Preuße, B. Paesler, C. Nelke, D. Cengiz, T. Müntefering, A. Roos, D. Amelin, Y. Allenbach, A. Uruha, C. Dittmayer, A. Hentschel, M. Pawlitzki, S. Hoffmann, S. Timm, S.L. Louis, N.F. Dengler, H. Wiendl, J.D. Lünemann, A. Sickmann, B. Hervier, S.G. Meuth, U. Schneider, A. Schänzer, S. Krause, S. Tomaras, E. Feist, R. Hassell, H.-H. Goebel, L. Gallay, N. Streichenberger, O. Benveniste, W. Stenzel, T. Ruck, Skeletal muscle provides the immunological micro-milieu for specific plasma cells in anti-synthetase syndrome-associated myositis, Acta Neuropathol. (2022), https://doi.org/10.1007/s00401-022-02438-z.
[27] A. Mauedanskas, O. Mölberg, N. Porat-Shliom, M. Sramkova, T. Wigand, P. Amornphimoltham, R. Weigert, Intravital microscopy, BioArchitecture 2 (2012) 143–157, https://doi.org/10.4161/bioa.21758.
[28] K. Flanagan, D. Moroziewicz, H. Kwak, H. Hörig, H.L. Kaufman, The lymphoid chemokine CCL21 costimulates naive T cell expansion and Th1 polarization of non-regulatory CD4+ T cells, Cell. Immunol. 231 (2004) 75–84, https://doi.org/10.1016/j.cellimm.2004.12.006.
[29] A.M. Afzali, T. Ruck, H. Wiendl, S.G. Meuth, Animal models in idiopathic inflammatory myopathies: how to overcome a translational roadblock? Autoimmun. Rev. 16 (2017) 478–494, https://doi.org/10.1016/j.autrev.2017.03.001.
[30] S. Stebe, K. Schellig, F. Lesage, H. Breer, J. Fleischer, The thermosensitive potassium channel TREK-1 contributes to coolness-evoked responses of Grueneberg ganglion neurons, Cell. Mol. Neurobiol. 34 (2014) 113–122, https://doi.org/10.1007/s10571-013-9992-x.
[31] T. Zyrianova, B. Lopez, R. Olcese, J. Belperio, C.M. Waters, L. Wong, V. Nguyen, S. Talapaneni, A. Schwingshackl, K2P2.1 (TREK-1) potassium channel activation protects against hyperoxia-induced lung injury, Sci. Rep. 10 (2020), 22011, https://doi.org/10.1038/s41598-020-78886-y.
[32] M. Tateyama, I. Nagano, M. Yoshioka, K. Chida, S. Nakamura, Y. Itoyama, Expression of tumor necrosis factor-α in muscles of polymyositis, J. Neurol. Sci. 146 (1997) 45–51, https://doi.org/10.1016/S0022-510X(96)00280-8.
[33] H. Varsani, S.C. Charman, C.K. Li, S.K.N. Marie, A.A. Amato, B. Banwell, K.E. Bove, A.M. Corse, A.M. Emslie-Smith, T.S. Jacques, I.E. Lundberg, C. Minetti, I. Nennesmo, E.J. Rushing, A.M.E. Sallum, C. Sewry, C.A. Pilkington, J.L. Holton, L. R. Wedderburn, UK Juvenile Dermatomyositis Research Group, Validation of a score tool for measurement of histological severity in juvenile dermatomyositis and association with clinical severity of disease, Ann. Rheum. Dis. 74 (2015) 204–210, https://doi.org/10.1136/annrheumdis-2013-203396.
[34] L.R. Wedderburn, H. Varsani, C.K.C. Li, K.R. Newton, A.A. Amato, B. Banwell, K. E. Bove, A.M. Corse, A. Emslie-Smith, B. Harding, J. Hoogendijk, I.E. Lundberg, S. Marie, C. Minetti, I. Nennesmo, E.J. Rushing, C. Sewry, S.C. Charman, C. A. Pilkington, J.L. Holton, UK Juvenile Dermatomyositis Research Group, International consensus on a proposed score system for muscle biopsy evaluation in patients with juvenile dermatomyositis: a tool for potential use in clinical trials, Arthritis Rheum. 57 (2007) 1192–1201, https://doi.org/10.1002/art.23012.
[35] Role of TREK-1 in Health and Disease, Focus on the Central Nervous System, (n.d.). https://www.ncbi.nlm.nih.gov/pmc/articles/PMC6470294/ (accessed March 12, 2022).
[36] R. Abou-Khalil, F. Le Grand, G. Pallafacchina, S. Valable, F.-J. Authier, M. A. Rudnicki, R.K. Gherardi, S. Germain, F. Chretien, A. Sotiropoulos, P. Lafuste, D. Montarras, B. Chazaud, Autocrine and paracrine angiopoietin 1/Tie-2 signaling promotes muscle satellite cell self-renewal, Cell Stem Cell 5 (2009) 298–309, https://doi.org/10.1016/j.stem.2009.06.001.
[37] C. Christov, F. Chrétien, R. Abou-Khalil, G. Bassez, G. Vallet, F.-J. Authier, Y. Bassaglia, V. Shinin, S. Tajbakhsh, B. Chazaud, R.K. Gherardi, Muscle satellite cells and endothelial cells: close neighbors and privileged partners, Mol. Biol. Cell 18 (2007) 1397–1409, https://doi.org/10.1091/mbc.e06-08-0693.
[38] M. Verma, Y. Asakura, B.S.R. Murakonda, T. Pengo, C. Latroche, B. Chazaud, L. K. McLoon, A. Asakura, Muscle satellite cell cross-talk with a vascular niche

maintains quiescence via VEGF and notch signaling, Cell Stem Cell 23 (2018) 530–543.e9, https://doi.org/10.1016/j.stem.2018.09.007.
[39] T. Ruck, S. Bock, S. Pfeuffer, C.B. Schroeter, D. Cengiz, P. Marciniak, M. Lindner, A. Herrmann, M. Liebmann, S. Kovac, L. Gola, L. Rolfes, M. Pawlitzki, N. Opel, T. Hahn, U. Dannlowski, T. Pap, F. Luessi, J.A. Schneider, B. Wünsch, T. Kuhlmann, G. Seebohm, B. Tackenberg, P. Seja, F. Döring, E. Wischmeyer, A.I. Chasan, J. Roth, L. Klotz, G. Meyer Zu Hörste, H. Wiendl, T. Marschall, S. Floess, J. Huehn, T. Budde, T. Bopp, S. Bittner, S.G. Meuth, K2P18.1 translates T cell receptor signals into thymic regulatory T cell development, Cell Res. 32 (2022) 72–88, https://doi.org/10.1038/s41422-021-00580-z.
[40] J. Masella, O. Péranzi, G. Lucas, C. Deval, S. Bérzud-Dufour, C. Gandin, M. El-Yacoubi, C. Widmann, A. Guyon, E. Chevet, S. Taouji, G. Conductier, A. Corinus, T. Coppola, G. Gobbi, J.-L. Nahon, C. Heurteaux, M. Borsotto, Spadin, a sortilin-derived peptide, targeting rodent TREK-1 channels: a new concept in the antidepressant drug design, PLoS Biol. 8 (2010), e1000355, https://doi.org/10.1371/journal.pbio.1000355.
[41] H. Huang, J.-Q. Liu, Y. Yu, L.-H. Mo, R.-T. Ge, H.-P. Zhang, Z.-G. Liu, P.-Y. Zheng, P.-C. Yang, Regulation of TWIK-related potassium channel-1 (Trek1) restitutes intestinal epithelial barrier function, Cell. Mol. Immunol. 13 (2016) 110–118, https://doi.org/10.1038/cmi.2014.137.
[42] I. Lauritzen, J. Chemin, E. Honoré, M. Jodar, N. Guy, M. Lazdunski, A. Jane Patel, Cross-talk between the mechano-gated K2P channel TREK-1 and the actin cytoskeleton, EMBO Rep. 6 (2005) 642–648, https://doi.org/10.1038/sj.embor.7400449.
[43] L. Pope, C. Arrigoni, H. Lou, C. Bryant, A. Gallardo-Godoy, A.R. Renslo, D.L. Minor, Protein and chemical determinants of BL-1249 action and selectivity for K2P channels, ACS Chem. Neurosci. 9 (2018) 3153–3165, https://doi.org/10.1021/acschemneuro.8b00337.

Acta Neuropathologica (2023) 146:725–745
https://doi.org/10.1007/s00401-023-02637-2

ORIGINAL PAPER

Senescent fibro-adipogenic progenitors are potential drivers of pathology in inclusion body myositis

Christopher Nelke[1] · Christina B. Schroeter[1] · Lukas Theissen[1] · Corinna Preusse[2] · Marc Pawlitzki[1] · Saskia Räuber[1] · Vera Dobelmann[1] · Derya Cengiz[1] · Felix Kleefeld[3] · Andreas Roos[4] · Benedikt Schoser[5] · Anna Brunn[6] · Eva Neuen-Jacob[6] · Jana Zschüntzsch[7] · Sven G. Meuth[1] · Werner Stenzel[2] · Tobias Ruck[1]

Received: 23 June 2023 / Revised: 18 September 2023 / Accepted: 19 September 2023 / Published online: 29 September 2023

Abstract
Inclusion body myositis (IBM) is unique across the spectrum of idiopathic inflammatory myopathies (IIM) due to its distinct clinical presentation and refractoriness to current treatment approaches. One explanation for this resistance may be the engagement of cell-autonomous mechanisms that sustain or promote disease progression of IBM independent of inflammatory activity. In this study, we focused on senescence of tissue-resident cells as potential driver of disease. For this purpose, we compared IBM patients to non-diseased controls and immune-mediated necrotizing myopathy patients. Histopathological analysis suggested that cellular senescence is a prominent feature of IBM, primarily affecting non-myogenic cells. In-depth analysis by single nuclei RNA sequencing allowed for the deconvolution and study of muscle-resident cell populations. Among these, we identified a specific cluster of fibro-adipogenic progenitors (FAPs) that demonstrated key hallmarks of senescence, including a pro-inflammatory secretome, expression of p21, increased β-galactosidase activity, and engagement of senescence pathways. FAP function is required for muscle cell health with changes to their phenotype potentially proving detrimental. In this respect, the transcriptomic landscape of IBM was also characterized by changes to the myogenic compartment demonstrating a pronounced loss of type 2A myofibers and a rarefication of acetylcholine receptor expressing myofibers. IBM muscle cells also engaged a specific pro-inflammatory phenotype defined by intracellular complement activity and the expression of immunogenic surface molecules. Skeletal muscle cell dysfunction may be linked to FAP senescence by a change in the collagen composition of the latter. Senescent FAPs lose collagen type XV expression, which is required to support myofibers' structural integrity and neuromuscular junction formation in vitro. Taken together, this study demonstrates an altered phenotypical landscape of muscle-resident cells and that FAPs, and not myofibers, are the primary senescent cell type in IBM.

Keywords Senescence · Inclusion body myositis · Acetylcholine receptor · Single nuclei · Myofiber · Complement

✉ Tobias Ruck
Tobias.Ruck@med.uni-duesseldorf.de

[1] Department of Neurology, Medical Faculty, Heinrich Heine University Duesseldorf, Moorenstr. 5, 40225 Duesseldorf, Germany

[2] Department of Neuropathology, Charité–University Medicine Berlin, Bonhoefferweg 3, 10117 Berlin, Germany

[3] Department of Neurology, Charité–University Medicine Berlin, Bonhoefferweg 3, 10117 Berlin, Germany

[4] Department of Neuropediatrics, Developmental Neurology and Social Pediatrics, Centre for Neuromuscular Disorders in Children, University Hospital Essen, University of Duisburg-Essen, Essen, Germany

[5] Friedrich Baur Institute at the Department of Neurology, LMU University Hospital, LMU Munich, 80336 Munich, Germany

[6] Institute of Neuropathology, Heinrich Heine University, University Hospital of Düsseldorf, Düsseldorf, Germany

[7] Department of Neurology, University Medical Center Göttingen, Robert-Koch-Str. 40, Göttingen, Germany

Introduction

The spectrum of idiopathic inflammatory myopathies (IIM) is characterized by muscle inflammation as a pathogenic hallmark [1, 36]. Among IIM, inclusion body myositis (IBM) is a unique entity due to its characteristic clinical presentation, advanced age at onset, and notable refractoriness to contemporary treatment strategies [17]. As such, IBM leads to progressive muscle damage and weakness resulting in an unmet need for novel treatment approaches.

One explanation for the treatment refractoriness of IBM might be the instigation of cell-autonomous mechanisms that promote disease progression independent of ongoing inflammatory activity. Skeletal muscle is constituted of myogenic and non-myogenic cells. The complex interplay of these cells is required to maintain muscle health and for the resolution of inflammation [39, 43]. However, IBM imposes a burden of chronic inflammation on the compartment, potentially shifting the cellular homeostasis to a detrimental muscle phenotype [7, 17, 40]. Indeed, in response to chronic stress or damage, cells may assume a state of stable cell cycle arrest termed cellular senescence [44]. These cells continue to influence their environment by engaging a specific senescence-associated secretory phenotype (SASP) characterized by immunomodulatory cytokines, growth factors, and proteases. Following this line of argumentation, accumulation of senescent cells in skeletal muscle may constitute a cell-autonomous mechanism by which muscle-resident cells promote compartmentalized inflammation and fibrotic remodelling in IBM.

Succeeding the identification and characterization of highly cytotoxic, terminally differentiated CD8 T cells [16, 18], renewed attention has been focused on the development of immunomodulatory strategies for IBM, e.g. the depletion of KLRG1$^+$ CD8 T cells [14]. However, addressing the deterioration of the skeletal muscle compartment might improve efficacy of those treatment strategies.

To understand whether IBM instigates cell-autonomous mechanisms, we studied cellular senescence in the skeletal muscles of IBM patients and compared them with those of non-diseased controls (NDC) and immune-mediated necrotizing myopathies (IMNM) as diseased control. Employing a single-nuclei transcriptomic approach, we describe a novel population of senescent fibro-adipogenic progenitors (FAPs) that may induce distinct alterations of the myogenic compartment. Given the growing interest and availability of senotherapeutics [21, 44], targeting these cells may provide an innovative strategy to ameliorate the muscle phenotype of IBM.

Methods

Ethics statement

The study was conducted in accordance with the Declaration of Helsinki and approved by the ethics committee of the Heinrich Heine University Duesseldorf (2016-053-f-S and 2021-1417) and the Charité Berlin (EA2/163/17). This study analysed skeletal muscle biopsies acquired from IIM patients and non-diseased controls (NDCs). All patients signed written informed consent before acquisition of the biopsy and clinical metadata.

Patient recruitment and clinical data

Patients were recruited from three tertiary centres specialized in the management of IIM (University Hospital Duesseldorf, Charité–University Medicine Berlin, and University Medical Center Göttingen). Patients treated in the outpatient clinic and patients admitted to the hospital were asked for study inclusion as well as written consent. Patients were recruited from January 2014 to January 2022. As disease control, we chose immune-mediated necrotizing myopathy (IMNM) as these patients rarely demonstrate extra-muscular manifestations, similar to IBM. IBM and IMNM patients were required to meet the European Neuromuscular Centre (ENMC) criteria for diagnosis [1, 2, 54]. NDCs served as an additional control cohort. As previously proposed by our group [53], these patients underwent muscle biopsy for diagnostic purposes, e.g. for myalgia. These patients were required not to have any objective muscle weakness or abnormal creatine kinase levels. On muscle histology, the patient's specimens were required to demonstrate no signs of inflammation or any other structural abnormalities. These patients had no myositis-specific or myositis-associated antibodies. Given the impact of age on the study readout of cellular senescence, NDC and IMNM patients were age-matched to IBM patients (maximum difference in age of 3 years). This study included 16 IBM, 16 NDC and 16 IMNM patients. The individual number of patients is given for each experiment as indicated. The disease duration was defined as the time between the first symptoms as reported by the patients to the time of muscle biopsy.

Biomaterial

All skeletal muscle specimens had been cryopreserved at − 80 °C before analysis according to the predefined standard operating procedure at the local biobank of the Heinrich Heine University Duesseldorf and the Charité Berlin.

Immunofluorescence

Immunofluorescence (IF) was performed as previously described [53]. Briefly, all stains were performed on 8 µm cryostat sections. We used irrelevant antibody stains (either mouse/rabbit monoclonal/polyclonal isotype controls) as negative controls, as well as omission of the primary antibody. The following antibodies were used for staining procedures: Laminin-β1 (Rabbit, 1:100, Novus Biologicals), p21 (Mouse, 1:50, Novus Biologicals), C3 (Rat, 1:100, Santa Cruz), PDGFRa (Mouse, 1:50, Novus Biologicals), α-bungarotoxin (Snake, 1:50, Invitrogen). The secondary antibodies for immunofluorescence were anti-rabbit (Alpaca, 1:200, Jackson ImmunoResearch), anti-rat (Alpaca, 1:200, Jackson ImmunoResearch) and anti-mouse (Alpaca, Jackson ImmunoResearch). Specimen were analysed using Zeiss Axio (for 10 and 20-fold magnification) or LSM 880, Zeiss (for 40 and 63-fold magnification) in cooperation with the Core Facility for Advanced Light Microscopy, Heinrich Heine University Düsseldorf. The biopsies were blinded for quantification with the diagnosis not possible to identify from the label. The scoring was performed in randomly distributed 10 high-power fields (HPF, based on the microscope used and the respective oculars ≙ 0.16 mm^2) as previously described [53].

Quantitative reverse transcription PCR (qRT-PCR)

Total RNA was extracted from muscle specimens as previously described [53]. cDNA was synthesized using the High-Capacity cDNA Archive Kit (Applied Biosystems, Foster City, CA). For reactions, 10 ng of cDNA were used on the 7900HT Fast Real-Time PCR System (Applied Biosystems, Foster City, CA) with the following running conditions: 95 °C 0:20, 95 °C 0:01, 60 °C 0:20, 45 cycles (values above 40 cycles were defined as "not expressed"). All targeted transcripts were run as triplicates. For each of these runs, the reference gene *PGK1* has been included as internal control to normalize the relative expression of the targeted transcripts. The $2^{-\Delta\Delta CT}$ method was used to quantify gene expression of IBM and IMNM patients compared to NDCs.

Isolation, purification, and cultivation of primary human muscle cells

Muscle tissue was dissociated using a muscle dissociation kit (Miltenyi Biotec, Bergisch Gladbach, Germany) according to the manufacturer's instructions. For primary human skeletal muscle cell (PHMC) purification, we used a CD56 (clone N901, Beckman Coulter) antibody combined with microbead magnetic separation. For cultivation, we used Biolaminin 521 LN coated 6-well plates and skeletal muscle cell growth medium (PELOBiotech, Planegg, Germany) according to the manufacturer's instructions. For all experiments, we used differentiated PHMCs by allowing cells to grow to 100% confluence. These PHMC cultures contain different degrees of myoblast differentiation as well as myotubes.

Flow cytometry

PHMC were analysed by flow cytometry. Cells were treated and cultivated as indicated in the corresponding section. Cells were then washed with ice-cold PBS and scraped. The cells were centrifuged, and the pellet was washed before staining. PHMC were stained with the α-bungarotoxin antibody (CF555, Invitrogen). 1 × 106 PHMC per well was co-cultivated with the indicated concentrations of collagen for 24 h. Recombinant COL1A1 and COL15A1 were purchased from Abbexa, Cambridge, England.

Live/dead assay

For the assessment of viability, we used the LIVE/DEAD Viability/Cytotoxicity Kit for mammalian cells (Invitrogen, Waltham, Massachusetts) according to the manufacturer's instructions. Briefly, 1 × 10^6 PHMC per well were co-cultivated with the indicated concentrations of collagen for 24 h. Cell viability was assessed by fluorescence microscopy. Live cells were identified by green-fluorescent calcein-AM indicating intracellular esterase activity. Dead cells were identified by red-fluorescent ethidium homodimer-1 indicating a loss of membrane integrity. For each sample, 100 cells were counted and the frequencies of live or dead cells were recorded.

ATPase staining

ATPase enzyme histochemical preparations at pH 4.3, 4.6, and 9.4 were performed according to standard protocols to highlight type 1 and type 2A and 2X fibers [10].

Isolation of single nuclei from muscle biopsies

Single nuclei were isolated from frozen muscle biopsy specimens. Approximately 60 mg of muscle was used for each sample. All biopsies were taken from the quadriceps muscle (vastus medialis) approximately 3 cm proximal to the knee joint.

The single nuclei suspension was obtained using GEXSCOPE® Single Nucleus RNA Library Kit V2 (Singleron Biotechnologies) as previously described [34]. Briefly, on ice, the tissue was immersed in a cold nucleus separation solution and cut into small pieces. Further homogenization was achieved by performing 5 strokes with pestle A and 5 strokes with pestle B of the Kimble

douncer (KIMBLE® KONTES® Dounce Tissue Grinder). The sample was then incubated on ice for 15 min, where the state of dissociation was monitored every 5 min under a light microscope. Following homogenization and digestion, the suspension was filtered using a 40 µm sterile strainer. The nuclei suspension was centrifuged at 200×*g* for 2 min at 4 °C, and the supernatant was centrifuged at 500×*g* for 5 min at 4 °C. The resulting pellet containing nuclei was resuspended in 0.25 ml cold nuclei suspension buffer. The quality of the nuclei was assessed by Trypan Blue staining (0.4% w/v, Gibco) under a light microscope. The nuclei were counted using propidium iodine with a Luma FX7 automated cell counter (Logos Biosystems, Villeneuve d'Ascq, France).

Library generation and sequencing

A total of 30 000 nuclei were loaded onto a microfluidic chip (Singleron GEXSCOPE® Single Nucleus RNA Library Kit V2) for a minimal capture of 6000 nuclei for each sample. Barcoded beads containing a unique cell barcode were loaded into the chip, and nuclei were lysed. After nuclei lysis, polyadenylated RNA was captured onto the Barcode Beads by the poly (dT) sequence. Barcode Beads with captured mRNA molecules were collected and subjected to reverse transcription reaction. The cDNA was then amplified and QC. NGS libraries generated were sequenced on an Illumina NovaSeq 6000 instrument using a paired-end 150 bp approach. The reads were demultiplexed on Illumina's BaseCloud, and fastq files were used to initiate data analysis.

Bioinformatics workflow

Illumina reads (fastq files) were processed to gene expression matrices using CeleScope™ (v1.14.1., www.github.com/singleron-RD/CeleScope; Singleron Biotechnologies). Briefly, fastq files were demultiplexed according to their respective cell barcodes and UMIs. Adapter sequences and poly-A tails were trimmed (cutadapt; https://cutadapt.readthedocs.io/en/stable/installation.html) and the trimmed Read2 reads were aligned to the GRCh38 version of the human genome with Ensembl version 92 gene annotations (STAR v2.6.1a_08-27 [https://github.com/alexdobin/STAR] and featureCounts 2.0.1). We excluded cells with a unique feature count over 2500 or below 200 or cells with a mitochondrial ratio of more than 5%. A combined digital expression matrix was constructed, containing all sequenced experiments, for downstream analysis. Analysis was performed in Seurat (v4.3.0). Data were normalized using the NormalizeData function and 2000 features with high cell-to-cell variation were calculated using the FindVariableFeatures function. For data integration of IBM and NDC samples, we employed the integration workflow as proposed for the Seurat workspace [57]. The FindIntegrationAnchors function was used to assemble all snRNA-seq datasets into an integrated and unbatched dataset. Next, to reduce dimensionality of the datasets, the RunPCA function was conducted with default parameters on linear-transformation scaled data generated by the ScaleData function. After integration, we performed a modularity-optimized Louvain clustering with a resolution of 0.8.

Cluster annotations

The FindAllMarkers function was used to identify cluster-specific markers with a fold-change threshold of 0.25 and min.pct set to 0.25. Clusters were then classified and annotated based on expressions of canonical markers of particular cell types. The complete list of markers for all clusters is available as Supplemental File 1.

Subclustering

As indicated, clusters of interest were extracted from the integrated dataset for in-depth analysis and subclustering. Principal component analysis and clustering were repeated as described above.

Differential expression testing and functional enrichment analysis

Differential gene expression testing was performed using the FindMarkers function using Wilcox testing and a fold-change threshold of 0.25. The Bonferroni correction was used based on the total number of genes in the dataset. Differentially expressed genes (DEGs) were selected based on the adjusted *p* value.

DEGs were used for gene set enrichment analysis (GSEA) using the ClusterProfiler package (v4.3.1) and the Gene Ontology (GO) "Biological Process" and the "Reactome" databases.

For targeted GSEA analysis, we used Genetrail (https://genetrail.bioinf.uni-sb.de/start.html) with the SenMayo gene set (v2023.1.Hs, available from https://www.gsea-msigdb.org/gsea/index.jsp as "SAUL_SEN_MAYO").

Cell–cell communication was analysed using the CellChat package (v1.5.0) as proposed by the developers.

Statistical analysis

Statistical analysis was performed using *R* 3.5.3. Data were presented as median with IQR, mean ± standard deviation (SD), as absolute (*n*) or relative frequencies (%). Differences between the two groups were analysed using the

Mann–Whitney *U* test. The Kruskal–Wallis test was used for multiple groups.

$p > 0.05$ was classified as not significant, $p < 0.05$ as significant (*), $p < 0.01$ (**), $p < 0.001$ (***).

Results

p21$^+$ senescent cells are abundant in the muscle of IBM

First, we sought to determine whether the number of senescent cells is altered in IBM compared to NDC and IMNM patients. For this purpose, we recruited a multicentric cohort of 48 patients (16 per group) in three tertiary centres specialized in managing IIMs. The clinical and epidemiological characteristics are given in Table 1. Given that age is likely to have a major impact on the development of cellular senescence, NDC and IMNM patients were matched to IBM by age to account for this confounder. For diagnosis of IBM and IMNM, patients were required to meet the current ENMC criteria for diagnosis, respectively [2, 35]. Briefly, IBM patients were 73 (45–87) years old with 7 males and 9 females. 5 out of 16 patients received intravenous immunoglobulin treatment at the time of biopsy. No other immunosuppressants were recorded for the IBM cohort.

As the first readout, we focused on the study of p21, an established marker for cellular senescence [15]. This choice was motivated by several recent studies in murine and human tissues demonstrating that p21 governs a senescent program in skeletal muscle and serves as a marker for muscle cell senescence [12, 50, 64]. We assessed the number of p21$^+$ cells by IF (Fig. 1a). Given the nuclear expression of p21, only cells that demonstrated clear co-localization of p21 and DAPI were considered to be p21$^+$. Indeed, the number of p21$^+$ cells was higher in IBM as compared to NDC and IMNM patients (Fig. 1b). To further corroborate this data, we also analysed p21 at the gene level by PCR observing an increased expression of *CDKN1A* (coding for p21) in IBM compared to NDC or IMNM patients

Table 1 Clinical and demographic characteristics

Characteristics	IBM ($n = 16$)	NDC ($n = 16$)	IMNM ($n = 16$)
Median age at diagnosis (years, range)	73 (45–87)	72 (44–86)	74 (46–85)
Median disease duration* (months, range)	7 (0–32)	3 (0–18)	2 (1–6)
Gender, *n* (%)			
Female	9 (56%)	8 (50%)	7 (44%)
Male	7 (44%)	8 (50%)	9 (56%)
Creatine kinase (U/l, mean, SD)	209 (45)	104 (98)	1509 (540)
Antibody status, *n* (%)			
Anti-cN-1A	9 (56%)	0 (0%)	0 (0%)
Anti-SRP	0 (0%)	0 (0%)	7 (44%)
Anti-HMGCR	0 (0%)	0 (0%)	8 (50%)
None	7 (44%)	16 (100%)	1 (6%)
Symptoms, *n* (%)			
Muscle weakness and atrophy	16 (100%)	0 (0%)	15 (94%)
Myalgia	2 (13%)	11 (69%)	11 (69%)
Dysphagia	12 (76%)	2 (13%)	7 (44%)
Lung involvement	0 (0%)	0 (0%)	4 (25%)
Treatment, *n* (%)			
Treatment naïve	11 (69%)	15 (94%)	2 (13%)
IVIG	5 (31%)	0 (0%)	4 (25%)
Steroids	2 (13%)	1 (6%)**	9 (56%)
Steroid dose per day (mean, SD)	10 (10)	5 (0)	30 (25)
Azathioprine	0 (0%)	0 (0%)	2 (13%)
Rituximab	0 (0%)	0 (0%)	2 (13%)

HMGCR HMG-CoA reductase; *IBM* inclusion body myositis; *IMNM* immune-mediated necrotizing myopathy; *NDC* non-diseased control; *SD* standard deviation; *SRP* signal recognition particle

*Disease duration was defined between the time of first symptoms as reported by the patient and the time of biopsy

**One NDC received steroids for the treatment of psoriasis

Fig. 1 p21$^+$ senescent cells are abundant in muscle of IBM. **a** Immunofluorescence staining of p21 (red), laminin-β1 (green), and DAPI (blue) in muscle specimens of NDCs ($n = 16$), IBM ($n = 16$), and IMNM ($n = 16$) patients. Patients were matched by age. Arrows indicate single p21$^+$ cells or clusters of p21$^+$ cells. **b** p21+cells were counted in randomly distributed 10 HPF (⌀ 0.16 mm^2). The biopsies were blinded for quantification, with the diagnosis impossible to identify from the label. p21$^+$ cells were defined as cells with a clear expression of p21 in the nucleus. **c** RT-qPCR analysis of *CDKN1A* coding for p21 in muscle specimen ($n = 16$ per group). The $2^{-\Delta\Delta CT}$ method was used for normalization. CDKN1A is significantly over-expressed to NDC for both IBM and IMNM. **d** Quantification of p21$^+$ myonuclei in muscle in muscle specimen ($n = 16$ per group). p21$^+$ myonuclei were defined as nuclei located inside a muscle fiber. **e** Exemplary image of a p21+nucleus located inside a myofiber. Differences between groups were analysed by Kruskal–Wallis test followed by post hoc testing. **f** Simple linear regression of the number of p21+cells and the disease duration of each IBM patient. The disease duration was defined as the time in months between the first symptoms as reported by the patient and the time of biopsy. The dotted line indicates the 95% confidence interval. Significance was tested by the likelihood test. *$p < 0.05$, **$p < 0.01$, ***$p < 0.001$. *NDC* non-diseased control; *HPF* high-power field; *IBM* inclusion body myositis; *IMNM* immune-mediated necrotizing myopathy; *r2* coefficient of determination; *RT-qPCR* real-time quantitative polymerase chain reaction

(Fig. 1c). Intriguingly, a substantial number of p21$^+$ cells were detected in the perimysial area in IBM. To clarify the origin of those p21$^+$ cells, we also counted the number of p21$^+$ myonuclei (Fig. 1d). Myonuclei were defined as nuclei localized inside the boundaries of the corresponding myofiber (Fig. 1e). IBM and IMNM patients demonstrated similar numbers of p21$^+$ myonuclei leading us to hypothesize that non-myogenic cells resident in skeletal muscle might primarily assume a senescent phenotype in IBM. Of note, longer disease durations were associated with an increased number of p21$^+$ cells (Fig. 1f). Following this line of argumentation, we aimed to study senescence at the level of single cells (or nuclei) in the landscape of myogenic and non-myogenic cells in the IBM muscle.

Single-nuclei RNA sequencing deconvolutes distinct cell populations and allocates senescence in IBM muscle mainly to fibro-adipogenic progenitors

For this purpose, we performed snRNA-seq of three IBM patients and three NDCs. We chose snRNA-seq as an alternative to single-cell RNA-seq due to the large size of myofibers that restricts the latter's use for studying skeletal muscle [30, 50]. For snRNA-seq, all muscle specimens were obtained from the quadriceps muscle, specifically the vastus medialis, approximately 3 cm proximal to the knee joint. IBM patients were 65, 68, and 71 years old with two male and one female subject. NDCs were age- and sex-matched. All IBM patients and all NDCs were treatment naïve.

After quality control, ~ 30,000 nuclei of which ~ 13,000 were obtained from IBM muscle and ~ 17,000 from NDC were integrated into a batch-corrected expression matrix for downstream analysis. Using graph-based clustering of uniform manifold approximation and projection (UMAP), we observed nine major cell types or subtypes based on differential marker expression (Fig. 2a, b). Cell types were assigned according to the expression of canonical markers (a full list of all marker genes is given in Supplemental File 1) based on previous transcriptomic studies of skeletal muscle [9, 30, 50, 52]. While non-myogenic cells were separated based on their transcriptomic profiles, the classification of myogenic cells was more challenging. Briefly, human skeletal muscle may be classified into slow-twitch (type 1) and fast-twitch (type 2A and type 2X) myofibers based on the presence or absence of specific myosin heavy chains (MYH) [42]. For this study, we annotated the myogenic compartment based on this classification, although it should be noted that some myofibers are considered hybrids falling between canonical subtypes [58]. First, we annotated type 1 myonuclei based on the expression of canonical markers such as *MYH7* or *MYH7B* (Fig. 2a, b) [50, 58]. Second, a subgroup of fast-twitch (type 2X) myonuclei were identified based on the expression of *MYH1* and the absence of *MYH7* [50, 58]. As previously described by Murgia et al., specific markers, except *MYH2*, for the type 2A subgroup of fast-twitch myofibers are currently lacking [42]. Following this line of argumentation, we annotated the final myonuclei cluster as type 2A given the absence of *MYH7* and *MYH1* expression specific for type 1 and type 2X fibers, respectively.

To understand the distribution of senescence in myogenic and non-myogenic cells, we determined the expression of *CDKN1A* across the dataset (Fig. 2c). To compare the cluster-specific frequencies, we calculated the number of *CDKN1A* expressing cells as percentage of all cells in a cluster for IBM and NDC (Fig. 2d). As described in the previous section, the relative frequencies of *CDKN1A*$^+$ nuclei were comparable between IBM and NDC for myonuclei. Intriguingly, the frequencies of *CDKN1A* expressing FAPs and monocytes/macrophages were strongly increased in IBM compared to NDC. However, it should be noted that the expression of a single gene is unlikely to capture the heterogeneity of cellular senescence across tissues. To address this caveat and to further corroborate the engagement of senescence pathways, we determined the differentially expressed genes (DEGs) between IBM and NDC for all cell clusters. Next, we employed the SenMayo gene set for enrichment analysis [56]. Briefly, the SenMayo gene set is a panel composed of 125 key genes associated with senescence signalling pathways. We chose SenMayo as this gene set has been benchmarked against existing senescence or SASP gene sets and outperformed the latter in the detection of senescent cells [56]. DEG lists of all clusters were entered into GSEA

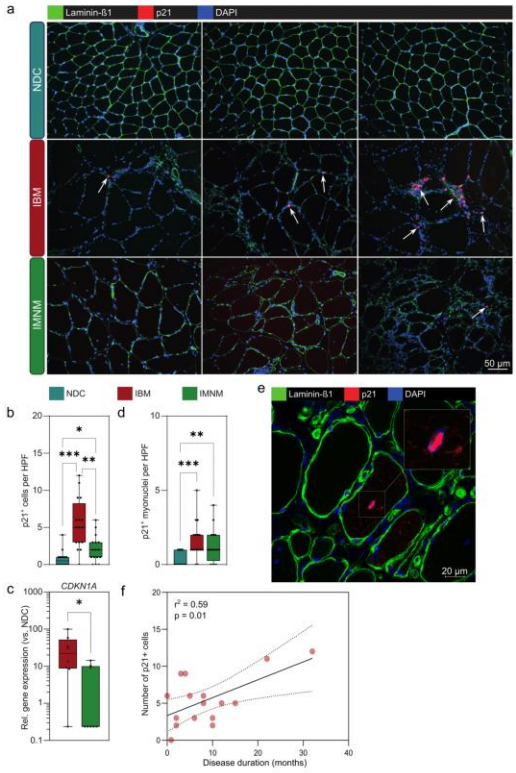

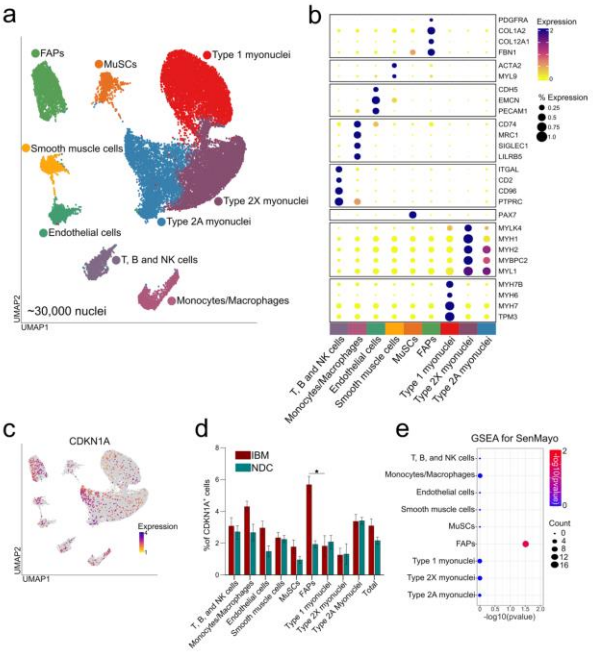

for the SenMayo gene set (Fig. 2e). Only the FAPs cell cluster was enriched for SenMayo in IBM compared to NDC. SnRNA-seq demonstrates the capability of discerning distinct cellular subtypes and suggests that non-myogenic cells assume a senescent phenotype in IBM.

Single-nuclei RNA sequencing identifies a novel population of senescent FAPs that resides in IBM muscle

Next, we focused on the FAP population and extracted this cell cluster for in-depth analysis (Fig. 3a). A total of ~ 3200 FAP nuclei were analysed. FAPs are the lineage precursors of specialized non-myogenic cells, including activated

◂**Fig. 2** Single-nuclei RNA sequencing of IBM and NDC muscle. A total of 6 frozen muscle specimens were processed for single nuclei-RNAseq (3 samples per group). A total of ~ 30,000 nuclei were included for downstream processing and clustering after quality control. **a** UMAP embedding demonstrating distinct clusters of cell types and subtypes. **b** Clustered dot plot visualization of top-regulated marker genes. The mean expression for each cluster is indicated by colour code. The dot size indicates the percent of expressing cells. Clusters were annotated based on marker genes. **c** Expression of CKDN1A (coding for p21) across the UMAP embedding. The mean expression for each cell is indicated by the colour code. **d** Frequency of CDKN1A+cells for each cell cluster as indicated for IBM patients and NDC. Differences between groups were analysed by the Kruskal–Wallis test followed by post hoc testing. **e** Gene set enrichment analysis (GSEA) for the SenMayo dataset. Differentially expressed genes were determined by the FindMarkers function using Wilcox testing and a fold-change threshold of 0.25. The Bonferroni correction was used for correction for multiple testing. DEGs specific to the IBM dataset were entered into the GSEA. The Kolmogorov–Smirnov test, followed by post hoc correction, was used to determine the significance. **$p<0.01$. *ACTA2* actin alpha 2; *CDKN1A* cyclin dependent kinase inhibitor 1A; *CDH5* cadherin 5; *COL* collagen; *EMCN* endomucin; *FBN1* fibrillin-1; *ITGAL* integrin subunit alpha L; *LILRB5* leukocyte immunoglobulin like receptor B5; *MRC1* mannose receptor C-type 1; *MYBPC2* myosin binding protein C2; *MYL9* myosin light chain 9; *NDC* non-diseased control; *IBM* inclusion body myositis; *SIGLEC1* sialic acid binding Ig like lectin 1; *TPM3* tropomyosin 3; *PECAM1* platelet and endothelial cell adhesion molecule 1; *PAX7* paired box 7; *PTPRC* protein tyrosine phosphatase type C (CD45); *UMAP* uniform manifold approximation and projection

fibroblasts, adipocytes, and osteogenic cells [8]. We performed subclustering on these cells and observed 4 subpopulations of FAPs (Fig. 3b, c). We determined marker genes for all FAP subtypes and compared these with previous studies [9, 55]. Although there currently exists no consensus regarding canonical marker genes of human FAPs, Perez et al. previously reported subtypes of FAPs associated with ageing based on the expression of the ryanodine receptor 1 (*RYR1*) and triadin (*TRDN*) [50]. In our dataset, the clusters FAPs2 and FAPs3 were also characterized by *RYR1* and *TRDN* expression. Given the advanced age of IBM patients and NDCs in our cohort, we suspect that these FAPs are reminiscent of these previously reported FAP phenotypes. In contrast, we also determined two clusters of FAPs only found in IBM patients, but not in NDCs. The first cluster was defined by the expression of lumican (*LUM*) and fibrillin-1 (*FBN1*). LUM^+FBN1^+ FAPs were previously described [55] and are thought to resemble neprilysin (*MME*) expressing FAPs associated with fatty infiltration of skeletal muscle. Intriguingly, we also investigated the expression of *CDKN1A* across FAP subtypes and found that the expression of this senescence marker is largely restricted to the LUM^+/FBN^+ FAP population. Consequently, we termed these FAPs $CDKN1A^+$ to underline their senescent phenotype and association with the p21 pathway. This FAP phenotype is found in IBM but not in NDCs (Fig. 3e). The identity of the fourth FAP subtype (FAPs3) is characterized by the expression of XIAP-associated factor 1 (*XAF1*) and dynamin-1 (*DNM1*). These markers were previously described in FAPs [19], however, their role is currently unknown.

Given the scope of this study, we focused our analysis on the $CDKN1A^+$ FAP population. To understand whether these FAPs exhibit senescence features, we determined the marker genes for this cell cluster and performed GSEA for the biological processes (BP) database (Fig. 3f). Here, the humoral immune response was the most enriched term for the $CDKN1A^+$ FAP population. This observation is consistent with current knowledge on the senescent phenotype, as these cells are known to engage a pro-inflammatory secretome (e.g. SASP). To further corroborate a senescent phenotype for these FAPs, we performed GSEA for the SenMayo gene set. Here, marker genes of $CDKN1A^+$ FAPs were enriched for SenMayo indicating the engagement of senescence pathways in these cells (Fig. 3g). We manually screened the marker genes of $CDKN1A^+$ FAPs and observed that these cells express endosialin (CD248), a glycoprotein and key regulator of tissue fibrosis [48, 51, 59]. CD248 expression was only detected in $CDKN1A^+$ FAPs but not in other FAP subtypes (Fig. 3h). Besides CD248, $CDKN1A^+$ FAPs also engage the Jun/JunB signalling pathway [37, 56]. This pathway has been reported to govern fibroblast senescence by inhibition of insulin growth factor-1 (IGF-1) [37]. Surprisingly, $CDKN1A^+$ FAPs also demonstrate upregulation of complement factors such as complement factor 3 (*C3*), complement factor H (*CFH*) or complement factor D (*CFD*). In respect to signalling, $CDKN1A^+$ FAPs express CD44, a pro-inflammatory cell-to-cell signalling receptor, as well as receptors for transforming growth factor beta (TGF-β, *TGFBR2*, and *TGFBR3*). To corroborate that the p21+ cells in the perimysium/endomysium are indeed the FAP phenotype detected in the transcriptomic dataset, we performed IF staining of IBM biopsy specimens (Suppl. Figure 1). Here, $p21^+$ cells located in the perimysium were identified by the canonical FAP marker platelet-derived growth factor receptor α (PDGRA).

To further cross-validate the engagement of senescence in these cells, we additionally investigated the activity of the senescence-associated β-galactosidase (SA-β-Gal) [38, 60]. To enable intracellular staining in tissue sections, we employed SPiDER-β-Gal which exerts higher cell permeability than traditional SA-β-Gal [29]. Indeed, p21 $(CDKN1A)^+$ FAPs were detected in the perimysium of IBM patients and stained positive for SA-β-Gal as an additional biomarker for cellular senescence (Suppl. Fig. 2a).

Succinctly, $CDKN1A+$ FAPs demonstrate key features of cellular senescence including expression of senescence markers, engagement of a pro-inflammatory secretory phenotype and pro-fibrotic surface molecules, the activity of SA-β-gal and a senescence-associated transcriptomic signature.

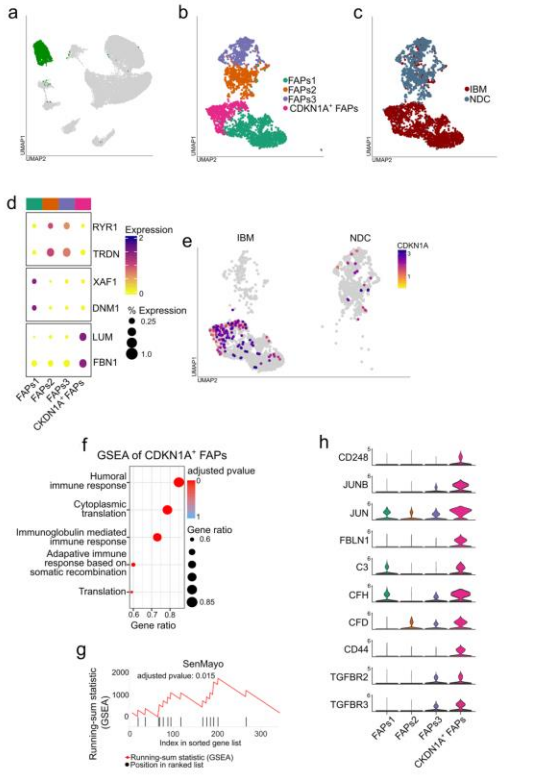

◂**Fig. 3** A novel population of senescent FAPs resides in IBM muscle. **a** UMAP embedding of the full dataset. FAPs are highlighted in green. All FAPs were extracted for downstream analysis and subclustering. **b** Subcluster analysis of the FAP population. Four FAP populations are identified based on their marker genes. **c** UMAP embedding displaying the origin for each nucleus. **d** Clustered dot plot visualization of top-regulated marker genes. The mean expression for each cluster is indicated by colour code. The dot size indicates the percent of expressing cells. Cluster were annotated based on marker genes. **e** Expression of CKDN1A (coding for p21) across the UMAP embedding split into the IBM (left) and NDC (right) datasets. The mean expression for each cell is indicated by the colour code. **f** Gene set enrichment analysis (GSEA) for the GO-BP dataset for the $CDKN1A^+$ FAP cluster. Differentially expressed genes were determined by the FindMarkers function using Wilcox testing and a fold-change threshold of 0.25. The Bonferroni correction was used for correction for multiple testing. DEGs specific to the IBM dataset were entered into the GSEA. The Kolmogorov–Smirnov test, followed by a post hoc correction, was used to determine the significance. **g** GSEA analysis for the SenMayo dataset for the DEGs obtained from the $CDKN1A^+$ FAP cluster. The running-sum statistic is in red, with the position in the ranked DEG list in black. Genes were sorted by fold change. The Kolmogorov–Smirnov test, followed by a post hoc correction, was used to determine the significance. **h** Violin plots displaying the normalized gene expression of the indicated genes for each FAP cluster. *CDKN1A* cyclin dependent kinase inhibitor 1A; *DNM1* dynamin-1; *FBN1* fibrillin-1; *GO-BP* gene ontology biological processes; *LUM* lumican; *NDC* non-diseased control; *IBM* inclusion body myositis; *RYR1* ryanodine receptor 1; *TRDN* triadin; *UMAP* uniform manifold approximation and projection; *XAF1* XIAP-associated factor 1

IBM demonstrates a pronounced loss of type 2A muscle fibers

Next, we analysed the myonuclear compartment of IBM and compared it to NDCs (Fig. 4a). Consistent with the current knowledge on IBM histopathology [17], the immune cell clusters of monocytes/macrophages and T, B, and NK cells were expanded in IBM compared to NDC (Fig. 4a, b). Further, we also observed that the number of type 2A and to a lesser extent type 2X myofibers were strongly reduced in IBM compared to NDC.

To gain further insight into the phenotype of myogenic cells in IBM, we extracted the myonuclei from the full dataset (Fig. 4c) and performed subclustering on these nuclei (Fig. 4d). ~ 20,000 myonuclei were analysed by this approach. Subclustering revealed five distinct populations of myonuclei. Briefly, we detected type 1 myonuclei defined by *MYH7* and *MYH7B* expression as well as type 2X myonuclei expressing *MYH1* (Fig. 4e). Type 2A myonuclei were defined, as above, by the lack of *MYH1* and *MYH7* while expressing *MYH2*. This subclustering revealed two additional clusters of myonuclei. First, we detected a population of myonuclei that were defined by the expression of the acetylcholine receptor (*CHRNA1*), the acetylcholine esterase (*ACHE*) and the muscle associated receptor tyrosine kinase (*MUSK*). Given their unique expression profile of NMJ proteins, these nuclei are likely to belong to myonuclei constituting the neuromuscular synapse (NMJ). Second, a cluster of myonuclei emerged that expressed high levels of pro-inflammatory molecules, such as *HLA-A*, *HLA-B* or *HLA-C* constituting the major histocompatibility complex (MHC) class 1. Further, these myonuclei displayed TNF alpha-induced protein 2 (*TNFAIP2*) and complement protein 3 (*C3*) as marker genes. Given their unique expression profile of pro-inflammatory genes, we termed these myonuclei as inflammatory. Phenotypically, these myonuclei express *MYH7* and *MYH7B* suggesting that they resemble type 1 myofibers. Comparing IBM and NDC, there was a strong reduction in the number of type 2A myonuclei (Fig. 4f). Concurrently, $CHRNA1^+$ myonuclei were also strongly reduced, while type 1 and type 2X myonuclei appeared largely unaltered.

For cross-validation of the specific loss of type 2A myofibers, we determined the frequency of myofiber types based on their ATPase staining after incubation at pH 4.6 [58]. We chose this approach to demonstrate the reduction in type 2A myofibers on the protein level and in a method independent of the MYH classification. Here, type 2A myofibers were markedly reduced in IBM compared to NDCs or IMNM patients (Fig. 4g, Suppl. Fig. 2b). In line, the relative frequency of type 1 myofibers was higher in IBM compared to the other groups. As such, a selective loss of type 2A myofibers appears to characterize the pathomorphology of IBM.

Skeletal muscle cells assume an inflammatory reprogramming in IBM

Next, we focused on the subpopulation of inflammatory myonuclei. Intriguingly, while this population was detected in IBM and NDC, their phenotype was altered depending on their origin (Fig. 5a). These myonuclei demonstrated high expression of marker genes such as *C3* or *HLA-A* only in IBM, but not in NDC. Notably, these inflammatory myonuclei were also the primary source of transforming growth factor beta (*TGFB1*). Further, we sought to cross-validate the presence of these myonuclei in muscle. For this purpose, we performed IF staining for intracellular C3 as expression for this gene was only detected in inflammatory myonuclei from IBM patients, but not in other subtypes of myonuclei in either NDC or IBM suggesting sufficient specificity to serve as a marker (Fig. 5b). Indeed, myofibers with intracellular C3 staining were abundant in IBM compared to NDC or IMNM muscle (Fig. 5c, d). To further characterize the phenotype of these myofibers, we computed the DEGs comparing inflammatory myonuclei between IBM and NDC. GSEA analysis of these DEGs for the GO-BP database indicated engagement of pro-inflammatory pathways, including the immunoglobulin mediated immune response, adaptive

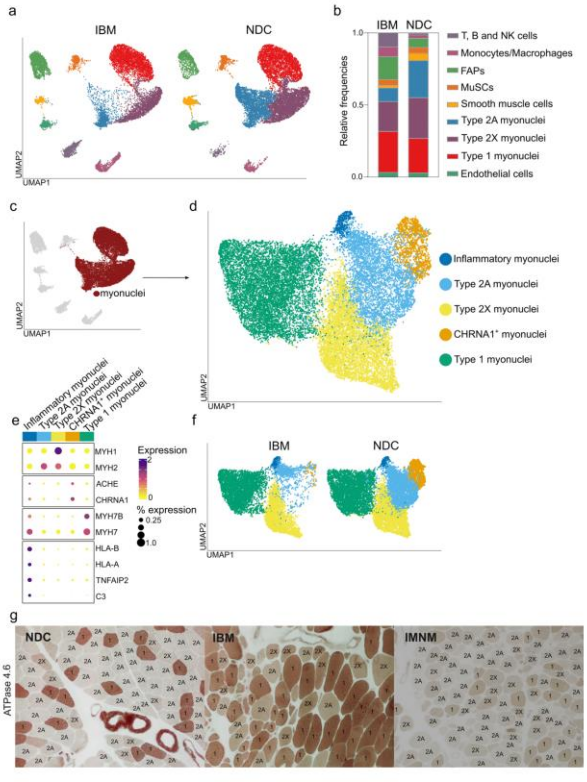

◂**Fig. 4** IBM demonstrates a pronounced loss of type 2A muscle fibers. **a** UMAP embedding of the full dataset split into IBM (left) and NDC (right). Cell populations are indicated by their colour code. **b** Relative frequency of each cell type or subtype in the IBM and the NDC dataset as a stacked bar plot. **c** UMAP embedding of the full dataset. Myonuclei are highlighted in dark red. These nuclei were extracted for downstream analysis **d** UMAP embedding of the myonuclei subclusters. A total of five populations were obtained from subclustering. **e** Clustered dot plot visualization of top-regulated marker genes. The mean expression for each cluster is indicated by colour code. The dot size indicates the percent of expressing cells. Clusters were annotated based on marker genes. **f** UMAP embedding for the myonuclei subcluster split into the IBM (left) and NDC (right) datasets. Subclusters are colour coded. **g** Exemplary ATPase staining for muscle specimens obtained from NDC, IBM, and IMNM patients. 8 patients were analysed by ATPase staining for each group. Muscle slices were incubated at a pH of 4.6, inactivating the myosin-ATPase of specific muscle fiber types. Type 1 muscle fibers are dark brown, type 2A is light brown, and type 2X are of an intermediate colour. The contrast and intensity vary between muscle specimens. A total of 10 high-power fields were counted. The corresponding statistical analysis is displayed in Suppl. Fig. 1B. *ACHE* acetylcholine esterase; *CHRNA1* cholinergic receptor nicotinic alpha 1 subunit; *FAP* fibro-adipogenic progenitor; *HLA* human leukocyte antigen; *IMNM* immune-mediated necrotizing myopathy; *MYH* myosin heavy chain; *MuSC* muscle stem cell; *NDC* non-diseased control; *IBM* inclusion body myositis; *TNFAIP2* TNF Alpha Induced Protein 2; *UMAP* uniform manifold approximation and projection

immune response, innate immune response and, interestingly, the B cell mediated immune response (Fig. 5e).

IBM myofibers lose their potential for endplate formation

To further characterize the changes to the myogenic compartment in IBM, we aimed to validate the reduction in AChR (*CHRNA1*) expressing muscle fibers (Fig. 6a). On the transcriptomic level, cells concurrently expressing the AChR as well as the acetylcholine esterase (*ACHE*) were reduced in IBM (Fig. 6b). Similarly, the expression of CHRNA1 in myonuclei was detected in NDC, but not in IBM (Fig. 6c). Formation of the NMJ is required for nerve-muscle communication. To visualize the neuromuscular endplate, we performed IF for α-bungarotoxin binding the AChR and counted the number of NMJs. Here, the number of NMJs was strongly reduced in IBM compared to NDCs or IMNM patients (Fig. 6d, e). NMJs were defined by the concurrent binding of α-bungarotoxin and their characteristic topography. These data suggest that endplate formation is impaired in IBM muscle potentially affecting nerve-muscle communication.

Conclusively, single nuclei analysis suggests that the myogenic compartment of IBM is characterized by the loss of type 2A myonuclei and of myonuclei that constitute the NMJ. Conversely, C3 expression identifies a distinct pro-inflammatory subpopulation of myonuclei residing in IBM muscle.

FAPs demonstrate a shifted collagen homeostasis with potential consequences for muscle health in IBM

Finally, we aimed to determine whether senescence of FAPs may be linked to changes to the myogenic compartment. FAPs and their fibroblast lineage are the primary sources of extracellular matrix proteins required for skeletal muscle homeostasis [6]. Manual screening of the top dysregulated genes in CDKN1A$^+$ FAPs revealed a shift in the expression of collagens, specifically of COL15A1, an isoform coding for collagen type XV, as well as COL1A1 and COL1A2, coding for collagen type I. Expression of all three collagen coding genes is allocated to the FAP cluster in both NDC and IBM (Fig. 7a). However, further analysis of the FAP subcluster indicates a shift of collagen expression between IBM and NDCs with CDKN1A$^+$ FAPs demonstrating a sharp downregulation of COL15A1 ($p = 5 \times 10^{-32}$), while engaging COL1A1 ($p = 1 \times 10^{-87}$) as well as COL1A2 ($p = 1 \times 10^{-70}$) expression (Fig. 7b, c). Both types of collagens are required to stabilize skeletal muscle cells and their differentiation. However, they vary in their biological functions [6, 24].

Following this line of argumentation, we suspected that differences in collagen might affect skeletal muscle cell homeostasis. To understand the communication between FAPs and myofibers better, we analyzed cell–cell communication across the transcriptomic dataset. We used the CellChat package to calculate the inferred intercellular communication based on an established receptor/ligand database [27]. We extracted all nuclei acquired from IBM patients and NDCs for individual analysis. Here, quantification of significantly over-expressed ligand/receptor pairings revealed that cell–cell communication is amplified across cell types and subtypes in IBM compared to NDCs (Fig. 7d). Intriguingly, FAPs appear to be a major communication hub interacting with myonuclei, immune cells and MuSCs. Indeed, the collagen and laminin signalling pathways constituted most outgoing ligands in IBM FAPs. Both signalling pathways belong to the KEGG pathway of extracellular matrix-receptor interaction (hsa04512). We suspect that a shift of the extracellular matrix composition might have functional implications for myofiber health in IBM.

To test this assumption in vitro, we cultivated primary human muscle cells (PHMC) and analysed them by flow cytometry. After reaching full confluence, PHMCs were treated with either 20 µg/ml of COL15A1 or COL1A1 [26, 33]. As specific collagen compositions are required for the successful maturation of the NMJ [33, 47], we analysed the amount of NMJ forming myofibers by quantification of α-bungarotoxin (Fig. 7e). In this setup, treatment with recombinant COL15A1 or with vehicle improved NMJ formation as compared to COL1A1. Next, we also aimed

◂**Fig. 5** Skeletal muscle cells assume an inflammatory reprogramming in IBM. **a** UMAP embedding of the myonuclei split into IBM (left) and NDC (right). The expression of each gene indicated on the right is colour coded. **b** Violin plot displaying the expression of complement factor 3 (C3) for each myonuclei subset for IBM and NDC. Only inflammatory myonuclei obtained from IBM patients express C3. **c** Exemplary staining for C3 (red) laminin-β1 (green) and DAPI (blue) for NDC, IBM, and IMNM patients. 16 patients were analysed for each group by immunofluorescence. **d** C3$^+$ myofibers were counted in randomly distributed 10 HPF (≙ 0.16 mm^2). The biopsies were blinded for quantification, making the diagnosis impossible to identify from the label. **e** Visualization of the gene set enrichment analysis (GSEA) for the GO-BP dataset as a gene concept network. GSEA was performed from the DEGs comparing inflammatory myonuclei from IBM patients and NDC. The Kolmogorov–Smirnov test followed by post hoc correction was used to determine the significance. The top five GO terms for the BP dataset are colour coded. A line connects the corresponding genes constituting each term. The fold change for each gene comprising the GO term comparing IBM and NDC is indicated in red. The number of genes for each GO term is indicated as a dot size. *CHRNA1* cholinergic receptor nicotinic alpha 1 subunit; *HLA* human leukocyte antigen; *HPF* high-power field; *MYH* myosin heavy chain; *NDC* non-diseased control; *IBM* inclusion body myositis; *TGFB1* transforming growth factor beta 1; *UMAP* uniform manifold approximation and projection

to understand if differences in collagen composition might affect PHMC survival. For this purpose, differentiated PHMCs were treated with 20 µg/ml of COL15A1 or 20 µg/ml COL1A1. To reflect inflammatory conditions in IBM, PHMCs were additionally treated with 10 ng/ml interferon-γ (INF-γ). After 48 h of incubation, we determined the number of dead PHMCs by live/dead staining (Fig. 7g, h). Interestingly, COL15A1 improved PHMC survival in response to INF-γ compared to COL1A1 or vehicle. These data suggest that senescent FAPs demonstrate an altered collagen homeostasis shifted towards collagen type I.

Discussion

FAPs are a mesenchymal cell population with high phenotypical plasticity that is crucially involved in skeletal muscle homeostasis and regeneration [5, 23]. Here, we report that tissue-resident FAPs, not myofibers, are the main cell type assuming a senescent phenotype in IBM. Depending on environmental cues, FAPs may differentiate into fibroblasts or adipocytes. In response to muscle damage, FAPs proliferate, expand and accumulate, constituting the main source of extracellular matrix proteins [23, 41]. Depletion of FAPs hinders muscle repair underscoring their functional importance [23, 41]. Conversely, in conditions of chronic muscle damage, FAPs may prove detrimental to muscle health. Their persistent activity cumulates in progressive tissue fibrosis and loss of normal tissue architecture [22, 23]. In line, we describe a novel population of senescent FAPs that reside in IBM muscle. These FAPs exhibit key hallmarks of cellular senescence including a pro-inflammatory secretome, engagement of the Jun/JunB-pathway and expression of senescence biomarkers (p21 and SA-β-Gal).

Besides their inflammatory properties, these FAPs also exhibit a shift in their collagen balance losing collagen type XV and increasing collagen type I expression. Interestingly, Col15a1 knockout mice lacking collagen type XV demonstrate a myopathy vulnerable to exercise-induced muscle injury, suggesting that this collagen type is required for muscle homeostasis [11]. Histopathologically, this myopathy is characterized by areas of degeneration and regeneration as well as variations in myofiber size [11]. Unlike other collagen types, collagen type XV is only encoded by a single gene (COL15A1) [25]. As such, a loss of COL15A1 expression, as seen in CDKN1A$^+$ FAPs, will likely result in impaired collagen type XV production. Collagen interacts with skeletal muscle via a number of receptors, such as integrins, mediating a plethora of downstream effects [63]. Besides differentiation and regeneration, collagen-muscle cell interaction is also required for the maturation and formation of the NMJ. Animal studies demonstrated that collagen type XIII and type XIX are needed for successful NMJ genesis [33, 47]. While the exact molecular pathways remain to be studied, we hypothesize that collagen dysregulation and persistent pro-inflammatory activity could link FAP senescence and the loss of structural integrity of the muscle compartment in IBM. Current immunosuppressive approaches are unlikely to inhibit or even affect the persistent activity of FAPs. Following this line of argumentation, senescent FAPs may represent a cell-autonomous mechanism that sustains inflammation and fibrotic remodelling in IBM despite therapeutically addressing immune cell pathology warranting further research.

Expanding on previous proteomics data that demonstrated a loss of type 2 myofibers linked to impaired glycolysis in IBM [49], snRNA-seq provides further insight into changes to the myogenic compartment in IBM at a high resolution. Here, the loss of type 2 fibers allocates specifically to the subtype of type 2A myofibers. Further, the transcriptomic landscape of IBM displays a rarefication of neuromuscular endplates and the engagement of an inflammatory muscle phenotype. Differences in composition and metabolic demands render individual myofibers vulnerable to distinct conditions. As such, type 2A myofibers rely primarily on oxidative phosphorylation for their ATP supply, while type 2X myofibers have an effective glycolytic ATP production [58]. Mitochondrial dysfunction is a primary

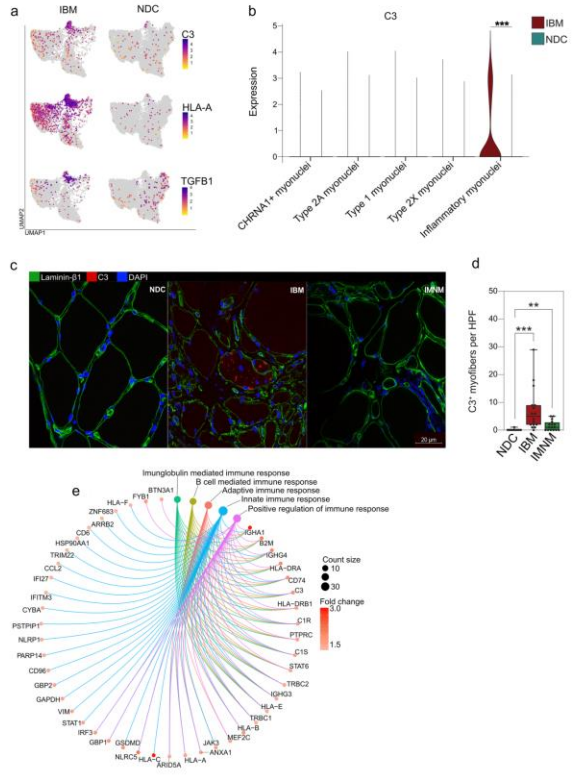

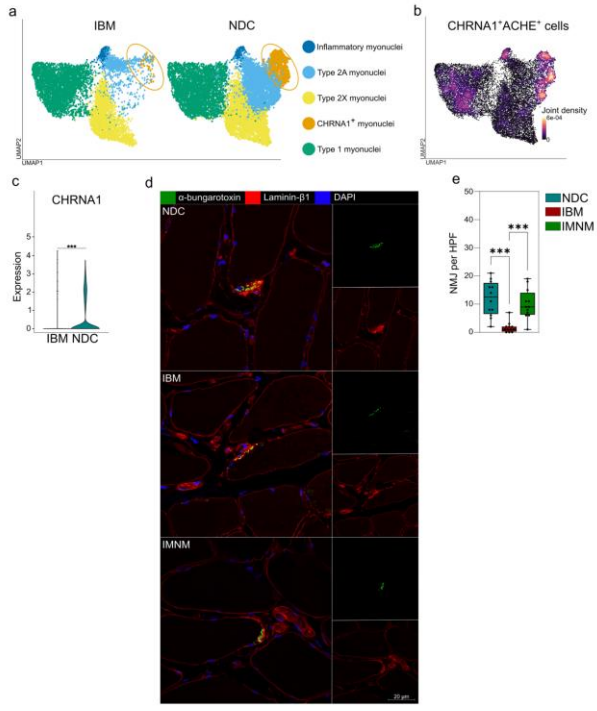

feature of IBM [46], thus providing a potential explanation for the pattern of myofiber loss observed. We hypothesize that type 2A myofibers are unable to meet their metabolic demand due to mitochondrial dysfunction in IBM, while type 2X myofibers may rely on glycolytic ATP. Further research on muscle metabolism and immunogenicity might prove valuable to better understand this understudied aspect of IBM pathophysiology. The importance of the myogenic

Fig. 6 IBM myofibers lose their potential for endplate formation. **a** UMAP embedding of the myonuclei split into IBM (left) and NDC (right). The myonuclei cluster expressing the acetylcholine receptor (CHRNA1) is marked in orange. **b** Density plot generated with the Nebulosa package of cells expressing acetylcholine receptor and acetylcholine esterase (ACHE). Areas of high cellular density are indicated in orange. **c** Violin plot for the CHRNA1 expression across the dataset. CHRNA1-expressing nuclei are largely absent in IBM muscle. **d** Exemplary staining of a NMJ in NDC, IBM, and IMNM patients, respectively. α-bungarotoxin was used to label the acetylcholine receptors of the NMJ in green. 12 patients were analysed for each group. **e** While NMJ was detected in all muscle samples, their frequency was strongly reduced in IBM. NMJ was defined by its characteristic topography and expression of the acetylcholine receptor. NMJ was counted in randomly distributed 10 HPF (≙ 0.16 mm^2). The biopsies were blinded for quantification, with the diagnosis impossible to identify from the label. 12 patients were analysed by immunofluorescence for each group. **f** Frequencies of NMJ in NDC, IBM, and IMNM patients. Differences between groups were analysed by Kruskal–Wallis test followed by post hoc testing. ***$p < 0.001$. *AChE* acetylcholine esterase; *CHRNA1* cholinergic receptor nicotinic alpha 1 subunit; *HPF* high-power field; *NDC* non-diseased control; *IBM* inclusion body myositis; *IMNM* immune-mediated necrotizing myopathy; *UMAP* uniform manifold approximation and projection

compartment is further stressed by the possibility of denervation contributing to pathology. Clinical, histomorphological and electrophysiological data suggest a neurogenic component and a failure of NMJ transmission in IBM [17, 45]. Here, we provide molecular evidence in favour of this hypothesis as myofibers constituting the NMJ appear to decline in IBM. Further research is warranted to understand this aspect of pathomorphology and whether treatment strategies addressing the NMJ, such as pyridostigmine, could prove valuable for the clinical management of IBM.

A recurrent observation across the transcriptomic dataset was the dysregulation of intracellular complement components. Historically, complement has been viewed as a serum-effective system that mediates the detection and removal of invading pathogens [62]. Intriguingly, recent studies challenged this classical view by demonstrating that complement activation not only occurs on the cell surface, but also in intracellular compartments, thereby regulating cell physiology of immune and non-immune cells [3, 31, 62]. In this study, we observed that inflammatory states of both myogenic and non-myogenic cells were accompanied by the upregulation of complement proteins, particularly of C3. Indeed, intracellular complement proteins are coded by the same set of genes that give rise to the circulatory complement system [62]. Moreover, intracellular complement regulates tissue inflammation and the transcriptomic programming of fibroblasts [13]. In response to repeated inflammatory challenges, fibroblasts in humans and mice assume a 'primed' phenotype that renders tissue susceptible to sustained inflammation. This transcriptomic program is controlled by C3 and the C3a-receptor as well as the mammalian target of rapamycin (mTOR). Following this line of argumentation, we suspect that the engagement of complement factors in this transcriptomic dataset suggests altered intracellular complement signalling as a potential contributor to IBM pathophysiology warranting further research.

Concurrently, an interesting argument for cellular senescence might arise from the effect of sirolimus in IBM. In a recent randomized, placebo-controlled trial for IBM, the mTOR inhibitor sirolimus did not meet the primary outcome of maximal voluntary isometric knee extension strength; however, secondary outcome measures such as 6-min walking distance, forced vital capacity and thigh fat fraction were ameliorated [4]. Aside from immunoregulatory effects, mTOR signalling has been linked to cellular senescence. In vivo and in vitro evidence demonstrated that the mTOR pathway suppresses the SASP, e.g. via Mitogen-activated protein kinase 2 (MAPK) signalling, of senescent cells [20, 32]. Hence, sirolimus is likely to inhibit pro-inflammatory fibroblasts requiring mTOR signalling, as described above [13]. Thus, it is tempting to speculate that the therapeutic effect of sirolimus is—at least in part—mediated by modulation of the senescent fibroblasts.

This study employs snRNA-seq as opposed to scRNA-seq. Both methodological approaches offer specific advantages and disadvantages. In respect to myofibers, the large size of individual cells limits the use of scRNA-seq rendering snRNA-seq a preferential choice [9, 50]. Concurrently, snRNA-seq also allows for the analysis of frozen tissues, thereby enabling the collection and analysis in a single run reducing the risk for batch effects [30]. A limitation of this approach is the complexity of multinucleated cells, as we cannot determine if certain nuclei originated from the same myofiber. Further, depending on the chosen method [59], specific cell populations might be underrepresented. In the study of liver tissue, snRNA-seq detected a lower number of immune cells than scRNA-seq [61]. Combining snRNA-seq with scRNA-seq might provide a more comprehensive picture of the muscle compartment than an individual method alone. Finally, a potential limitation to this study is introduced by the focus on the distal segment of the quadriceps muscle. The highest concentration of NMJs is located within the equatorial region of the muscle [28]. This topographic disparity should be considered when interpreting these findings as further research is warranted to understand whether the reduction of NMJs in IBM patients is also present in the high-density equatorial segment of the muscle.

Taken together, this study highlights the contribution of dysfunctional tissue-resident cells to IBM pathophysiology.

Fig. 7 FAPs demonstrate a shifted collagen homeostasis with potential consequences for muscle health in IBM. **a** UMAP embedding of the full dataset with the corresponding gene expression indicated by the colour code. The FAP cluster is in the upper left. **b** UMAP of the FAP subclusters split into their origin of IBM patients or NDC. The annotation of the corresponding subcluster is given beside the plot. $CDKN1A^+$ FAPs are in the lower left. **c** UMAPs demonstrating COL1A1, COL1A2, and COL15A1 expression across the FAP cluster and its subclusters. COL15A1 is largely absent in the $CDKN1A^+$ FAP subcluster. **d** Analysis of the cell–cell communication across the IBM and NDC datasets using the CellChat package. The number of the inferred ligand/receptor interactions is indicated by the size of an arrow connecting two cell populations. The larger the arrow, the higher the number of interactions between the cell populations. The ligand/receptor pairings were tested against the CellChat library for significance. **e** Representative flow cytometry scatter plots displaying SSC vs α-bungarotoxin for primary human muscle cells (PHMC) treated with COL15A1 or COL1A1. **f** Percentage of α-bungarotoxin + PHMC treated with COL15A1 or COL1A1 or vehicle. $N = 8$ per group. **g** Representative live/dead staining for PHMCs incubated with COL15A1 or COL1A1 in addition to 10 ng/ml interferon-γ (INF-γ). Live cells were identified by green-fluorescent calcein-AM, indicating intracellular esterase activity. Dead cells were identified by red-fluorescent ethidium homodimer-1, indicating a loss of membrane integrity. **h** 100 cells were counted for each sample, and the frequencies of live or dead cells were recorded. $N = 8$ per group. Differences between groups were analysed by Kruskal–Wallis test followed by post hoc testing. *$p < 0.05$, **$p < 0.01$. ***$p < 0.001$. *CDKN1A* cyclin dependent kinase inhibitor 1A; *COL* collagen; *FAP* fibro-adipogenic progenitor; *NDC* non-diseased control; *IBM* inclusion body myositis; *IMNM* immune-mediated necrotizing myopathy; *UMAP* uniform manifold approximation and projection

Treatment strategies for IBM may benefit from exploring an integrative approach that targets invading immune cells while also addressing detrimental tissue-resident cells such as FAPs and their senescent phenotype.

Supplementary Information The online version contains supplementary material available at https://doi.org/10.1007/s00401-023-02637-2.

Acknowledgements We thank the patients and their families for their support. We acknowledge the support from the Core Facility for Advanced Light Microscopy and the support from the Friedrich-Baur-Institut.

Author contributions CN and TR designed the study and methods. CN, LT, CP, and VD performed the experiments. CP and WS provided clinical data. BS, AB, ENJ, JZ, and SGM provided resources. CN and TR wrote the manuscript. SGM, WS, and TR supervised the study. The manuscript was revised by CBS, LT, CP, MP, SR, VD, FK, AR, BS, AB, ENJ, and JZ.

Funding Open Access funding enabled and organized by Projekt DEAL. The funding source had no influence on the study design, on the collection, analysis, and interpretation of data, on the writing of the manuscript, and the decision to submit the paper for publication. This work was directly funded by the Else Kröner-Fresenius-Stiftung to CN (2023_EKEA.38). Further, this work was supported by the internal research funding program of the Heinrich Heine University to CN, CBS and TR. This research was supported by the Myositis Netz e.V. for CN. Further study funding from the BMBF (Bundesministeriums für Bildung und Forschung, 01EC1901A) to TR, by the EKFS (Else Kröner-Fresenius-Stiftung, 2018_A03) to TR, the DGM (Deutsche Gesellschaft für Muskelkranke, Ru2/1 and Sc22/4) to TR, and to CN (Deutsche Gesellschaft für Muskelkranke, Ne4/1) and by the DFG (RU 2169/2-1, Deutsche Forschungsgemeinschaft) to TR.

Data availability The raw transcriptomic data are publicly available under the accession number: SCP2253 at https://singlecell.broadinstitute.org/single_cell. All further data are available from the corresponding author upon reasonable request.

Declarations

Conflict of interest The authors declare no competing interests.

References

1. Allenbach Y, Benveniste O, Goebel H-H, Stenzel W (2017) Integrated classification of inflammatory myopathies. Neuropathol Appl Neurobiol 43:62–81. https://doi.org/10.1111/nan.12380
2. Allenbach Y, Mammen AL, Benveniste O, Stenzel W, Allenbach Y, Amato A et al (2018) 224th ENMC international workshop: clinico-sero-pathological classification of immune-mediated necrotizing myopathies Zandvoort, the Netherlands, 14–16 October 2016. Neuromuscul Disord 28:87–99. https://doi.org/10.1016/j.nmd.2017.09.016
3. Arbore G, Kemper C, Kolev M (2017) Intracellular complement—the complosome—in immune cell regulation. Mol Immunol 89:2–9. https://doi.org/10.1016/j.molimm.2017.05.012
4. Benveniste O, Hogrel J-Y, Belin L, Annoussamy M, Bachasson D, Rigolet A et al (2021) Sirolimus for treatment of patients with inclusion body myositis: a randomised, double-blind, placebo-controlled, proof-of-concept, phase 2b trial. Lancet Rheumatol 3:e40–e48. https://doi.org/10.1016/S2665-9913(20)30280-0
5. Biferali B, Proietti D, Mozzetta C, Madaro L (2019) Fibro–adipogenic progenitors cross-talk in skeletal muscle: the social network. Front Physiol 10:1074. https://doi.org/10.3389/fphys.2019.01074
6. Chapman MA, Meza R, Lieber RL (2016) Skeletal muscle fibroblasts in health and disease. Differentiation 92:108–115. https://doi.org/10.1016/j.diff.2016.05.007
7. Chen Y-W, Shi R, Geraci N, Shrestha S, Gordish-Dressman H, Pachman LM (2008) Duration of chronic inflammation alters gene expression in muscle from untreated girls with juvenile dermatomyositis. BMC Immunol 9:43. https://doi.org/10.1186/1471-2172-9-43
8. Contreras O, Rossi FMV, Theret M (2021) Origins, potency, and heterogeneity of skeletal muscle fibro-adipogenic progenitors—time for new definitions. Skeletal Muscle 11:16. https://doi.org/10.1186/s13395-021-00265-6
9. De Micheli AJ, Spector JA, Elemento O, Cosgrove BD (2020) A reference single-cell transcriptomic atlas of human skeletal muscle tissue reveals bifurcated muscle stem cell populations. Skeletal Muscle 10:19. https://doi.org/10.1186/s13395-020-00236-3
10. Dubowitz, Sewry, Oldfors muscle biopsy: a practical approach. 5th edn. ISBN: 978-7020-7471-4. Pages 21-22
11. Eklund L, Piuhola J, Komulainen J, Sormunen R, Ongvarrasopone C, Fässler R et al (2001) Lack of type XV collagen causes a skeletal myopathy and cardiovascular defects in mice. Proc Natl Acad Sci USA 98:1194–1199. https://doi.org/10.1073/pnas.98.3.1194
12. Englund DA, Jolliffe A, Aversa Z, Zhang X, Sturmlechner I, Sakamoto AE et al (2023) p21 induces a senescence program and skeletal muscle dysfunction. Molecular Metabolism 67:101652. https://doi.org/10.1016/j.molmet.2022.101652
13. Frišćić J, Böttcher M, Reinwald C, Bruns H, Wirth B, Popp S-J et al (2021) The complement system drives local inflammatory tissue priming by metabolic reprogramming of synovial fibroblasts. Immunity 54:1002-1021.e10. https://doi.org/10.1016/j.immuni.2021.03.003
14. Goel N, Needham M, Soler-Ferran D, Cotreau MM, Escobar J, Greenberg S (2022) Pos1342 depletion of Klrg1+ T cells in a first-in-human clinical trial of Abc008 in inclusion body myositis (ibm). Ann Rheum Dis 81:1008–1009. https://doi.org/10.1136/annrheumdis-2022-eular.2141
15. Gorgoulis V, Adams PD, Alimonti A, Bennett DC, Bischof O, Bishop C et al (2019) Cellular senescence: defining a path forward. Cell 179:813–827. https://doi.org/10.1016/j.cell.2019.10.005
16. Goyal NA, Coulis G, Duarte J, Farahat PK, Mannaa AH, Cauchii J et al (2022) Immunophenotyping of inclusion body myositis blood T and NK cells. Neurology 98:e1374–e1383. https://doi.org/10.1212/WNL.0000000000200013
17. Greenberg SA (2019) Inclusion body myositis: clinical features and pathogenesis. Nat Rev Rheumatol 15:257–272. https://doi.org/10.1038/s41584-019-0186-x
18. Greenberg SA, Pinkus JL, Kong SW, Baecher-Allan C, Amato AA, Dorfman DM (2019) Highly differentiated cytotoxic T cells in inclusion body myositis. Brain 142:2590–2604. https://doi.org/10.1093/brain/awz207
19. Grimaldi A, Comai G, Mella S, Tajbakhsh S (2022) Identification of bipotent progenitors that give rise to myogenic and connective tissues in mouse. Elife 11:e70235. https://doi.org/10.7554/eLife.70235
20. Herranz N, Gallage S, Mellone M, Wuestefeld T, Klotz S, Hanley CJ et al (2015) mTOR regulates MAPKAPK2 translation to control the senescence-associated secretory phenotype. Nat Cell Biol 17:1205–1217. https://doi.org/10.1038/ncb3225
21. Hickson LJ, Langhi Prata LGP, Bobart SA, Evans TK, Giorgadze N, Hashmi SK et al (2019) Senolytics decrease senescent cells in humans: preliminary report from a clinical trial of dasatinib plus quercetin in individuals with diabetic kidney disease. EBioMedicine 47:446–456. https://doi.org/10.1016/j.ebiom.2019.08.069
22. Hinz B, Lagares D (2020) Evasion of apoptosis by myofibroblasts: a hallmark of fibrotic diseases. Nat Rev Rheumatol 16:11–31. https://doi.org/10.1038/s41584-019-0324-5
23. Hogarth MW, Uapinyoying P, Mázala DAG, Jaiswal JK (2022) Pathogenic role and therapeutic potential of fibro-adipogenic progenitors in muscle disease. Trends Mol Med 28:8–11. https://doi.org/10.1016/j.molmed.2021.10.003
24. Hu L-Y, Mileti CJ, Loomis T, Brashear SE, Ahmad S, Chellakudam RR et al (2021) Skeletal muscle progenitors are sensitive to collagen architectural features of fibril size and cross linking. Am J Physiol Cell Physiol 321:C330–C342. https://doi.org/10.1152/ajpcell.00065.2021
25. Huebner K, Cannizzaro LA, Jabs EW, Kiyirikko S, Manzone H, Pihlajaniemi T et al (1992) Chromosomal assignment of a gene encoding a new collagen type (COL15A1) to 9q21 → q22. Genomics 14:220–224. https://doi.org/10.1016/S0888-7543(05)80209-5
26. Hurskainen M, Ruggiero F, Hägg P, Pihlajaniemi T, Huhtala P (2010) Recombinant human collagen XV regulates cell adhesion and migration. J Biol Chem 285:5258–5265. https://doi.org/10.1074/jbc.M109.033787
27. Jin S, Guerrero-Juarez CF, Zhang L, Chang I, Ramos R, Kuan C-H et al (2021) Inference and analysis of cell-cell communication using cellchat. Nat Commun 12:1088. https://doi.org/10.1038/s41467-021-21246-9
28. Jones RA, Harrison C, Eaton SL, Llavero Hurtado M, Graham LC, Alkhammash L et al (2017) Cellular and molecular anatomy of the human neuromuscular junction. Cell Rep 21:2348–2356. https://doi.org/10.1016/j.celrep.2017.11.008
29. Kim SR, Eirin A, Zhang X, Lerman A, Lerman LO (2019) Mitochondrial protection partly mitigates kidney cellular senescence in swine atherosclerotic renal artery stenosis. Cell Physiol Biochem 52:617–632. https://doi.org/10.33594/000000044
30. Kim M, Franke V, Brandt B, Lowenstein ED, Schöwel V, Spuler S et al (2020) Single-nucleus transcriptomics reveals functional compartmentalization in syncytial skeletal muscle cells. Nat Commun 11:6375. https://doi.org/10.1038/s41467-020-20064-9
31. Kolev M, Friec GL, Kemper C (2014) Complement — tapping into new sites and effector systems. Nat Rev Immunol 14:811–820. https://doi.org/10.1038/nri3761
32. Laberge R-M, Sun Y, Orjalo AV, Patil CK, Freund A, Zhou L et al (2015) MTOR regulates the pro-tumorigenic senescence-associated secretory phenotype by promoting IL1A translation. Nat Cell Biol 17:1049–1061. https://doi.org/10.1038/ncb3195
33. Latvanlehto A, Fox MA, Sormunen R, Tu H, Oikarainen T, Koski A et al (2010) Muscle-derived collagen XIII regulates maturation of the skeletal neuromuscular junction. J Neurosci 30:12230–12241. https://doi.org/10.1523/JNEUROSCI.5518-09.2010
34. Li M-L, Wu S-H, Song B, Yang J, Fan L-Y, Yang Y et al (2022) Single-cell analysis reveals transcriptomic reprogramming in aging primate entorhinal cortex and the relevance with Alzheimer's disease. Aging Cell 21:e13723. https://doi.org/10.1111/acel.13723
35. Lloyd TE, Mammen AL, Amato AA, Weiss MD, Needham M, Greenberg SA (2014) Evaluation and construction of diagnostic criteria for inclusion body myositis. Neurology 83:426–433. https://doi.org/10.1212/WNL.0000000000000642
36. Lundberg IE, de Visser M, Werth VP (2018) Classification of myositis. Nat Rev Rheumatol 14:269–278. https://doi.org/10.1038/nrrheum.2018.41
37. Maity P, Singh K, Krug L, Koroma A, Hainzl A, Bloch W et al (2021) Persistent JunB activation in fibroblasts disrupts stem cell niche interactions enforcing skin aging. Cell Rep 36:109634. https://doi.org/10.1016/j.celrep.2021.109634
38. Martínez-Zamudio RI, Dewald HK, Vasilopoulos T, Gittens-Williams L, Fitzgerald-Bocarsly P, Herbig U (2021) Senescence-associated β-galactosidase reveals the abundance of senescent CD8+ T cells in aging humans. Aging Cell 20:e13344. https://doi.org/10.1111/acel.13344
39. McLeish E, Slater N, Sooda A, Wilson A, Coudert JD, Lloyd TE et al (2022) Inclusion body myositis: the interplay between ageing, muscle degeneration and autoimmunity. Best Pract Res Clin Rheumatol 36:101761. https://doi.org/10.1016/j.berh.2022.101761
40. Morosetti R, Broccolini A, Sancricca C, Gliubizzi C, Gidaro T, Tonali PA et al (2010) Increased aging in primary muscle cultures of sporadic inclusion-body myositis. Neurobiol Aging 31:1205–1214. https://doi.org/10.1016/j.neurobiolaging.2008.08.011
41. Mozzetta C, Consalvi S, Saccone V, Tierney M, Diamantini A, Mitchell KJ et al (2013) Fibroadipogenic progenitors mediate the ability of HDAC inhibitors to promote regeneration in dystrophic

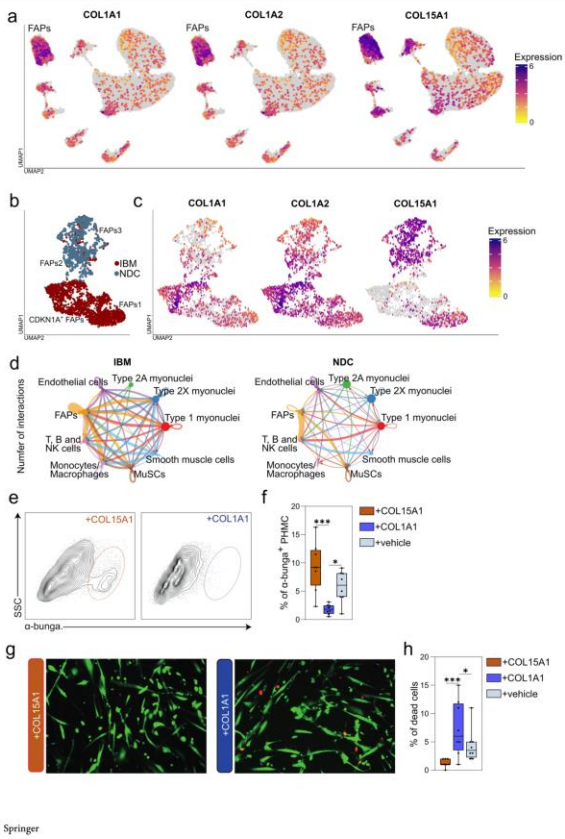

muscles of young, but not old Mdx mice. EMBO Mol Med 5:626–639. https://doi.org/10.1002/emmm.201202096
42. Murgia M, Nogara L, Baraldo M, Reggiani C, Mann M, Schiaffino S (2021) Protein profile of fiber types in human skeletal muscle: a single-fiber proteomics study. Skeletal Muscle 11:24. https://doi.org/10.1186/s13395-021-00279-0
43. Nelke C, Dziewas R, Minnerup J, Meuth SG, Ruck T (2019) Skeletal muscle as potential central link between sarcopenia and immune senescence. EBioMedicine 49:381–388. https://doi.org/10.1016/j.ebiom.2019.10.034
44. Nelke C, Schroeter CB, Pawlitzki M, Meuth SG, Ruck T (2022) Cellular senescence in neuroinflammatory disease: new therapies for old cells? Trends Mol Med 28:850–863. https://doi.org/10.1016/j.molmed.2022.07.003
45. Noda S, Murakami A, Kazuta T, Hirano S, Kimura S, Nakanishi H et al (2022) Clinical implication of denervation in sporadic inclusion body myositis. J Neurol Sci 439:120317. https://doi.org/10.1016/j.jns.2022.120317
46. Oldfors A, Moslemi AR, Fyhr IM, Holme E, Larsson NG, Lindberg C (1995) Mitochondrial DNA deletions in muscle fibers in inclusion body myositis. J Neuropathol Exp Neurol 54:581–587. https://doi.org/10.1097/00005072-199507000-00012
47. Oprişoreanu A-M, Smith HL, Arya S, Webster R, Zhong Z, Eaton-Hart C et al (2019) Interaction of axonal chondrolectin with collagen XIXa1 is necessary for precise neuromuscular junction formation. Cell Rep 29:1082-1098.e10. https://doi.org/10.1016/j.celrep.2019.09.033
48. Pai C-H, Lin S-R, Liu C-H, Pan S-Y, Hsu H, Chen Y-T et al (2020) Targeting fibroblast CD248 attenuates CCL17-expressing macrophages and tissue fibrosis. Sci Rep 10:16772. https://doi.org/10.1038/s41598-020-73194-x
49. Parker KC, Kong SW, Walsh RJ, Salajegheh M, Moghadaszadeh B, Amato AA et al (2009) Fast-twitch sarcomeric and glycolytic enzyme protein loss in inclusion body myositis. Muscle Nerve 39:739–753. https://doi.org/10.1002/mus.21230
50. Perez K, Ciotlos S, McGirr J, Limbad C, Doi R, Nederveen JP et al (2022) Single nuclei profiling identifies cell specific markers of skeletal muscle aging, frailty, and senescence. Aging (Albany NY) 14:9393–9422. https://doi.org/10.18632/aging.204435
51. Petrus P, Fernandez TL, Kwon MM, Huang JL, Lei V, Safikhan NS et al (2019) Specific loss of adipocyte CD248 improves metabolic health via reduced white adipose tissue hypoxia, fibrosis and inflammation. eBioMedicine 44:489–501. https://doi.org/10.1016/j.ebiom.2019.05.057
52. Pinal-Fernandez I, Quintana A, Milisenda JC, Casal-Dominguez M, Muñoz-Braceras S, Derfoul A et al (2023) Transcriptomic profiling reveals distinct subsets of immune checkpoint inhibitor induced myositis. Ann Rheum Dis 82:829–836. https://doi.org/10.1136/ard-2022-223792
53. Preuße C, Paesler B, Nelke C, Cengiz D, Müntefering T, Roos A et al (2022) Skeletal muscle provides the immunological micro-milieu for specific plasma cells in anti-synthetase syndrome-associated myositis. Acta Neuropathol. https://doi.org/10.1007/s00401-022-02438-z
54. Rose MR, ENMC IBM Working Group (2013) 188th ENMC International Workshop: Inclusion Body Myositis, 2–4 December 2011, Naarden, The Netherlands. Neuromuscul Disord 23:1044–1055. https://doi.org/10.1016/j.nmd.2013.08.007
55. Rubenstein AB, Smith GR, Raue U, Begue G, Minchev K, Ruf-Zamojski F et al (2020) Single-cell transcriptional profiles in human skeletal muscle. Sci Rep 10:229. https://doi.org/10.1038/s41598-019-57110-6
56. Saul D, Kosinsky RL, Atkinson EJ, Doolittle ML, Zhang X, LeBrasseur NK et al (2022) A new gene set identifies senescent cells and predicts senescence-associated pathways across tissues. Nat Commun 13:4827. https://doi.org/10.1038/s41467-022-32552-1
57. Stuart T, Butler A, Hoffman P, Hafemeister C, Papalexi E, Mauck WM et al (2019) Comprehensive integration of single-cell data. Cell 177:1888-1902.e21. https://doi.org/10.1016/j.cell.2019.05.031
58. Talbot J, Maves L (2016) Skeletal muscle fiber type: using insights from muscle developmental biology to dissect targets for susceptibility and resistance to muscle disease. Wiley Interdiscip Rev Dev Biol 5:518–534. https://doi.org/10.1002/wdev.230
59. Teicher BA (2019) CD248: a therapeutic target in cancer and fibrotic diseases. Oncotarget 10:993–1009. https://doi.org/10.18632/oncotarget.26590
60. Valieva Y, Ivanova E, Fayzullin A, Kurkov A, Igrunkova A (2022) Senescence-associated β-galactosidase detection in pathology. Diagnostics (Basel) 12:2309. https://doi.org/10.3390/diagnostics12102309
61. Wen F, Tang X, Xu L, Qu H (2022) Comparison of single-nucleus and single-cell transcriptomes in hepatocellular carcinoma tissue. Mol Med Rep 26:339. https://doi.org/10.3892/mmr.2022.12855
62. West EE, Kemper C (2023) Complosome—the intracellular complement system. Nat Rev Nephrol. https://doi.org/10.1038/s41581-023-00704-1
63. Zhang W, Liu Y, Zhang H (2021) Extracellular matrix: an important regulator of cell functions and skeletal muscle development. Cell Biosci 11:65. https://doi.org/10.1186/s13578-021-00579-4
64. Zhang X, Habiballa L, Aversa Z, Ng YE, Sakamoto AE, Englund DA et al (2022) Characterization of cellular senescence in aging skeletal muscle. Nat Aging 2:601–615. https://doi.org/10.1038/s43587-022-00250-8

Eculizumab treatment alters the proteometabolome beyond the inhibition of complement

Christopher Nelke,[1] Christina B. Schroeter,[1] Frauke Stascheit,[2,3] Niklas Huntemann,[1] Marc Pawlitzki,[1] Alice Willison,[1] Saskia Räuber,[1] Nico Melzer,[1] Ute Distler,[4] Stefan Tenzer,[4,5,6] Kai Stühler,[7] Andreas Roos,[8] Andreas Meisel,[2,3,9] Sven G. Meuth,[1] and Tobias Ruck[1]

[1]Department of Neurology, Medical Faculty, Heinrich Heine University Düsseldorf, Düsseldorf, Germany. [2]Charité – Universitätsmedizin Berlin, corporate member of Freie Universität Berlin and Humboldt Universität zu Berlin, Department of Neurology and Experimental Neurology, Berlin, Germany. [3]Charité – Universitätsmedizin Berlin, corporate member of Freie Universität Berlin and Humboldt Universität zu Berlin, Neuroscience Clinical Research Center, Berlin, Germany. [4]University Medical Center of the Johannes-Gutenberg University Mainz, Mainz, Germany. [5]Helmholtz Institute for Translational Oncology (HI-TRON) Mainz, Germany. [6]Deutsches Krebsforschungszentrum (DKFZ), Heidelberg, Germany. [7]Molecular Proteomics Laboratory, Heinrich Heine University, Düsseldorf, Germany. [8]Department of Neuropediatrics, University of Duisburg-Essen, Essen, Germany. [9]Charité – Universitätsmedizin Berlin, corporate member of Freie Universität Berlin and Humboldt Universität zu Berlin, Center for Stroke Research Berlin, Berlin, Germany.

Therapeutic strategies targeting complement have revolutionized the treatment of myasthenia gravis (MG). However, a deeper understanding of complement modulation in the human system is required to improve treatment responses and identify off-target effects shaping long-term outcomes. For this reason, we studied a cohort of patients with MG treated with either eculizumab or azathioprine as well as treatment-naive patients using a combined proteomics and metabolomics approach. This strategy validated known effects of eculizumab on the terminal complement cascade. Beyond that, eculizumab modulated the serum proteometabolome as distinct pathways were altered in eculizumab-treated patients, including the oxidative stress response, mitogen-activated protein kinase signaling, and lipid metabolism with particular emphasis on arachidonic acid signaling. We detected reduced levels of arachidonate 5-lipoxygenase (ALOX5) and leukotriene A_4 in eculizumab-treated patients. Mechanistically, ligation of the C5a receptor (C5aR) is needed for ALOX5 metabolism and generation of downstream leukotrienes. As eculizumab prevents cleavage of C5 into C5a, decreased engagement of C5aR may inhibit ALOX5-mediated synthesis of pro-inflammatory leukotrienes. These findings indicate distinct off-target effects induced by eculizumab, illuminating potential mechanisms of action that may be harnessed to improve treatment outcomes.

Authorship note: CN and CBS are co–first authors.

Conflict of interest: CN reports personal fees from Argenx, Alexion Pharmaceuticals Inc., Merck, and UCB. AM has received speaker honoraria, consulting fees, or (institutional) financial research support from Alexion Pharmaceuticals Inc., Argenx, Grifols SA, Hormosan Pharma GmbH, Janssen, Octapharma, and UCB. He is chair of the medical advisory board of the German Myasthenia Gravis Society. TR reports grants from German Ministry of Education, Science, Research and Technology; grants and personal fees from Sanofi-Genzyme, Argenx, and Alexion Pharmaceuticals Inc.; personal fees from Argenx, Biogen, Roche, and Teva; and personal fees and nonfinancial support from Merck Serono.

Submitted: January 24, 2023
Accepted: May 23, 2023
Published: July 10, 2023

Reference information: *JCI Insight*. 2023;8(13):e169135. https://doi.org/10.1172/jci.insight.169135.

Introduction

Immunotherapies have long been used to treat autoimmunity. With the advent of targeted immunotherapies, a new generation of treatment options emerged for autoimmune diseases. These agents may provide sustained immune modulation with a more beneficial adverse effect profile than traditional immunosuppressants (**1**). One of these agents is the monoclonal antibody (Ab) eculizumab used to treat complement-mediated diseases (**2**, **3**). Eculizumab specifically binds to complement protein C5, preventing its cleavage into C5a and C5b, thereby precluding the formation of the terminal complement cascade (**4**). While eculizumab has demonstrated high efficacy even in cases of treatment-refractory autoimmune disease (**2**, **5**, **6**), studies investigating the long-term safety and mechanistic consequences are needed (**7**). Even more recently, a number of C5 inhibitors were developed, including ravulizumab, a monoclonal Ab with enhanced effect duration (**8**), and zilucoplan, a small molecule inhibitor of C5 (**9**), among others, which have revolutionized the treatment of several autoimmune disorders. This trend underlines the need for a deeper understanding of terminal complement inhibition. Following this line of thought, novel functions for complement have emerged besides its critical role in innate immunity, including regulation of effector T cell differentiation and

of metabolic pathways (**10**, **11**). Consequently, therapeutic ablation of the terminal complement cascade is likely to influence human biology beyond innate immune response inhibition.

Thus, we employed an in-depth proteomics and metabolomics approach to dissect the serological profile of anti–acetylcholine receptor antibody–positive (anti-AChR Ab^+) myasthenia gravis (MG) patients treated with eculizumab. Insight into the advantageous and disadvantageous consequences of treatment may prove valuable for patient selection and development of risk mitigation strategies.

Results

Eculizumab affects the terminal complement cascade. Aiming to explore the influence of eculizumab on the serum proteome and metabolome, we included 3 age- and sex-matched cohorts of patients with MG, treated with eculizumab or azathioprine (as most common first-line therapy) and treatment-naive patients (as control group). Patients were approximately 55 years old at baseline, with 2 women and 8 men in each group (**Table 1**). Eculizumab-treated patients received 2.8 (SD 1.6) previous ISTs, while azathioprine-treated patients received 1.5 (SD 2.5). Thymectomy had been performed in 3 eculizumab-treated, 1 treatment-naive, and 5 azathioprine-treated patients. Thymectomy was performed at least 6 months before study inclusion for all patients. No differences in steroid dosage were observed between eculizumab- and azathioprine-treated patients ($P = 0.68$). We performed in-depth proteomic analysis of patient serum samples using shotgun mass spectrometry (**Figure 1A**). To underline the feasibility of a proteomics approach, we first analyzed the common complement cascade of patients treated with eculizumab compared with all other patients. Complement proteins were readily detected (**Figure 1B**). Eculizumab forms a complex with C5 precluding the latter from cleavage, thus reducing the levels of free C5 in serum (**12**). Following lysis for proteomic analysis, the eculizumab-C5 complex was broken down and the individual peptides were recorded. Consequently, C5 levels were unchanged when measured by proteomics as compared to ELISA (**Supplemental Figure 4A**; supplemental material available online with this article; https://doi.org/10.1172/jci.insight.169135DS1) (**12**). In line with the inhibitory effect of eculizumab on C5 cleavage, proteomics detected increased levels of C6 and C7. To validate these results, we performed ELISA studies of C6 and C7 levels and verified that these proteins were increased in eculizumab-treated patients (**Figure 1B**). Intriguingly, while downstream complement factors C6 and C7 accumulated in eculizumab-treated patients, levels of C8 and C9 remained unchanged.

Taken together, analysis of the serum proteome corroborates eculizumab's mechanism of action.

Eculizumab alters the serum proteome beyond complement inhibition. Next, we assessed changes to the serum proteome eculizumab treatment induced. To this end, we reduced data set complexity by principal component analysis (PCA) (**Figure 2A**). Here, azathioprine-treated and treatment-naive patients were indistinguishable, while eculizumab-treated patients displayed altered clustering. Consistent with this, superimposing hierarchical clustering on the heatmap visualization separated eculizumab patients from all others (**Figure 2B**). Aside from shared protein patterns, we analyzed unique proteins for each cohort. As displayed in **Figure 2C**, the azathioprine and treatment-naive cohorts were characterized by 7 unique proteins. In contrast, the eculizumab cohort demonstrated no unique proteins.

To further dissect the proteome patterns resulting from eculizumab treatment, we performed functional enrichment analyses of differentially expressed proteins. Here, eculizumab treatment showed marked alterations of Gene Ontology (GO) terms and functional pathways when compared with azathioprine or treatment-naive patients (**Figure 3, A and D**). For MFs, the eculizumab cohort was enriched for antioxidant activity and cholesterol transfer activity, among others. In contrast, antigen binding was significantly enriched in treatment-naive and azathioprine-treated patients' serum samples but not in eculizumab-treated patients (**Figure 3, B and C**). For BPs, we found functional alterations for complement activation and regulation of complement activation in the eculizumab cohort, likely due to accumulation of terminal complement factors. Interestingly, serum from eculizumab-treated patients also revealed significantly altered high-density lipoprotein particle remodeling, regulation of wound healing, and cellular detoxification processes compared with azathioprine or treatment-naive patients. For CCs, we observed GO term enrichment for immunoglobulin complexes and blood microparticles in the eculizumab group, among others. Functional analysis of the KEGG pathway showed upregulation of complement and coagulation cascades in the eculizumab cohort. Analysis of the HPA database revealed no significant functional enrichment.

Together, these findings point toward highly complex consequences of eculizumab treatment, with alterations in multiple biological pathways that go beyond complement inhibition.

Table 1. Clinical and demographic baseline data of eculizumab-treated patients

Baseline characteristic	Eculizumab	Treatment-naive	Azathioprine
Age at baseline, years, mean (SD)	55.4 (12.8)	55.2 (11.8)	56.0 (13.0)
Age at diagnosis, years, mean (SD)	47.5 (12.3)	51.2 (26.9)	51.1 (16.9)
Early onset, *n* (%)	6 (60%)	6 (60%)	5 (50%)
Female, *n* (%)	2 (20%)	2 (20%)	2 (20%)
Number of previous ISTs, mean (SD)	2.8 (1.6)	0	1.5 (2.5)
Thymectomy, *n* (%)	3 (30%)	1 (10%)	5 (50%)
Anti-AChR Ab positive, *n* (%)	10 (100%)	10 (100%)	10 (100%)
Mean steroid dosage, mg, mean (SD)	5.5 (6.2)	0	6.5 (7.4)

Baseline is defined as time of blood sampling. Groups were matched by age and sex. Ab, antibody; AChR, acetylcholine receptor; IST, immunosuppressive therapy.

Distinct immunometabolic pathways are altered in eculizumab-treated patients. Aiming to dissect proteome patterns induced by terminal complement ablation, we compared individual proteins between groups (**Figure 4, A and B**, and **Figure 5A**). Here, we observed a marked increase of C4BP in serum of eculizumab-treated patients as compared with the other groups (**Figure 4C**). Besides, TF was increased in eculizumab-treated patients (**Figure 4D**). To validate these findings with a different method, C4BP and TF levels were measured by ELISA, corroborating the observations of proteomic analysis (**Supplemental Figure 4**, A and B). Consistent with the patterns observed for the GO term analysis, ALOX5 and APOC3/4 were altered in eculizumab-treated patients, pointing toward changes of the lipid metabolism in response to terminal complement ablation (**Figure 4E**). ALOX5 levels were verified by ELISA measurement (**Supplemental Figure 4C**). A further pattern emerged for the oxidative stress response with the MPO being reduced in the eculizumab group, while the antioxidant enzymes PRDX2/6 were increased (PRDX2 was significantly increased only when compared with treatment-naive patients) (**Figure 4F**). MAPKs are a ubiquitous group of enzymes that orchestrate cellular responses to a wide range of stimuli, including pro-inflammatory cytokines or osmotic stress (**13**).

Interestingly, various members of this group were altered in serum of eculizumab-treated patients: levels of MAPK8 were decreased compared with the azathioprine cohort, while MAP3K8 levels were significantly increased (**Figure 5B**). MAP3K8 is of interest as it represents a promoter for production of TNF-α and IL-2 in T lymphocytes. SKAP2 is required for macrophage migration and actin reorganization (**14**). We detected reduced SKAP2 levels in eculizumab-treated patients compared with azathioprine patients or treatment-naive controls (**Figure 5B**). Concurrently, the chemokine CCL22 was reduced in eculizumab-treated patients as compared with controls. The change of CCL22 was validated by ELISA (**Supplemental Figure 4D**).

Integration of metabolites indicates alterations of arachidonic acid metabolism by eculizumab. Next, we analyzed our metabolome data set, aiming to elaborate observed patterns following complement treatment. After data pre-processing and metabolite identification, a total of 289 unique metabolites were permitted for downstream analysis. Given the ability of sparse partial least squares discriminant analysis (sPLS-DA) to analyze noisy data with high collinearity (**15**), we tuned a model to fit our metabolomics data and reduce data set dimensionality (**Figure 6A** and **Supplemental Figure 1**). Here, all 3 groups demonstrated individual metabolome signatures. To identify altered pathways, we performed functional enrichment analysis of the eculizumab cohort using the KEGG database (**Figure 6B**). Interestingly, linoleic acid metabolism was the most enriched functional pathway in the eculizumab cohort. Given our previous observation of reduced ALOX5 levels, we suspected that arachidonic acid (AA) metabolism is altered due to complement blockade in eculizumab-treated patients. Linoleic acid is a precursor lipid metabolized to AA. Thus, we investigated metabolites correlating with ALOX5 by constructing a circos plot using the mixOmicsR package as adapted from González et al. (**16**) (**Figure 5C**). 5-HPETE was positively correlated with ALOX5. As such, we hypothesized that reduced ALOX5 levels result in altered AA metabolism and inhibition of downstream production of leukotrienes (**17**). AA is metabolized by ALOX5, resulting in 5-HPETE, which is further processed to LTA_4 (**17**). Indeed, comparison between groups revealed that 5-HPETE was reduced in the serum of eculizumab patients (**Figure 6C**). 5-HPETE is metabolized to LTA_4, a precursor of downstream leukotriene synthesis (**18**). However, LTA_4 could not be unambiguously detected in our metabolomics approach. In addition to its role in the leukotriene pathway, AA is also a

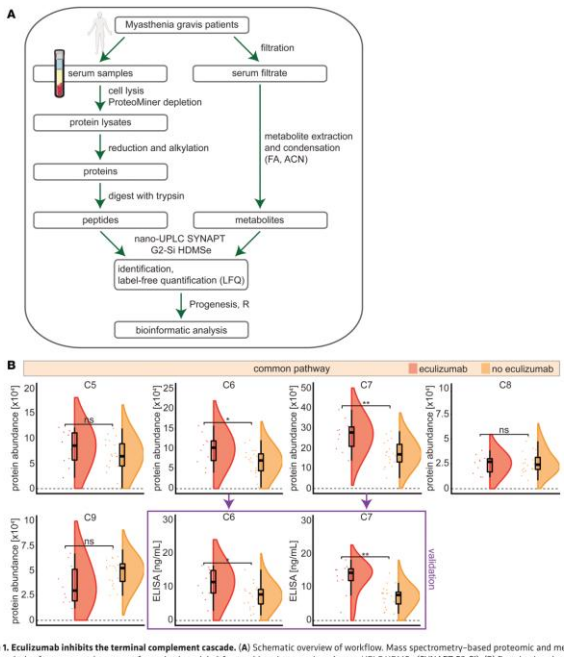

Figure 1. Eculizumab inhibits the terminal complement cascade. (**A**) Schematic overview of workflow. Mass spectrometry–based proteomic and metabolomic analysis of serum samples was performed using a label-free, unbiased approach and nano-UPLC HDMSe (**SYNAPT G2-Si**). (**B**) Protein abundance of serum proteins determined by proteomics displayed as raincloud plots. Protein levels were determined by ELISA measurement for C6 and C7 as validation. Whiskers are 1.5 IQR. Differences were determined by the 2-sided Student's *t* test for eculizumab (red) ($n = 10$) and no eculizumab (orange) ($n = 20$). ACN, acetonitrile; FA, formic acid; HDMSe, high-definition mass spectrometry; UPLC, ultra-performance liquid chromatography. $^{**}P < 0.01$, $^{*}P < 0.05$.

key precursor of prostaglandins. To investigate whether prostaglandin metabolism is also disturbed, we investigated levels of PGH_2 resulting from enzymatic activity of the PGH_2 synthase (**Figure 6D**). PGH_2 levels were unchanged across groups. Finally, we aimed to corroborate our previous data in a different methodical readout. To this end, we performed targeted analysis of PGH_2 and LTA_4 by ELISA. We analyzed these metabolites as they constitute important precursor metabolites for both prostaglandin and leukotriene metabolism. Here, LTA_4 levels were diminished in eculizumab-treated patients, while PGH_2

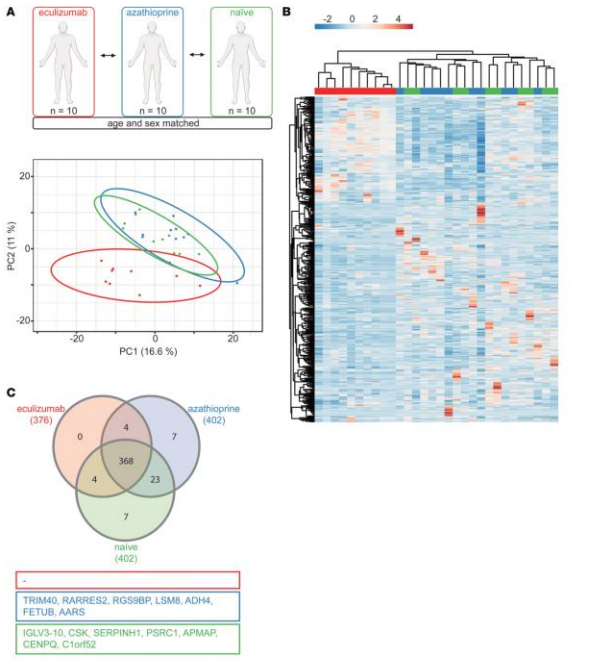

Figure 2. Eculizumab shapes the serum proteome. (**A**) PCA of serum proteome. SVD was used to calculate principal components. The *x* and *y* axes show principal component 1 and principal component 2, respectively. Prediction ellipses are such that with probability 0.95, a new observation from the same group will fall inside the ellipse. (**B**) Heatmap of serum proteome. Rows (proteins) and columns (replicates, here: patients) were clustered using correlation distance and average linkage. For multivariate analysis, rows were centered and unit variance scaling was applied. *P* value for significance was set to <0.05. (**C**) Venn diagram of serum proteome showing overlapping as well as unique expression profiles of the 3 analyzed data sets ($n = 10$ for each group). $N = 10$ per group. PCA, principal component analysis; SVD, singular value decomposition.

was unaltered across groups (Figure 6, E and F). To validate these observations, we acquired longitudinal samples from eculizumab-treated patients. We collected serum samples from 5 patients treated with azathioprine who were switched to eculizumab (Figure 6G). These patients were on average 52.5 years old (range 31 to 73) with 3 men and 2 women (Table 2). After the switch, azathioprine was discontinued,

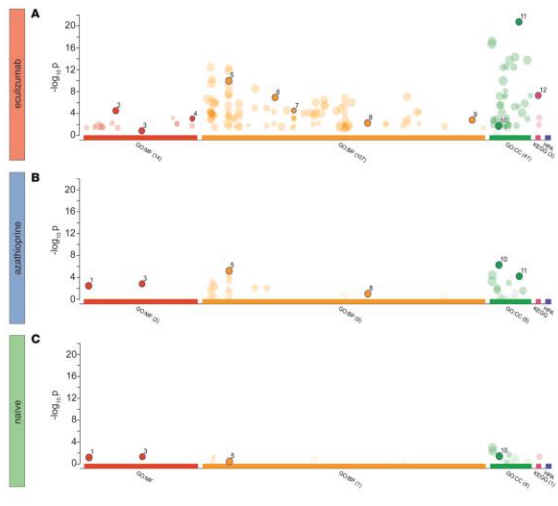

ID	Source	Term name	p (eculizumab)	p (azathioprine)	p (naive)
1	GO-MF	antigen binding	1.000	3.795×10^{-3}	7.216×10^{-2}
2	GO-MF	antioxidant activity	3.405×10^{-6}	1.000	1.000
3	GO-MF	immunoglobulin receptor binding	1.572×10^{-7}	1.651×10^{-3}	5.236×10^{-2}
4	GO-MF	cholesterol transfer activity	9.141×10^{-4}	1.000	1.000
5	GO-BP	complement activation	1.168×10^{-10}	6.749×10^{-6}	4.002×10^{-1}
6	GO-BP	regulation of complement activation	1.296×10^{-7}	1.000	1.000
7	GO-BP	high-density lipoprotein particle remodeling	3.029×10^{-6}	1.000	1.000
8	GO-BP	regulation of wound healing	5.789×10^{-3}	1.072×10^{-1}	1.000
9	GO-BP	cellular detoxification	1.661×10^{-3}	1.000	1.000
10	GO-CC	immunoglobulin complex	2.138×10^{-2}	5.858×10^{-7}	4.086×10^{-2}
11	GO-CC	blood microparticle	2.016×10^{-21}	6.743×10^{-5}	1.000
12	KEGG	complement and coagulation cascades	5.420×10^{-8}	1.000	1.000

Figure 3. Terminal complement inhibition influences functional pathways. (**A**–**C**) Manhattan plot illustrating functional enrichment of differentially regulated proteins (fold-change > 1.5) from the MF (molecular function), BP (biological process), CC (cellular component), KEGG (Kyoto Encyclopedia of Genes and Genomes), and HPA (Human Protein Atlas) databases, respectively. The analysis was performed using the R package gprofiler2 with g:SCS multiple-testing correction method applying significance threshold of 0.05. The $-\log_{10} P$ value is indicated on the *y* axis. IDs next to circles are annotated in **D**. Related GO terms and functional pathways were clustered together. The number in parentheses behind all depicted GO terms on the *x* axis denotes the number of found GO terms and functional pathways. (**D**) Table displaying GO terms and functional pathways of interest shown in **A**–**C**. $N = 10$ per group. GO, gene ontology.

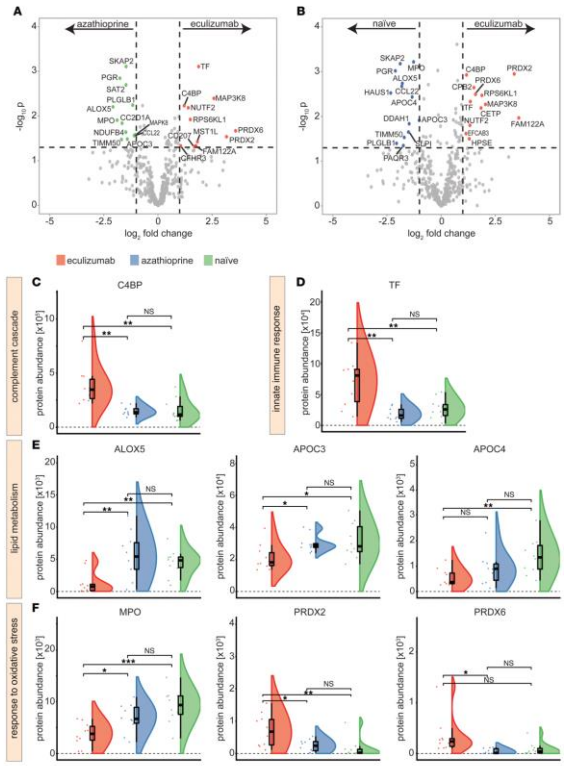

Figure 4. Unique protein signatures are observed for eculizumab-treated patients. (**A**) Volcano plot comparing azathioprine and eculizumab constructed by plotting $\log_2$ values of protein fold-changes between the 2 treatment groups against their $-\log_{10} P$ values. Differential regulation of expression levels was calculated by 1-way ANOVA. The horizontal dashed line indicates the significance cutoff value, which was set to $P < 0.05$. The vertical dashed lines indicate a fold-change cut-off of 1.0. (**B**) Volcano plot comparing treatment-naive and eculizumab-treated patients. (**C**–**F**) Protein abundance of

significantly regulated serum proteins of interest in **A** displayed as raincloud plots. Whiskers are 1.5 IQR. To account for multiple comparisons, statistical significance was corrected by the false discovery rate (FDR) approach. A threshold of q = 5% was used for FDR. One-way ANOVA testing was used for comparison of multiple groups. $N = 10$ per group. ALOX5, arachidonat-5-lipoxygenase; APOC3/4, apolipoprotein CIII/IV; C4BP, C4b-binding protein; CRP, C-reactive protein; MPO, myeloperoxidase; PRDX2/6, peroxiredoxin-2/6; TF, transferrin. ***$P < 0.001$, **$P < 0.01$, *$P < 0.05$.

patients were kept on eculizumab for 3 months, and serum samples were collected. Glucocorticoid dosages were kept stable for all patients with an average of 5 mg (SD 2.5). We measured LTA_4 and PGH_2 levels by ELISA comparing the status under treatment with eculizumab and before. Here, LTA_4 was decreased in eculizumab-treated patients, while PGH_2 levels remained unchanged (Figure 6, H and I).

Our data suggest that terminal complement blockade induces distinct alterations of AA homeostasis with inhibition of leukotriene production via ALOX5 metabolism (Figure 6J).

Interaction of C5a with the C5a receptor is needed for AA processing by ALOX5. Last, we aimed to understand the mechanistic link between terminal complement inhibition and altered ALOX5 metabolism. Two previous studies demonstrated that ligation of the C5a receptor (C5aR) induces synthesis and release of leukotriene B_4 (LTB_4) (**19**, **20**). LTB_4 is a downstream product of AA and LTA_4 exhibiting pro-inflammatory properties. As such, ALOX5 processing is required for LTB_4 generation (**19**, **20**). We suspected that reduced engagement of the C5aR downregulates ALOX5 activity in response to C5 inhibition, thereby decreasing LTA_4 and LTB_4 levels. To test this hypothesis, we investigated an in vitro model employing polymorphonuclear leukocytes (PMNs), the immune cells primarily involved in ALOX5 metabolism (**21**, **22**). To validate the ability of ALOX5 to produce LTB_4 in PMNs, we incubated these cells with increasing concentrations of recombinant C5a (Figure 7A). LTB_4 was quantified using an ELISA. In line with previous reports (**19**, **20**), C5a induced LTB_4 release in a dose-dependent manner. Based on these observations, we chose 500 ng/mL of C5a for further experiments. Next, we wanted to demonstrate that C5aR is required for LTB_4 release on PMNs. For this purpose, PMNs were incubated with C5a as well as PBS as control (Figure 7B). We used the C5aR inhibitor PMX53 (**23**) to test if the interaction of C5a and C5aR is needed for LTB_4 generation. Indeed, co-incubation with PMX53 (10 nM) diminished LTB_4 release. Second, PMNs were incubated with C5a and the ALOX5 inhibitor zileuton (**24**) (100 μM), also resulting in reduced LTB_4 levels. Taken together, these data suggest that interaction of C5a and C5aR triggers leukotriene synthesis by ALOX5.

Next, as the C5 inhibitor eculizumab prevents cleavage of C5 and release of C5a, we suspect that this mechanism is responsible for the observed effects. To test this hypothesis, we incubated PMNs with the serum of the 10 treatment-naive patients employed in this study as well as serum from the eculizumab-treated patients (Figure 7C). In response to the serum of treatment-naive patients, we recorded higher levels of LTB_4 as compared with incubation with eculizumab-treated serum or PBS. We also treated PMNs with the serum of treatment-naive patients as well as the C5aR inhibitor PMX53. In this setup, LTB_4 levels were also reduced, suggesting that the interaction of C5a and C5aR is required for the effect of eculizumab on downstream products of ALOX5 metabolism.

Taken together, eculizumab is likely to prevent ligation of C5aR on PMNs by inhibiting the generation of C5a. C5aR activation is needed to induce ALOX5 processing of AA; thus, eculizumab may decrease the generation of downstream leukotrienes.

Discussion

Eculizumab-mediated ablation of terminal complement activation has proved effective for treatment of anti-AChR Ab^+ MG patients (**3**). In order to improve treatment outcomes, knowledge of the consequences of complement modulation in the human system might be of value.

To this end, we analyzed the proteometabolome in a cohort of eculizumab patients, observing distinct patterns of signaling pathways induced by terminal complement ablation. First, we were interested in dissecting eculizumab's mechanism of action using a proteomics approach. Interestingly, eculizumab-mediated complement blockade is not without contestation, as previous immunoassays failed to detect reduced C5a levels in response to eculizumab treatment (**25**). This might be due to eculizumab inducing a C5a neopeptide falsely detected by immunoassays (**26**). Analysis of our proteomics data revealed an accumulation of C6 and C7 in serum of eculizumab-treated patients. These findings corroborate the mechanisms of action of eculizumab as eculizumab inhibits the cleavage of C5. Interestingly, levels of C8 and C9 remained unchanged using a proteomics approach. In this context, the influence of eculizumab on the peripheral level of terminal

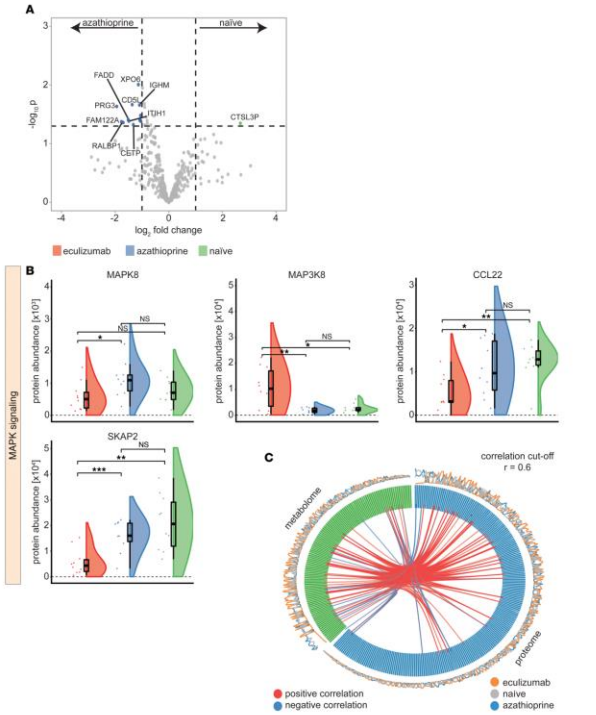

Figure 5. Eculizumab-associated changes to the proteometabolome. (**A**) Volcano plot comparing azathioprine and treatment-naive patients constructed by plotting $\log_2$ values of protein fold-changes between the 2 treatment groups against their $-\log_{10} P$ values. Differential regulation of expression levels was calculated by 1-way ANOVA. The horizontal dashed line indicates the significance cutoff value, which was set to $P < 0.05$. The vertical dashed lines indicate a fold-change cutoff of 1.0. (**B**) Protein abundance of significantly regulated serum proteins of interest displayed as raincloud plots. Whiskers are 1.5 IQR. To account for multiple comparisons, statistical significance was corrected by the false discovery rate (FDR) approach. A threshold of $q = 5\%$ was used for FDR. (**C**) Circos plot visualizing correlations between the proteome (blue) and metabolome (green). Correlations were calculated by pairwise variable association for large data matrixes. Inner lines display positive (red) and negative (blue) correlations between individual metabolites above the threshold of $r = 0.6$. The outer circle displays the serum abundance of individual data points measured by mass spectrometry.

One-way ANOVA testing was used for comparison of multiple groups. $N = 10$ per group. CCL22, CC motif chemokine ligand 22; MAPK8, mitogen-activated protein kinase 8; MAP3K8, mitogen-activated protein kinase kinase kinase 8; PGR, progesterone receptor; SKAP2, Src kinase-associated phosphoprotein 2. $^{***}P < 0.001$, $^{**}P < 0.01$, $^{*}P < 0.05$.

complement components remains heterogenous. In patients with atypical hemolytic uremic syndrome (**27**) or thrombotic microangiopathy after hematopoietic stem cell transplantation (**28**), eculizumab reduced sC5b-9 concentrations, while other studies did not observe a change in response to treatment (**29**). Indeed, eculizumab-mediated complement inhibition is dependent on pretreatment complement levels as well as on the underlying disease (**30**). Consequently, terminal complement patterns due to eculizumab treatment are likely subject to variation between diseases and individual patients.

We analyzed the serum proteome in order to elucidate the intricate relationship between complement modulation and cellular processes, observing alterations in the lipid metabolism; factors of innate immunity, e.g., TF; the oxidative stress response; and the heterogenous group of MAPK signaling pathways. Indeed, complement has been shown to induce MAPK signaling (**31**). As such, C5a-C5aR interaction contributes to renal injury by MAPK activation and release of pro-inflammatory cytokines in a trichloroethylene-sensitized mouse model (**31, 32**). Consistent with this, we observed alterations of proteins associated with MAPKs, e.g., upregulation of MAP3K8 and downregulation of SKAP2 or MAPK8. Interestingly, we also detected proteins with antioxidant function, e.g., PRDX2 and PRDX6, to be abundant in serum of eculizumab-treated patients. Complement activity contributes to tissue injury in response to oxidative stress with the classical and the lectin — but not the alternative — pathways mediating complement activation (**33, 34**). In contrast, little is known about the retrograde influence of complement inhibition on the oxidative stress response. Our data point to a potentially beneficial influence of eculizumab on the oxidative stress response.

Intriguingly, we also observed metabolic alterations in eculizumab-treated patients. AA metabolism is localized at the intersection point of cardiovascular and inflammatory biology (**35, 36**). Three distinct enzyme systems metabolize AA, resulting in a plethora of biological effects. First, cyclooxygenases generate prostanoids, such as thromboxane A_2 or prostaglandins, from AA. Second, the cytochrome P450 system metabolizes AA, generating hydroxyeicosatetraenoic acids capable of mediating pro-inflammatory signals (**37**). Last, the lipoxygenase pathway results in the formation of leukotrienes (**38**). ALOX5, perhaps the most studied lipoxygenase, inserts oxygen at the C-5 position of AA to promote the formation of 5-HPETE and finally LTA_4, the precursor of downstream leukotrienes (**17**). The biological relevance of this pathway is underlined by the efficacy of leukotriene antagonists, and ALOX5 inhibitors are used to treat bronchial asthma and seasonal allergies (**38, 39**). Of note, C5a has been demonstrated to recruit ALOX5 to process AA and stimulate leukotriene metabolism (**40**). Concurrently, liberation of thromboxane B2 and other metabolic products of AA degradation increases in the presence of complement proteins (**41, 42**). Following this line of argument, proteomic and metabolomic analyses corroborated that AA metabolism was blunted in response to eculizumab as 5-HPETE and LTA_4 — downstream products of AA processing by ALOX5 — were reduced compared with treatment-naive or azathioprine-treated patients. As an immunometabolic regulator, ALOX5 is primarily expressed by immune cells, such as granulocytes, macrophages/monocytes, and dendritic cells (**43**). Leukotrienes resulting from AA metabolism exert chemotactic properties and regulate immune cell activity and bronchoconstriction (**43, 44**). On a mechanistic level, C5a is required for ALOX5-mediated leukotriene generation by interacting with C5aR. Alterations of ALOX5 and downstream metabolites indicate the modulation of AA by terminal complement ablation as a potential off-target effect of eculizumab. Further studies are needed to understand whether modulation of leukotriene metabolism is indeed beneficial and to what extent this effect contributes to the clinical efficacy of eculizumab.

Given the rarity of MG and further aggravation by the limited application of eculizumab in clinical settings, this study is confined to a sample size of 10 patients for the eculizumab group. However, this study is designed as an explorative approach to better understand complement-modulating therapies. Consistent with this, the scope of an omics approach in a human model is not suited to deduce causality, but rather to highlight understudied or unknown mechanisms and stimulate further research. Further, assessment of metabolite levels is influenced by a plethora of confounders, including nutritional or environmental factors. Accordingly, additional studies are needed to account for potential external factors influencing metabolite readouts.

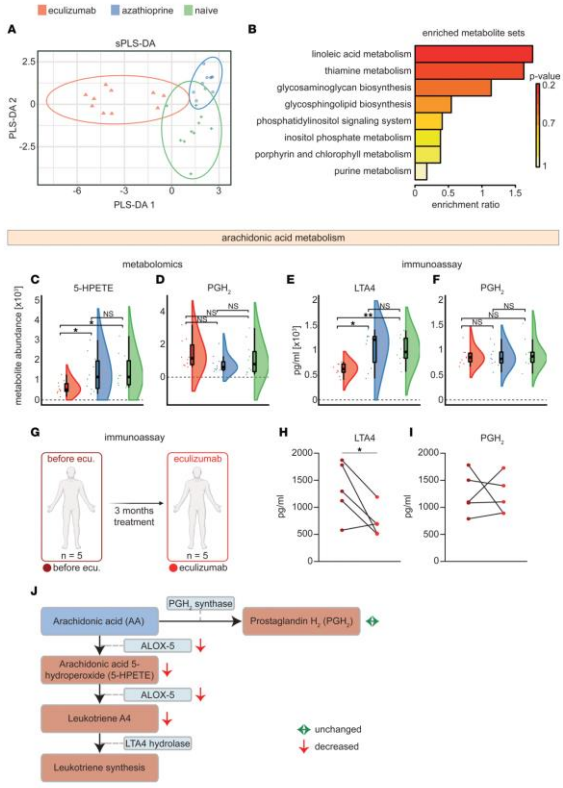

Figure 6. Immunometabolic pathways are altered in eculizumab-treated patients. (**A**) sPLS-DA score plot showing the metabolite data set for different groups. Prediction ellipses are 95% CI. (**B**) Functional enrichment analysis of the eculizumab cohort compared with other groups. Enrichment was performed by MetaboAnalystR package version 3.0 set to GSEA using the KEGG database. (**C** and **D**) Metabolite abundance of 5-HPETE and PGH_2 displayed

as raincloud plots. Metabolite levels were determined by metabolomic analysis. (**E** and **F**) Metabolite abundance of LTA_4 and PGH_2 displayed as raincloud plots. Metabolite levels were determined by immunoassay. Whiskers are 1.5 IQR. (**G**) For longitudinal analysis, samples were acquired from 5 patients before and under eculizumab treatment. (**H**) Longitudinal analysis shows reduction of LTA_4 level in eculizumab-treated patients. (**I**) PGH_2 levels remained unchanged after switching to eculizumab. "Before eculizumab" and "eculizumab" are represented in dark red and red, respectively. (**J**) Schematic overview of AA metabolism. Changes observed in this study are indicated by arrows. To account for multiple comparisons, statistical significance was corrected by the false discovery rate (FDR) approach. A threshold of $q = 5\%$ was used for FDR. ANOVA testing was used for comparison of multiple groups. $N = 10$ per group. 5-HPETE, arachidonic acid 5-hydroperoxide; GSEA, gene set enrichment analysis; LTA_4, leukotriene A_4; PGH_2, prostaglandin H_2; sPLS-DA, sparse partial least squares discriminant analysis.

Nonetheless, these findings demonstrate that the eculizumab-induced proteometabolome is a valuable model for understanding the influence of terminal complement ablation on human biology and for exploring potential mechanisms shaping treatment outcomes beyond inhibition of the complement cascade.

Methods

Ethics and human participants. All patients were required to meet the national guidelines for the diagnosis of MG (**45**). We included 3 age- and sex-matched cohorts with a total of 30 patients for cross-sectional comparison ($n = 10$ per group). Clinical and demographic baseline data are given in **Table 1**. We compared eculizumab patients with azathioprine (as a prominent first-line therapy) and treatment-naive patients. Patients were required to be treated with eculizumab for at least 3 months prior to blood sampling. To adjust for disease severity as a potential confounder, patients treated with eculizumab and patients treated with azathioprine were required to meet the following criteria defining a therapy-refractory course of disease in accordance with national guidelines (**45**): (**a**) Clinical severity: Myasthenia Gravis Foundation of America status of ≥III. (**b**) Previous immunotherapies: 2 previous immunotherapies with a treatment period of at least 12 months for azathioprine, mycophenolate, cyclosporine A, methotrexate, or steroids at maximum tolerable dose without sufficient symptom control. (**c**) Adverse effects: discontinuation of at least 2 previous immunotherapies due to intolerable adverse effects. (**d**) Myasthenic crisis: myasthenic crises requiring intensive care treatment.

For this study, patients treated with eculizumab and azathioprine were required to fulfil criterion (**a**) and at least 1 other criterion. Azathioprine-treated patients were required to be eligible for eculizumab treatment. Treatment-naive patients were required not to meet any of criteria (**b**) to (**d**). Both eculizumab- and azathioprine-treated patients were required not to be concurrently treated with a second IST. Low-dose steroids (<10 mg/d) were permitted.

Biomaterial and patient cohort. Serum samples were acquired after obtaining written informed consent. At the time of sampling, patients were required to have no evidence of infection. Serum samples from patients were stored according to the predefined standard operating procedure at the local biobanks of the Heinrich Heine University Düsseldorf and the Charité Berlin at –80°C. Later, they were transferred for measurement on dry ice to the Core Unit Proteomics facility of the University of Münster.

Lysate generation and processing for proteomic deep mapping. Serum samples (200 μL) were depleted according to the instructions of the manufacturer using the ProteoMiner kit (Bio-Rad Laboratories Inc.). This subproteome was placed in Pall Nanosep 10K Omega filter units (10 kDa cutoff) and centrifuged (12,500*g*, room temperature, 30 minutes). The analyte was washed by adding 100 μL of urea buffer (8 M urea, 100 mM Tris base) to the filter unit and was centrifuged (room temperature, 200*g*, and 30 minutes; same centrifuge settings used throughout). For reduction (45 minutes), 100 μL of 50 mM dithiothreitol in urea buffer was added to the filter unit. Subsequently, the unit was again centrifuged, and the sample was rinsed with 100 μL urea buffer. For alkylation, 50 mM iodoacetamide in urea buffer was placed into the filter unit. Incubation proceeded in the dark for 30 minutes at room temperature. Following centrifugation and rinsing twice with 300 μL 50 mM NH_4HCO_3 containing 10% acetonitrile in urea buffer and 200 μL of 0.01 μg/μL trypsin in 50 mM NH_4HCO_3 containing 10% acetonitrile were added to the filter unit. Incubation proceeded at 37°C overnight. Peptides were collected by rinsing the filter thrice with 5% acetonitrile/0.1% formic acid followed by centrifugation. Samples were dried using a Speedvac (Thermo Fisher Scientific) and redissolved in 10 μL 5% acetonitrile/0.1% formic acid.

Mass spectrometry–based proteomics. Peptide solutions (0.5 μL) were analyzed by reversed-phase chromatography coupled to ion mobility mass spectrometry with SYNAPT G2-Si/M-Class nano-UPLC (Waters Corporation) using PharmaFluidics C18 μPAC columns (trapping and 50 cm analytical). Data were analyzed using Progenesis for Proteomics (Waters Corporation) and the UniProt human database. One missed

Table 2. Clinical and demographic baseline data of eculizumab-treated patients switched from azathioprine

Number of patients	5
Age at baseline, years, mean (SD)	52.5 (24.2)
Age at diagnosis, years, mean (SD)	45.5 (14.5)
Early onset, *n* (%)	2 (40%)
Female, *n* (%)	2 (40%)
Number of previous ISTs, mean (SD)	1 (0)
Thymectomy, *n* (%)	2 (40%)
Anti-AChR Ab positive, *n* (%)	5 (100%)
Mean steroid dosage, mg, mean (SD)	5 (2.5)
Clinical indication for switch (for each patient)	Patient 1: elevated liver enzymes Patient 2: elevated liver enzymes Patient 3: insufficient treatment response Patient 4: elevated liver enzymes Patient 5: insufficient treatment response
Individual washout period (for each patient)	Patient 1: 3 months Patient 2: 4.5 months Patient 3: 6 months Patient 4: 3.5 months Patient 5: 12 months

Baseline is defined as time of blood sampling. The washout period is defined as the time between the end of the azathioprine therapy and the start of eculizumab. Ab, antibody; AChR, acetylcholine receptor; IST, immunosuppressive therapy.

cleavage was allowed, carbamidomethylation was set as fixed, and methionine oxidation was set as a variable modification. A short list of the protein output was created by demanding protein assignment by at least 2 peptides. Histograms of the acquired proteome (**Supplemental Figure 1**) illustrate normal distribution of included patient samples.

Lysate generation and processing for metabolomic profiling. Serum (10 μL) was filtered using Pall Nanosep 10K Omega units (3.5 kDa cutoff), washed thrice with 5% acetonitrile/0.1% formic acid, dried, and redissolved in 10 μL 5% acetonitrile/0.1% formic acid.

Mass spectrometry–based metabolomics. Mass spectrometry was performed using above instrumentation in MSe mode. For data analysis we used Progenesis with Metascope, LipidBlast, ChemSpider, and Metlin databases. Hits with multiple substance assignments were not used. Metabolites were identified based on their mass, retention time, and mass spectra. A total of 8,893 hits were recorded. After metabolite extraction and exclusion of missing values, 289 unique metabolites were permitted for downstream analyses. Distribution of metabolites across patient samples is illustrated as histograms (**Supplemental Figure 2**).

ELISAs. The patients' serum samples were tested protein levels via ELISA kits according to the manufacturer's instructions. These included ALOX5 (Abbexa, catalog abx250809), C4BP (MyBioSource, catalog MBS9303010), C6 (Abcam, catalog ab230934), C7 (Abcam, catalog ab125964), CCL22 (Bio-Techne, catalog DMD00), LTA_4 (Abbexa, catalog abx150355), LTB_4 (Abbexa, catalog abx257172), and TF (Abcam, catalog ab220653). We performed dilution series and used dilutions of 1:50 for the final assays. Samples were measured in technical duplicates with the Tecan plate reader Infinite M200 Pro.

Cell culture experiments. PMNs were isolated from peripheral blood from healthy donors as previously described based on density gradients (**22**). PMNs were resuspended in DMEM in 6-well dishes with 10^6 cells per sample. PMNs were incubated at 37°C and 5% CO_2. PMNs were treated with substances at indicated concentrations or with serum samples for 6 hours. Afterward, supernatants were harvested and stored at −80°C. Concentration of LTB_4 was determined by ELISA according to the manufacturer's instructions. For stimulation with C5a, we used recombinant C5a (R&D Systems). PMX53 and zileuton were purchased from R&D Systems. For co-incubation with human serum, 500 mL of serum was added to each well containing 1 mL of DMEM.

Visualization. Figures were created using Adobe Illustrator (version 2020) and Servier Medical Art (https://smart.servier.com).

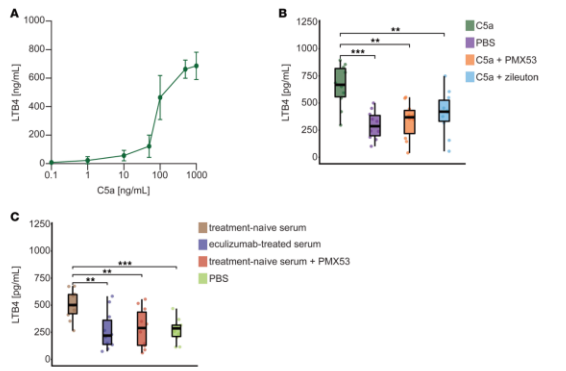

Figure 7. Interaction of C5a with the C5aR is needed for AA processing by ALOX5. (**A**) PMNs were incubated with indicated concentrations of recombinant C5a for 6 hours. Concentrations of LTB_4 were determined by ELISA ($n = 5$). (**B**) PMNs were incubated with indicated substances (C5a 500 ng/mL, C5a + PMX53 10 nM, C5a + zileuton 100 μM, or PBS) for 6 hours ($n = 10$ per group). (**C**) PMNs were incubated with indicated serum from treatment-naive patients with MG or eculizumab-treated patients with MG for 6 hours. PMNs were also incubated with treatment-naive serum and a final concentration of PMX53 of 10 nM or PBS for 6 hours ($n = 10$ per group). Box plots show the interquartile range (box), median (line), and minimum and maximum (whiskers). Groups were compared by 2-sided Student's *t* test. ***$P < 0.001$, **$P < 0.01$. ALOX5, arachidonate 5-lipoxygenase; LTB_4, leukotriene B_4; PMNs, polymorphonuclear leukocytes.

Statistics. Statistical analysis was performed using R 3.5.3. Data were presented as median (IQR), mean (SD), or *n* (%). Differences between groups were analyzed using unpaired Student's *t* test or Mann-Whitney *U* test as appropriate. One-way ANOVA test or Kruskal-Wallis test was used for multiple groups as appropriate.

Prior to multivariate analysis, data were centered, and unit variance scaling was utilized. For PCA, each patient was treated as 1 data point. For heatmaps, rows and columns were clustered using correlation distance and average linkage. Raincloud plots were constructed as previously described (**46**). Volcano plots were created by plotting $\log_2$ values of the relative difference between the mean protein expression values against the $-\log_{10}$ *P* values. For simple regression analysis, we included the Quantitative MG score, MG Activities of Daily Living score and the MG Quality of Life score as dependent variables. sPLS-DA was performed on normalized metabolomics data using mixOmics package version 6.16 as previously described (**47**, **48**) (**Supplemental Figure 3A**). The model was tuned using a 3-fold internal cross validation repeated 50 times to minimize the balanced error rate (**Supplemental Figure 3B**).

For enrichment analysis, differentially expressed proteins were defined as having an adjusted *P* value of < 0.05. We employed the following databases to identify the enriched MFs and associated biological pathways: GO (**49**), KEGG (**50**), and the HPA (**51**). The functional enrichment analysis for proteomics was performed using the R package gProfiler (version 0.70) with g:SCS multiple-testing correction method applying significance threshold of 0.05 (**52**). Functional enrichment of metabolite data was performed with the MetaboAnalyst R package version 3.0 set to GSEA as previously described (**53**). Differences were considered statistically significant with the following *P* values: *$P < 0.05$, **$P < 0.01$, ***$P < 0.001$, and ****$P < 0.0001$.

Study approval. All work performed in this study was in accordance with the Declaration of Helsinki. For this study, patients were recruited from the University Hospital Düsseldorf (Ethikkomission der HHU, Düsseldorf, Germany; ethics approval: 2016-053-f-S and 2021-1417) and the Charité Berlin

(Ethikkomission der Charité Berlin, Berlin, Germany; ethics approval: EA1/281/10). Patients provided oral and written informed consent before inclusion.

Data availability. The full data set is available via ProteomeXchange with identifier PXD040786. The analytical code for the manuscript is available from the corresponding author on reasonable request.

Author contributions

CBS, CN, SGM, and TR designed the study and methods; formal analysis was done by CBS and CN; CBS and CN performed the experiments and were responsible for data analysis; clinical data were provided by CBS, CN, FS, MP, AM, SGM, and TR; resources were provided by FS, AM, SGM, and TR; CBS and CN wrote the original draft; FS, NH, MP, AW, SR, NM, UD, ST, KS, AR, AM, SGM, and TR reviewed and edited the manuscript; figures were created by CBS, CN, and NH; funding acquisition was performed by SGM and TR; and supervision was provided by AM, SGM, and TR. CN and CBS contributed equally. The order was determined by coin flip.

Acknowledgments

Mass spectrometry–based measurements were performed by Simone König (Core Unit Proteomics, Interdisciplinary Center for Clinical Research, Medical Faculty, University of Münster, Münster, Germany). This work was supported by the internal research funding program of the Heinrich Heine University to CN, CBS, and TR (2021-40).

Address correspondence to: Tobias Ruck, Department of Neurology, Heinrich Heine University Düsseldorf, Moorenstraße 5, D-40225 Düsseldorf, Germany. Phone: 0049.0.211.81.17880; Email: tobias.ruck@uni-duesseldorf.de.

1. Bucktrout SL, et al. Recent advances in immunotherapies: from infection and autoimmunity, to cancer, and back again. *Genome Med*. 2018;10(1):79.
2. Pittock SJ, et al. Eculizumab in aquaporin-4-positive neuromyelitis optica spectrum disorder. *N Engl J Med*. 2019;381(7):614–625.
3. Howard JF Jr., et al. Safety and efficacy of eculizumab in anti-acetylcholine receptor antibody-positive refractory generalised myasthenia gravis (REGAIN): a phase 3, randomised, double-blind, placebo-controlled, multicentre study. *Lancet Neurol*. 2017;16(12):976–986.
4. Thomas TC, et al. Inhibition of complement activity by humanized anti-C5 antibody and single-chain Fv. *Mol Immunol*. 1996;33(17):1389–1401.
5. Muppidi S, et al. Long-term safety and efficacy of eculizumab in generalized myasthenia gravis. *Muscle Nerve*. 2019;60(1):14–24.
6. Nelke C, et al. Eculizumab versus rituximab in generalised myasthenia gravis. *J Neurol Neurosurg Psychiatry*. 2022;93(5):548–554.
7. Menon D, et al. Novel treatments in myasthenia gravis. *Front Neurol*. 2020;11:538.538.
8. Vu T, et al. Terminal complement inhibitor ravulizumab in generalized myasthenia gravis. *NEJM Evid*. 2022;1(5):1–12.
9. Howard JF, et al. Clinical effects of the self-administered subcutaneous complement inhibitor zilucoplan in patients with moderate to severe generalized myasthenia gravis: results of a phase 2 randomized, double-blind, placebo-controlled, multicenter clinical trial. *JAMA Neurol*. 2020;77(5):1–592.
10. Hess C, Kemper C. Complement-mediated regulation of metabolism and basic cellular processes. *Immunity*. 2016;45(2):240–254.
11. Liszewski MK, et al. Intracellular complement activation sustains T cell homeostasis and mediates effector differentiation. *Immunity*. 2013;39(6):1143–1157.
12. Monteleone JPR, et al. Eculizumab pharmacokinetics and pharmacodynamics in patients with generalized myasthenia gravis. *Front Neurol*. 2021;12:696385.
13. Zhang W, Liu HT. MAPK signal pathways in the regulation of cell proliferation in mammalian cells. *Cell Res*. 2002;12(1):9–18.
14. Alenghat FJ, et al. Macrophages require Skap2 and Sirpα for integrin-stimulated cytoskeletal rearrangement. *J Cell Sci*. 2012;125(22):5535–5545.
15. Bujak R, et al. PLS-based and regularization-based methods for the selection of relevant variables in non-targeted metabolomics data. *Front Mol Biosci*. 2016;3:35.
16. González I, et al. Visualising associations between paired 'omics' data sets. *BioData Min*. 2012;5(1):19.
17. Shimizu T, et al. Characterization of leukotriene A4 synthase from murine mast cells: evidence for its identity to arachidonate 5-lipoxygenase. *Proc Natl Acad Sci U S A*. 1986;83(12):4175–4179.
18. Peters-Golden M, Henderson WR. Leukotrienes. *N Engl J Med*. 2007;357(18):1841–1854.
19. Miyabe Y, et al. Complement C5a receptor is the key initiator of neutrophil adhesion igniting immune complex-induced arthritis. *Sci Immunol*. 2017;2(7):eaaj2195.
20. Sadik CD, et al. Neutrophils orchestrate their own recruitment in murine arthritis through C5aR and FcγR signaling. *Proc Natl Acad Sci U S A*. 2012;109(46):E3177–E3185.
21. Poirier SJ, et al. LPS induces ALOX5 promoter activation and 5-lipoxygenase expression in human monocytic cells. *Prostaglandins Leukot Essent Fatty Acids*. 2020;154:102078.
22. Cui C, et al. Isolation of polymorphonuclear neutrophils and monocytes from a single sample of human peripheral blood. *STAR Protoc*. 2021;2(4):100845.

23. Kumar V, et al. Preclinical pharmacokinetics of complement C5a receptor antagonists PMX53 and PMX205 in mice. *ACS Omega*. 2020;5(5):2345–2354.
24. Rossi A, et al. The 5-lipoxygenase inhibitor, zileuton, suppresses prostaglandin biosynthesis by inhibition of arachidonic acid release in macrophages. *Br J Pharmacol*. 2010;161(3):555–570.
25. Burwick RM, et al. Eculizumab fails to inhibit generation of C5a in vivo. *Blood*. 2014;124(23):3502–3503.
26. Nilsson PH, et al. Eculizumab-C5 complexes express a C5a neoepitope in vivo: consequences for interpretation of patient complement analyses. *Mol Immunol*. 2017;89:111–114.
27. Cofiell R, et al. Eculizumab reduces complement activation, inflammation, endothelial damage, thrombosis, and renal injury markers in aHUS. *Blood*. 2015;125(21):3253–3262.
28. Jodele S, et al. Variable eculizumab clearance requires pharmacodynamic monitoring to optimize therapy for thrombotic microangiopathy after hematopoietic stem cell transplantation. *Biol Blood Marrow Transplant*. 2016;22(2):307–315.
29. Morris M, et al. Dynamics of complement activation in aHUS and how to monitor eculizumab therapy. *Blood*. 2014;124(11):1715–1726.
30. Wijnsma KL, et al. Pharmacology, pharmacokinetics and pharmacodynamics of eculizumab, and possibilities for an individualized approach to eculizumab. *Clin Pharmacokinet*. 2019;58(7):859–874.
31. Fattahi F, et al. Complement-induced activation of MAPKs and Akt during sepsis: role in cardiac dysfunction. *FASEB J*. 2017;31(9):4129–4139.
32. Zhang J, et al. Complement C5a-C5aR interaction enhances MAPK signaling pathway activities to mediate renal injury in trichloroethylene sensitized BALB/c mice. *J Appl Toxicol*. 2016;36(2):271–284.
33. Collard CD, et al. Complement activation after oxidative stress: role of the lectin complement pathway. *Am J Pathol*. 2000;156(5):1549–1556.
34. Collard CD, et al. Reoxygenation of hypoxic human umbilical vein endothelial cells activates the classic complement pathway. *Circulation*. 1997;96(1):326–333.
35. Wang B, et al. Metabolism pathways of arachidonic acids: mechanisms and potential therapeutic targets. *Signal Transduct Target Ther*. 2021;6(1):94.
36. Zhang T, et al. The associations of plasma phospholipid arachidonic acid with cardiovascular diseases: a Mendelian randomization study. *EBioMedicine*. 2021;63:103189.
37. Capdevila J, et al. Cytochrome P-450-dependent oxygenation of arachidonic acid to hydroxyicosatetraenoic acids. *Proc Natl Acad Sci U S A*. 1982;79(3):767–770.
38. Lewis RA, et al. Leukotrienes and other products of the 5-lipoxygenase pathway. Biochemistry and relation to pathobiology in human diseases. *N Engl J Med*. 1990;323(10):645–655.
39. Diamant Z, et al. Montelukast in the treatment of asthma and beyond. *Expert Rev Clin Immunol*. 2009;5(6):639–658.
40. Clancy RM, et al. Arachidonate metabolism by human polymorphonuclear leukocytes stimulated by N-formyl-Met-Leu-Phe or complement component C5a is independent of phospholipase activation. *Proc Natl Acad Sci U S A*. 1983;80(23):7200–7204.
41. Polley MJ, et al. Human complement in the arachidonic acid transformation pathway in platelets. *J Exp Med*. 1981;153(2):257–268.
42. Imagawa DK, et al. Consequences of cell membrane attack by complement: release of arachidonate and formation of inflammatory derivatives. *Proc Natl Acad Sci U S A*. 1983;80(21):6647–6651.
43. Häfner A-K, et al. Beyond leukotriene formation-the noncanonical functions of 5-lipoxygenase. *Prostaglandins Other Lipid Mediat*. 2019;142:24–32.
44. Yokomizo T, et al. Leukotriene receptors as potential therapeutic targets. *J Clin Invest*. 2018;128(7):2691–2701.
45. Diener HC, et al. 68 Diagnostik und Therapie der Myasthenia gravis und des Lambert-Eaton-Syndroms. https://www.thieme-connect.de/products/ebooks/lookinside/10.1055/b-0034-37851. Accessed June 1, 2023.
46. Allen M, et al. Raincloud plots: a multi-platform tool for robust data visualization. *Wellcome Open Res*. 2019;4:63.
47. Rohart F, et al. mixOmics: an R package for 'omics feature selection and multiple data integration. *PLoS Comput Biol*. 2017;13(11):e1005752.
48. Lê Cao K-A, et al. Sparse PLS discriminant analysis: biologically relevant feature selection and graphical displays for multiclass problems. *BMC Bioinformatics*. 2011;12(1):253.
49. Mi H, et al. PANTHER version 14: more genomes, a new PANTHER GO-slim and improvements in enrichment analysis tools. *Nucleic Acids Res*. 2019;47(D1):D419–D426.
50. Kanehisa M, Sato Y. KEGG Mapper for inferring cellular functions from protein sequences. *Protein Sci*. 2020;29(1):28–35.
51. Uhlen M, et al. A pathology atlas of the human cancer transcriptome. *Science*. 2017;357(6352):eaan2507.
52. Raudvere U, et al. g:Profiler: a web server for functional enrichment analysis and conversions of gene lists (2019 update). *Nucleic Acids Res*. 2019;47(w1):W191–W198.
53. Pang Z, et al. MetaboAnalyst 5.0: narrowing the gap between raw spectra and functional insights. *Nucleic Acids Res*. 2021;49(w1):W388–W396.

Journal of Neuroinflammation

RESEARCH Open Access

Independent risk factors for myasthenic crisis and disease exacerbation in a retrospective cohort of myasthenia gravis patients

Christopher Nelke[1,4†], Frauke Stascheit[2,3†], Carmen Eckert[4], Marc Pawlitzki[1,5], Christina B. Schroeter[1], Niklas Huntemann[1], Philipp Mergenthaler[2,3,11], Ercan Arat[1], Menekse Öztürk[1], Dirk Foell[6], Stefanie Schreiber[7,14,15], Stefan Vielhaber[7,14,15], Asmae Gassa[8], Henning Stetefeld[9], Michael Schroeter[9], Benjamin Berger[10], Andreas Totzeck[11], Tim Hagenacker[11], Sven G. Meuth[1], Andreas Meisel[2,3,12,13], Heinz Wiendl[4] and Tobias Ruck[1,4*]

Abstract

Background: Myasthenic crisis (MC) and disease exacerbation in myasthenia gravis (MG) are associated with significant lethality and continue to impose a high disease burden on affected patients. Therefore, we sought to determine potential predictors for MC and exacerbation as well as to identify factors affecting outcome.

Methods: We examined a retrospective, observational cohort study of patients diagnosed with MG between 2000 and 2021 with a mean follow-up of 62.6 months after diagnosis from eight tertiary hospitals in Germany. A multivariate Cox regression model with follow-up duration as the time variable was used to determine independent risk factors for MC and disease exacerbation.

Results: 815 patients diagnosed with MG according to national guidelines were included. Disease severity at diagnosis (quantitative MG score or Myasthenia Gravis Foundation of America class), the presence of thymoma and anti-muscle specific tyrosine kinase-antibodies were independent predictors of MC or disease exacerbation. Patients with minimal manifestation status 12 months after diagnosis had a lower risk of MC and disease exacerbation than those without. The timespan between diagnosis and the start of immunosuppressive therapy did not affect risk. Patients with a worse outcome of MC were older, had higher MGFA class before MC and at admission, and had lower vital capacity before and at admission. The number of comorbidities, requirement for intubation, prolonged mechanical ventilation, and MC triggered by infection were associated with worse outcome. No differences between outcomes were observed comparing treatments with IVIG (intravenous immunoglobulin) vs. plasma exchange vs. IVIG together with plasma exchange.

Conclusions: MC and disease exacerbations inflict a substantial burden of disease on MG patients. Disease severity at diagnosis and antibody status predicted the occurrence of MC and disease exacerbation. Intensified monitoring with emphasis on the prevention of infectious complications could be of value to prevent uncontrolled disease in MG patients.

Keywords: Myasthenic crisis, Myasthenia gravis, Disease exacerbation, Risk factors, Predictors

Graphical Abstract

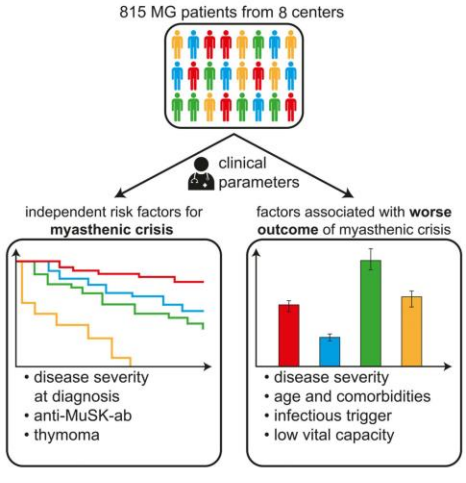

*Correspondence: tobias.ruck@med.uni-duesseldorf.de
†Christopher Nelke and Frauke Stascheit contributed equally to this work.
[1] Department of Neurology, Medical Faculty, Heinrich Heine University Düsseldorf, Moorenstraße 5, 40225 Duesseldorf, Germany
Full list of author information is available at the end of the article

Background

Myasthenia gravis (MG) is an acquired autoimmune disorder of the neuromuscular junction characterized by dysfunction of the post-synaptic membrane [1]. Owing to improved treatment strategies and diagnostic tools, therapeutic outcomes have improved for the majority of MG patients [2]. However, a clinically distinct subgroup of patients, often referred to as refractory, remains symptomatic despite therapy [2, 3]. Exacerbation of disease and myasthenic crisis (MC) are frequent in these patients and substantially contribute to disease burden [4]. Despite diagnostic and therapeutic advances for the management of MG, patients experiencing MC continue to face a substantial mortality rate of approximately 5–12% [5, 6]. The requirement for hospitalisation, the associated burden of disease and the cost of available rescue therapies, underline the importance of the prevention and management of MC [7, 8].

Hindered by the rarity of MG, our understanding of the underlying pathophysiological mechanisms related to insufficient disease control remains fragmented. A range of potential triggers for the manifestation of MC or disease exacerbations have been observed including infections, surgery, adverse effects of medication, comorbidity, pregnancy or tapering of immunosuppressive medication [9, 10]. Prognostic factors identifying patients at risk for MC or disease exacerbations remain incompletely understood and have only been characterized for MG patients presenting with a thymoma [11, 12]. However, factors predicting the occurrence of MC especially in patients without thymoma remain largely elusive. Finally, factors defining the outcome of MC are incompletely identified, but urgently needed to guide the clinical management of these patients. Our analysis aims at understanding factors predicting clinical deteriorations. We therefore analysed a cohort of 815 MG patients to identify potential risk factors for MC and disease exacerbations.

Methods

Study design and participants

Our cohort study is a retrospective analysis of 815 patients from eight university hospitals in Germany (Charité—Universitätsmedizin Berlin and University Hospitals Cologne, Duesseldorf, Essen, Freiburg, Magdeburg, Muenster and Regensburg). Patients requiring intensive care were treated on specialized neurological intensive care units (NICU). Patients were identified by searching the on-site database for the corresponding ICD-10 code (ICD-10-GM-2019 G70.-). Overall, 1645 patients were screened, of whom 815 were included in the analysis (Fig. 1). Diagnosis of MG was established by characteristic clinical presentation in accordance with national guidelines [13], independent of disease duration or severity. All centres are certified as integrated myasthenia centre (iMC) by the German Myasthenia Gravis Society applying standardised clinical pathways for patient management. Diagnosis was supported by antibody findings and repetitive nerve stimulation. Antibody testing was performed by enzyme-linked- or radio-immunoassay (Euroline). Suspected cases without established diagnosis, with a change to their diagnosis ($n=609$) or with insufficient case documentation were excluded (<6 months of longitudinal documentation) ($n=127$) (Fig. 1). The final cohort consisted of patients diagnosed between January 2000 and July 2021. Patients with an established diagnosis and sufficient longitudinal documentation of >6 months were included during this time period. Socio-demographics (age, sex, disease duration), antibody (ab) status (acetylcholine-receptor (AChR), muscle specific receptor tyrosine kinase (MuSK), lipoprotein-related protein 4 (LRP4), seronegative), MG specific medication (cholinesterase-inhibitors, glucocorticoids, and long-term immunosuppressant's), history of thymoma-status, and comorbidities were collected from patient' charts. The follow-up strategy was standardized across centres. According to iMC standards, patients with a stable course were seen every 6 months and instable patients more frequently. MG-specific scoring was performed by the treating neurologist at the time of presentation.

Definitions

For this cohort analysis, we differentiated between MC and disease exacerbation as distinct clinical events.

A MC was defined as a rapid clinical decline requiring non-invasive ventilation, intubation or parenteral nutrition [14]. Dysphagia severe enough to require a nasogastric tube was also included as criterion for MC.

A disease exacerbation was defined as fulfilment all of the following criteria as adapted from national guidelines [15]:

- Objective: QMG (quantitative myasthenia gravis) score [16] of ≥ 8 points and a minimum increase of ≥ 5 points from the previous visit. Ocular findings must not account for more than 5 points on the QMG score.
- Subjective: progressive clinical deterioration due to weakness of bulbo-pharyngeal or limb muscles or reduced respiratory function impacting activities of daily living.
- Period of time: progress of symptoms no longer than 30 days.

A clinical event matching both the definition of MC and disease exacerbation was classified as MC. The outcome of MC was defined according to the MGFA (Myasthenia Gravis Foundation of America) post-intervention status (MGFA–PIS) [17, 18]: Specifically, improved signifies that QMG score at hospital discharge was reduced by ≥ 3 points compared to pre-admission, worse signifies that QMG score hospital discharge was increased by ≥ 3 points compared to before the admission and unchanged signifies that neither the criteria for improved nor worse were met. Patients with worse outcome were discharged for further rehabilitation. The threshold was defined to be that a score of 3 points in a single item of the QMG score reflects severe impairment [18]. The cutoff between early-(EOMG) and late-onset (LOMG) MG was set at 50 years as previously defined [19]. Minimal manifestation status (MMS) was defined in accordance with the MGFA–PIS as no symptoms of functional limitation from MG but weakness on examination only detectable by examination [17, 20, 21]. For MMS, immunosuppressive therapy and symptomatic therapy, e.g., cholinesterase inhibitors, were permitted (analogous to MMS-3 as proposed by the MGFA–PIS) [17, 20, 21].

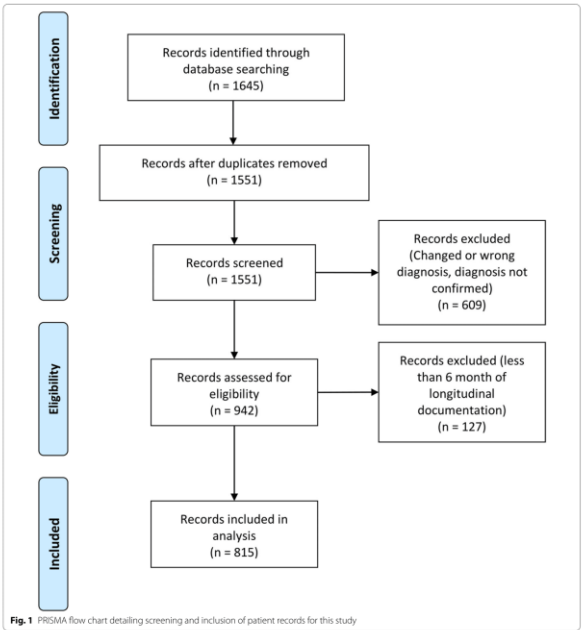

Fig. 1 PRISMA flow chart detailing screening and inclusion of patient records for this study

Standard protocol approvals, registrations, and patient consents

The study was approved by the local ethics committee and institutional review boards (no. AZ 2020-010-f-S, no. AZ 07/2017, 19-8973-BO, AZ 21-1265, AZ 21-1331). Data were anonymized and collected retrospectively according to the standardized requirements of the German register for myasthenia.

Statistical analysis

Statistical Analysis was performed using GraphPad Prism 9.3 (GraphPad Software, Inc., San Diego, CA) and

R (R Core Team, 2020). Data were presented as median (IQR = interquartile range), mean (standard deviation = SD), or *n* (%). For univariate logistic regression, goodness of fit was assessed by Cox-Snell's generalized R squared or Tjur's Pseudo R squared as appropriate. Significance was assessed by the likelihood ratio test. The odds ratio (OR) was assessed using a multivariate Cox regression model with follow-up as the time variable. Experiencing at least one MC or disease exacerbation compared to no event was used as the status variable. For analysis of time between diagnosis and MC or disease exacerbation the Kaplan–Meier method was used. Statistical significance between survival curves was determined by a pairwise log rank test. Analysis of variance (ANOVA) testing was performed for the analysis of groups for continuous variables and Fisher's exact test for categorial variables. To account for multiple comparisons, statistical significance was corrected by the false discovery rate (FDR). Anonymized data will be shared by request from any qualified investigator. For regression analysis of MGFA class II to IV, MGFA classes A and B were combined to allow for statistical analysis. Therefore, analysis is limited to MGFA classes without distinguishing the distribution of muscle weakness.

Results

Baseline characteristics and clinical features

Clinical and demographic data are presented in Table 1. Mean age at disease onset was 52.7 years (SD 20.0) and at diagnosis 53.5 years (SD 19.8). Early disease onset before the age of 50 years occurred in 300 patients (36.8%), while 510 cases (62.6%) were LOMG. The follow-up time was 62.6 months (SD 73.3) after diagnosis.

MGFA class at diagnosis was available for 782 patients (96.3%). 236 (28.9%) patients presented with ocular weakness (Class I); 309 (37.9%) with mild symptoms (Class II); 169 (20.8%) with moderate symptoms (Class III); 43 patients (5.3%) with severe muscle weakness (Class IV) and for 25 patients a history of intubation (3.0%) (Class V) was documented. Disease severity at diagnosis was classified by assessment of QMG score and was available for 687 patients (84.4%) [22]. Median QMG score at diagnosis was 4 points (IQR 2.0–8.0).

With respect to ab status, 714 (87.6%) patients were seropositive, whereas 86 (10.5%) were seronegative. The ab-status included anti-AChR-ab ($n = 641$), anti-MuSK-ab ($n = 71$), and anti-LRP4-ab ($n = 2$). 436 patients (53.5%) received corticosteroids following diagnosis with a mean dosage of 15 mg (SD 10). The average time between diagnosis and the start of the first immunosuppressive therapy (IST) was 1.3 years (SD 3.7). 451 patients (54.6%) received their first IST less than 1 year after diagnosis and were considered as early IST, while 111 patients

Table 1 Clinical and demographic baseline characteristics of patients

Characteristic	*n*	%
Total	**815**	**100**
Sex		
Male/Female	361/454	44.4/55.6
Age, y		
Mean age at first manifestation, years	52.7 ± 20.0	
Mean age at diagnosis, years	53.5 ± 19.8	
Early-onset MG (< 50 years)	300	36.9
Decremental response		
Positive	368	45.2
Negative	446	54.8
Increment		
Positive	6	0.7
Generalized MG at diagnosis		
Ocular MG	215	26.3
Generalized MG	589	72.7
MGFA class at diagnosis		
I (ocular)	236	28.9
II	309	37.9
III	169	20.8
IV	43	5.3
V	25	3.0
Missing	30	3.7
QMG-score at diagnosis, median ± IQR	4.0 (2.0–8.0)	
Antibody status		
Seronegative	86	10.5
Seropositive	714	87.6
Anti-AchR-ab	641	89.9
Anti-MuSK-ab	71	9.9
Anti-LRP4-ab	2	0.3
Anti-Titin-ab	156	21.8
Missing	15	1.8
Thymectomy	294	36.1
MRI or CT		
Thymoma-suspect	98	12.0
Histology		
Thymoma	158	19.4
First IST		
Azathioprine	475	58.2
MMF	46	5.6
Methotrexate	41	5.0
Cyclosporine	0	0
Mean corticosteroid dosage following diagnosis, mg	15 ± 10	
Concomitant diseases		
Cardiovascular	379	46.6
Arterial hypertension	289	35.4
Heart failure (any cause)	59	7.3
Aortic stenosis	64	7.8
Cardiac arrythmia	45	5.5

Table 1 (continued)

Characteristic	*n*	%
Other	111	13.6
Pulmonary	133	16.3
Chronic obstructive pulmonary disease	74	9.1
Asthma	28	3.5
Smoking	89	10.9
Other	23	2.8
Metabolic	185	22.7
Diabetes mellitus (type 1 or 2)	166	20.4
Hypercholesterolemia	155	19.0
Other	21	2.5
Gastrointestinal	167	20.5
Celiac disease	18	2.2
Gastroesophageal reflux disease	91	11.1
Liver failure (any cause)	15	18.4
Inflammatory bowel disease	8	0.9
Other	12	14.7
Malignancy other than thymoma	91	11.2
Lung cancer	22	2.7
Prostate cancer	33	4.0
Breast cancer	12	1.4
Other	15	1.8
Autoimmune disease	152	18.7
Hashimoto's disease	44	5.3
Rheumatoid arthritis	32	3.9
Psoriasis	34	4.2
Multiple sclerosis	3	0.3
Other	22	2.7
Months of follow-up	62.6 ± 73.3	

Baseline characteristics of included patients with myasthenic syndromes. *ab* antibody, *anti-AChR-ab* anti-acetylcholine-receptor-ab, *anti-MuSK-ab* anti-muscle-specific tyrosine kinase-ab, *anti-LRP4-ab* anti-low-density lipoprotein receptor-related protein 4-ab, *MC* myasthenic crisis, *MG* myasthenia gravis, *MMF* mycophenolate-mofetil, *IST* immunosuppressive therapy, *IQR* interquartile range, *SD* standard deviation. Unless otherwise reported, values are mean ± SD (range), median ± IQR (range) or *n* (%); QMG-score = quantitative myasthenia gravis-score

(13.5%) received IST after 1 year or more and were considered late IST. The remaining patients did not receive IST during the observation period.

Predictive factors for MC and disease exacerbation

Overall, 217 patients (26.3%) experienced a MC during their disease course while 225 patients (27.6%) experienced a disease exacerbation. To assess potential risk factors for the occurrence of MC or disease exacerbation, we employed a model of univariate logistic regression (Additional file 1: Table S1). We assessed the risk for experiencing at least one MC or disease exacerbation compared to patients experiencing no event. Aiming to identify independent risk factors, we entered risk factors

Table 2 Risk factors for MC and exacerbation—Multivariate analysis

	Odds ratio	95%CI	*p*-value
MC			
Age at diagnosis	1.01	0.87–1.25	0.32
Sex	0.96	0.81–1.43	0.86
QMG score at diagnosis	1.23	1.14–1.66	**< 0.0001**
MGFA status at diagnosis	1.83	1.65–1.97	**< 0.0001**
Anti-MuSK-ab	2.18	1.76–2.59	**0.02**
Thymoma	3.71	3.01–4.41	**< 0.0001**
Cardiovascular disease	1.29	0.72–1.66	0.35
Heart failure (any cause)	1.11	0.71–1.78	0.48
Pulmonary disease	1.36	0.88–1.44	0.25
Chronic obstructive pulmonary disease	1.41	0.91–1.48	0.11
Exacerbation			
Sex	0.82	0.66–1.17	0.24
Age at diagnosis	1.03	0.76–1.51	0.45
Generalized disease at diagnosis	1.83	1.23–2.39	**0.03**
QMG score at diagnosis	1.12	1.09–1.44	**< 0.0001**
MGFA status at diagnosis	1.03	0.75–1.48	0.11
Anti-MuSK-ab	1.07	1.01–1.28	**0.003**
Thymoma	1.64	1.29–2.07	**0.02**
Pulmonary disease	1.22	0.71–1.47	0.32
Chronic obstructive pulmonary disease	1.32	0.92–1.41	0.12

Risk factors for MC and exacerbation in multivariate Cox regression analysis. *anti-Musk-ab* anti-muscle-specific tyrosine kinase-ab, *MGFA* Myasthenia Gravis Foundation of America, *SD* standard deviation, *QMG* quantitative myasthenia gravis score. Variables with a *p*-value < 0.05 in the univariate analysis and clinically relevant variables (sex, age) were included in the multivariate analysis. For highly collinear factors (thymoma, thymectomy and imaging suspect for thymoma as well as age at onset, age at diagnosis and early onset) we included only one variable to avoid overfitting. Risk is presented as odds ratio. A *p*-value below 0.05 was considered statistically significant. Statistically significant results are bold. 95% CI = 95% confidence interval

reaching statistical significance ($p < 0.05$) in univariate analysis in a model of multivariate Cox regression. In addition, we included clinical parameters (sex and age) as they were related to clinical outcomes in previous studies [5]. To avoid overfitting, factors facing high collinearity were excluded (age at manifestation, thymectomy, imaging suggestive of thymoma). Accordingly, multivariate analysis revealed that QMG score at diagnosis [OR 1.23 95% confidence interval (95%CI) 1.14–1.66, $p < 0.0001$], MGFA class at diagnosis (OR 1.83 95% CI 1.65–1.97, $p < 0.001$), anti-MuSK-ab (OR 2.18 95% CI 1.76–2.59, $p < 0.05$) and the presence of a thymoma (OR 3.71 95% CI 3.01–4.41, $p < 0.0001$) predicted the occurrence of MC as independent risk factors (Table 2). Multivariate analysis of risk factors for disease exacerbation identified generalized disease (OR 1.83 95% CI 1.23–2.39, $p < 0.05$), QMG score at diagnosis (OR 1.12 95% CI 1.09 to 1.44, $p < 0.001$), anti-MuSK-ab (OR 1.07 95% CI 1.01–1.28, $p < 0.01$) and the presence of a thymoma (OR 1.56 95% CI 1.29–2.07, $p < 0.05$) as independent risk factors. Next, we applied the Kaplan–Meier method to our data set. Here, we observed an inverse relation between MGFA class and the occurrence of MC (Fig. 2A, B). In addition, we observed that anti-MuSK-ab status correlates with the risk for experiencing MC (Fig. 2C) or disease exacerbation (Fig. 2D) (Table 2).

Finally, we investigated whether therapeutic management of MG influences the occurrence of MC and exacerbation during the disease course. To assess the time between diagnosis and treatment as a potential risk factor, we separated the patient cohort by the time between diagnosis and the start of the first standard IST. Standard IST comprised of azathioprine, MMF, methotrexate and cyclosporine. Here, the risk for MC and disease exacerbation was not different for patients with early vs. late IST, respectively (MC: OR 0.38 95% CI 0.22–0.87, $p = 0.79$, exacerbation: OR 0.86 95% CI 0.65–0.99, $p = 0.38$). In addition to the time to treatment, we investigated the effect of treatment response on the occurrence of MC or exacerbation. We analysed the risk for MC and exacerbation for patients achieving MMS at 12 months after diagnosis and those who did not. To exclude bias due to patients presenting with MC or exacerbation as first manifestation, patients with a clinical event up to 6 months after diagnosis were excluded from the analysis of treatment response. Indeed, the risk was reduced for achieving MMS for MC (OR 0.32 95% CI 0.17–0.61, $p = 0.002$) and for exacerbation (OR 0.50 95% CI 0.34–0.70, $p < 0.001$). Next, using the Kaplan–Meier method we observed treatment non-responders as at risk to experience MC and exacerbations early in their disease as compared to treatment responders (Fig. 2E, F). To further dissect the importance of therapeutic management, we analyzed both cortisone treatment, as binary variable, and dosage, as continuous variable, as predictors for MC or exacerbation. Here, the risk for MC (OR 1.12 95% CI 1.05–1.33, $p = 0.16$) and exacerbation (OR 1.09 95% CI 1.01–1.45, $p = 0.42$) were similar for patients receiving cortisone following diagnosis compared with those who did not. In the group of cortisone-treated patients, assessment of cortisone dose did not reveal an association with the risk for MC (OR 1.27 95% CI 1.16–1.65, $p = 0.23$) or exacerbation (OR 1.52 95% CI 1.34–1.72, $p = 0.18$).

Factors determining the outcome of MC

Given the substantial mortality and lasting functional impairment associated with MC [5, 23], we further investigated potential factors affecting the outcome of MC. As detailed above, patients experiencing MC were grouped into three cohorts (improved, unchanged and worse). Clinical, demographic, diagnostic and therapeutic data were assessed for each cohort (Additional file 2: Table S2). Overall, 235 MC were recorded. In-hospital mortality was recorded for 6 patients (0.25%). To prevent bias (i.e., shorter ventilation time despite worse outcome), patients had died to MC were not included. Comparison of groups was performed on the remaining 229 MC. Recorded trigger factors are presented in Additional file 3: Table S3. Outcomes after MC were defined as improved for 143 MC (62.4%), unchanged for 33 MC (14.4%) and worse for 53 MC (23.2%) (Table 3).

Patients experiencing a worse outcome of following MC were older at the time of MC as compared to improved patients, while sex displayed no association with the outcome. MGFA class at admission as well as the last most recent measurement of MGFA class before prior to admission were lower in patients improving who improved. Interestingly, MC triggered by infections were was associated with a worse outcome. Consistent with previous reports, patients with a high number of comorbidities at admission had a worse outcome. Of note, vital capacity (VC) at admission, as well as the last recorded VC before MC, were was lower in patients worseningwho worsened. In addition, patients who were intubated, who had a longer time of mechanical ventilation or total hospital stay, and who developed pneumonia or sepsis had a poor outcome.

Finally, we analysed the impact of the available rescue therapies on the outcome of MC. Here, we compared the effect of IVIG (43 patients) vs. plasma exchange [PLEX (plasmapheresis) or IA (immunoadsorption)] (90 patients) vs. IVIG combined with plasma exchange (47 patients) vs. no rescue therapy (49 patients) (Table 3). Out of 49 patients with no rescue therapy, 31 were unable to receive therapy due to comorbidities (e.g., sepsis, renal failure), while 18 patient charts contained insufficient data on rescue treatments. Assessing the outcome of different rescue therapies revealed no differences between IVIG, plasma exchange, and the combination of both. However, patients receiving no rescue therapy had

(See figure on next page.)

Fig. 2 Survival analysis of MC and disease exacerbation. Survival curves displaying the time (in months) between diagnosis and the first MC (myasthenic crisis) or exacerbation. (**A**) Survival graph displaying the time to MC according to MGFA class. (**B**) Survival graph displaying the time to exacerbation according to MGFA class. (**C**) Survival graph displaying the time to MC according to anti-Musk-ab status. (**D**)Survival graph displaying the time to exacerbation according to anti-Musk-ab status. (**E**) Survival graph displaying the time to MC according to minimal manifestation status (MMS) at 12 months after diagnosis. (**F**) Survival graph displaying the time to exacerbation according to MMS at 12 months after diagnosis. Significance between survival curves was assessed by logrank testing. ****$p < 0.0001$ ***$p < 0.001$, **$p < 0.01$, *$p < 0.05$

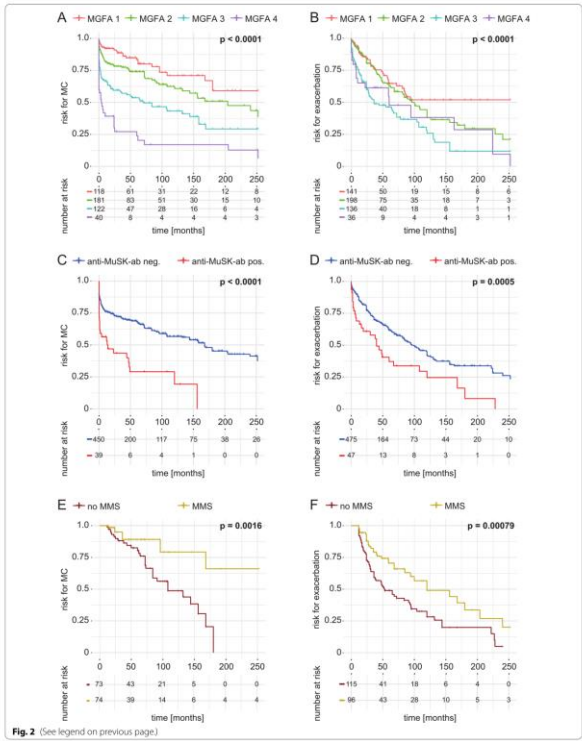

Fig. 2 (See legend on previous page.)

Table 3 Factors affecting outcome of MC

	Improved (*p* value compared to worse)	Unchanged (*p* value compared to worse)	Worse
Female (% of patients)	51.5% (0.89[#])	40.5% (0.62[#])	48.1%
Age at MC [Year, mean (SD)]	57.9 (21.8) (**0.01**[+])	60.7 (17.8) (0.14[+])	67.5 (15.0)
Time between diagnosis and MC [Months, mean (SD)]	31.1 (50.7) (0.77[+])	27.5 (61.0) (0.77[+])	36.4 (52.5)
MGFA before MC [MGFA, median (IQR)]	2 (1) (**0.006**[+])	2 (1) (0.38 +)	3 (2)
MGFA at admission [MGFA, median (IQR)]	3 (1) (<**0.001**[+])	3 (1) (**0.008**[+])	4 (2)
Treated with IST at start of MD (% of patients)	63.1% (0.13[#])	60.0% (0.49[#])	50.9%
MC triggered by infection (% of MC triggered by infections)	33.5% (**0.005**[#])	42.4% (0.26[#])	56.6%
VC before MC [VC in ml, mean (SD)]	2192 (822) (0.14[+])	1938 (739) (<**0.001**[+])	1533 (581)
VC at admission [VC in ml, mean (SD)]	1292 (800) (**0.04**[+])	1263 (598) (**0.006**[+])	871 (348)
Comorbidities [Number of comorbidities at admission, median (IQR)]	2 (2) (<**0.001**[+])	2 (2) (<**0.001**[+])	4 (2)
Time of hospitalisation [days, mean (SD)]	20.2 (16.1) (<**0.001**[+])	24.7 (25.8) (0.11[+])	34.1 (32.4)
Intubated (% of patients)	26.9% (<**0.001**[#])	26.7% (**0.002**[#])	64.2%
Time of invasive ventilation (days, mean)	7.8 (13.8) (**0.002**[+])	4.1 (8.9) (**0.001**[+])	22.6 (39.2)
Pneumonia (% of patients)	26.1% (<**0.001**[#])	20.0% (<**0.001**[#])	57.1%
Sepsis (% of patients)	6.6% (**0.002**[#])	3.3% (**0.013**[#])	25.0%
Treated with PLEX or IA (% of patients)	57.8% (0.11[#])	45.5% (0.99[#])	34.2%
Treated with IVIG and PLEX or IA (% of patients)	24.3% (0.24[#])	12.2% (0.76[#])	15.3%
Treated with no IVIG, PLEX or IA (% of patients)	18.0% (<**0.001**[#])	15.2% (<**0.001**[#])	60.3%

Factors affecting the outcome of MC. *SD* standard deviation, *IQR* interquartile range, *MC* myasthenic crisis, *MGFA* Myasthenia Gravis Foundation of America, *IST* immunosuppressive therapy, *IVIG* intravenous immunoglobulin, *IA* immunoadsorption, *PLEX* plasmapheresis, *VC* vital capacity. Patients who died during the MC were excluded from the analysis as to prevent bias of data due to early death. Significance for groups was assessed by ANOVA (denoted by [+]) or Fisher's exact test (denoted by [#]). To account for multiple comparisons, statistical significance was corrected by the false discovery rate (FDR). A *p*-value below 0.05 was considered statistically significant. Statistically significant results are bold. Unless otherwise specified, values are mean ± SD (range), median ± IQR (range) or *n* (%)

worse outcome compared to patients that received rescue therapy.

The six patients not surviving MC were on average 70 (SD 11.6) years. All 6 patients were intubated at admission, and the treating physician recorded an infection as the trigger for MC (pneumonia in all 6 cases). The average time of ventilation was 36.3 (SD32.5) days. Four patients died due to sepsis. One patient was treated with PLEX, one patient received both PLEX and IVIGs, while 4 patients did not receive rescue therapies.

Discussion

Despite therapeutic advances, 10–20% of MG patients experience MC during their disease course [3, 6, 24]. To ameliorate the burden of disease incurred by uncontrolled disease, identification of patients at risk for these events as well as factors and strategies promoting MC remission are of high importance for clinical practice. To guide identification and—by extension—management of patients at risk, we analysed a large cohort of MG patients, which reflected previously reported demographic and clinical characteristics [6]. In essence, our data implicate disease severity at diagnosis as a readily accessible and reliable predictor for MC. Treatment strategies should be tailored to the severity of initial symptoms, potentially reducing the likelihood for MC or exacerbation. In addition, our data underlines that the prevention and resolution of infections are pivotal factors defining MC outcome.

Previous observational studies regarding possible risk factors are mostly available for the subgroup of MG patients that received thymectomy [11, 12]. Investigating patients with and without thymoma, our study corroborates the presence of thymoma as a risk factor. Corroborating previous studies [25, 26], we also identified anti-MuSK-ab positivity as an independent risk factor for disease deterioration. Anti-MuSK-ab positive has also been associated with poor outcome of MC [27]. Interestingly, disease severity as assessed by clinical scoring was a robust predictor for patients at risk for MC or exacerbation, underlining the importance of standardized clinical evaluation of MG patients. Patients presenting with severe disease should receive intensified disease monitoring to recognize and, if possible, prevent the occurrence of MC.

Analysing the impact of disease management, we observed that treatment response influenced the risk for MC. Here, patients achieving MMS were at an reduced risk for MC and exacerbation than those who did not. MMS was proposed by the International Consensus Guidance for Management of MG as treatment target [17, 20]. We analyzed this parameter to understand if achieving the proposed treatment target is associated with a reduced risk for MC [17]. Treatment strategies were previously suggested to affect the course of disease in MG. As such, a recent meta-analysis suggested that cortisone treatment reduces the risk for secondary generalization for MG patients with ocular manifestation [28]. Thymectomy is also evidenced to improve clinical readouts over a 3-year time span as demonstrated in a recent, randomized, controlled trial [19, 20]. Taken together, successful treatment approaches appear to influence long-term outcomes.

Knowledge of factors affecting the outcome of MC are of high clinical importance to promote remission and functional independence [6], with most studies reporting factors associated with prolonged ventilation as a surrogate marker for clinical outcome of MC [6, 23, 29]. Following analysis of patients experiencing MC according to the MGFA post-intervention-status [17], we observed an association between prolonged ventilation time and a worse outcome, suggesting that ventilation time correlates with functional status at discharge. However, our cohort also revealed that VC might be a valuable biomarker for risk stratification of MC as VC predicted the outcome if assessed at admission. Interestingly, a previous retrospective cohort analysing 5 patients with MC found no link between VC and the need for mechanical ventilation [30]. Corroborating VC as a predictive biomarker in other neuromuscular diseases such as Guillain-Barré syndrome [31], our study contrasts the findings from the previous cohort with the difference potentially attributed to the substantial variance in cohort size implicating that monitoring and improvement of ventilation might allow clinicians to avert severe courses of MC. Intriguingly, an infectious trigger of MC was both frequent and associated with an unfavourable outcome compared to other triggers. Hence, prevention and early management of infection in MG patients, notably in MG patients with impaired ventilatory capacities, constitutes a cornerstone in the management of MC. We suggest that treatment of comorbidities making patients vulnerable to infection and resolute adhesion to vaccination protocols should be employed to reduce the risk of infection for MG patients.

The retrospective design of this study might be vulnerable to confounding factors as data were collected during routine clinical practice rather than a formal study setting making data sensitive to variation both in quantity and quality between individual patients and time points. Nonetheless, data quality was improved by collection according to standardised requirements of the German Myasthenia register. A focus on tertiary centers might introduce a bias towards severe cases. However, given the rarity of the disorder, most MG patients are treated in specialized centres [32]. Thus, our cohort is likely to be representative of the general MG population. Regarding the analysis of predictors, a potential limitation is that patients initially presenting with MC or exacerbation could not be included. These patients potentially constitute a distinct clinical subtype as they are expected to have fewer co-morbidities and are likely to be treated more aggressively [6]. Furthermore, definitions for MG exacerbation are heterogenous and diverging interpretations have been previously proposed, e.g., de Meel et al. included an increase in immunosuppressive therapy in their operational definition for exacerbation [33]. A caveat to the analysis of rescue therapies is that the subgroup of patients receiving no treatment for MC is biased to severe cases as these patients were often unable to be treated due to comorbidities (e.g., sepsis or renal failure).

Conclusions

Our study highlights that disease severity at diagnosis is a valuable clinical marker to identify patients at risk for MC or disease exacerbation. Intensified monitoring with emphasis on the prevention of infectious complications is pivotal for management of patients at risk.

Abbreviations

ANOVA: Analysis of variance; ab: Antibody; anti-AChR-ab: Anti-acetylcholine-receptor-ab; anti-LRP4-ab: Anti-low-density lipoprotein receptor-related protein 4-ab; anti-MuSK-ab: Anti-muscle-specific tyrosine kinase-ab; anti-VGCC-ab: Anti-voltage-gated calcium channel-ab; EOMG: Early-onset MG; FDR: False discovery rate; IA: Immunoadsorption; IMC: Integrated Myasthenia Centre; IQR: Interquartile range; IST: Immunosuppressive therapy; IVIG: Intravenous immunoglobulin; LOMG: Late-onset MG; MC: Myasthenic crisis; MG: Myasthenia gravis; MGFA: Myasthenia Gravis Foundation of America; MGFA–PIS: Myasthenia Gravis Foundation of America post-intervention status; MMF: Mycophenolate-mofetil; NICU: Neurological Intensive Care Unit; OR: Odds ratio; PLEX: Plasmapheresis; SD: Standard deviation.

Supplementary Information

The online version contains supplementary material available at https://doi.org/10.1186/s12974-022-02448-4.

Additional file 1. Suppl. Table 1. Risk factors for MC and exacerbation – Univariate analysis.

Additional file 2. Suppl. Table 2. Clinical and demographic characteristics of included MC.

Additional file 3. Suppl. Table 3. Trigger factors.

Acknowledgements

We thank the patient and their families for their contribution.

Author contributions

CN, FS and TR designed the study and methods. Formal analysis was done by CN and FS. Clinical data was provided by FS, CE, MP, CBS, NH, PM, EA, MO, DF, SS, SV, AG, HS, MS, BB, AT and TH. Resources were provided by SGM, AM, HW and TR. CN, FS and TR wrote the original draft. CE, MP, CBS, NH, PM, EA, EÖ, DF, SS, SV, AG, HS, MS, BB, AT, TH, SGM, AM and HW reviewed and edited the manuscript. Figures were created by CN, CBS and NH. Subversion was provided by SGM, AM, HW and TR. All authors read and approved the final manuscript.

Funding

Open Access funding enabled and organized by Projekt DEAL. PM is Einstein Junior Fellow funded by the Einstein Foundation Berlin, and is supported by grants from the Bundesministerium für Bildung und Forschung (Grants no. 16GW0191 and NUM-COVID 19—Organo-Strat 01KX2021).

Availability of data and materials

The datasets used and/or analysed during the current study are available from the corresponding author on reasonable request.

Declarations

Ethics approval and consent to participate

The study was approved by the local ethics committee and institutional review boards (no. AZ 2020-010-f-S, no. AZ 07/2017, 19-8973-BO, AZ 21-1265, AZ 21-1331). Data were anonymized and collected retrospectively according to the standardized requirements of the German register for myasthenia.

Consent for publication

Not applicable.

Competing interests

Dr. Nelke reports no disclosures. Dr. Stascheit received speaking Honoria from Biogen and Alexion. Cand. med. Eckert reports no disclosures. Dr. Pawlitzki received speaker honoraria and travel/accommodation/meeting expenses from Novartis. Dr. Mergenthaler is on the Advisory Board of HealthNextGen Inc. and has equity interest in the company. His research is funded by the Bundesministerium für Bildung und Forschung (BMBF), the European Union, the Else Kröner-Fresenius Stiftung, the Volkswagen Stiftung, and the Einstein Foundation Berlin. Dr Schroeter reports no disclosures. Dr. Arat reports no disclosures. Dr. Öztürk reports no disclosures. Prof. Föll reports no disclosures. Prof. Schreiber reports no disclosures. Prof. Vielhaber reports no disclosures. Dr. Gassa reports no disclosures. Dr. Stetefeld reports not disclosures. Prof. Schroeter reports no disclosures. Dr. Berger received travel grants and/or training expenses from Bayer Vital GmbH, IpsenPharma GmbH, Norvartis, Biogen GmbH and Genzyme, as well as lecture fees from Ipsen Pharma GmbH, Alexion Pharma GmbH, Merck, Sanofi Genzyme and Roche. Dr. Totzeck reports no disclosures. Dr. Hagenacker received speaker and advisory board honoraria from Alexion, Biogen and Roche. Prof. Meuth receives honoraria for lecturing, and travel expenses for attending meetings from Almirall, Amicus Therapeutics Germany, Bayer Health Care, Biogen, Celgene, Diamed, Genzyme, MedDay Pharmaceuticals, Merck Serono, Novartis, Novo Nordisk, ONO Pharma, Roche, Sanofi-Aventis, Chugai Pharma, QuintilesIMS and Teva. His research is funded by the German Ministry for Education and Research (BMBF), Bundesinstitut für Risikobewertung (BfR), Deutsche Forschungsgemeinschaft (DFG), Deutsche Multiple Sklerose Gesellschaft (DMSG), Else Kröner Fresenius Foundation, Gemeinsamer Bundesausschuss (G-BA), German Academic Exchange Service, Hertie Foundation, Interdisciplinary Center for Clinical Studies (IZKF) Muenster, German Foundation Neurology and Alexion, Almirall, Amicus Therapeutics Germany, Biogen, Diamed, Fresenius Medical Care, Genzyme, HERZ Burgdorf, Merck Serono, Novartis, ONO Pharma, Roche, and Teva. Prof. Wiendl receives honoraria for acting as a member of Scientific Advisory Boards, Biogen, Evgen, Genzyme, MedDay Pharmaceuticals, Merck Serono, Novartis, Roche Pharma AG, and Sanofi-Aventis as well as speaker honoraria and travel support from Alexion, Biogen, Cognomed, F. Hoffmann-La Roche Ltd., Gemeinnützige Hertie-Stiftung, Merck Serono, Novartis, Roche Pharma AG, Genzyme, TEVA, and WebMD Global. Prof. Wiendl is acting as a paid consultant for Abbvie, Actelion, Biogen, IGES, Johnson & Johnson, Novartis, Roche, Sanofi-Aventis, and the Swiss Multiple Sclerosis Society. His research is funded by the German Ministry for Education and Research (BMBF), Deutsche Forschungsgemeinschaft (DFG), Else Kröner Fresenius Foundation, Fresenius Foundation, the European Union, Hertie Foundation, NRW Ministry of Education and Research, Interdisciplinary Center for Clinical Studies (IZKF) Muenster and RE Children's Foundation, Biogen, GlaxoSmithKline GmbH, Roche Pharma AG, Sanofi-Genzyme. Prof. Meisel received speaker honoraria from Alexion, argnx, GRIFOLS and Hormosan. He received honoraria from Alexion, argnx, UCB, Janssen and Vitaccess for consulting services and financial research support from Octapharma and Alexion. Andreas Meisel is chairman of the medical advisory board of the German Myasthenia Gravis Society. Dr. Ruck reports grants from German Ministry of Education, Science, Research and Technology, grants and personal fees from Sanofi-Genzyme and Alexion; personal fees from Biogen, Roche and Teva; personal fees and nonfinancial support from Merck Serono, outside the submitted work.

Author details

[1]Department of Neurology, Medical Faculty, Heinrich Heine University Düsseldorf, Moorenstraße 5, 40225 Duesseldorf, Germany. [2]Charité, Universitätsmedizin Berlin, corporate member of Freie Universität Berlin, Department of Neurology With Experimental Neurology, Humboldt-Universität zu Berlin, Berlin, Germany. [3]Charité, Universitätsmedizin Berlin, corporate member of Freie Universität Berlin, NeuroCure Clinical Research Center, Humboldt-Universität zu Berlin, Berlin, Germany. [4]Department of Neurology with Institute of Translational Neurology, University and University Hospital Münster, Munster, Germany. [5]Department of Child and Adolescent Psychiatry and Psychotherapy, University Hospital Münster, Munster, Germany. [6]Department for Pediatric Rheumatology and Immunology, University of Münster, Munster, Germany. [7]Department of Neurology, University of Magdeburg, Magdeburg, Germany. [8]Department of Cardiothoracic Surgery, University of Cologne and University Hospital Cologne, Cologne, Germany. [9]Department of Neurology, University of Cologne, Faculty of Medicine and University Hospital Cologne, Cologne, Germany. [10]Clinic of Neurology and Neurophysiology, Medical Center, Faculty of Medicine, University of Freiburg, Freiburg, Germany. [11]Department of Neurology and Center for Translational Neuro- and Behavioral Sciences (C-TNBS), University Hospital Essen, University of Duisburg-Essen, Essen, Germany. [12]Charité, Universitätsmedizin Berlin, corporate member of Freie Universität Berlin, Center for Stroke Research Berlin, Humboldt-Universität zu Berlin, Berlin, Germany. [13]German Myasthenia Gravis Society, Berlin, Germany. [14]German Center for Neurodegenerative Diseases, Bonn, Germany. [15]Center for Behavioral Brain Sciences, Magdeburg, Germany.

Received: 6 December 2021 Accepted: 29 March 2022
Published online: 12 April 2022

References

1. Gilhus NE, et al. Myasthenia gravis—autoantibody characteristics and their implications for therapy. Nat Rev Neurol. 2016;12:259–68.
2. Mantegazza R, Antozzi C. When myasthenia gravis is deemed refractory: clinical signposts and treatment strategies. Ther Adv Neurol Disord. 2018; 1–11.
3. Schneider-Gold C, Hagenacker T, Melzer N, Ruck T. Understanding the burden of refractory myasthenia gravis. Ther Adv Neurol Disord. 2019;12:1–16.
4. Lacomis D. Myasthenic crisis. 2005. https://doi.org/10.1385/Neurocrit.
5. Alshekhlee A, Miles JD, Katirji B, Preston DC, Kaminski HJ. Incidence and mortality rates of myasthenia gravis and myasthenic crisis in US hospitals. Neurology. 2009;72:1548–54.
6. Neumann B, et al. Myasthenic crisis demanding mechanical ventilation. Neurology. 2020;94:e299–313.
7. Barth D, Nabavi Nouri M, Ng E, Nwe P, Bril V. Comparison of IVIg and PLEX in patients with myasthenia gravis. Neurology. 2011;76:2017–23.
8. Gajdos P, Chevret S, Clair B, Tranchant C, Chastang C. Clinical trial of plasma exchange and high-dose intravenous immunoglobulin in myasthenia gravis. Ann Neurol. 1997;41:789–96.
9. Gummi RR, Kukulka NA, Deroche CB, Govindarajan R. Factors associated with acute exacerbations of myasthenia gravis. Muscle Nerve. 2019;60:693–9.
10. Wendell LC, Levine JM. Myasthenic crisis. Neurohospitalist. 2011;1:16–22.
11. Geng Y, Zhang H, Wang Y. Risk factors of myasthenia crisis after thymectomy among myasthenia gravis patients: a meta-analysis. Medicine. 2020;99:e18622.
12. Xue L, et al. Risk factors of myasthenic crisis after thymectomy for thymoma patients with myasthenia gravis† . Eur J Cardiothorac Surg. 2017;52:692–7.
13. 68 Diagnostik und Therapie der Myasthenia gravis und des Lambert-Eaton-Syndroms. in Leitlinien für Diagnostik und Therapie in der Neurologie. 2014. https://doi.org/10.1055/b-0034-37851.
14. Bedlack RS, Sanders DB. On the concept of myasthenic crisis. J Clin Neuromuscul Dis. 2002;4:40–2.
15. Schroeter M, Thayssen G, Kaiser J. Myasthenia gravis—exacerbation and crisis. Neurol Int Open. 2018;02:E10–5.
16. Bedlack RS, et al. Quantitative myasthenia gravis score: assessment of responsiveness and longitudinal validity. Neurology. 2005;64:1968–70.
17. Sanders DB, et al. International consensus guidance for management of myasthenia gravis: executive summary. Neurology. 2016;87:419–25.
18. Katzberg HD, Barnett C, Merkies IS, Bril V. Minimal clinically important difference in myasthenia gravis: outcomes from a randomized trial. Muscle Nerve. 2014;49:661–5.
19. Wolfe GI, et al. Randomized trial of thymectomy in myasthenia gravis. N Engl J Med. 2016;375:511–22.
20. Narayanaswami P, et al. International consensus guidance for management of myasthenia gravis. Neurology. 2021;96:114–22.
21. America, T. F. of the M. S. A. B. of the M. G. F. of et al. Myasthenia gravis: recommendations for clinical research standards. Neurology. 2000;55: 16–23.
22. Besinger UA, et al. Myasthenia gravis: long-term correlation of binding and bungarotoxin blocking antibodies against acetylcholine receptors with changes in disease severity. Neurology. 1983;33:1316–21.
23. Thomas CE, et al. Myasthenic crisis: clinical features, mortality, complications, and risk factors for prolonged intubation. Neurology. 1997;48:1253–60.
24. Maggi L, et al. Thymoma-associated myasthenia gravis: outcome, clinical and pathological correlations in 197 patients on a 20-year experience. J Neuroimmunol. 2008;201:257–44.
25. Evoli A, et al. Clinical correlates with anti-MuSK antibodies in generalized seronegative myasthenia gravis. Brain. 2003;126:2304–11.
26. Guptill JT, Sanders DB, Evoli A. Anti-MuSK antibody myasthenia gravis: clinical findings and response to treatment in two large cohorts. Muscle Nerve. 2011;44:36–40.
27. Konig N, et al. MuSK-antibodies are associated with worse outcome in myasthenic crisis requiring mechanical ventilation. J Neurol. 2021. https://doi.org/10.1007/s00415-021-10603-9.
28. Li M, et al. Do early prednisolone and other immunosuppressant therapies prevent generalization in ocular myasthenia gravis in Western populations: a systematic review and meta-analysis. Ther Adv Neurol Disord. 2019;12:1756286419876521.
29. Liu Z, et al. Predictors of extubation outcomes following myasthenic crisis. J Int Med Res. 2016;44:1524–33.
30. Rieder P, Louis M, Jolliet P, Chevrolet JC. The repeated measurement of vital capacity is a poor predictor of the need for mechanical ventilation in myasthenia gravis. Intensive Care Med. 1995;21:663–8.
31. Racca F, Del Sorbo L, Mongini T, Vianello A, Ranieri VM. Respiratory management of acute respiratory failure in neuromuscular diseases. Minerva Anestesiol. 2010;76:51–62.
32. Wiendl H. Diagnostik und Therapie der Myasthenia gravis und des Lambert-Eaton-Syndroms. 2014.
33. de Meel RHP, Lipka AF, van Zwet EW, Niks EH, Verschuuren JJGM. Prognostic factors for exacerbations and emergency treatments in myasthenia gravis. J Neuroimmunol. 2015;282:123–5.

OPEN ACCESS

Original research

Eculizumab versus rituximab in generalised myasthenia gravis

Christopher Nelke ,[1] Christina B Schroeter,[1] Frauke Stascheit ,[2,3] Marc Pawlitzki,[1,4] Liesa Regner-Nelke,[1] Niklas Huntemann,[1] Ercan Arat,[1] Menekse Öztürk,[1] Nico Melzer,[1] Philipp Mergenthaler ,[2,3] Asmae Gassa,[5] Henning Stetefeld,[6] Michael Schroeter,[7] Benjamin Berger,[8] Andreas Totzeck,[9] Tim Hagenacker,[9] Stefanie Schreiber ,[10] Stefan Vielhaber,[11] Hans-Peter Hartung,[1] Andreas Meisel,[2,3,12] Heinz Wiendl,[13] Sven G Meuth,[1] Tobias Ruck[1]

► Additional supplemental material is published online only. To view, please visit the journal online (http://dx.doi.org/10.1136/jnnp-2021-328665).

For numbered affiliations see end of article.

Correspondence to
Dr Tobias Ruck, Department of Neurology, Heinrich Heine University Düsseldorf, Dusseldorf, Germany; Tobias.Ruck@med.uni-duesseldorf.de

CN and CBS contributed equally.

CN and CBS are joint first authors.

Received 16 December 2021
Accepted 22 February 2022
Published Online First 4 March 2022

ABSTRACT

Objective Myasthenia gravis (MG) is the most common autoimmune disorder affecting the neuromuscular junction. However, evidence shaping treatment decisions, particularly for treatment-refractory cases, is sparse. Both rituximab and eculizumab may be considered as therapeutic options for refractory MG after insufficient symptom control by standard immunosuppressive therapies.

Methods In this retrospective observational study, we included 57 rituximab-treated and 20 eculizumab-treated patients with MG to compare the efficacy of treatment agents in generalised, therapy-refractory anti-acetylcholine receptor antibody (anti-AChR-ab)-mediated MG with an observation period of 24 months. Change in the quantitative myasthenia gravis (QMG) score was defined as the primary outcome parameter. Differences between groups were determined in an optimal full propensity score matching model.

Results Both groups were comparable in terms of clinical and demographic characteristics. Eculizumab was associated with a better outcome compared with rituximab, as measured by the change of the QMG score at 12 and 24 months of treatment. Minimal manifestation of disease was more frequently achieved in eculizumab-treated patients than rituximab-treated patients at 12 and 24 months after baseline. However, the risk of myasthenic crisis (MC) was not ameliorated in either group.

Interpretation This retrospective, observational study provides the first real-world evidence supporting the use of eculizumab for the treatment of refractory, anti-AChR-ab positive MG. Nonetheless, the risk of MC remained high and prompts the need for intensified monitoring and further research effort aimed at this vulnerable patient cohort.

To cite: Nelke C, Schroeter CB, Stascheit F, *et al*. *J Neurol Neurosurg Psychiatry* 2022;**93**:548–554.

INTRODUCTION

Myasthenia gravis (MG) is the most common autoimmune disorder affecting the neuromuscular junction, characterised by antibody (ab)-mediated dysfunction of the postsynaptic membrane.[1] The hallmark of MG is fluctuating weakness of ocular, bulbar, limb and respiratory muscles, with corresponding morbidity and mortality.[2]

In the majority of patients with MG, disease is sufficiently controlled by immunosuppressive treatment, while a clinically distinct subgroup of patients, often referred to as refractory, continues to experience severe disease despite therapy.[2 3] Nonetheless, a consensus for the definition of refractory MG is currently lacking, with various studies employing heterogeneous definitions.[3] Treatment strategies are evolving with novel biological agents complementing existing standards of therapy. Rituximab, a B cell-depleting monoclonal antibody (ab), has been discussed as potential therapy for patients with MG whose disease is refractory to standardised immunotherapies.[4] This viewpoint is supported by findings from a meta-analysis of smaller case series as well as observational studies investigating rituximab for new-onset MG in patients who are anti-acetylcholine receptor (AChR)-ab positive[5] and for anti-muscle-specific tyrosine kinase (MuSK)-ab positive.[6] Concurrently, identification of complement as major driver of disease activity in anti-AChR-ab MG[7] led to the development of complement-targeted therapies. As such, eculizumab is a humanised, monoclonal ab that specifically recognises and inhibits cleavage of complement C5.[8] Ablation of terminal complement activation by eculizumab has proven efficacious for treating patients with anti-AChR-ab positive treatment-refractory (TR) MG in the phase 3, randomised, placebo-controlled REGAIN trial.[9]

Both biologicals, that is, rituximab and eculizumab, may be considered as treatment options for refractory MG after failure of immunosuppressive standard therapies (ISTs).[1 9 10] However, evidence guiding treatment strategies is sparse. Thus, we compared rituximab and eculizumab for the treatment of generalised, therapy-refractory anti-AChR-ab positive MG in a retrospective, observational study. The change to baseline quantitative myasthenia gravis (QMG) score was employed as the primary outcome parameter with a follow-up period of 24 months. Study outcomes were specified prior to data analysis.

MATERIAL AND METHODS

Study cohort

Our cohort is a retrospective, observational multicentric analysis of patients from six university hospitals (University Medicine Charité Berlin, University Hospital Cologne, University Hospital Duesseldorf,

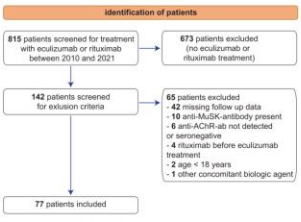

Figure 1 Flow chart detailing patient recruitment. Seventy-seven patients were included in the final study for rituximab (n=57) and eculizumab treatment (n=20). ab, antibody; AChR, acetylcholine receptor; MuSK, muscle-specific tyrosine kinase.

University Hospital Freiburg, University Hospital Magdeburg and University Hospital Regensburg). A total of 815 patients with MG were recruited with a focus on TR cases. Diagnosis of MG was established by characteristic clinical presentation and supported by characteristic antibody (ab) findings in accordance with national guidelines.[11] Participating centres are established as the integrated Myasthenia Centre (iMC) by the German Myasthenia Gravis Society, employing standardised workflows for patient management. According to the iMC protocol, patients with a stable course were seen every 6 months and unstable patients more frequently. Data were collected according to the standards of the German Myasthenia registry and included sociodemographic data (age, sex and disease duration), ab-status (AChR, MuSK, lipoprotein-related protein 4 or seronegative), MG-specific medication (cholinesterase inhibitors, glucocorticoids and immunosuppressants), history of thymectomy, and comorbidities. The scoring of MG-specific parameters was performed by the treating neurologist. No clinical scoring was applied retrospectively.

Patient cohort and selection

We identified 142 patients treated with rituximab or eculizumab between 2010 and 2021 (figure 1).

The following inclusion criteria were applied:

- Confirmed diagnosis of MG in accordance with national guidelines.
- Confirmed serological detection of anti-AChR-ab.
- Age≥18 at start of rituximab or eculizumab treatment.
- Treatment refractory MG according to the following definition[3]: persistent impairment due to MG despite adequate standard therapy for more than 12 months or persistent intolerable side effects. In this study, we employed generalised disease with a QMG score of ≥6 as operational definition for persistent impairment. Standard therapy was defined as having received two previous first-line ISTs or one first-line IST and prednisolone at maximum tolerable dose for a minimum treatment duration of 6 months each without achieving disease control or until treatment has to be stopped due to intolerable side effects. Standard ISTs included azathioprine, mycophenolate mofetil, methotrexate or cyclosporine. Acetylcholinesterase inhibitors were required to be at a maximum tolerable dose. Thymectomy was performed if indicated.
- Sufficient clinical follow-up data with at least three out of four QMG scores assessed by a trained neurologist at baseline, that is, start of rituximab or eculizumab treatment, as well as at 6 months, 12 months and 24 months after therapy initiation.

Additionally, the following exclusion criteria was applied during patient selection:

- Presence of ab other than anti-AChR-ab (anti-titin-ab were permitted as these are considered complementary markers to anti-AChR-ab).
- Presence of IST or a biological agent other than rituximab or eculizumab (rescue treatments including plasmapheresis (PLEX), intravenous immunoglobulins (IVIG) and immune adsorption (IA) were permitted).
- Previous treatment with rituximab for eculizumab patients or eculizumab for rituximab patients.
- Pregnancy during the treatment period.

Following selection using the inclusion and exclusion criteria, 57 patients treated with rituximab and 20 patients treated with eculizumab were included in the analysis (figure 1). The first patient of this cohort was treated with rituximab in 2010. Until 2017, a total of 39 patients received rituximab. The remaining 18 rituximab-treated patients were included between 2017 and 2021. After formal approval for MG, the first patient received eculizumab in 2017. All eculizumab-treated patients were recruited between 2017 and 2021. During this period, eculizumab was preferentially offered due to its on-label status. If patients declined eculizumab, rituximab was offered instead.

Dosing regime

Rituximab and eculizumab treatment regimens were performed in accordance with local standard operating procedure. For rituximab, a dose of 1000 mg was given 14 days apart. The treatment interval for maintenance therapy with 1000 mg was 6–9 months, depending on clinical response.[11] For eculizumab, treatment started with 900 mg weekly for 4 weeks followed by maintenance therapy at week 5 with 1200 mg in a biweekly application scheme.

Definitions

Myasthenic crisis (MC) was defined as a rapid clinical deterioration requiring non-invasive or invasive ventilation.[12] An age of 50 years at disease onset was used as a cut-off point between early (<50 years) and late-onset (≥50 years) MG.[13] IVIG, PLEX and IA were considered as rescue therapies if given for an exacerbation of MG concurrently with IST or biological agents. Recurrent IVIG infusions were defined as IST if given without other IST or biological agents. Minimal manifestation (MM) was defined based on the Myasthenia Gravis Foundation of America post-intervention status.[14] For MM status, the patient was required to have no functional limitations due to MG except for minimal weakness on examination. In our study, residual weakness was required to be a QMG score of ≤3 points. For MM, symptomatic treatment with cholinesterase inhibitors was permitted. MM required that no rescue therapy was needed in the last 6 months at the time of assessment.

Standard protocol approvals, registrations and patient consents

This study was conducted in accordance with the Declaration of Helsinki. Data were anonymised and collected retrospectively according to the standards of the German Register for Myasthenia.

Study outcomes

The change from baseline QMG score after 12 months of therapy was the primary study outcome. The QMG is a 13-item scale with each item scored from 0 (no impairment) to 3 (severe impairment), for a total score ranging from 0 to 39 points.[15] The change from baseline QMG score after 24 months of therapy, the time to MC and the number of patients reaching minimal manifestation at 12 and 24 months of therapy were secondary study outcomes. Patients presenting with MC that overlapped with specified time points were to be considered as missing data for the analysis of the QMG score. During this study, no overlap between MC and the specified time points of 12 and 24 months were detected. Transient worsening (that did not qualify as MC) and acute rescue therapies overlapping with the specified time points was permitted and the corresponding QMG score was recorded. Study outcomes were specified prior to data analysis.

Data availability

All analysed data are presented in the manuscript and available on reasonable request from qualified investigators.

Statistical analysis

Statistical analysis was performed using RStudio V.1.4.1103 (R-Tools Technology). Data are presented as the mean (SD) or n (%). To account for pretreatment disease severity and reduce selection bias, we employed a model of propensity score matching. The propensity scores were calculated for each patients using a logistic regression model with a priori selected covariates (sex, age at diagnosis, age at baseline, thymoma and QMG at baseline). The obtained propensity scores were subsequently entered in an Average Treatment effect on the Treated weighting model to provide a balanced sample of patients except for their respective treatment. Due to differences in sample sizes, we preferred an optimal full matching approach as to avoid a selection of patients to remain unmatched.[16] As previously described,[16 17] the balance between the two groups was assessed by comparing the standardised mean differences of the covariates before and after propensity score adjustment. Using a model of optimal full matching, we achieved standardised mean differences for the selected covariates below 0.1 indicating adequate balance of the two groups (online supplemental figure 1). Differences between groups were analysed using a two-tailed, unpaired T test for quantitative variables and two-tailed Fisher's exact test for categorical variables. Group differences for time to MC were assessed through Kaplan-Meier curves and the logrank test for comparison of MC distribution. Differences were considered statistically significant with the following p values: *p<0.05, **p<0.01, ***p<0.001.

Missing data

A total of three rituximab-treated (5.3%) and one eculizumab-treated (5%) patients were lost to follow-up. Clinical and demographic baseline data were indistinguishable from patients completing the full observation period (data not shown). All patients lost to follow-up were missing, that is, patients who did not complete follow-up visits and did not state a specific reason. As we detected no systematic differences between patients with missing data and those with complete data, we assumed that these data points were missing completely at random.[18] Consequently, listwise deletion was applied to handle missing data points.

RESULTS

Out of 142 patients receiving rituximab or eculizumab, we included 77 patients in the final analysis (figure 1). Distribution of baseline characteristics were comparable between the two groups (table 1). The majority of patients in both groups were women (rituximab 35 (62.5%) vs eculizumab 12 (54.6%), p=0.61), with an early onset of disease (rituximab 36 (63.1%) vs eculizumab 16 (72.7%), p=0.59). The average age at the start of rituximab and eculizumab treatment was 46.5 (SD 17.1) and 45.4 (SD 15.2) years, respectively (p=0.791). Disease severity in both groups was high with QMG scores at baseline of 10.7 (5.1) for rituximab and 13.25 (5.2) or eculizumab (p=0.056). Previous numbers of ISTs were comparable with rituximab-treated and eculizumab-treated patients receiving a median of two previous ISTs (IQR 2–3). Azathioprine was the most common previous IST in the rituximab and eculizumab group with 49 (63.4%) and 18 (90.0%) patients, respectively (p=0.126). Prednisone dose at baseline was similar, with rituximab-treated patients receiving 6.0 mg (SD 10.3) and eculizumab-treated patients 10.4 mg (SD 12.6) prednisone (p=0.121). Thymectomy was performed before baseline for all included patients. Eight rituximab-treated and four eculizumab-treated patients had a confirmed thymoma (p=0.487). No deaths or meningococcal infections were recorded during the observation period. Adverse events were in line with the known spectrum of both agents (ie, headache, nausea, diarrhoea, fever, joint pain and upper airway infections).[4 19]

We compared the change to QMG baseline after 12 months of treatment with rituximab (n=56) and eculizumab (n=20) using a model of full optimal propensity score matching. After matching, the standardised mean differences of all included covariates were below 0.1 indicating adequate balance (online supplemental figure 1). Eculizumab-treated patients demonstrated a significantly greater benefit from treatment as compared with rituximab patients (QMG at 12 months for rituximab 11.2 (SD 7.3) and eculizumab 8.4 (SD 6.1); p=0.021, figure 2). In addition, we compared rituximab (n=54) and eculizumab (n=19) cohorts for changes of their QMG score to baseline at 24 months (figure 2). Here, we observed a significantly greater benefit from eculizumab treatment compared with rituximab (QMG at 24 months for rituximab 11.2 (SD 6.4) and eculizumab 9.6 (SD 8.5); p<0.001). Thymoma status did not impact the change to the QMG score at 12 or 24 months (p=0.123 and p=0.848, respectively). For two rituximab-treated and one eculizumab-treated patient, the prespecified time point of 12 months coincided with application of IVIGs. Excluding these patients from the analysis did not affect study outcomes (QMG at 12 months for rituximab 10.8 (SD 7.6) and eculizumab 8.1 (SD 6.9), p=0.038). To account for selection bias, we analysed the rituximab cohort included before 2017 (n=39) and after 2017 (n=18) (table 2). Both groups of rituximab-treated patients were similar in terms of demographic and clinical data. The change to baseline QMG at 12 months (QMG before 2017: 10.5 (SD 7.1), after 2017: 11.1 (SD 6.8), p=0.633) was comparable for both groups of rituximab-treated patients.

Next, we analysed the time to MC in both groups. During the 24-month observation period, nine patients experienced a MC in the rituximab group, while two patients deteriorated in the eculizumab group, which did not reach statistical significance (MC, n (%), rituximab 15 (15.8%) vs eculizumab 2 (10.0%), p=0.510). The time to MC did not differ between rituximab and eculizumab patients (figure 3A). For both groups, infection was the most common trigger for MC as recorded by the treating physician with 7 out of 9 MC for rituximab and 2 out of 2 MC for eculizumab. For the remaining MC, the trigger remained unknown.

At 12 months, the rate of MM differed between the two groups with six patients achieving MM in the rituximab (n=56, 10.7%) and seven patients in the eculizumab treatment group (n=19,

Table 1 Baseline characteristics of patients, total n=77

	Rituximab-treated patients	Eculizumab-treated patients	P value
Patients, n	57	20	
Age at baseline, years, mean (SD)	46.5 (17.1)	45.4 (15.2)	0.791
Age at diagnosis, years, mean (SD)	40.8 (18.2)	36.5 (12.2)	0.351
Early onset MG, n (%)	36 (63.1)	16 (80.0)	0.266
Late onset MG, n (%)	21 (36.9)	4 (20.0)	0.266
Female patients, n (%)	35 (62.5)	12 (54.6)	0.610
Disease duration, years, mean (SD)	6.3 (4.5)	8.8 (6.3)	0.068
QMG score at baseline, mean (SD)	10.7 (5.1)	13.2 (5.2)	0.056
MGFA status at maximum severity, n (%)			
I	0 (0.0)	0 (0.0)	0.335
II	16 (28.1)	10 (50.0)	
III	20 (35.1)	5 (25.0)	
IV	16 (28.1)	3 (15.0)	
V	7 (12.2)	2 (10.0)	
History of thymectomy, n (%)	29 (50.8)	13 (65)	0.308
Confirmed thymoma, n (%)	8 (14.0)	4 (20.0)	0.487
Total number of previous ISTs, median (minimum–maximum)	2 (2–3)	2 (2–3)	0.285
Previous disease modifying therapy, n (%)			
Azathioprine	49 (85.9)	18 (90.0)	0.729
Mycophenolate	26 (45.6)	14 (70.0)	0.072
Methotrexate	24 (42.1)	7 (35.0)	0.608
Cyclosporine	7 (12.2)	5 (25.0)	0.279
Cortisone at baseline, mg, mean (SD)	6.0 (10.3)	10.4 (12.6)	0.121
Number of previous MC, median (minimum–maximum)	1 (0–3)	1 (0–3)	0.971

Baseline refers to the first infusion of rituximab or eculizumab. Disease duration was defined as the time between symptom onset and baseline. Patients with rituximab were compared with patients receiving eculizumab by two-sided Student's t-test (*) or Fisher's exact test (#). P values are given; significance cut-off was p<0.05.
IST, immunosuppressive therapy; MC, myasthenic crisis; MG, myasthenia gravis; MGFA, Myasthenia Gravis Foundation of America; QMG, quantitative myasthenia gravis.

36.8%; p=0.031, figure 3B). At 24 months, the effect persisted with seven patients reaching MM after rituximab (n=54, 12.9%) and seven patients after eculizumab treatment (n=19, 36.8%; p=0.015). One eculizumab patient and three rituximab patients were excluded from the analysis due to insufficient information regarding rescue therapies. The use of rescue therapies did not differ significantly between the rituximab and eculizumab groups as measured by the number of rescue therapies required for each patient during the 24 months observation period (number of rescue therapies per patient (SD) rituximab 2.20 (1.83), eculizumab 1.42 (1.81) p=0.073) (figure 3C). Lastly, both groups were able to reduce prednisone dose after treatment initiation (figure 3D). We detected no significant difference between the groups regarding the change to baseline prednisone dose at 12 months (prednisone dose at 12 months, mg (SD) rituximab 4.01 (4.90), eculizumab 5.30 (5.63), p=0.721) or at 24 months of treatment (prednisone dose at 24 months, mg (SD) rituximab 2.75 (3.67), eculizumab 3.17 (2.88), p=0.871).

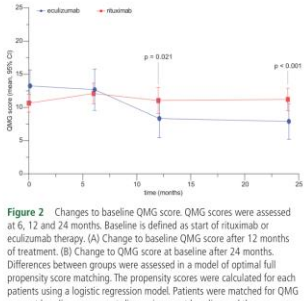

Figure 2 Changes to baseline QMG score. QMG scores were assessed at 6, 12 and 24 months. Baseline is defined as start of rituximab or eculizumab therapy. (A) Change to baseline QMG score after 12 months of treatment. (B) Change to QMG score at baseline after 24 months. Differences between groups were assessed in a model of optimal full propensity score matching. The propensity scores were calculated for each patients using a logistic regression model. Patients were matched for QMG score at baseline, sex, age at diagnosis, age at baseline and thymoma. Error bars display mean (95% CI). QMG quantitative myasthenia gravis. ***p<0.001, **p<0.01, *p<0.05, p≥0.05, not significant.

DISCUSSION

Clinical evidence is sparse in the therapeutic landscape of MG,[20] but necessary to shape informed treatment decisions. To this end, we compared rituximab and eculizumab for treatment of refractory, generalised anti-AChR-ab positive MG. Eculizumab was more effective at ameliorating disease severity than rituximab as measured by QMG score after 12 and 24 months of treatment. Eculizumab-treated patients also achieved MM more frequently than rituximab-treated patients at 12 and at 24 months of treatment, while the risk for MC was comparable between both groups. Both groups were able to reduce average prednisone doses; however, no statistically significant difference was observed between the groups.

The role of eculizumab in the therapeutic landscape of MG is evolving as new evidence emerges. The REGAIN trial supports the use of eculizumab for refractory, anti-AChR-ab

Table 2 Characteristics of rituximab-treated patients before and after 2017

	Rituximab-treated patients before 2017	Rituximab-treated patients after 2017	P value
Patients, n	39	18	
Age at baseline, years, mean (SD)	40.3 (16.3)	44.9 (16.7)	0.221
Age at diagnosis, years, mean (SD)	38.1 (17.4)	42.1 (19.9)	0.442
Early onset MG, n (%)	26 (66.7)	13 (72.2)	0.695
Late onset MG, n (%)	13 (33.3)	5 (27.8)	0.695
Female patients, n (%)	25 (64.1)	14 (77.8)	0.136
Disease duration, years, mean (SD)	7.1 (5.6)	9.4 (9.7)	0.098
QMG score at baseline, mean (SD)	11.5 (4.4)	10.3 (6.4)	0.438
MGFA status at maximum severity, n (%)			
I	0 (0.0)	0 (0.0)	0.119
II	12 (30.1)	6 (33.3)	
III	15 (38.4)	7 (38.9)	
IV	9 (23.1)	5 (27.8)	
V	4 (10.2)	2 (11.1)	
History of thymectomy, n (%)	18 (46.1)	10 (55.5)	0.726
Confirmed thymoma, n (%)	5 (12.8)	3 (16.7)	0.698
Total number of previous ISTs, median (minmum–maximum)	2 (2–3)	2 (2–3)	0.331
Previous disease modifying therapy, n (%)			
Azathioprine	36 (92.3)	13 (72.2)	0.093
Mycophenolate	20 (51.3)	6 (33.3)	0.174
Methotrexate	13 (33.3)	11 (61.0)	0.082
Cyclosporine	5 (12.8)	2 (11.1)	0.999
Cortisone at baseline, mg, mean (SD)	9.8 (11.2)	10.8 (12.1)	0.841
Number of previous MC, median (minmum–maximum)	1 (0–3)	1 (0–2)	0.865

Disease duration was defined as the time between symptom onset and baseline. Rituximab-treated patients included before 2017 were compared with rituximab-treated patients included after 2017 by two-sided Student's t-test (*) or Fisher's exact test (#). P values are given; significance cut-off was p<0.05.
IST, immunosuppressive therapy; MC, myasthenic crisis; MG, myasthenia gravis; MGFA, Myasthenia Gravis Foundation of America; QMG, quantitative myasthenia gravis.

mediated MG.[9 10] Despite not reaching the prespecified primary endpoint of change from baseline in the MG activities of daily living (ADL) score, post-hoc sensitivity analysis and secondary outcome measures demonstrated the efficacy of eculizumab in this patient collective.[9] Analysis of the open-label extension reported that eculizumab's effect was maintained throughout the 3 years of treatment.[10] However, given its novelty and high cost, eculizumab remains reserved for cases with severe disease in current guidelines and direct comparisons to other therapies are lacking.[21] Pathophysiological considerations might further strengthen the use of eculizumab as aberrant complement activation has been evidenced in humans and in animal models.[22] Selective targeting of the complement cascade might therefore improve clinical outcomes while offering a beneficial profile of adverse effects.[10] Consistent with this, data from our observational study underlines the efficacy of eculizumab as potential treatment option for refractory MG. It should be noted, that eculizumab is currently limited to anti-AChR-ab positive MG, which is mediated by IgG1 (and IgG3) subtype autoantibodies capable to activate the complement cascade. In contrast, MG mediated by pathogenic IgG4 subtype, for example, anti-MuSK MG, is unlikely to benefit from treatment due the lack of complement activation.[23] By contrast, rituximab is efficacious in MG with anti-MuSK-ab as evidenced in a nationwide retrospective study.[24] A shorter time to response might be expected for eculizumab in comparison to rituximab. Following infusion, complement is rapidly inhibited and therapeutic effects are seen as early as 3 days after treatment.[25] Maximum efficacy is expected after 12 weeks of treatment as demonstrated in the REGAIN trial.[26] As a general rule, rituximab effects are delayed for 6–8 weeks after infusion, and some patients require repeated cycles to achieve clinical benefits.[27 28] Surprisingly, differences in treatment efficacy between the therapies persisted at 12 and 24 months after therapy initiation. Both treatment options carry a risk of severe infection, especially in combination with other immunosuppressants. Specifically, eculizumab is accompanied by an increased risk for meningococcal infections with approximately 0.1 events per 100 patient years,[29 30] leading to obligatory anti-meningococcal vaccination before starting therapy.

Comparison between the two groups revealed no meaningful differences in the time to MC. With 10% and 16% of patients experiencing a MC during the 24 months observation period, the risk for MC remained high, underlining the need for intensified care and monitoring for patients with MG during a refractory course of disease.[7] A potential explanation for the high rate for MC observed in both groups might be the frequency of infectious complications accounting for the majority of MC triggers. Treatment might dampen autoimmunity and improve symptoms, but not protect patients from infectious agents, resulting in disease flare-ups. However, the current sample size of eculizumab-treated patients might not be powered to detect effects on MC and prospective trials are required to better understand the long-term efficacy of eculizumab compared with established treatment strategies. In the open-label extension of the REGAIN trial, MG worsening occurred in ~13% and MC in 3% of patients in a time period of 22 months,[10] indicating potential differences between study settings and real-world data. The current coronavirus disease 2019 (COVID-19) pandemic is a further factor shaping treatment decisions, as treatment agents such as rituximab increase the risk of hospitalisation due to

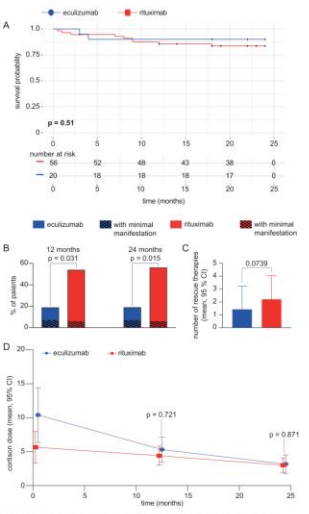

Figure 3 Time to myasthenic crisis after baseline. (A) Kaplan-Meier curve displaying time to myasthenic crisis after baseline. Baseline is defined as start of rituximab or eculizumab therapy. Differences between groups were assessed by logrank test. (B) Number of patients achieving minimal manifestation after 12 and 24 months of treatment according to treatment. (C) Number of rescue therapies per patient in the 24 months observation period. Differences between groups were assessed by two-sided Student's t-test. (D) Change to cortisone dose at baseline at 12 and 24 months of treatment. Error bars display mean (95% CI). **p<0.01, *p<0.05, p≥0.05, not significant.

immunosuppression.[31 32] In contrast, data on the safety profile of ongoing eculizumab-treatment for COVID-19 is mostly lacking.

A limitation to this study is the retrospective, observational design, potentially introducing a selection bias for treatment decisions. In addition, limitations include data collection during routine clinical practice rather than a defined study setting. This might result in variances in data quality and quantity between patients. For example, the MG-ADL score was not routinely assessed during clinical practice and could not serve as an additional outcome parameter. Further, a conclusive definition for a treatment refractory status is currently lacking. For this study, we adapted a previously published definition of treatment refractory status as operational definition.[3] However, we appreciate that the definition of treatment refractory disease at baseline, as employed for this study, is provisional until a consensus has been achieved for treatment refractoriness in the field of MG. The scope of our study is limited to the comparison of rituximab and eculizumab. Further studies investigating the efficacy of either agents against untreated patients in a real-world setting might be of scientific interest. Due to the clinical heterogeneity and rarity of the disease, MG has been historically difficult to study in the context of clinical trials.[20] Thus, a strength of this study is the use of a well-defined MG cohort with high diagnostic certainty, providing novel data for treatment decisions for refractory MG. Moreover, data collection was standardised across participating centres in accordance with the German Myasthenia Gravis Register. Collectively, the results of this retrospective, observational study support the treatment of refractory, anti-AChR-ab MG with eculizumab and indicates certain advantages compared with rituximab in this subgroup. Based on our data, a randomised, prospective trial comparing rituximab and eculizumab in the setting of severe, generalised MG is required to establish the most effective treatment strategy for this disease course.

Author affiliations
[1]Department of Neurology, Heinrich Heine University Düsseldorf, Dusseldorf, Germany
[2]Department of Neurology, Charité — Universitätsmedizin Berlin, corporate member of Freie Universität Berlin and Humboldt-Universität zu Berlin, Berlin, Germany
[3]NeuroCure Clinical Research Center, Charité — Universitätsmedizin Berlin, corporate member of Freie Universität Berlin and Humboldt-Universität zu Berlin, Berlin, Germany
[4]Department of Neurology with Institute of Translational Neurology, University Hospital Münster, Münster, Germany
[5]Department of Cardiothoracic Surgery, University Hospital Cologne, Koln, Germany
[6]Departement of Neurology, Uniklinik Koln, Koln, Nordrhein-Westfalen, Germany
[7]Department of Neurology, University of Cologne, Koln, Germany
[8]Department of Neurology and Neurophysiology, University Hospital Freiburg, Freiburg, Germany
[9]Department of Neurology, University Hospital Essen, Essen, Germany
[10]Department of Neurology, Otto-von-Guericke University, Magdeburg, Germany
[11]Otto von Guericke Universität Magdeburg, Magdeburg, Sachsen-Anhalt, Germany
[12]Center for Stroke Research Berlin, Charité — Universitätsmedizin Berlin, corporate member of Freie Universität Berlin and Humboldt-Universität zu Berlin, Berlin, Germany
[13]Department of Neurology - Inflammatory Disorders of the Nervous System and Neurooncology, University of Münster, Münster, Germany

Acknowledgements We thank the patients and their families for their valuable contribution and support.

Contributors CN, CBS and TR designed the study and methods. Formal analysis was done by CN and CBS. Clinical data were provided by CN, CBS, FS, MP, AG, HS, MS, BB, AT, TH, SS, SV, AM, HW, SGM and TR. Resources were provided by FS, AM, SGM and TR. CN and CBS wrote the original draft. FS, MP, LR-N, NM, AG, HS, MS, BB, AT, TH, SS, SV, AM, SGM and TR reviewed and edited the manuscript; Figures were created by CN and CBS. Supervision by AM, SGM and TR. Guarantor of the study is TR.

Funding PM is Einstein Junior Fellow funded by the Einstein Foundation Berlin, and is supported by grants from the Bundesministerium für Bildung und Forschung (grants no. 16GW0191 and NUM-COVID 19 – Organo-Strat 01KX2021).

Competing interests CN reports no conflicts of interest. CBS reports no conflicts of interest. FS received speaking honoraria from Biogen and Alexion. MP received speaker honoraria and travel/accommodation/meeting expenses from Novartis. LR-N reports no disclosures. NM reports no conflicts of interest. PM is on the Advisory Board of HealthNextGen and has equity interest in the company. His research is funded by the Bundesministerium für Bildung und Forschung (BMBF), the European Union, the Else Kröner-Fresenius Stiftung, the Volkswagen Stiftung and the Einstein Foundation Berlin. AG reports no conflicts of interest. HS reports no conflicts of interest. MS reports no conflicts of interest. BB received travel grants and/or training expenses from Bayer Vital GmbH, IpsenPharma GmbH, Novartis, Biogen GmbH and Genzyme, as well as lecture fees from Ipsen Pharma GmbH, Alexion Pharma GmbH, Merck, Sanofi Genzyme and Roche. AT reports on conflicts of interest. TH received speaker honoraria and advisor honoraria from Alexion, Argenx, Biogen, Roche, Sanofi-Genzyme, Novartis and Hormosan. SS reports no conflicts of interest. SV reports no conflicts of interest. AM received speaker honoraria, consulting services and/or research support research from Alexion, argnx, GRIFOLS, Hormosan, Janssen, Octapharma, UCB and Vitaccess. He serves as chairman of the medical advisory board of the German Myasthenia Gravis Society. HW receives honoraria for acting as a member of Scientific Advisory Boards, Biogen, Evgen, Genzyme, MedDay Pharmaceuticals, Merck Serono, Novartis, Roche Pharma AG and Sanofi-Aventis as well as speaker honoraria and travel support from Alexion, Biogen, Cognomed, F. Hoffmann-La Roche, Gemeinnützige Hertie-Stiftung, Merck Serono, Novartis, Roche Pharma AG, Genzyme, TEVA and WebMD Global. HW is acting as a paid consultant for AbbVie, Actelion, Biogen, IGES, Johnson & Johnson, Novartis, Roche, Sanofi-Aventis and the Swiss Multiple Sclerosis Society. His research is funded by the German Ministry for Education and Research (BMBF), Deutsche Forschungsgemeinschaft (DFG), Else Kröner Fresenius Foundation, Fresenius Foundation, the European Union, Hertie Foundation, NRW Ministry of Education and Research, Interdisciplinary Center for Clinical Studies (IZKF) Muenster and RE Children's Foundation, Biogen, GlaxoSmithKline GmbH, Roche Pharma AG, Sanofi-Genzyme. SGM receives honoraria for lecturing, and travel expenses for attending meetings from Almirall, Amicus Therapeutics Germany, Bayer Health Care, Biogen, Celgene, Diamed, Genzyme, MedDay Pharmaceuticals, Merck Serono, Novartis, Novo Nordisk, ONO Pharma, Roche, Sanofi-Aventis, Chugai Pharma, QuintilesIMS and Teva. His research is funded by the German Ministry for Education and Research (BMBF), Bundesinstitut für Risikobewertung (BfR), Deutsche Forschungsgemeinschaft (DFG), Deutsche Multiple Sklerose Gesellschaft (DMSG), Else Kröner Fresenius Foundation, Gemeinsamer Bundesausschuss (G-BA), German Academic Exchange Service, Hertie Foundation, Interdisciplinary Center for Clinical Studies (IZKF) Muenster, German Foundation Neurology and Alexion, Almirall, Amicus Therapeutics Germany, Biogen, Diamed, Fresenius Medical Care, Genzyme, HERZ Burgdorf, Merck Serono, Novartis, ONO Pharma, Roche and Teva. HW receives honoraria for acting as a member of Scientific Advisory Boards, Biogen, Evgen, Genzyme, MedDay Pharmaceuticals, Merck Serono, Novartis, Roche Pharma AG and Sanofi-Aventis as well as speaker honoraria and travel support from Alexion, Biogen, Cognomed, F. Hoffmann-La Roche, Gemeinnützige Hertie-Stiftung, Merck Serono, Novartis, Roche Pharma AG, Genzyme, TEVA and WebMD Global. TR reports grants from German Ministry of Education, Science, Research and Technology, grants and personal fees from Sanofi-Genzyme and Alexion; personal fees from Biogen, Roche and Teva; personal fees and non-financial support from Merck Serono, outside the submitted work.

Patient consent for publication Not applicable.

Ethics approval The study was approved by the corresponding ethic boards (no. AZ 2020-010-f-S, no. AZ 07/2017, 19-8973-BO, AZ 21-1265, AZ 21-1331). Participants gave informed consent to participate in the study before taking part.

Provenance and peer review Not commissioned; externally peer reviewed.

Data availability statement Data are available upon reasonable request. All data relevant to the study are included in the article or uploaded as supplementary information. All analysed data are presented in the manuscript and available upon reasonable request from qualified investigators.

ORCID iDs
Christopher Nelke http://orcid.org/0000-0002-6048-7143
Frauke Stascheit http://orcid.org/0000-0001-5306-7880
Philipp Mergenthaler http://orcid.org/0000-0002-9753-6711
Stefanie Schreiber http://orcid.org/0000-0003-4439-4374

REFERENCES

1 Gilhus NE, Tzartos S, Evoli A, *et al*. Myasthenia gravis. *Nat Rev Dis Primers* 2019;5:30.
2 Grob D, Brunner N, Namba T, *et al*. Lifetime course of myasthenia gravis. *Muscle Nerve* 2008;37:141–9.
3 Schneider-Gold C, Hagenacker T, Melzer N, *et al*. Understanding the burden of refractory myasthenia gravis. *Ther Adv Neurol Disord* 2019;12:1756286419832242.
4 Iorio R, Damato V, Alboini PE, *et al*. Efficacy and safety of rituximab for myasthenia gravis: a systematic review and meta-analysis. *J Neurol* 2015;262:1115–9.
5 Brauner S, Eriksson-Dufva A, Hietala MA, *et al*. Comparison between rituximab treatment for new-onset generalized myasthenia gravis and refractory generalized myasthenia gravis. *JAMA Neurol* 2020;77:974–81.
6 Hehir MK, Hobson-Webb LD, Benatar M, *et al*. Rituximab as treatment for anti-MuSK myasthenia gravis: multicenter blinded prospective review. *Neurology* 2017;89:1069–77.
7 Kusner LL, Kaminski HJ, Soltys J. Effect of complement and its regulation on myasthenia gravis pathogenesis. *Expert Rev Clin Immunol* 2008;4:43–52.
8 Rother RP, Rollins SA, Mojcik CF, *et al*. Discovery and development of the complement inhibitor eculizumab for the treatment of paroxysmal nocturnal hemoglobinuria. *Nat Biotechnol* 2007;25:1256–64.
9 Howard JF, Utsugisawa K, Benatar M, *et al*. Safety and efficacy of eculizumab in anti-acetylcholine receptor antibody-positive refractory generalised myasthenia gravis (REGAIN): a phase 3, randomised, double-blind, placebo-controlled, multicentre study. *Lancet Neurol* 2017;16:976–86.
10 Muppidi S, Utsugisawa K, Benatar M, *et al*. Long-term safety and efficacy of eculizumab in generalized myasthenia gravis. *Muscle Nerve* 2019;60:14–24.
11 Wendl H. *Diagnostik und therapie der myasthenia gravis und des lambert-eaton-syndroms*, 2014.
12 Bedlack RS, Sanders DB. On the concept of myasthenic crisis. *J Clin Neuromuscul Dis* 2002;4:40–2.
13 Wolfe GI, Kaminski HJ, Aban IB, *et al*. Randomized trial of thymectomy in myasthenia gravis. *N Engl J Med* 2016;375:511–22.
14 America TF, Jaretzki A, Barohn RJ. Myasthenia gravis: recommendations for clinical research standards. *Neurology* 2000;55:16–23.
15 Thomsen JLS, Andersen H. Outcome measures in clinical trials of patients with myasthenia gravis. *Front Neurol* 2020;11.
16 Austin PC, Xin Yu AY, Vyas MV, *et al*. Applying propensity score methods in clinical research in neurology. *Neurology* 2021;97:856–63.
17 Vollmer B, Ontaneda D, Bandyopadhyay A, *et al*. Discontinuation and comparative effectiveness of dimethyl fumarate and fingolimod in 2 centers. *Neurol Clin Pract* 2018;8:292–301.
18 Donner A. The relative effectiveness of procedures commonly used in multiple regression analysis for dealing with missing values. *Am Stat* 1982;36:378–81.
19 Kasi PM, Tawbi HA, Oddis CV, *et al*. Clinical review: Serious adverse events associated with the use of rituximab - a critical care perspective. *Crit Care* 2012;16:231.
20 Nguyen-Cao TM, Gelinas D, Griffin R, *et al*. Myasthenia gravis: historical achievements and the "golden age" of clinical trials. *J Neurol Sci* 2019;406:116428.
21 Narayanaswami P, Sanders DB, Wolfe G, *et al*. International consensus guidance for management of myasthenia gravis: 2020 update. *Neurology* 2021;96:114–22.
22 Christadoss P, Tüzün E, Li J, *et al*. Classical complement pathway in experimental autoimmune myasthenia gravis pathogenesis. *Ann N Y Acad Sci* 2008;1132:210–9.
23 Kawa S. The immunobiology of immunoglobulin G4 and complement activation pathways in IgG4-related disease. *Curr Top Microbiol Immunol* 2017;401:61–73.
24 Topakian R, Zimprich F, Iglseder S, *et al*. High efficacy of rituximab for myasthenia gravis: a comprehensive nationwide study in Austria. *J Neurol* 2019;266:699–706.
25 Tsai H-M, Kuo E. Eculizumab therapy leads to rapid resolution of thrombocytopenia in atypical hemolytic uremic syndrome. *Adv Hematol* 2014;2014:1–7.
26 Dhillon S. Eculizumab: a review in generalized myasthenia gravis. *Drugs* 2018;78:367–76.
27 Safety and efficacy of eculizumab in anti-acetylcholine receptor antibody-positive refractory generalised myasthenia gravis (REGAIN): a phase 3, randomised, double-blind, placebo-controlled, multicentre study - The Lancet Neurology. Available: https://www.thelancet.com/journals/laneur/article/PIIS1474-4422(17)30369-1/fulltext [Accessed 7 Jun 2021].
28 Nowak RJ, Dicapua DB, Zebardast N, *et al*. Response of patients with refractory myasthenia gravis to rituximab: a retrospective study. *Ther Adv Neurol Disord* 2011;4:259–66.
29 Langerels JD, van den Broek B, Franssen S, *et al*. Eculizumab impairs Neisseria meningitidis serogroup B killing in whole blood despite 4CMenB vaccination of PNH patients. *Blood Adv* 2020;4:3615–20.
30 Patriquin CJ, Kulasekararaj A, Peffault de Latour R, *et al*. Prophylactic antibiotic use and risk of meningococcal infections in patients with paroxysmal nocturnal hemoglobinuria (PNH) treated with eculizumab who received meningococcal vaccination: results from the International PNH registry. *Blood* 2019;134:4802.
31 Sormani MP, De Rossi N, Schiavetti I, *et al*. Disease-modifying therapies and coronavirus disease 2019 severity in multiple sclerosis. *Ann Neurol* 2021;89:780–9.
32 Gianfrancesco M, Hyrich KL, Al-Adely S, *et al*. Characteristics associated with hospitalisation for COVID-19 in people with rheumatic disease: data from the COVID-19 global rheumatology alliance physician-reported registry. *Ann Rheum Dis* 2020;79:859–66.

Review

Cellular senescence in neuroinflammatory disease: new therapies for old cells?

Christopher Nelke,[1,2] Christina B. Schroeter,[1,2] Marc Pawlitzki,[1] Sven G. Meuth,[1] and Tobias Ruck[1,*]

Neuroinflammatory diseases remain a therapeutic challenge, notably when progressing towards neurodegeneration. In this context, multiple sclerosis represents a central nervous system (CNS) disorder that combines pathogenic inflammatory and degenerative processes. Immunosuppression is effective for managing inflammatory activity, but neurodegenerative processes secondary to chronic inflammation are often refractory to contemporary treatments. Recent evidence indicates that pathways involved in chronic neuroinflammation demonstrate features of cellular senescence. These features could provide a framework that could serve as a target for senotherapeutics. In this review, we discuss the unmet need for strategies capable of overcoming the treatment resistance of neuroinflammatory diseases, and we discuss the potential of cellular senescence towards developing these strategies.

Highlights

There is an unmet need for novel therapeutic strategies that can halt neuroinflammatory disorders progressing towards a degenerative phenotype.

Accumulating evidence links cellular senescence to a plethora of human diseases.

Initial data indicate the presence of cellular senescence in neuroinflammatory disorders, suggesting it as a potential driver of pathogenesis.

Senotherapeutics were able to reduce the senescent burden in animal models and, more recently, in humans.

Incorporating senotherapeutics in the field of neuroinflammation could improve treatment outcomes.

Are senotherapeutics the key to treatment refractoriness in neuroinflammatory disorders?

The cellular state of senescence is characterized by the inability of a cell to proliferate despite sufficient resources and stimuli [1,2]. This concept was first described in 1961 and has since attracted considerable scientific interest, particularly over the past 5 years [3]. Indeed, senotherapeutic research has advanced exponentially and demonstrated that targeting **cellular senescence** (see Glossary) is a promising treatment strategy for otherwise incurable diseases, at least in animal models [4,5]. For example, pharmacological depletion of senescent cells improved functional outcomes in a murine model of Alzheimer's disease (AD) [6]. Following these results, **senotherapies** (Box 1) are currently being tested in clinical trials for neurodegenerative diseases such as AD [7], as well as for other pathologies (e.g., cardiometabolic or age-associated conditions) [5]. By contrast, research and literature focusing on cellular senescence in the context of neuroinflammation is sparse. Neuroinflammatory diseases are characterized by autoimmunity directed against components of the nervous system. Contemporary treatment options are often able to halt neuroinflammation to a considerable extent [8]. However, neuroinflammatory disorders that have a degenerative component often respond poorly to therapy and constitute an unmet need for novel therapeutic approaches [9]. This concept is perhaps best exemplified by **multiple sclerosis (MS)**. Immunosuppression may dampen inflammation in relapsing–remitting MS (RRMS), effectively reducing disability progression [8,10]. By contrast, once RRMS advances to the secondary progressive course of the disease (SPMS), neurodegeneration and disease progression are often insidious and unresponsive to therapeutic modulation [11].

Effective strategies to ameliorate secondary degenerative processes following chronic inflammation are yet to be successfully translated into clinical practice. Senotherapies may be a promising approach to improve therapeutic outcomes of neuroinflammatory diseases that have an unsatisfactory response to immunosuppressive treatment alone. In this review, we provide a current overview of the current knowledge on cellular senescence and its role in neuroinflammatory disorders. For the latter, we focus on MS as a neuroinflammatory disease exhibiting neurodegenerative components. However, we also discuss inflammatory pathologies of the peripheral nervous system (PNS) and skeletal muscle, as these areas of research have progressed recently and share common pathogenic traits with CNS disorders. We further demonstrate how senotherapeutics may be used as new treatment strategies to overcome treatment refractoriness in those diseases. Overall, this review intends to stimulate further research in the emerging field of senotherapeutics.

[1]Department of Neurology, Medical Faculty, Heinrich Heine University Düsseldorf, Düsseldorf, Germany
[2]Contributed equally as first authors

*Correspondence:
Tobias.Ruck@med.uni-duesseldorf.de (T. Ruck).

850 Trends in Molecular Medicine, October 2022, Vol. 28, No. 10 https://doi.org/10.1016/j.molmed.2022.07.003

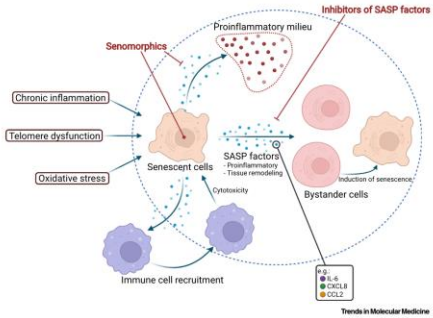

Small-fiber neuropathy: a type of peripheral neuropathy that affects the small nerve fibers in the skin.
Xenotransplantation: a heterologous transplant of living cells, tissues, or organs from one species to another.

Figure 1. Cellular senescence in neuroinflammation. Different triggers may establish a senescent phenotype. Oxidative stress, telomere dysfunction, and chronic inflammation are examples of factors promoting cellular senescence. The senescence-associated secretory phenotype (SASP) attracts further immune cells, provides a local proinflammatory milieu, and induces senescence in bystander cells. The SASP composition is heterogeneous and includes proinflammatory and tissue remodeling factors such as IL-6, CXCL8, or CCL2 among others. Therapeutic agents targeting mechanisms of cellular senescence are indicated in red. This figure was created with BioRender. Abbreviations: CCL2, CC-chemokine ligand 2; CXCL8, chemokine (C-X-C motif) ligand 8.

environment [22–24]. Following this line of argument, cells with a senescent phenotype resistant to apoptosis might provide a proinflammatory microenvironment sustaining the progression of neuroinflammatory diseases, which we discuss in the following subsections.

The challenge of treating progressive MS

MS is a common autoimmune disease of the CNS resulting in demyelination and axonal degeneration [26]. Around 80% of MS patients are first diagnosed as having RRMS. Here, patients experience unpredictable relapses of inflammatory activity, often linked to persisting disability. A substantial proportion of RRMS patients, ranging from 25% to 60% as demonstrated by natural history studies [27,28], advance to a progressive phase of the disease termed SPMS. The remaining 10–20% of MS patients have a primary progressive MS course (PPMS) from disease onset. Both progressive forms of MS are characterized by sustained disability accumulation, with only a minor fluctuation of symptoms [27]. Indeed, a current study on the natural history of MS demonstrated that 75–100% of PPMS patients experience substantial disease worsening as compared to ~55% of RRMS patients [8]. While clear clinical or pathological criteria defining transition from RRMS to SPMS remain to be defined, the distinction between RRMS and progressive MS is crucial as their pathophysiological mechanisms and therapeutic responses differ [27]. The current viewpoint on progressive MS recognizes chronic inflammation compartmentalized behind a closed blood–brain barrier as a pathogenic hallmark [27]. Persistent activation of immune cells and microglia, as well as mitochondrial damage, leads to neurodegeneration with progredient neuroaxonal cell

852 Trends in Molecular Medicine, October 2022, Vol. 28, No. 10

Box 1. Senotherapeutics

Senotherapeutics (from Latin senex = old) aim to reduce the burden of cellular senescence. Senotherapeutic strategies can be broadly divided into two categories (senolytics and senomorphics) based on their mechanism of action. First, senolytics selectively induce cell death in senescent cells. Most senolytics target prosurvival and/or anti-apoptotic cellular pathways such as p53, p21, B cell lymphoma (Bcl-2) family proteins, HSP90, or protein kinase B (Akt). Different senolytic agents target distinct subpopulations of senescent cells, depending on their mechanism of action. Second, senomorphics aim to suppress the senescence-associated secretory phenotype (SASP) without inducing cell death. Most senomorphics target cellular pathways mediating senescent reprogramming, such as nuclear factor κB (NF-κB), mTOR, JAK 1/2 inhibitors, rho-kinase 1 (ROCK1), or p38 MAPK. As the field of senotherapeutics is rapidly evolving, a conclusive definition of therapeutic subgroups is currently lacking. It is worth noting that individual agents often exhibit mechanisms that qualify for one or more subgroups of senotherapy: for example, senolytics might also act as senomorphics and vice versa. An overview of contemporary senotherapeutics is given in Table 1 in main text.

Cellular senescence: current concepts in the field

Cellular senescence is the consequence of endogenous and exogenous stress. Among other things, these stressors include DNA damage, telomere dysfunction, oncogene activation, and chronic inflammation [1,2]. Pathways of cellular senescence and apoptosis are intimately linked and mediated, in part, by p53 signaling [12]. However, the factors shaping a cell's trajectory towards apoptosis or senescence remain to be established [2,13]. Intriguingly, senescence is not confined to the cell experiencing stress, but exhibits the ability to spread. **Xenotransplantation** of senescent fibroblasts into skeletal muscle of young mice induces expression of a senescent phenotype in bystander cells [14]. These bystander cells included fibroblasts and myofibers. One mechanism that may explain the dissemination of senescence is the secretory phenotype of senescent cells establishing a microenvironment perpetuating cellular senescence. Although subject to variation across tissues, the corresponding **senescence-associated secretory phenotype (SASP)** is characterized by a set of proinflammatory cytokines, growth factors, and proteases (Figure 1) [15,16]. The composition of the SASP is heterogeneous, with unique quantitative and qualitative features depending on the corresponding trigger, cell type, and tissue [17]. Even within the CNS, SASP profiles diverge between cell types (the phenotypes are discussed in detail by Papadopoulos *et al.* [17]). The senescent **secretome** includes a range of proinflammatory and immunomodulatory cytokines (e.g., IL-6, IL-7), chemokines [e.g., CC-chemokine ligand 2 (CCL2), CCL8], growth factors [e.g., epidermal growth factor (EGF) and vascular endothelial growth factor (VEGF)], and proteases (e.g., MMP-1/3) [18,19]. Senescent cells also interact by specific receptors [e.g., intercellular adhesion molecule-1 (ICAM-1), urokinase receptor (uPAR), tumor necrosis factor (TNF) receptors], non-protein molecules [e.g., prostaglandin E2 (PGE2)], insoluble factors (e.g., fibronectin, collagens), **exosomes**, and **ectosomes** [20]. Thus, both soluble and insoluble interaction molecules are employed by senescent cells to influence the local microenvironment. The effect of the SASP is highly dynamic. Initially, it is characterized by immunosuppressive and profibrotic effects, preserving or restoring tissue homeostasis [21]. However, with accumulation of senescent cells during inflammation and aging, its proinflammatory and potentially detrimental characteristics dominate and result in inflammation, tissue damage, and detrimental growth responses in bystander cells [22–24]. Thus, the SASP is increasingly recognized as a key driver of age-related pathologies, such as chronic inflammation [25]. Of note, SASP components are effective proinflammatory cytokines capable of attracting and activating immune cells, thereby promoting an inflammatory tissue

Glossary

Autophagy: intracellular degradation system which removes cellular debris.
β-Galactosidase: a family of glycoside hydrolase enzymes associated with cellular senescence.
Cellular senescence: a state of irreversible stable cell cycle arrest.
Chemotherapy-induced peripheral neuropathy (CIPN): damage to peripheral nerves induced by chemotherapies.
Chronic inflammatory demyelinating polyradiculoneuropathy (CIDP): a chronic inflammatory disease of peripheral nerves.
Ectosome: an extracellular vesicle generated by outward budding from the plasma membrane.
Endoneural: from the endoneurium, a layer of connective tissue surrounding the myelin sheath of nerves.
Exosome: an extracellular vesicle released on exocytosis of multivesicular bodies.
Idiopathic inflammatory myopathies (IIMs): a group of autoimmune disorders affecting skeletal muscle.
Immunosenescence: age-related changes to the immune system.
Inclusion body myositis (IBM): an acquired IIM preferentially affecting older patients with distinct clinical features.
Mammalian target of rapamycin (mTOR): a kinase encoded by the *mTOR* gene regulating a number of cellular processes.
Multiple sclerosis (MS): a frequent, chronic autoimmune disease affecting the central nervous system.
Oligodendrocyte precursor cells (OPCs): a subtype of glia in the central nervous system acting as precursors to oligodendrocytes.
Progression independent of relapse activity (PIRA): disability accumulating in multiple sclerosis independent of relapse activity.
Secretome: a set of proteins secreted into the extracellular space.
Senescence-associated secretory phenotype (SASP): a distinct secretome assumed by senescent cells, including proinflammatory cytokines, growth factors, and proteases, among others.
Senotherapies: therapeutic agents targeting senescent cells.
Sirolimus (rapamycin): a commonly used mTOR inhibitor.

death. Altered ion-channel function and imbalance of reactive oxygen species (ROS) likely amplify inflammatory conditions [29–31]. Only a few immunosuppressive drugs have shown limited efficacy in the treatment of progressive MS [9]. Consequently, treatment approaches for progressive MS remain unsatisfactory, as contemporary immunosuppressants are unable to effectively halt neurodegeneration. The challenge of managing progressive MS is highlighted by the (un)availability of treatment agents. While over 15 drugs have been approved for RRMS, only two (siponimod and cladribine) have demonstrated limited efficacy in SPMS and only one (ocrelizumab) in PPMS [10]. However, the efficacy of approved agents for progressive MS is linked mainly to treating features of acute inflammatory activity [32]. However, **progression independent of relapse activity (PIRA)** recently emerged as a major driver of disability accumulation [33]. Indeed, over a period of 96 weeks, confirmed disability accumulation occurred in 80–90% of RRMS patients as PIRA. By contrast, only ~17% of disability was attributed to clinical relapses [33]. This observation challenges the dichotomy of RRMS and progressive MS and highlights the need for treatment strategies capable of preventing insidious neurodegeneration independent of inflammatory activity. Interestingly, aside from the transition to a progressive form, age at baseline was more frequently associated with negative results for treatment trials of drugs proven to be effective in RRMS [9]. Consequently, evidence for therapeutic efficacy is not available for the majority of established drugs when treating patients over the age of 55 years [9].

Taken together, novel strategies are needed to effectively manage progressive MS. Senotherapeutics are a promising potential solution to this issue. In the following sections, we will discuss the current (albeit preliminary) data on cellular senescence in MS.

MS and cellular senescence: a bidirectional link

Chronic inflammation and oxidative stress are pathogenic hallmarks of MS [34–36]. Accumulating evidence supports senescent cells as a source of chronic inflammation [20]. Vice versa, data on chronic inflammation promoting cellular senescence are less robust, warranting further research in the bidirectional interplay of senescence and inflammation. Senescent cells promote an inflammatory milieu by secretion of proinflammatory cytokines, chemokines, and ROS [37]. Consequently, DNA damage and telomerase dysfunction lead to cell cycle arrest in adult progenitor cells exceeding the regenerative capacity of the CNS and resulting in dysfunction of resident cell types such as **oligodendrocyte precursor cells (OPCs)** (Figure 2) [38–40]. Consistent with this, senescent glial cells were detected in the white and gray matter of demyelinating lesions in a murine cuprizone-induced demyelination model of MS [41,42]. These cells were identified by **β-galactosidase** and lipofuscin histochemistry. Senescence of OPCs and other neural progenitor cells is thought to play a role in remyelination failure in MS, thereby promoting transition from nonprogressive to progressive MS [40,43]. Indeed, in aged rodents, OPCs exhibit a senescent phenotype unresponsive to differentiation signals and impaired metabolic homeostasis [44]. Premature **immunosenescence** of T cells has been described in MS, as well as in rheumatoid arthritis [45]. Specifically, our group previously demonstrated that premature immune aging, especially in the $CD8^+$ T cell compartment, occurs in young MS patients and may impact disease severity [46]. Moreover, expression of immunoinhibitory molecules was decreased while a premature immune aging signature consisting of KLRG1, LAG3, CTLA-4, and CD226 was identified [46]. Interestingly, the loss of age-dependent regulation was more prominent in PPMS than in RRMS patients and correlated with disease severity [46]. Likewise, there is evidence that premature senescence of B cells promotes inflammation and disease progression in MS [47]. Induced pluripotent stem-cell lines isolated from peripheral-blood mononuclear cells displayed increased markers of cellular senescence as evidenced by β-galactosidase activity in patients with PPMS and RRMS compared with controls [48]. Differentiation of this cell line into neural progenitor cells also demonstrated increased expression of senescence markers [48].

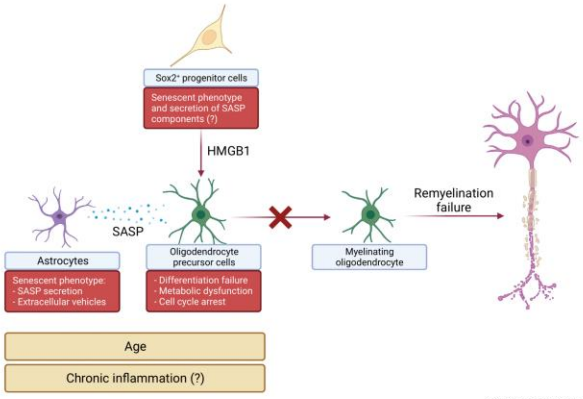

Figure 2. Oligodendrocyte precursor cell (OPC) failure as a potential intersection for cellular senescence in the central nervous system. Age and chronic inflammation might putatively underlie pathways promoting cellular senescence. Aged astrocytes can secrete senescence-associated secretory phenotype (SASP) components and extracellular vesicles impairing OPC function. Sox2$^+$ progenitor cells display a senescent phenotype in primary progressive multiple sclerosis (PPMS) and reduce OPC differentiation via high mobility group box 1 (HMGB1) signaling. It remains unknown whether progenitor cell senescence is a result of PPMS or whether senescence of progenitor cells promotes the development of PPMS. Impaired differentiation of OPCs into myelinating oligodendrocytes results in remyelination failure. This figure was created with BioRender.

Further insight into cellular senescence in the CNS might be gained from studying a model of AD (Box 2). In both humans and mice, OPCs surrounding aggregates of amyloid-β exhibit a senescent phenotype characterized by activation of the p16 pathway and β-galactosidase activity [6]. The

Box 2. Cellular senescence in AD

AD is the most common cause of dementia, contributing to 60–80% of cases. Aging is the greatest risk factor for development of AD [48]. The pathogenic hallmarks of AD are accumulation of abnormally folded amyloid-β, neurofibrillary tangles containing the protein tau, and neuroinflammation [50]. In AD, microglia and astrocytes release proinflammatory cytokines that allow for crosstalk between CNS-resident cells [49,50]. Amyloid-β oligomers, neurofibrillary tangles, and inflammatory conditions induce a senescent phenotype in CNS-resident cells. Among others, OPCs and oligodendrocytes become senescent as evidenced by elevated p16 and p21 levels [51]. Concurrently, neurons may also engage a senescent phenotype [51,52]. These cells promote inflammatory conditions by secretion of the SASP linking neuroinflammation to cellular senescence [50]. Consequently, senescent cells are considered a promising therapeutic target in the field of AD. Indeed, in murine models of AD [8] – tau pathology [53] and age-related cognitive impairment [51] – senolytics reduced neuroinflammation while improving cognitive function. Based on these findings, a number of clinical trials are currently studying the efficacy of senotherapeutics in human AD.

corticosteroids or immunoglobulins [65]. In response to these therapies, around 40% of patients require sustained treatment, while 13% accumulate severe disability [65]. Interestingly, patients with a chronic disease course did not experience remission at 5 years, while remission occurred in 43% of CIDP patients with subacute disease onset [65]. Moreover, chronic progression was more frequent in elderly patients affected by CIDP, and functional recovery was less frequent in this group when compared with younger patients [66]. Therapeutic management of CIDP is challenging, particularly when facing the progressive course of disease. Following this line of argument, advanced age is potentially associated with an imbalance of regulatory T cells (Tregs) and Th17 cells, infiltration of natural killer T cells, and alterations to the CD8$^+$ T cell repertoire in CIDP [66]. Likewise, the number and proinflammatory activity of macrophages is increased in older CIDP patients [67,68]. Yuan *et al.* demonstrated that age-related degenerative changes in peripheral nerves progressing to neuropathy can be attributed to **endoneural** macrophage

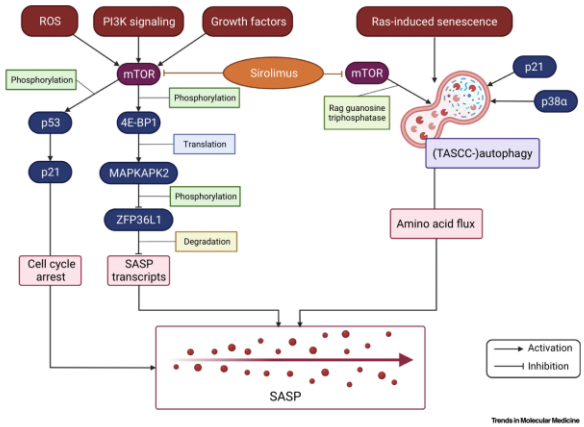

Figure 3. Potential mechanisms for mammalian target of rapamycin (mTOR) modulation on cellular senescence. mTOR is a protein kinase belonging to the phosphatidylinositol 3-kinase-related kinase family, which is preserved across eukaryotic species. Still incompletely understood, mTOR activity is likely regulated by nutrient availability and cellular stress. The mTOR pathway is linked to cellular senescence and establishment of the senescence-associated secretory phenotype (SASP) by multiple pathways. mTOR might signal via the p53/p21 pathway, inducing cell cycle arrest and a senescent phenotype. Phosphorylation of 4E-BP is also thought to contribute to the availability of gene transcripts for SASP expression. In Ras-induced senescence, mTOR is thought to colocalize with specialized lysosomes [TOR-**autophagy** spatial coupling compartment (TASCC)] in a Rag guanosine triphosphatase-dependent manner. Amino acid catabolism might then provide the flux necessary to sustain production of SASP components. p21/p38α also contribute to upregulation of autophagy and a senescent phenotype. This figure was created with BioRender. Abbreviations: 4E-BP1, eukaryotic translation initiation factor 4E-binding protein 1; MAPKAPK2, MAPK activated protein kinase 2; ROS, reactive oxygen species; ZFP36L1, ZFP36 ring finger protein like 1.

local plaque environment demonstrates an activated senescent and proinflammatory genetic signature. Ablation of senescent OPCs by the senolytic cocktail dasatinib and quercetin (DQ) reduced microglial activation and levels of proinflammatory cytokines while also improving hippocampus-dependent learning and memory deficits [6]. It is interesting to note that the same cell type, OPC, engages a senescent programming upon stress both in MS [40] and when challenged by amyloid-β aggregates [6]. Consequently, senotherapies directed at OPC reprogramming might be of translational interest for targeting MS.

The concept of cellular senescence might be of particular interest in progressive MS as this subtype responds poorly, if at all, to immunosuppressants. Accumulation of ROS contributes to progressive MS [54]. Concurrently, oxidative stress induces cellular senescence as evidenced by *in vivo* and *in vitro* studies [55,56]. In a murine model, deletion of the nuclear constitutive photomorphogenesis 9 (COP9) signalosome component CSN5 (JAB1) in oligodendrocytes results in DNA damage and cellular progression into a senescent phenotype [57]. The authors used phosphorylated H2A histone family member X (p-H2AX) and β-galactosidase activity to detect senescent cells. These mice exhibited progressive CNS demyelination, inflammation, and neurodegeneration reminiscent of progressive MS. Targeting microglial inflammation did not influence severity, whereas inhibition of the p53 pathway via p21^{Cip1} (but not p16ink4a) ameliorated disease severity [57]. These results suggest a prominent role for cellular senescence in perpetuating degeneration in the context of neuroinflammation. These findings are of particular interest from a translational perspective. Neurodegeneration is a major driver of disability in progressive MS and remains refractory to contemporary treatment approaches [11]. While immunosuppression appeared futile in JAB1-knockout mice, deletion of senescence-associated pathways dampened disease progression. It remains to be established whether this conceptual framework can be replicated in other models of CNS inflammation, and whether it can be translated to humans. It is interesting to note that even in RRMS, 80–90% of disability accumulated as PIRA [33]. This observation is supported by imaging data reporting a similar loss of brain volume across MS subtypes [58]. These data challenge the dichotomy of relapsing and progressive MS and point to shared mechanisms underlying disease progression. As outlined above, recent evidence supports a role for cellular senescence in MS, particularly in progressive MS. Therefore, targeting senescent cells might alleviate the proinflammatory microenvironment exerted by these cells and help overcome treatment resistance. Specifically, DQ might be a viable approach to treat progressive MS, as this drug has been shown to be effective at clearing senescent cells in humans [59] and is already being tested in a clinical trial for AD [7]. Importantly, DQ has been shown to cross the blood–brain barrier [6], while data on CNS permeability of other senotherapies are currently lacking. An advantage of DQ might be the route of administration. A dose of 100 mg D and 1000 mg Q can be administered orally for 2 consecutive days every 2 weeks [7]. Senolytic treatment by DQ could be of interest as a novel approach to managing progressive MS and warrants further research.

Cellular senescence may contribute to disease progression in polyneuropathies

Autoimmunity in the field of neuroinflammation is not restricted to the CNS but may also affect structures of the PNS. Indeed, immune-mediated neuropathies are heterogeneous disease entities affecting the peripheral nerves [60]. Among these, **chronic inflammatory demyelinating polyradiculoneuropathy (CIDP)** is characterized by immune-mediated demyelination of peripheral nerves and a chronic progressive or relapsing–remitting course of disease [61]. Clinical hallmarks are a progressive loss of motor function and sensory disturbances [62]. In typical CIDP, this pattern is often symmetric. While the exact pathophysiological mechanisms remain unknown, CIDP is thought to be mediated by autoimmunity directed against components of the PNS [62]. In a subset of patients (5–15%), autoantibodies against structures of the PNS, such as the node of Ranvier, could be detected [63,64]. CIDP patients are mostly treated with

infiltration in mice [69]. Interestingly, upon depletion of macrophages with the selective colony-stimulating factor 1 receptor (CSF1R) inhibitor PLX5622, pathological alterations in the peripheral nerves were reduced and neuropathy was ameliorated [69]. The SASP exerted by senescent cells can recruit immune cells, including macrophages, using the chemoattractant CCL2 [70]. In the context of sustained endoneural inflammation, it is tempting to speculate that senescent cells secreting CCL2 might mediate immune cell recruitment of macrophages and promote nerve damage. Studies of the endoneural microstructure might be valuable to better understand the impact of senescence in CIDP pathophysiology. Further, elevated levels of SASP factors IL-6 and IL-8 were detected in skin punch biopsies of patients affected by **small-fiber neuropathy** [71]. IL-6 and IL-8 secretion is not restricted to the SASP, and other sources are plausible. Nonetheless, the SASP is a potential origin of proinflammatory cytokines in the local microenvironment of small-fiber neuropathy, and further studies on the importance of senescent pathways in its pathophysiology are of interest.

A further link between cellular senescence and nerve damage is demonstrated by **chemotherapy-induced peripheral neuropathy (CIPN)**. In the context of CIPN, dorsal root ganglia sensory neurons may undergo a senescence-like response instead of apoptosis [72]. Indeed, in response to cisplatin, mouse dorsal root ganglia display markers of cellular senescence such as increased β-galactosidase activity and accumulation of cytosolic p16ink4a [73]. Senolysis using the p16-3MR transgene or application of the broad-spectrum senolytic agent ABT263 [74] improved symptoms of CIPN as measured by the response to mechanical or thermal stimuli in a murine model [73]. The question arises whether the observed effect could be replicated in immune-mediated neuropathies such as CIDP.

Effective treatment strategies for immune-mediated neuropathies remain an unmet need. Further studies should address whether senotherapeutics are effective agents for abrogating tissue damage mediated by the SASP and reducing immune cell – particularly macrophage – invasion in aged CIDP patients. Based on the current data in mice, we suspect that a senolytic strategy might be feasible for targeting senescence in CIDP. Currently, the senolytic cocktail DQ is supported by the most evidence as this approach has already been proven in humans [59].

Old cells in skeletal muscle: implications for inclusion-body myositis

Finally, we will discuss autoimmunity in the context of skeletal muscle with a focus on **inclusion-body myositis(IBM)**. The spectrum of **idiopathic inflammatory myopathies (IIMs)** is characterized by muscle inflammation as a pathophysiological hallmark [75]. IBM is unique among IIMs due to its characteristic clinical presentation, advanced age at onset, and notable refractoriness to contemporary treatment approaches [76]. Indeed, IBM primarily affects elderly patients and is characterized by progressive muscle weakness of finger flexors and knee extensors. Clonal expansion of terminally differentiated cytotoxic CD8$^+$ T cells emerged as the pathogenic hallmark, mediating damage to skeletal muscle (a current view on the pathophysiology of IBM is discussed in detail by Greenberg [76]). The identification of circulating autoantibodies (anti-cN1A) [77] and the detection of a cytotoxic T cell signature in gene expression studies [78,79] underline autoimmunity as the driver of disease in IBM. Despite its autoimmune etiology and numerous clinical trials, contemporary immunosuppressive strategies are ineffective in treating IBM [76]. Progressive disability results in a loss of ambulation for most patients by 10 years after diagnosis [80]. Immunosuppressants such as prednisone [81], methotrexate [82], natalizumab [83], or alemtuzumab [84] are unable to halt disease progression. Given its treatment refractoriness, and that it primarily affects elderly patients, a contribution from senescent pathways is plausible. Indeed, protein aggregations associated with tissue degeneration were described in IBM muscle. Detection of TAR DNA-binding protein 43 (TDP-43) aggregates in IBM myofibers ranges between 12% and 23% of cases [85,86], while other markers, including β-amyloid, are exceedingly rare [76]. However, autoimmunity likely

Clinician's corner

Treatment options for neuroinflammatory disorders have evolved substantially. Nevertheless, neuroinflammation progressing to a degenerative phenotype often remains refractory to contemporary treatment.

In both animal models and humans, features of cellular senescence have been detected in neuroinflammatory disorders. However, it remains to be established how the senescent burden influences clinical outcomes.

In a recent landmark trial, the senolytic treatment DQ eliminated senescent cells in patients with diabetic kidney disease. Although no adverse effects were observed, caution is warranted as long-term effects are currently unknown, and cellular senescence is an important mechanism protecting tissues against neoplasia.

Further senotherapeutic strategies are currently in development or are already being tested in humans.

Neuroinflammatory diseases resistant to immunosuppression might potentially benefit from senotherapies.

precedes the appearance of degenerative biomarkers, and the majority of protein aggregates present are not specific for IBM but are also detected in other muscle diseases, such as hereditary IBM or HIV-associated myositis [76,87]. While protein aggregation is likely unspecific, studying myoblasts from IBM patients *in vivo* demonstrated impaired proliferative capacities and increased telomere shortening, suggestive of a senescent phenotype [88]. Primary muscle cultures from IBM patients also overexpress β-catenin [88]. Together with Wnt, β-catenin signaling is thought to induce cellular senescence *in vitro* [89,90]. Following this line of argument, accumulation of senescent muscle cells might influence the microenvironment by excretion of the SASP, and provide proinflammatory stimuli sustaining T cell pathology. An interesting argument for senescence might arise from the effect of **sirolimus (rapamycin)** in IBM. In the latest randomized, placebo-controlled trial for IBM, the **mammalian target of rapamycin (mTOR)** inhibitor sirolimus was tested in 44 IBM patients [91]. Sirolimus did not meet the primary outcome of maximal voluntary isometric knee extension strength; however, secondary outcome measures – such as 6-min walking distance, forced vital capacity, and thigh fat fraction – were improved [91]. The trend observed for secondary outcomes is noteworthy and warranted further investigation in a multicenter Phase 3 study [91]. Aside from immunoregulatory effects, mTOR signaling has been linked to cellular senescence (Figure 3). *In vivo* and *in vitro* evidence demonstrated that the mTOR pathway regulates the SASP, for example, via mitogen-activated protein kinase (MAPK)-activated protein kinase 2 signaling [92,93]. Consequently, the mTOR inhibitor sirolimus suppressed the SASP of senescent cells [92,94]. Thus, it is tempting to speculate that the therapeutic effect of sirolimus is, at least in part, mediated by modulation of the SASP. Studies investigating mTOR inhibition for treatment of IBM might be improved by integrating analyses that are able to detect changes to cellular senescence in skeletal muscle. Based on current evidence, skeletal muscle cells might engage a senescent phenotype in IBM and consequently respond to senotherapeutics [88]. Consequently, β-galactosidase staining of skeletal muscle before and after treatment could serve as a potential readout. Currently, a Phase 3 trial is planned to investigate sirolimus in IBM [91]. Sirolimus is taken orally at a dose of 2 mg per day. The results of this trial are of particular interest as they will provide additional data on the efficacy of sirolimus, a drug with senomorphic properties [94].

It is worthy of discussion that the function of skeletal muscle is not only impaired in pathological conditions such as IBM, but also in response to physiological aging [15]. However, despite comprising 40–50% of the total body mass, studies investigating cellular senescence in the context of skeletal muscle are sparse. Two recent studies in mice provided novel evidence for senescence in aging muscle. As evidenced by β-galactosidase and p21 immunohistochemistry, muscle of old mice displayed increased numbers of senescent cells following a bout of exercise when compared with young mice [95]. Similar to humans, muscle hypertrophy is impaired in aged mice. Interestingly, treatment of old mice with the senolytic DQ resulted in enhanced muscle and muscle fiber size as well as improvements in functional testing [95,96]. In response to chemical muscle injury induced by barium chloride, muscle regeneration was improved by DQ treatment, as compared to vehicle, in old mice [96]. Muscle regeneration was measured by fiber cross-sectional area. Interestingly, DQ did not improve muscle regeneration in young mice, suggesting that the framework in which senolytics are effective is affected by age in skeletal muscle [96]. Although limited to mice, these findings underline the importance of understanding how muscle tissue responds to cellular stress, and how senescence is implicated in this process. Particularly in old age, senotherapeutics could provide a promising tool to improve muscle function in health and disease, warranting further research in this field.

Concluding remarks

Cells with a senescent phenotype promote disease chronicity in neuroinflammation and potentially diminish treatment responses to immunosuppression (Figure 4). Current senotherapeutics include

Outstanding questions

The influence of cellular senescence on neuroinflammatory diseases is understudied. Future research might benefit from targeting the following questions. What are the implications of cellular senescence for disease outcomes in individual disorders? At what time point does the senescent burden become relevant? What are the functional implications?

Primary pathways of senescence have already been studied in the field of neuroimmunology. What other specific cells and pathways are implicated in cellular senescence following neuroinflammation? Are these concepts disease-specific or a broader response to chronic inflammation? Can we transfer these concepts from one disease entity to another?

Can senotherapeutics be beneficial for patients suffering from neuroinflammatory diseases? And if so, in what context? What is the optimal timing for treatment? Should immunosuppressive agents be coadministered? What are the short- and long-term adverse effects of senotherapeutics?

senolytics [e.g., fisetin [97], DQ [59], or heat shock protein 90 (HSP90) inhibitors [98]] and senomorphics [e.g., rapamycin [94], novel small-molecule therapeutics [99], or Janus kinase (JAK) 1/2 inhibitors [100]] (Table 1). For a current overview of senotherapeutics, see [101].

Table 1. Overview of current senotherapeutics and their effect mechanisms[a]

Senotherapeutic	Subgroup	Substance	Molecular mechanism	Route of application	Refs
Senomorphics	Glucocorticoids	Corticosterone	Suppression of senescence-associated IL-6 secretion Nuclear translocation of glucocorticoid receptor in senescent cells	Oral (p.o.) or intravenous (i.v.)	[102]
		Cortisol	Suppression of IL-1α expression on mRNA level Impairment of the IL-1α/NF-κB pathway Suppression of the ability of the SASP to stimulate tumor-cell invasion	p.o. or i.v.	
	Novel small molecules	Nutlin-3a	Inhibition of MDM2–p53 interaction Increase in p53 levels and its transcriptional target p21 Induction of senescence growth arrest	p.o. or i.v.	[99]
		MI-63		p.o. or i.v.	
		Oridonin	Reduced NF-κB activity, phosphorylation and expression of p38 in senescent cells Reduced secretion of IL-6 and IL-8	p.o.	[103]
		Y-27632	Reduced IL-1α, IL-1β, IL-6, and IL-8 secretion in keratinocytes	Unknown	[104]
	JAK inhibitors	JAK inhibitors	Inhibition of the JAK/STAT[b] pathway Reduced phosphorylated STAT3 in adipose tissue Reduced levels of systemic inflammation	p.o. or i.v.	[100]
	Sirolimus (rapamycin)	mTOR inhibitor	Inhibition of mTOR Inhibition of the Stat3-pathway	p.o.	[94]
Senolytics	N-terminal ansamycin-derived HSP90 inhibitors	Geldanamycin 17-AAG (tanespimycin) 17-DMAG (alvespimycin)	Inhibition of HSP90 (molecular chaperone, important for protein stabilization and degradation) Selective cell death of senescent cells Downregulation of anti-apoptotic PI3K/AKT pathway	i.v.	[98]
	Flavanoids	Fisetin	Reduction in viability of senescent cells without affecting proliferating cells Antioxidant activity Reduction of senescence (e.g., SA-β-gal) and SASP markers (e.g., IL-6, IL-8, MCP-1) Reduction in $p16^{INK4A}$, $p21^{CIP1}$ expressing cells	p.o.	[97]
	Tyrosine kinase inhibitor (BCR/Abl)	Dasatinib and quercetin (DQ)	Reduction in $p16^{INK4A}$, $p21^{CIP1}$ expressing cells Reduction in SA-β-gal-expressing cells Decrease in cells with limited replicative potential Reduction in circulating SASP factors (e.g., IL-1α, IL-6, MMP-9 and -12)	p.o.	[59]
	BCL-2/Bcl-xL inhibitors	ABT263 (navitoclax)	Inhibition of the anti-apoptotic proteins BCL-2 and BCL-xL Reduced aging in response to total-body irradiation in hematopoietic cells Apoptosis of aged cholangiocytes	p.o.	[4,105,106]
		ABT-737			
		A1331852			
		A1155463			
		UBX-1325			
	Ubiquitin-specific peptidase 7 (USP7) inhibitors	P5091	RNA interference with USP7 Induction of p53 and proapoptotic pathways in senescent cells	Unknown	[107]

[a]This is not a complete list of known senotherapeutics, but provides examples of common classes that are in development.
[b]Abbreviation: STAT, signal transducer and activator of transcription proteins.

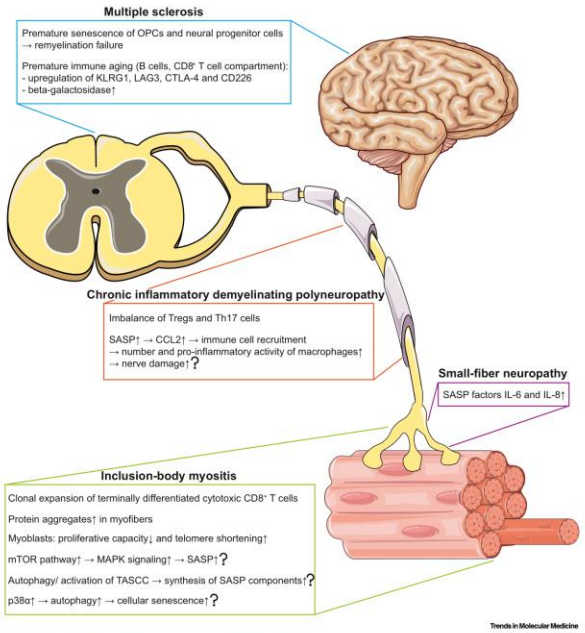

Figure 4. Outline of cellular senescence in exemplary neuroinflammatory conditions. Multiple sclerosis (MS), chronic inflammatory demyelinating polyneuropathy (CIDP), small-fiber neuropathy, and inclusion-body myositis (IBM) are characterized by chronic inflammation. Boxes display potential mechanisms by which cellular senescence may influence the respective pathophysiology. Senescent cells might serve as treatment targets; however, further research is needed to understand the impact in individual diseases. This figure was created with Adobe Illustrator. Abbreviations: OPCs, oligodendrocyte progenitor cells; SASP, senescence-associated secretory phenotype; TASCC, TOR-autophagy spatial coupling compartment; Tregs, regulatory T cells.

Senomorphics suppress the SASP without inducing cell death, while senolytics promote cell death in senescent cells. Consistent with this, a recent landmark trial provided the first evidence that DQ reduces senescent cells in humans as measured by $p16^{INK4A}$ and $p21^{CIP1}$ expression [59]. Consequently, plasma levels of SASP factors IL-1α, -2, -6, and -9 were significantly reduced [59]. However, caution is warranted when translating these findings, as studies investigating the adverse effects profile (especially in the long term) of senolytic drugs are sparse in humans. By employing a 'hit and run' strategy (i.e., pulsatile treatment with DQ over 2 consecutive days with 100 mg D and 1000 mg Q), toxicity might be reduced [4]. However, at least in a healthy state, cellular senescence is a powerful tumor-suppressive mechanism, protecting tissue from malignancy in response to chronic stress. Long-term outcomes are therefore of particular importance to assess the risk:benefit ratio of senotherapeutics (see Outstanding questions). In this context, the individual and socioeconomic burden of disease for treatment-refractory neuroinflammatory disorders such as progressive MS or IBM is immense [11]. Thus, the risk for adverse effects may well be outweighed by potential benefits. By targeting specific cells and pathways, as evidenced for OPC in CNS inflammation, adverse effects might be further reduced.

The field of senotherapeutic research is further complicated by the lack of conclusive readouts used to define a senescent state. A plethora of markers is associated with cellular senescence, including, among others, β-galactosidase activity, p16INK4a, or p21. However, none of these is a specific biomarker for cellular senescence. External conditions, such as pH in the case of β-galactosidase activity [101], also affect senescence markers, potentially impairing readouts. Consequently, the discovery of novel and more specific biomarkers is needed to advance the field. Combining senotherapeutics with immunomodulatory approaches could be valuable for neuroinflammatory diseases that do not respond to contemporary therapies (see also Clinician's corner). Studies should focus on identifying the senescent burden in individual disorders to enable a better understanding of potential benefits and drawbacks of senotherapeutics in neuroinflammation.

Acknowledgments

T.R. was supported by the Deutsche Forschungsgemeinschaft (DFG) (RU 2169/2-1), the Else Kröner-Fresenius-Stiftung (2018_A03), the Federal Ministry of Education and Research (BMBF, 01EC1901A), and the Deutsche Gesellschaft für Muskelkranke e.V. (DGM, Ru2/1 and Sc22/4). C.N. was supported by the Deutsche Gesellschaft für Muskelkranke e.V. (DGM, Ne4/1) and the Interne Forschungsförderung of the Medical Faculty of the Heinrich Heine University Duesseldorf.

Declaration of interests

No interests are declared.

References

1. Jurk, D. *et al.* (2014) Chronic inflammation induces telomere dysfunction and accelerates ageing in mice. *Nat. Commun.* 5, 4172
2. Di Micco, R. *et al.* (2021) Cellular senescence in ageing: from mechanisms to therapeutic opportunities. *Nat. Rev. Mol. Cell Biol.* 22, 75–95
3. Hayflick, L. and Moorhead, P.S. (1961) The serial cultivation of human diploid cell strains. *Exp. Cell Res.* 25, 585–621
4. Kirkland, J.L. and Tchkonia, T. (2020) Senolytic drugs: from discovery to translation. *J. Intern. Med.* 288, 518–536
5. Raffaele, M. and Vinciguerra, M. (2022) The costs and benefits of senotherapeutics for human health. *Lancet Healthy Longev.* 3, e67–e77
6. Zhang, P. *et al.* (2019) Senolytic therapy alleviates Aβ-associated oligodendrocyte progenitor cell senescence and cognitive deficits in an Alzheimer's disease model. *Nat. Neurosci.* 22, 719–728
7. Gonzales, M.M. *et al.* (2022) Senolytic therapy to modulate the progression of Alzheimer's disease (SToMP-AD): a pilot clinical trial. *J. Prev. Alzheimers Dis.* 9, 22–29
8. University of California, San Francisco MS-EPIC Team *et al.* (2019) Long-term evolution of multiple sclerosis disability in the treatment era. *Ann. Neurol.* 85, 499–510
9. Rollins, L. *et al.* (2020) Failed, interrupted, or inconclusive trials on immunomodulatory treatment strategies in multiple sclerosis: update 2015–2020. *BioDrugs Clin. Immunother. Biopharm. Gene Ther.* 34, 587–610
10. Cree, B.A.C. *et al.* (2021) Secondary progressive multiple sclerosis: new insights. *Neurology* 97, 378–388
11. Wallin, M.T. *et al.* (2019) Global, regional, and national burden of multiple sclerosis 1990–2016: a systematic analysis for the Global Burden of Disease Study 2016. *Lancet Neurol.* 18, 269–285
12. Mijit, M. *et al.* (2020) Role of p53 in the regulation of cellular senescence. *Biomolecules* 10, E420
13. Milanovic, M. *et al.* (2018) Senescence-associated reprogramming promotes cancer stemness. *Nature* 553, 96–100
14. da Silva, P.F.L. *et al.* (2019) The bystander effect contributes to the accumulation of senescent cells *in vivo*. *Aging Cell* 18, e12848

15. Nelke, C. *et al.* (2019) Skeletal muscle as potential central link between sarcopenia and immune senescence. *eBioMedicine* 49, 381–388.
16. Kirkland, J.L. and Tchkonia, T. (2017) Cellular senescence: a translational perspective. *eBioMedicine* 21, 21–28
17. Papadopoulos, D. *et al.* (2020) Aging, cellular senescence, and progressive multiple sclerosis. *Front. Cell. Neurosci.* 14, 178
18. Acosta, J.C. *et al.* (2008) Chemokine signaling via the CXCR2 receptor reinforces senescence. *Cell* 133, 1006–1018
19. Basisty, N. *et al.* (2020) A proteomic atlas of senescence-associated secretomes for aging biomarker development. *PLoS Biol.* 18, e3000599
20. Gorgoulis, V. *et al.* (2019) Cellular senescence: defining a path forward. *Cell* 179, 813–827
21. Newe, J. *et al.* (2013) Of flies, mice, and men: evolutionarily conserved tissue damage responses and aging. *Dev. Cell* 32, 9–18
22. Tchkonia, T. *et al.* (2013) Cellular senescence and the senescent secretory phenotype: therapeutic opportunities. *J. Clin. Invest.* 123, 966–972
23. Kuilman, T. and Peeper, D.S. (2009) Senescence-messaging secretome: SMS-ing cellular stress. *Nat. Rev. Cancer* 9, 81–94
24. Acosta, J.C. *et al.* (2013) A complex secretory program orchestrated by the inflammasome controls paracrine senescence. *Nat. Cell Biol.* 15, 978–990
25. Tominaga, K. (2015) The emerging role of senescent cells in tissue homeostasis and pathophysiology. *Pathobiol. Aging Age Relat. Dis.* 5, 27743
26. Attfield, K.E. *et al.* (2022) The immunology of multiple sclerosis. *Nat. Rev. Immunol.* Published online May 4, 2022. http://doi.org/10.1038/s41577-022-00718-z
27. Fassner, S. *et al.* (2018) Progressive multiple sclerosis: from pathophysiology to therapeutic strategies. *Nat. Rev. Drug Discov.* 18, 905–922
28. Scalfari, A. *et al.* (2014) Onset of secondary progressive phase and long-term evolution of multiple sclerosis. *J. Neurol. Neurosurg. Psychiatry* 85, 67–75
29. Bittner, S. *et al.* (2013) Endothelial TWIK-related potassium channel-1 (TREK1) regulates immune-cell trafficking into the CNS. *Nat. Med.* 19, 1161–1165
30. Ruck, T. *et al.* (2022) K2P18.1 translates T cell receptor signals into thymic regulatory T cell development. *Cell Rep.* 32, 72–88
31. Bittner, S. *et al.* (2014) TREK-king the blood–brain-barrier. *J. Neuroimmune Pharmacol.* 9, 293–301
32. Hauser, S.L. *et al.* (2017) Ocrelizumab versus interferon beta-1a in relapsing multiple sclerosis. *N. Engl. J. Med.* 376, 221–234
33. Kappos, L. *et al.* (2020) Contribution of relapse-independent progression vs relapse-associated worsening to overall confirmed disability accumulation in typical relapsing multiple sclerosis in a pooled analysis of 2 randomized clinical trials. *JAMA Neurol.* 77, 1132–1140
34. Wiley, C.D. *et al.* (2016) Mitochondrial dysfunction induces senescence with a distinct secretory phenotype. *Cell Metab.* 23, 303–314
35. López-Otín, C. *et al.* (2013) The hallmarks of aging. *Cell* 153, 1194–1217
36. Oost, W. *et al.* (2018) Targeting senescence to delay progression of multiple sclerosis. *J. Mol. Med. (Berl.)* 96, 1153–1166
37. Passos, J.F. *et al.* (2010) Feedback between p21 and reactive oxygen production is necessary for cell senescence. *Mol. Syst. Biol.* 6, 347
38. Purcell, M. *et al.* (2014) Gene expression profiling of replicative and induced senescence. *Cell Cycle* 13, 3927–3937
39. Koutsoudaki, P.N. *et al.* (2020) Cellular senescence and failure of myelin repair in multiple sclerosis. *Mech. Ageing Dev.* 192, 111366
40. Nicaise, A.M. *et al.* (2019) Cellular senescence in progenitor cells contributes to diminished remyelination potential in progressive multiple sclerosis. *Proc. Natl. Acad. Sci. U. S. A.* 116, 9030–9039
41. Klein, B. *et al.* (2018) Age influences microglial activation after cuprizone-induced demyelination. *Front. Aging Neurosci.* 10, 278
42. Karamita, M. *et al.* (2018) Cellular senescence correlates with demyelination, brain atrophy and motor impairment in a model of multiple sclerosis (P2.405). *Neurology* 90, P2.405
43. Cantuti-Castelvetri, L. *et al.* (2018) Defective cholesterol clearance limits remyelination in the aged central nervous system. *Science* 359, 684–688
44. Neumann, B. *et al.* (2019) Metformin restores CNS remyelination capacity by rejuvenating aged stem cells. *Cell Stem Cell* 25, 473–485.e8
45. Thewissen, M. *et al.* (2005) Premature immunosenescence in rheumatoid arthritis and multiple sclerosis patients. *Ann. N. Y. Acad. Sci.* 1051, 255–262
46. Eschborn, M. *et al.* (2021) Evaluation of age-dependent immune signatures in patients with multiple sclerosis. *Neurol. Neuroimmunol. Neuroinflamm.* 8, e1094
47. Claes, N. *et al.* (2016) Age-associated B cells with proinflammatory characteristics are expanded in a proportion of multiple sclerosis patients. *J. Immunol.* 197, 4576–4583
48. Mutukula, N. *et al.* (2021) Generation of RRMS and PPMS-specific iPSCs as a platform for modeling multiple sclerosis. *Stem Cell Res.* 53, 102319
49. De Strooper, B. and Karran, E. (2016) The cellular phase of Alzheimer's disease. *Cell* 164, 603–615
50. Guerrero, A. *et al.* (2021) Cellular senescence at the crossroads of inflammation and Alzheimer's disease. *Trends Neurosci.* 44, 714–727
51. Ogrodnik, M. *et al.* (2021) Whole-body senescent cell clearance alleviates age-related brain inflammation and cognitive impairment in mice. *Aging Cell* 20, e13296
52. Angelova, D.M. and Brown, D.R. (2018) Altered processing of β-amyloid in SH-SY5Y cells induced by model senescent microglia. *ACS Chem. Neurosci.* 9, 3137–3152
53. Bussian, T.J. *et al.* (2018) Clearance of senescent glial cells prevents tau-dependent pathology and cognitive decline. *Nature* 562, 578–582
54. Redondo, J. *et al.* (2018) Dysregulation of mesenchymal stromal cell antioxidant responses in progressive multiple sclerosis. *Stem Cells Transl. Med.* 7, 748–758
55. Komarova, J.S. *et al.* (2018) High doses of synthetic antioxidants induce premature senescence in cultivated mesenchymal stem cells. *Sci. Rep.* 9, 1296
56. Liguori, I. *et al.* (2018) Oxidative stress, aging, and diseases. *Clin. Interv. Aging* 13, 757–772
57. Rivellini, C. *et al.* (2022) JAB1 deletion in oligodendrocytes causes senescence-induced inflammation and neurodegeneration in mice. *J. Clin. Invest.* 132, e145071
58. De Stefano, N. *et al.* (2013) Assessing brain atrophy rates in a large population of untreated multiple sclerosis subtypes. *Neurology* 74, 1868–1876
59. Hickson, L.J. *et al.* (2019) Senolytics decrease senescent cells in humans: preliminary report from a clinical trial of Dasatinib plus Quercetin in individuals with diabetic kidney disease. *eBioMedicine* 47, 446–456
60. Kiesseier, B.C. *et al.* (2018) Immune-mediated neuropathies. *Nat. Rev. Dis. Primer* 4, 31
61. Bunschoten, C. *et al.* (2019) Progress in diagnosis and treatment of chronic inflammatory demyelinating polyradiculoneuropathy. *Lancet Neurol.* 18, 784–794
62. Mahdi-Rogers, M. and Rajabally, Y.A. (2013) Overview of the pathogenesis and treatment of chronic inflammatory demyelinating polyneuropathy with intravenous immunoglobulins. *Biol. Targets Ther.* 4, 45–49
63. Querol, L. *et al.* (2017) Antibodies against peripheral nerve antigens in chronic inflammatory demyelinating polyradiculoneuropathy. *Sci. Rep.* 7, 14411
64. Cortese, A. *et al.* (2020) Antibodies to neurofascin, contactin-1, and contactin-associated protein 1 in CIDP: clinical relevance of IgG isotype. *Neurol. Neuroimmunol. Neuroinflamm.* 7, e639
65. Kuwabara, S. *et al.* (2006) Long-term prognosis of chronic inflammatory demyelinating polyneuropathy: a five year follow-up of 38 cases. *J. Neurol. Neurosurg. Psychiatry* 77, 66–70
66. Hagen, K.M. and Ousman, S.S. (2021) The immune response and aging in chronic inflammatory demyelinating polyradiculoneuropathy. *J. Neuroinflammation* 18, 78
67. Büttner, R. *et al.* (2018) Inflammaging impairs peripheral nerve maintenance and regeneration. *Aging Cell* 17, e12833
68. van Beek, A.A. *et al.* (2019) Metabolic alterations in aging macrophages: ingredients for inflammaging? *Trends Immunol.* 40, 113–127
69. Yuan, X. *et al.* (2018) Macrophage depletion ameliorates peripheral neuropathy in aging mice. *J. Neurosci.* 38, 4610–4620

70. Chambers, E.S. *et al.* (2021) Recruitment of inflammatory monocytes by senescent fibroblasts inhibits antigen-specific tissue immunity during human aging. *Nat. Aging* 1, 101–113
71. Uçeyler, N. *et al.* (2013) Elevated proinflammatory cytokine expression in affected skin in small fiber neuropathy. *Neurology* 74, 1806–1813
72. Calls, A. *et al.* (2021) Cisplatin-induced peripheral neuropathy is associated with neuronal senescence-like response. *Neuro-Oncol.* 23, 88–99
73. Acklin, S. *et al.* (2023) Depletion of senescent-like neuronal cells alleviates cisplatin-induced peripheral neuropathy in mice. *Sci. Rep.* 10, 14179
74. Chang, J. *et al.* (2016) Clearance of senescent cells by ABT263 rejuvenates aged hematopoietic stem cells in mice. *Nat. Med.* 22, 78–83
75. Lundberg, I.E. *et al.* (2018) Classification of myositis. *Nat. Rev. Rheumatol.* 14, 269–278
76. Greenberg, S.A. (2019) Inclusion body myositis: clinical features and pathogenesis. *Nat. Rev. Rheumatol.* 15, 257–272
77. Nihtinuis, H. *et al.* (2014) G.P.6(b) the utility of anti-cN1A autoantibody for the diagnosis of sporadic inclusion body myositis. *Neuromuscul. Disord.* 24, 815
78. Goyal, N.A. *et al.* (2022) Immunophenotyping of inclusion body myositis blood T and NK cells. *Neurology* 98, e1374–e1383
79. Greenberg, S.A. *et al.* (2019) Highly differentiated cytotoxic T cells in inclusion body myositis. *Brain* 142, 2590–2604
80. Shelly, S. *et al.* (2021) Epidemiology and natural history of inclusion body myositis: a 40-year population-based study. *Neurology* 96, e2653–e2661
81. Barohn, R.J. *et al.* (1995) Inclusion body myositis: explanation for poor response to immunosuppressive therapy. *Neurology* 45, 1302–1304
82. Badrising, U.A. *et al.* (2002) Comparison of weakness progression in inclusion body myositis during treatment with methotrexate or placebo. *Ann. Neurol.* 51, 369–372
83. Saperstein, D. and Levine, T. (2016) Interim analysis of a pilot trial of rataliximab in inclusion body myositis (P3.161). *Neurology* 86, P3.161
84. Dalakas, M.C. *et al.* (2009) Effect of alemtuzumab (CAMPATH 1-H) in patients with inclusion-body myositis. *Brain* 132, 1536–1544
85. Salajegheh, M. *et al.* (2009) Sarcoplasmic redistribution of nuclear TDP-43 in inclusion body myositis. *Muscle Nerve* 40, 19–31
86. Dubourg, O. *et al.* (2011) Diagnostic value of markers of muscle degeneration in sporadic inclusion body myositis. *Acta Myol. Myopathies Cardiomyopathies* 30, 103–109
87. Hinker, A. *et al.* (2016) T cell-mediated inflammatory myopathies in HIV-positive individuals: a histologic study of 19 cases. *J. Neuropathol. Exp. Neurol.* 75, 239–245
88. Morosetti, R. *et al.* (2010) Increased aging in primary muscle cultures of sporadic inclusion-body myositis. *Neurobiol. Aging* 31, 1206–1214
89. Gu, Z. *et al.* (2014) Wnt/β-catenin signaling mediates the senescence of bone marrow-mesenchymal stem cells from systemic lupus erythematosus patients through the p53/p21 pathway. *Mol. Cell. Biochem.* 387, 27–37
90. Lehmann, M. *et al.* (2023) Chronic WNT/β-catenin signaling induces cellular senescence in lung epithelial cells. *Cell. Signal.* 70, 109588
91. Benveniste, O. *et al.* (2021) Sirolimus for treatment of patients with inclusion body myositis: a randomised, double-blind, placebo-controlled, proof-of-concept, phase 2b trial. *Lancet Rheumatol.* 3, e40–e48
92. Herranz, N. *et al.* (2015) mTOR regulates MAPKAPK2 translation to control the senescence-associated secretory phenotype. *Nat. Cell Biol.* 17, 1205–1217
93. Laberge, R.-M. *et al.* (2015) MTOR regulates the pro-tumorigenic senescence-associated secretory phenotype by promoting IL1A translation. *Nat. Cell Biol.* 17, 1049–1061
94. Wang, R. *et al.* (2017) Rapamycin inhibits the secretory phenotype of senescent cells by a Nrf2-independent mechanism. *Aging Cell* 16, 564–574
95. Dungan, C.M. *et al.* (2022) Senolytic treatment rescues blunted muscle hypertrophy in old mice. *GeroScience*. Published online March 24, 2022. http://doi.org/10.1007/s11357-022-00542-2
96. Dungan, C.M. *et al.* (2022) Deletion of SA β-Gal+ cells using senolytics improves muscle regeneration in old mice. *Aging Cell* 21, e13528
97. Yousefzadeh, M.J. *et al.* (2018) Fisetin is a senotherapeutic that extends health and lifespan. *eBioMedicine* 36, 18–28
98. Fuhrmann-Stroissnigg, H. *et al.* (2017) Identification of HSP90 inhibitors as a novel class of senolytics. *Nat. Commun.* 8, 422
99. Wiley, C.D. *et al.* (2018) Small-molecule MDM2 antagonists attenuate the senescence-associated secretory phenotype. *Sci. Rep.* 8, 2410
100. Xu, M. *et al.* (2015) JAK inhibition alleviates the cellular senescence-associated secretory phenotype and frailty in old age. *Proc. Natl. Acad. Sci. U. S. A.* 112, E6301–E6310
101. de Mera-Rodríguez, J.A. *et al.* (2021) Is senescence-associated β-galactosidase a reliable *in vivo* marker of cellular senescence during embryonic development? *Front. Cell Dev. Biol.* 9, 623175
102. Laberge, R.-M. *et al.* (2012) Glucocorticoids suppress selected components of the senescence-associated secretory phenotype. *Aging Cell* 11, 569–578
103. Yasuda, S. *et al.* (2022) Ordonin inhibits SASP by blocking p38 and NF-κB pathways in senescent cells. *Biochem. Biophys. Res. Commun.* 590, 55–62
104. Niklander, S. *et al.* (2023) ROCK inhibition modulates the senescence-associated secretory phenotype (SASP) in oral keratinocytes. *FEBS Open Bio* 13, 2740–2749
105. Moncsek, A. *et al.* (2018) Targeting senescent cholangiocytes and activated fibroblasts with B-cell lymphoma-extra large inhibitors ameliorates fibrosis in multidrug resistance 2 gene knockout (Mdr2$^{-/-}$) mice. *Hepatology* 67, 247–259
106. Yosef, R. *et al.* (2016) Directed elimination of senescent cells by inhibition of BCL-W and BCL-XL. *Nat. Commun.* 7, 11190
107. He, Y. *et al.* (2023) Inhibition of USP7 activity selectively eliminates senescent cells in part via restoration of p53 activity. *Aging Cell* 19, e13117